



Numerical Precision Calculations for LHC Physics

Dissertation

zur Erlangung des Grades

”Doktor der Naturwissenschaften”

am Fachbereich Physik, Mathematik und Informatik

der Johannes Gutenberg - Universität

in Mainz

Vorgelegt von

Christian Andreas Reuschle,

geboren in Heilbronn

Mainz, den 15. November 2012

D77 / Dissertation der Johannes Gutenberg - Universität Mainz

1. Berichterstatter: –

2. Berichterstatter: –

Datum der Mündlichen Prüfung: 5. Februar 2013

To –

Abstract / Zusammenfassung

In this thesis I present aspects of QCD calculations, which are related to the fully numerical evaluation of next-to-leading order (NLO) QCD amplitudes, especially of the one-loop contributions, and the efficient computation of associated collider observables. Two interrelated topics have thereby been of concern to the thesis at hand, which give rise to two major parts. One large part is focused on the general group-theoretical behavior of one-loop QCD amplitudes, with respect to the underlying $SU(N_c)$ theory, in order to correctly and efficiently handle the color degrees of freedom in QCD one-loop amplitudes. To this end a new method is introduced that can be used in order to express color-ordered partial one-loop amplitudes with multiple quark-antiquark pairs as shuffle sums over cyclically ordered primitive one-loop amplitudes. The other large part is focused on the local subtraction of divergences off the one-loop integrands of primitive one-loop amplitudes. A method for local UV renormalization has thereby been developed, which uses local UV counterterms and efficient recursive routines. Together with suitable virtual soft and collinear subtraction terms, the subtraction method is extended to the virtual contributions in the calculations of NLO observables, which enables the fully numerical evaluation of the one-loop integrals in the virtual contributions. The method has been successfully applied to the calculation of jet rates in electron-positron annihilation to NLO accuracy in the large- N_c limit.

In dieser Arbeit stelle ich Aspekte zu QCD Berechnungen vor, welche eng verknüpft sind mit der numerischen Auswertung von NLO QCD Amplituden, speziell der entsprechenden Einschleifenbeiträge, und der effizienten Berechnung von damit verbundenen Beschleunigerobservablen. Zwei Themen haben sich in der vorliegenden Arbeit dabei herauskristallisiert, welche den Hauptteil der Arbeit konstituieren. Ein großer Teil konzentriert sich dabei auf das gruppentheoretische Verhalten von Einschleifenamplituden in QCD, um einen Weg zu finden die assoziierten Farbfreiheitsgrade korrekt und effizient zu behandeln. Zu diesem Zweck wird eine neue Herangehensweise eingeführt welche benutzt werden kann, um farbgeordnete Einschleifenpartialamplituden mit mehreren Quark-Antiquark Paaren durch Shufflesummation über zyklisch geordnete primitive Einschleifenamplituden auszudrücken. Ein zweiter großer Teil konzentriert sich auf die lokale Subtraktion von zu Divergenzen führenden Poltermen in primitiven Einschleifenamplituden. Hierbei wurde im Speziellen eine Methode entwickelt, um die primitiven Einschleifenamplituden lokal zu renormieren, welche lokale UV Counterterme und effiziente rekursive Routinen benutzt. Zusammen mit geeigneten lokalen soften und kollinearen Subtraktionstermen wird die Subtraktionsmethode dadurch auf den virtuellen Teil in der Berechnung von NLO Observablen erweitert, was die voll numerische Auswertung der Einschleifenintegrale in den virtuellen Beiträgen der NLO Observablen ermöglicht. Die Methode wurde schließlich erfolgreich auf die Berechnung von NLO Jetraten in Elektron-Positron Annihilation im farbführenden Limes angewandt.

Contents

	Page
1 Introduction	1
1.1 Processes in Hadron Colliders	2
1.2 Perturbative Calculations	6
1.3 Divergences in Infrared Safe Observables	10
1.4 Subtracting Virtual Divergences	13
2 Color Management	17
2.1 Tree-Level Color Decomposition	19
2.1.1 Tree-Level Gluon Amplitudes	19
2.1.2 Tree-Level Amplitudes with Gluons and Quarks	24
2.2 Color Flow in $SU(N_c)$ Theories	27
2.2.1 Tree-Level Gluon Amplitudes in the Color-Flow Basis	29
2.2.2 Tree-Level Amplitudes with Gluons and Quarks in the Color-Flow Basis	30
2.3 Squared Amplitudes and the Color Matrix	32
2.4 Gluon Amplitudes in the Adjoint Basis	38
2.5 One-Loop Color Decomposition	40
2.5.1 One-Loop Gluon Amplitudes	43
2.5.2 One-Loop Amplitudes with Gluons and One Quark-Antiquark Pair	48
2.5.3 One-Loop Amplitudes with Gluons and Multiple Quark-Antiquark Pairs	52
3 Virtual Subtraction Method	79
3.1 Pole Structure of QCD Amplitudes	81
3.2 Virtual Subtraction Terms	87
3.2.1 Local Soft and Collinear Subtraction Terms	89
3.2.2 Local UV Subtraction Terms / Local UV Renormalization	92
3.3 Remarks	102
3.4 One-Loop Integration	105

4	Recursive Relations	113
4.1	Tree-Level Recurrence Relations	115
4.2	One-loop Recurrence Relations	118
4.3	UV Recurrence Relations	123
4.4	Cross-Checking the Recursive Interplay	125
5	Application to Jet Rates in Electron-Positron Annihilation	131
5.1	Optimization of the Virtual Subtraction Terms in the UV	131
5.2	Direct One-Loop Contour Deformation for the Process $e^+e^- \rightarrow jets$	136
5.3	Jet Rates in Electron-Positron Annihilation in the Leading Color Approximation	141
6	Conclusions and Outlook	147
A	QCD Feynman Rules	151
A.1	Propagators	151
A.2	Vertices	153
B	Generating Cyclic Classes	159
C	UV Divergent Ordered One-Loop Diagrams in QCD	165
D	Local UV Counterterms to Ordered One-Loop QCD Corrections	175
E	One-Loop Integrals to Integrate the Local UV Counterterms	183
F	One-Loop Recurrence Relations in Leading Color Approximation	191
F.1	Ordered One-Loop Gluon Currents	191
F.2	Ordered One-Loop Quark and Antiquark Currents	195
F.3	One-Loop Recursion for $e^+e^- \rightarrow (n-2)$ jets	199
G	UV Recurrence Relations in Leading Color Approximation	203
G.1	Ordered One-Loop Gluon Currents	203
G.2	Ordered One-Loop Quark and Antiquark Currents	206
G.3	UV Recursion for $e^+e^- \rightarrow (n-2)$ jets	210
H	Monte Carlo Integration and Phase-Space Points for Small Two-Particle Invariants	213
H.1	Monte Carlo Integration	213
H.2	Generating Phase-Space Points for Small Two-Particle Invariants	216

Chapter 1

Introduction

High energy colliders allow us to study the fundamental forces of nature in a well-defined environment. With the start of the Large Hadron Colliders (LHC) in Geneva so far unexplored energies of up to a design energy of 14 TeV in the center-of-mass frame of the two colliding protons are thereby now in reach. The main research program at the LHC focuses on the search for the Higgs boson in the Standard Model (SM) and on the search for signals of new physics (NP) beyond the Standard Model (BSM). The recent discovery of a new resonance at around 125 GeV [1, 2] by both the main experiments ATLAS and CMS marks thereby a tremendous success but also the advent of high precision measurements in high energetic hadronic scattering processes. Since the experiments at the LHC are faced with high QCD jet rates and also a plethora of other SM processes, it is unavoidable in any signal search to determine the associated QCD or SM background with equally high precision. A selection of such background processes is given in table 1.1. In addition to hadron induced scattering processes also the scattering of two leptons in the initial state can be important for QCD predictions, where jet rates in electron-positron annihilation for example constitute rather clean observables from which the strong coupling constant can be determined with high precision [3]. The development of reliable and efficient computational tools for the automated computation of many-particle (QCD) processes at high energies is thereby an important task, where special focus these days is given to the automated computation of many-particle processes at the next-to-leading order (NLO) accuracy in the perturbative expansion in the strong coupling constant. Numerical Monte Carlo methods are thereby natural candidates for the implementation of such tools, where one has to distinguish between parton level Monte Carlo programs and general purpose Monte Carlo event generators like Pythia 8, Herwig++ or Sherpa [4-6], which use the parton level programs to evaluate the perturbative hard scattering processes and complement them with additional perturbative and

1.1 Processes in Hadron Colliders

Background process	Associated signal process
$pp \rightarrow VV + jet$	$t\bar{t}H$, NP
$pp \rightarrow H + 2jets$	VBF $\rightarrow H$
$pp \rightarrow t\bar{t}b\bar{b}$	$t\bar{t}H$
$pp \rightarrow t\bar{t} + 2jets$	$t\bar{t}H$
$pp \rightarrow VVb\bar{b}$	VBF $\rightarrow H \rightarrow VV$, $t\bar{t}H$, NP
$pp \rightarrow VV + 2jets$	VBF $\rightarrow H \rightarrow VV$
$pp \rightarrow V + 3jets$	NP
$pp \rightarrow VVV$	NP

Table 1.1: A selection of Standard Model background processes, as given in [7], on the left and the associated signal processes on the right. Many of the background processes are associated with QCD processes.

non-perturbative components like parton distribution functions, parton showers and hadronization models.

1.1 Processes in Hadron Colliders

For physics predictions in hadron colliders the strategy in the development of theoretical tools is to "divide and conquer", whereby the scattering process at high energies is understood to be factorizable into several contributions as depicted in figure 1.1, and where the scattering process between the initial (parent) protons is modeled to some extent by and around the hard scattering process between their partonic (daughter) constituents, due to the property of asymptotic freedom of QCD at high energies. The protons are defined to be color neutral. Upon separation of the partonic constituents from the parent proton, however, we separate a color neutral state into a color charged main constituent and a color charged remnant. Figure 1.1 depicts thereby the separation and subsequent interaction of the partonic main constituents, the main event. The color charged remnants can of course also undergo further interactions, which has to be modeled as part of the underlying events. The corresponding formula to calculate an observable from the main event can, in a rather condensed notation, be written as [8]

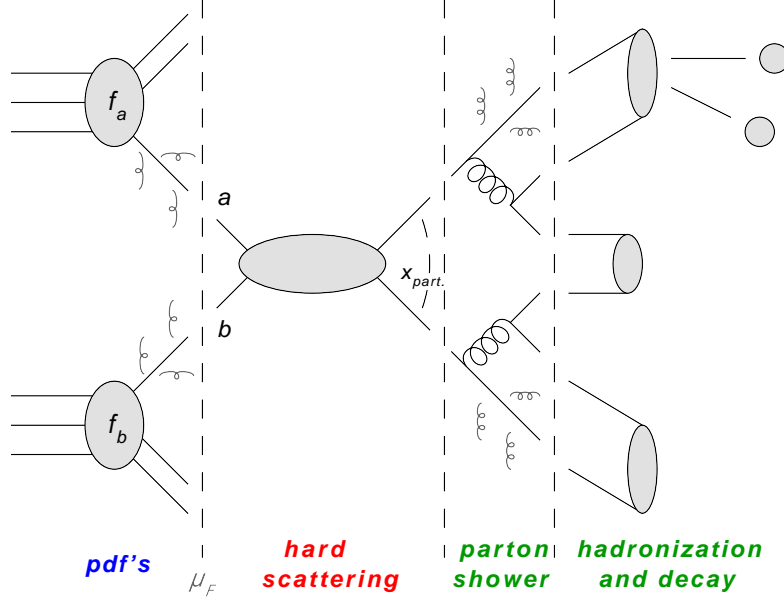


Figure 1.1: The scattering of two protons described by the PDFs f_a and f_b . The hard scattering process is described by the scattering between the corresponding partonic constituents a and b respectively, with a partonic center-of-mass energy squared \hat{s} . The consecutive radiation of soft and/or collinear partons off the partons from the hard scattering process is governed by a parton shower. The partons in the parton shower hadronize at a certain scale $\Lambda_{QCD}^2 \ll \hat{s}$ around $\Lambda_{QCD} \approx 1 \text{ GeV}$, and may subsequently decay. Not depicted are the underlying events alongside the main event.

$$\langle O \rangle = \sum_{a,b} \int dx_1 dx_2 f_a(x_1) f_b(x_2) \frac{1}{F(\hat{s})} \frac{1}{S_a S_b} \frac{1}{C_a C_b} \times \\ \times \sum_n \int d\phi_{n-2} O(p_1, \dots, p_n) |\mathcal{A}_n(\hat{s})|^2 \quad (1.1)$$

where the $f_a(x_1)$ and $f_b(x_2)$ denote the parton distribution functions or parton density functions (PDFs) of the protons 1 and 2 to contribute the partons a and b with corresponding momentum fractions x_1 and x_2 respectively, and where we sum over the possible parton configurations. $F(\hat{s})$ is a typical flux factor, i.e. two times the center-of-mass energy squared of the incoming partons $2\hat{s}$. The averaging over the S_i and C_i is over the numbers of the spin and color degrees of freedom of the incoming partons, where we have two spin degrees of freedom for (anti-)quarks as well as gluons, and three color degrees of freedom for (anti-)quarks and eight color degrees of freedom for gluons. The second sum is over the possible numbers of final-state particles in the hard n -particle scattering process, where the integration is over the phase-space of the $(n-2)$

final-state particles. $|\mathcal{A}_n(\hat{s})|^2$ is the matrix element squared of the hard scattering process with n particles, summed over all color and spin degrees of freedom.

The given picture portrays a "snapshot" of the evolution of the protons during the scattering process, where we pick an arbitrary scale μ_F^2 to factorize off the actual hard interaction between the partonic constituents. The hard scattering process is then described at a certain hard scale beyond the factorization scale μ_F^2 . The PDFs $f_i(x_j, Q^2)$ are non-perturbative objects which describe the distributions of partons inside the protons, i.e. the probability density for a parent proton j to contain a partonic constituent of flavor i with a certain longitudinal momentum fraction x_j at a scale Q^2 . The partonic distribution within a proton cannot be calculated from first principles in perturbation theory. The evolution of a specific parton to the point of the factorization scale μ_F^2 , i.e. the behavior of the PDFs with the variation of the scale Q^2 , can however be calculated in perturbation theory, which results in the DGLAP equations [9–11]. Thus the PDFs can be measured in experiment at a certain fixed scale Q_0^2 and can then be extrapolated to a different scale, where the factorization scale μ_F^2 is typically chosen to be close to a hard scale. The corresponding scale-dependence of the PDFs is reduced if we consider higher orders in the perturbative expansion in the strong coupling constant, where the scale-variation of the PDFs introduces thereby poles of collinear origin, which are partly absorbed into the definition of the PDFs.

The hard scattering process, which can be calculated completely in perturbation theory, is now described entirely by the interaction between the partonic main constituents at a certain hard energy scale, where the partonic center-of-mass energy squared \hat{s} is determined from the initial hadronic center-of-mass energy squared s by $\hat{s} = x_1 x_2 s$. The central object in any computation to the hard scattering process is thereby the hard scattering matrix element $\mathcal{A}_n(\hat{s}, \mu_F^2, \mu_R^2)$ of the hard scattering process of n particles with a center-of-mass energy squared \hat{s} and is generally determined up to another arbitrary scale μ_R^2 . In practical calculations the factorization scale μ_F^2 from the PDFs and the renormalization scale μ_R^2 are often identified via $\mu^2 = \mu_F^2 = \mu_R^2$. In this thesis we focus upon aspects in the automatized computation of multi-particle hard matrix elements in QCD up to NLO accuracy in the strong coupling constant.

The experiments detect events at the hadronic level. Parton showers are hereby used in the computation in order to describe cascades of soft and/or collinear radiation, which govern the evolution from the hard scale of the hard partonic scattering process down to a hadronization scale $\Lambda_{QCD} \sim \mathcal{O}(1 \text{ GeV})$, at which the partons in the shower are expected to recombine into

color neutral hadronic states. Parton showers are perturbative objects which make use of the fact that QCD matrix elements are in general enhanced in the soft and collinear regions and can thus be approximated accordingly by appropriately chosen splitting kernels. The Sudakov form factors at the heart of the parton showers, whose evolution is governed by the DGLAP equations and contain the DGLAP splitting kernels, describe thereby sequences of (no-)emission probabilities for soft and/or collinear radiation. The subsequent hadronization cannot be calculated in perturbation theory and has to be modeled. Parton showers approximate the behavior of matrix elements essentially up to arbitrary orders in the strong coupling constant, but are trustworthy only in the soft and/or collinear regions. This approximation is reasonable since matrix elements are in general enhanced in these regions, however, it is such that it is naively only correct up to the so called leading logarithmic behavior. A more detailed overview on the matter of parton showers and general purpose event generators can be found in [12].

Accompanying the main event are the underlying events, which are soft and collinear interactions of the proton remnants. In addition there are multiple interactions, which originate in additional interactions between the remnants from the partonic separation off the main event, or pile up events, which originate in the scattering between a different proton pair from the same proton bunch in the beam. The strong model dependence in the non-perturbative parts of the main event and in the underlying events limits the accuracy of the theoretical predictions. For a certain class of observables, which depend not as much on showering and hadronization, we can however still rely on the perturbative calculations. This is the class of infrared safe observables, which means that the observables do not change in the limit in which additional soft or collinear particles are imposed. An infrared safe observable O is thereby defined to behave as follows

$$O_{n-1}(p_1, \dots, p_i, \dots, p_{n-1}) \rightarrow O_{n-2}(p_1, \dots, \cancel{p_i}, \dots, p_{n-1}) \text{ if } p_i \rightarrow 0 \quad (1.2)$$

$$O_{n-1}(p_1, \dots, p_i, \dots, p_j, \dots, p_{n-1}) \rightarrow O_{n-2}(p_1, \dots, p_i + p_j, \dots, p_{n-1}) \text{ if } p_i || p_j \quad (1.3)$$

$$O_{n-2}(p_1, \dots, p_{n-2}) \rightarrow 0 \text{ if } p_i \cdot p_j \rightarrow 0 \text{ for any } i, j \quad (1.4)$$

An important class of observables is the class of jet observables, whereby some definitions of the corresponding jet algorithms possess the property of being infrared safe. The crude picture of a jet is that of a more or less central parton, which radiates off additional (soft and/or collinear) partons inside a "cone" of a certain "opening angle" around the central parton. Several formulations to define such jet algorithms are available, where some fulfill the above criterion of infrared safeness and some do not. The property of being an additional soft and/or collinear parton or not is thereby governed by either residing inside or outside the cone, i.e. whether the

1.2 Perturbative Calculations

associated jet variable is either smaller than a certain defined jet resolution parameter y_{cut} or gets cut away. We speak thereby of unresolved or resolved partons. A more detailed overview on the matter of jet observables can be found in [12, 13].

Jets can either be modeled on the partonic level or on the hadronic level after showering, or even after hadronization, where the momenta of the jets are usually given by the sum of the momenta of the contributing partons. At leading order (LO) in the perturbative expansion in the strong coupling constant partonic jets are thereby modeled by only the central parton. At NLO jets are modeled by up to two partons, i.e. up to one additional unresolved parton. At NNLO jets are modeled by up to two additional unresolved partons, and so on. This is depicted in figure 1.2. One can now compute for example the matrix element of a hard scattering process with two partons in the partonic final state, run the parton shower, and get a bunch of partons at the hadronic level just before hadronization. At the partonic level of the hard scattering we can then have two resolved LO jets or one resolved NLO jet, depending on up to which order we want to compute the observable. At the hadronic level we can have more jets at various desired orders, depending on the number of partons after the showering. Parton showers approximate jets up to an arbitrary order in the strong coupling but are only correct in the soft and/or collinear regions of phase space. These are the regions where real emission is dominant and the contributions are approximated by $(n + x)$ -parton tree-level matrix elements with x additional unresolved radiated partons. Since the shower is only correct in the soft and/or collinear regions, however, this means that any additional jets compared to the partonic level of the hard scattering do not contribute correctly to the observable. Any additional resolved jet should thus be provided directly from the matrix element, which explains the importance of providing multi-particle matrix elements at higher orders. The problem of how to match a matrix element calculation to a parton shower in order to get the best out of both, and how to do this properly at higher orders in perturbation theory, is a topic on its own and will not be covered in this thesis. A more detailed overview on the matter of matching and merging can be found in [12, 13].

1.2 Perturbative Calculations

QCD is asymptotically free, and at high energies the strong coupling constant therefore becomes small. The matrix element of the hard scattering process can therefore be computed in perturbation theory. The one-loop renormalization group equation, which governs the scale dependence of the strong coupling constant α_s , is thereby given by

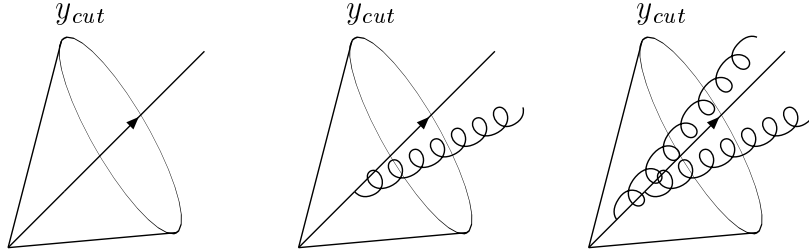


Figure 1.2: At LO jets are modeled by one parton. At NLO jets are modeled by up to two partons, i.e. up to one additional unresolved parton. At NNLO jets are modeled by up to two additional unresolved partons. The picture is taken from [8].

$$\mu^2 \frac{d}{d\mu^2} \left(\frac{\alpha_s}{2\pi} \right) = -\frac{1}{2} \beta_0 \left(\frac{\alpha_s}{2\pi} \right)^2 + \mathcal{O}(\alpha_s^3) \quad (1.5)$$

where $\beta_0 = (\frac{11}{3}N_c - \frac{2}{3}n_f)$ and in QCD $N_c = 3$. With $\alpha_s = g_s^2/4\pi$ this can also be written as the Callan–Symanzik β -function $\mu \frac{dg_s}{d\mu} \equiv \beta(g_s) = -\frac{\beta_0 g_s^3}{(4\pi)^2}$, which is negative for $n_f \leq 16$. From equation 1.5 we can determine

$$\alpha_s(Q^2) = \frac{4\pi}{\beta_0 \ln \left(\frac{Q^2}{\Lambda_{QCD}^2} \right)} \propto 1 / \ln \left(\frac{Q^2}{\Lambda_{QCD}^2} \right) \quad (1.6)$$

with the two bounds of integration given by Q^2 , an arbitrary upper scale, and Λ_{QCD}^2 , a lower cut-off scale at which perturbative QCD is expected to break down and non-perturbative effects start to take over. One notes the "running" behavior of $\alpha_s(Q^2)$, with confinement in the non-perturbative regime and asymptotic freedom for large Q^2 , which is depicted on the left of figure 1.3.

The scale dependence of the strong coupling constant enters also the computation of observables, where for example the LO prediction for the cross section to the process $pp \rightarrow t\bar{t} + jet + X$ is proportional to α_s^3 [15] and therefore highly scale dependent. The inclusion of higher orders in the perturbative expansion in α_s reduces this scale dependence and enhances thus the predictive power of the computation. This is depicted on the right of figure 1.3.

For an observable whose LO prediction is given by an n -parton tree-level amplitude the following

1.2 Perturbative Calculations

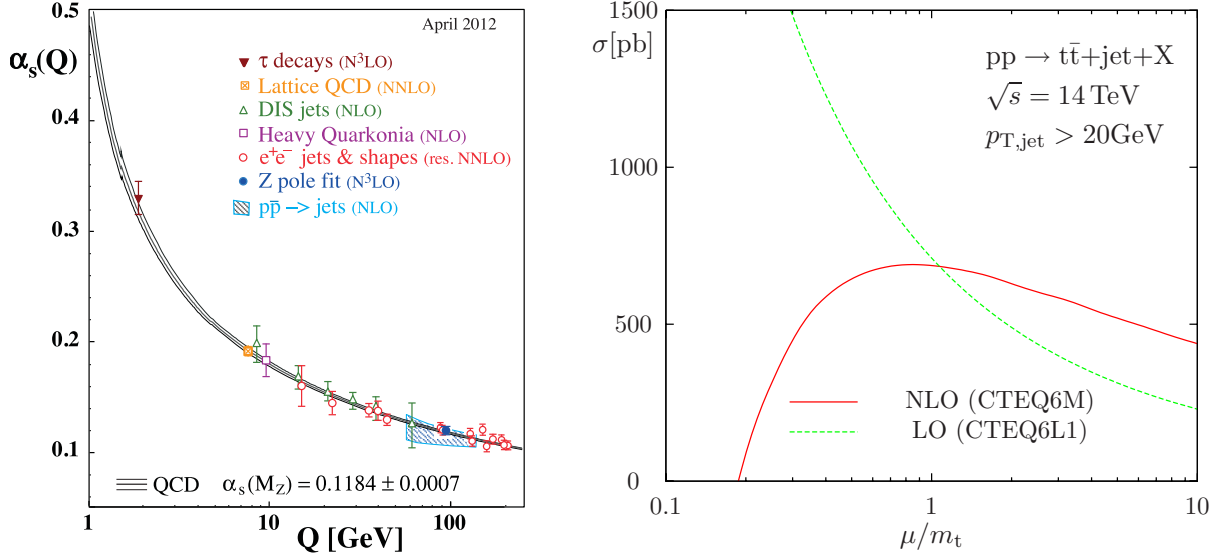


Figure 1.3: Left: Running of $\alpha_s(Q)$, plot taken from [14]. Right: Scale dependence of $\sigma(pp \rightarrow t\bar{t} + \text{jet} + X)$ at LO and NLO, plot taken from [15].

expansions are relevant for the calculations of the NLO and NNLO predictions [8]

$$\alpha_s^{n-2} |\mathcal{A}_n|^2 = \alpha_s^{n-2} \left(|\mathcal{A}_n^{(0)}|^2 + \alpha_s 2\text{Re}(\mathcal{A}_n^{(0)*} \mathcal{A}_n^{(1)}) + \alpha_s^2 2\text{Re}(\mathcal{A}_n^{(0)*} \mathcal{A}_n^{(2)}) + \alpha_s^2 |\mathcal{A}_n^{(1)}|^2 \right) \quad (1.7)$$

$$\alpha_s^{n-2} |\mathcal{A}_{n+1}|^2 = \alpha_s^{n-2} \left(\alpha_s |\mathcal{A}_{n+1}^{(0)}|^2 + \alpha_s^2 2\text{Re}(\mathcal{A}_{n+1}^{(0)*} \mathcal{A}_{n+1}^{(1)}) \right) \quad (1.8)$$

$$\alpha_s^{n-2} |\mathcal{A}_{n+2}|^2 = \alpha_s^{n-2} \left(\alpha_s^2 |\mathcal{A}_{n+2}^{(0)}|^2 \right) \quad (1.9)$$

where the dependence of the squared n -parton QCD amplitude on the strong coupling constant at LO has been explicitly pulled out for clarification. The LO contribution in green is simply given by the square of the tree-level matrix element with n partons $|\mathcal{A}_n^{(0)}|^2$. The NLO contributions in red originate from two different regions with respect to the phase-space: One contribution comes from the interference term of the virtual one-loop matrix element with the corresponding tree-level matrix element with n partons, the other comes from the squared $(n+1)$ -parton tree-level matrix element with one additional parton. The two NLO contributions "live" on different phase-spaces as far as final-state phase-space integration is concerned. In gray are the NNLO contributions. Up to NNLO we include the radiation of up to two additional partons. For jet observables, as described above, this means that up to NNLO jets are modeled by up to two additional partons, up to NLO they are modeled by up to one additional parton. In this thesis we will focus entirely on the evaluation of the NLO contributions.

In order to compute (QCD) matrix elements in perturbation theory one relies usually on a Feynman diagrammatic picture, where the necessary Feynman rules are derived from the corresponding Lagrangian density. The Lagrangian for QCD is thereby given by

$$\mathcal{L}_{QCD} = -\frac{1}{4}F^{a,\mu\nu}(x)F_{\mu\nu}^a(x) - \frac{1}{2\xi}(\partial^\mu A_\mu^a(x))^2 + \sum_q \bar{q}(x)(i\gamma^\mu D_\mu - m_q)q(x) + \mathcal{L}_{FP\ ghost} \quad (1.10)$$

with $F_{\mu\nu}^a(x) = \partial_\mu A_\nu^a(x) - \partial_\nu A_\mu^a(x) + g_s f^{abc} A_\mu^b(x)A_\nu^c(x)$ and $D_\mu = \partial_\mu - ig_s T^a A_\mu^a(x)$. The gluon field is hereby denoted by $A_\mu^a(x)$ and the quark field in a short-hand notation by $q(x)$, where we sum over all quark-flavors and $\bar{q}(x)$ denotes the corresponding conjugated spinor. The summation over contracted color indices is usually not shown explicitly, according to Einstein's summation convention for repeated indices. The first and the second term cover the pure gluonic contributions, where the first term contributes to the non-abelian gluonic three- and four-valent interactions and together with the second term to the gluonic quadratic self-interaction, which results in the gluon propagator. To define the generating functional properly a gauge parameter has to be introduced in the second term. Physical observables are independent of the choice of the gauge and we thus use the Feynman-'t Hooft gauge with $\xi = 1$, which is to some extent the most simple to use. For the computation of amplitudes in the Feynman gauge we have to introduce auxiliary fields, the Faddeev-Popov ghost fields, to cancel unphysical degrees of freedom introduced through the gluon propagator in the Feynman gauge. Their action is governed by the fourth term $\mathcal{L}_{FP\ ghost}$, which is not shown explicitly. The third term governs the quadratic contribution of the quark fields with mass m_q , which leads to the (massive) quark propagator, and the interaction between gluons and quarks through the covariant derivative D_μ , which leads to the quark-gluon vertex. We have collected all the necessary QCD Feynman rules in appendix A. In equation 1.10 γ^μ denotes the Dirac gamma matrices, which are four-dimensional matrices in spin-space and are for massless QCD in the high energy limit best chosen in the Weyl representation. The matrices T_{ij}^a are the generators of the $SU(N_c)$ algebra in the fundamental representation, carrying an adjoint index $a = 1, \dots, N_c^2 - 1$, a fundamental index $i = 1, \dots, N_c$ and an antifundamental index $\bar{j} = 1, \dots, N_c$. In equation 1.10 we have suppressed the (anti-)fundamental indices of the color matrices as well as the spin indices on the quark fields and the Dirac matrix. Further details can be found in any textbook on particle physics and quantum field theory.

Multi-parton QCD calculations are in the usual Feynman diagrammatic approach complicated by the combinatorics and the complex non-abelian structure, expressed in the algebraically complex Feynman rules for the non-abelian vertices. In the usual Feynman diagrammatic ap-

proach this results in a plethora of Feynman diagrams which have to be computed, where for example for pure gluon tree-level amplitudes the number of Feynman diagrams which have to be computed grows factorially with the number of external gluons. A large part of this thesis is concerned with a method to get the organization of the color degrees of freedom in one-loop amplitudes straight. Color-ordering helps therefor by exploring the general properties of the underlying gauge theory, which will be discussed in great detail in chapter 2.

1.3 Divergences in Infrared Safe Observables

Infrared safe observables constitute an important class of observables for physics predictions in particle collider processes. The various contributions to the NLO computations of such observables, however, are stricken by soft and collinear singularities. Consider the two-particle scattering process $2 \rightarrow (n-2)$, with $(n-2)$ particles in the final state. In a rather condensed notation the LO and NLO contributions to an infrared safe observable O_x , with x particles in the final state, are given by

$$\langle O \rangle^{LO} = \int_{n-2} O_{n-2} d\sigma^B \quad (1.11)$$

where $d\sigma^B = |\mathcal{A}_n^{(0)}|^2 d\phi_{n-2}$ denotes the Born contribution, determined by the square of the tree-level matrix element with n particles, and

$$\langle O \rangle^{NLO} = \int_{n-1} O_{n-1} d\sigma^R + \int_{n-2} O_{n-2} d\sigma^V + \int_{n-2} O_{n-2} d\sigma^C \quad (1.12)$$

where $d\sigma^R = |\mathcal{A}_{n+1}^{(0)}|^2 d\phi_{n-1}$ denotes the contribution from additional real emission, determined by the square of the tree-level matrix element with $(n+1)$ particles. The virtual contribution $d\sigma^V = 2\text{Re}(\mathcal{A}_n^{(0)*} \mathcal{A}_n^{(1)}) d\phi_{n-2}$ is determined by the interference term of the one-loop amplitude with n particles with the corresponding n -particle tree-level matrix element. In processes with partonic initial state particles $d\sigma^C$ denotes a collinear subtraction term to subtract remaining initial state collinear singularities. In general $d\phi_x$ denotes the $(3x-4)$ -dimensional final-state phase-space element for x final-state particles [16].

Taken separately the NLO contributions are divergent, where we encounter divergences from the soft and collinear regions of phase-space for the real emission contributions and divergences from the soft, collinear and ultraviolet (UV) regions of loop-momentum space for the virtual

contributions. These divergences are for example made apparent in dimensional regularization through explicit poles in the dimensional regularization parameter ε . Usually $\int_{n-2} O_{n-2} d\sigma^V$ denotes the UV renormalized virtual contribution, which thus contains only soft and collinear poles. According to a theorem due to Kinoshita, Lee and Nauenberg [17, 18] the soft and collinear poles cancel upon summation of the various contributions, where the soft and collinear poles of the real emission contributions, the soft and collinear poles of the virtual contributions and the poles from the initial state collinear remainders cancel against each other. According to this $\langle O \rangle^{NLO}$ is thus free of any IR or UV poles. For a large number of particles, however, analytic phase-space integration is practically impossible and one needs to resort to numerical methods, as for example Monte Carlo integration. There are two requirements, however, which the integrand in any numerical integration has to fulfill in order to be integrable over a finite number of integration dimensions. Firstly, the integrand has to be free of poles in the integration region. Secondly, the combined integration of two different integrand functions is only possible if the integration regions are identical or can at least be continuously mapped onto each other. An excellent introduction to Monte Carlo integration is given in [19]. Although $\langle O \rangle^{NLO}$ is free of any IR and UV poles it cannot be trivially integrated numerically, since its separate contributions are defined on different phase-spaces of different dimensionality. The separate contributions, however, are not free of poles and can thus not be integrated separately. This poses a problem for the numerical evaluation of multi-parton processes.

A popular solution to this problem is presented by the subtraction method, originally introduced in the application to specific processes [20–25] and later generalized by Catani and Seymour through the dipole subtraction method for multi-parton amplitudes [26, 27]. The dipole subtraction method has been intensively studied and extended since then [28–32]. The idea is drafted as follows. One subtracts and adds back a suitably chosen piece $d\sigma^A$

$$\langle O \rangle^{NLO} = \int_{n-1} (O_{n-1} d\sigma^R - O_{n-2} d\sigma^A) + \int_{n-2} (O_{n-2} d\sigma^V + O_{n-2} d\sigma^C + O_{n-2} \int_1 d\sigma^A) \quad (1.13)$$

where $d\sigma^A$ is chosen such that the subtraction term approximates the real emission contributions locally in the soft and collinear regions of the real emission phase-space, and is proportional to the Born level. This renders the first bracket in the above formula finite by definition, such that $(O_{n-1} d\sigma^R - O_{n-2} d\sigma^A)$ is integrable over the $(n-1)$ -particle final-state phase-space of the real emission contributions. On the other hand is $d\sigma^A$ chosen such that an analytical integration over the unresolved one-particle phase-space yields a simple result that cancels the poles from the

1.3 Divergences in Infrared Safe Observables

virtual contributions and from the initial state collinear remainder. The second bracket above is thus integrable over the $(n - 2)$ -particle final-state phase-space. The limit $\varepsilon = 0$ can then safely be performed, such that

$$\langle O \rangle^{NLO} = \int_{n-1} \left(O_{n-1} d\sigma^R \Big|_{\varepsilon=0} - O_{n-2} d\sigma^A \Big|_{\varepsilon=0} \right) + \int_{n-2} \left(O_{n-2} d\sigma^V + O_{n-2} d\sigma^C + O_{n-2} \int_1 d\sigma^A \right) \Big|_{\varepsilon=0} \quad (1.14)$$

In the dipole subtraction method $d\sigma^A$ is given by a sum over appropriately chosen dipole terms $\mathcal{D}_{ij,k}(p_1, \dots, p_{n-1})$, which contain all singularities in the limit $p_i \cdot p_j = 0$, i.e. i and j being collinear or either one of them being soft. The $\mathcal{D}_{ij,k}$ are thereby given by

$$\mathcal{D}_{ij,k}(p_1, \dots, p_{n-1}) = \frac{-1}{2p_i \cdot p_j} \mathcal{A}_{n-2}^{(0)*}(1, \dots, \tilde{i}\tilde{j}, \dots, \tilde{k}, \dots, n-1) \frac{\mathbf{T}_k \mathbf{T}_{ij}}{\mathbf{T}_{ij}^2} \mathbf{V}_{ij,k} \mathcal{A}_{n-2}^{(0)}(1, \dots, \tilde{i}\tilde{j}, \dots, \tilde{k}, \dots, n-1) \quad (1.15)$$

where $\tilde{i}\tilde{j}$ is a (pair of) emitter parton(s) and \tilde{k} is a spectator parton. The $(n - 1)$ -parton phase-space is mapped onto the $(n - 2)$ -parton phase-space by an appropriate choice of the combined four-momentum $p_{\tilde{i}\tilde{j}}$ of the emitter parton and the four-momentum $p_{\tilde{k}}$ of the spectator parton. The \mathbf{T}_k and \mathbf{T}_{ij} are the color charge operators of the spectator and the emitter respectively and determine the corresponding color correlation. The $\mathbf{V}_{ij,k}$ are matrices in the spin/helicity space of the emitter, which determine the corresponding spin correlation. They encode the singularities from the splittings and are related to the D -dimensional Altarelli-Parisi splitting functions [26, 10]. Whenever the real emission phase-space enters a collinear or soft region the squared matrix element of the real emission approximates continuously one of the dipole terms and the particular set of parton momenta $\{p_1, \dots, p_i, \dots, p_j, \dots, p_k, \dots, p_{n-1}\}$ in that region approximates the dipole configuration $\{p_1, \dots, p_{\tilde{i}\tilde{j}}, p_{\tilde{k}}, \dots, p_{n-1}\}$, such that in total

$$\int_{n-1} (O_{n-1} d\sigma^R - O_{n-2} d\sigma^A) \quad (1.16)$$

is free of any collinear or soft singularities for O_x an infrared safe observable with x particles in the final state. Consider, for example, the real emission contribution only from the final state partons, then the subtraction term is given by

$$O_{n-2}d\sigma^A \equiv \sum_{(i,j)} \sum_{k \neq i,j} \mathcal{D}_{ij,k}(p_1, \dots, p_{n-1}) O_{n-2}(p_1, \dots, p_{\tilde{i}}, p_{\tilde{j}}, p_{\tilde{k}}, \dots, p_{n-1}) \quad (1.17)$$

On the other hand defines the integrated subtraction term the dipole insertion operator \mathbf{I} via

$$\int_{n-1} O_{n-2}d\sigma^A = \int_{n-2} O_{n-2} \left(\int_1 d\sigma^A \right) = \int_{n-2} O_{n-2} \mathbf{I} \otimes d\sigma^B \quad (1.18)$$

where \mathbf{I} contains now all the explicit poles in the dimensional regularization parameter ε , and when combined with the virtual part $\int_{n-2} O_{n-2}d\sigma^V$ the explicit poles cancel. Further details will follow in chapter 3.1.

1.4 Subtracting Virtual Divergences

In order to compute the virtual part, which has been considered a bottle-neck in multi-leg calculations for a long time but has witnessed tremendous progress in the past years, one usually relies on rather traditional methods based on Feynman graphs and/or tensor reduction [33–51] or on more modern methods based on generalized unitarity and cut-techniques [52–70, 67, 71–73]. We will give a brief introduction in chapter 3.4, reviews can be found in [8, 74–77].

In contrast to these methods we seek to compute the virtual part fully numerical, where also the one-loop integrals are to be evaluated directly with Monte Carlo integration. These methods have been discussed in the past [78–86] and also more recently [87–89]. It was thereby shown that the direct numerical method can be efficiently applied to relevant physics processes [90, 91]. We stress, however, that therefor the phase-space and loop-momentum integrations have to be and can be performed together in one combined Monte Carlo integration. We will discuss the basics of one-loop integration and Monte Carlo integration, and the necessary numerical deformation of the one-loop integration contour into the complex plane, further in the chapters 3.4 and 5.2, and in appendix H.

To be able to perform the one-loop integral numerically, i.e. safely integrating over the physical four dimensions of loop-momentum space, we need to subtract the divergent poles off the one-loop integrand in the virtual contributions, quite in analogy to the subtraction method for the real emission contributions. Local virtual subtraction terms for multi-parton processes have

1.4 Subtracting Virtual Divergences

been discussed in the past for the application on a diagrammatic level [92]. In contrast to this we extend the subtraction method to the virtual contributions in a more generic framework, i.e. on the amplitude level [93, 87, 91].

The renormalized virtual part contains after the integration no more UV divergences. However, locally the usual counterterms do not suffice. We thus split the renormalized virtual part into the bare part and the corresponding counterterm. In the condensed notation from above this reads

$$\int_{n-2} O_{n-2} d\sigma^V \equiv \int_{n-2} O_{n-2} \int_{loop} d\sigma_{bare}^V + \int_{n-2} O_{n-2} d\sigma_{CT}^V \quad (1.19)$$

where $d\sigma_{bare}^V = 2Re(\mathcal{A}^{(0)*} \mathcal{G}_{bare}^{(1)}) d^4k d\phi_{n-2}$ contains the total bare one-loop integrand, which leads to IR as well as UV poles, and $d\sigma_{CT}^V = 2Re(\mathcal{A}^{(0)*} \mathcal{A}_{CT}) d\phi_{n-2}$ contains the total counterterm from UV renormalization, which leads to the corresponding UV poles. We subtract and add back another suitably chosen piece $d\sigma^L$ locally, i.e. on the one-loop integrand level, by

$$\int_{n-2} O_{n-2} d\sigma^V \equiv \int_{n-2} O_{n-2} \int_{loop} (d\sigma_{bare}^V - d\sigma^L) + \int_{n-2} O_{n-2} (d\sigma_{CT}^V + \int_{loop} d\sigma^L) \quad (1.20)$$

where $d\sigma^L$ is chosen such that it approximates the one-loop integrand of the bare virtual part in the soft, collinear and UV regions of loop-momentum space, and is proportional to the Born level. This renders the first bracket in equation 1.20 finite by definition, so that $(d\sigma_{bare}^V - d\sigma^L)$ is integrable over the four-dimensional loop-momentum space. On the other hand $d\sigma^L$ is chosen such that analytic one-loop integration yields a simple result, which cancels the poles from the counterterm as well as from the unresolved one-particle integrated real emission contributions and from the initial state collinear remainder. The limit $\varepsilon = 0$ can then again safely be performed, such that

$$\begin{aligned} \langle O \rangle^{NLO} &= \int_{n-1} (O_{n-1} d\sigma^R|_{\varepsilon=0} - O_{n-2} d\sigma^A|_{\varepsilon=0}) + \int_{(n-2, loop)} (O_{n-2} d\sigma_{bare}^V|_{\varepsilon=0} - O_{n-2} d\sigma^L|_{\varepsilon=0}) \\ &+ \int_{n-2} (O_{n-2} d\sigma_{CT}^V + O_{n-2} \int_{loop} d\sigma^L + O_{n-2} \int_1 d\sigma^A + O_{n-2} d\sigma^C)|_{\varepsilon=0} \end{aligned} \quad (1.21)$$

where all three brackets can now be safely integrated numerically. The local virtual subtraction

method will be explained in greater detail in chapter 3, where we discuss the pole structure of one-loop QCD amplitudes in chapter 3.1 and the necessary local virtual subtraction terms for the soft, the collinear as well as the ultraviolet regions in loop-momentum space in chapter 3.2.

The thesis at hand evolved within the framework of a more comprehensive collaborative effort between multiple parties in order to develop a computer program for the automated and fully numerical evaluation of NLO multi-parton processes, which resulted so far in the publication of several articles. A general overview of the method was given in [87]. The first application to a physics process, and proof of principle of the method, was reported on in [90], followed by a more detailed account about the necessary improvements in [91]. The method was also discussed in several proceedings [94–96].

Regarding the local virtual subtraction method in chapter 3.2 the author puts special focus on the local virtual UV subtraction, to which end a local renormalization method is introduced and local UV counterterms are derived. This constitutes a large part of the thesis and will be explained in great detail in chapter 3.2.2. The associated recursive constructions of the bare one-loop integrands and the corresponding total local UV subtraction terms in the leading color approximation are further discussed in great detail in chapter 4, especially in the sections 4.2, 4.3 and 4.4, and the associated appendices. Improvements to the numerical stability of the local virtual subtraction terms in the UV region are discussed in chapter 5.1. The contents in the chapters 3.2.2 and 4.3, and in the associated appendices, have not been published in this detailed form. The general idea and the corresponding results, however, have been presented already in several articles [87, 91, 95, 96].

A second major part of the thesis at hand, as already mentioned, is concerned with the color management in one-loop QCD amplitudes, where the author puts special focus on one-loop amplitudes with multiple external quark-antiquark pairs and an arbitrary number of external gluons. This will be explained in great detail in chapter 2, especially in section 2.5 and subsection 2.5.3, and in the associated appendices. The method which is thereby presented is new and has not yet been published.

The remainder of the thesis at hand is structured as follows. In chapter 2 we will discuss the color decomposition of QCD amplitudes and especially of one-loop QCD amplitudes with multiple external quark-antiquark pairs. In chapter 3 we will discuss the local virtual subtraction method and especially the local virtual UV subtraction. We will also briefly introduce some basics of

analytical and numerical one-loop integration in this chapter. In chapter 4 we will discuss the recursive relations to construct QCD amplitudes and especially to construct the bare integrands and the total local UV subtraction terms of one-loop QCD amplitudes. In chapter 5 we will discuss the application of our numerical method to jet rates in electron-positron annihilation and the associated methods to improve the numerical stability of the virtual subtraction terms and in the numerical loop integration. The thesis will finally conclude with an outlook in chapter 6. All other necessary information, which is not included in the chapters of the main body of the thesis, is collected in several appendices followed by a list of references.

Chapter 2

Color Management

The traditional perturbative approach in order to calculate the hard matrix element to a given high energy scattering process is to compute the sum of all necessary Feynman diagrams, as outlined in the introduction. The rich mathematical structure of the QCD Feynman rules leads thereby to a proliferation of terms, especially in the computation of the square of the hard matrix element, and therefore to rather lengthy and complex expressions. In pure gluon tree-level amplitudes, for example, the number of Feynman diagrams grows factorially with the number of external legs [97, 31]. In addition, in order to reduce the resulting terms, one has to rely heavily on the application of the corresponding $SU(N_c)$ algebra relations in each Feynman diagram, where in QCD $N_c = 3$. In automated computations of multi-parton amplitudes this is obviously not the most effective approach. In order to have a better handle on the perturbative QCD calculations one can do better regarding the systematic organization of the corresponding $SU(N_c)$ or color algebra by the use of color decomposition, which was initially studied for Yang–Mills tree-level amplitudes [98–107], also referred to as the dual expansion due to the similarity to string amplitudes [108–110], and then extended to include additional quark–antiquark pairs [111–113, 97, 31]. The application to one-loop amplitudes was initially introduced for the case of external gluons only [114–116], where the similarity to super Yang–Mills amplitudes has been noted, before it was extended to include additional external quark–antiquark pairs [117–120, 73]. A comprehensive overview on the available methods in the one-loop case can also be found in [76, 77], some application and further comments in [121, 122, 69, 123].

Any $SU(N_c)$ -amplitude can be factorized or decomposed into group-theoretical (color) factors multiplied by purely kinematical factors, called partial amplitudes. If we consider all Feynman diagrams to a given matrix element and separate the color factors from the kinematical factors,

to subsequently collect all those kinematical factors which multiply the same color factor C_i into one partial amplitude A_i , the amplitude reads

$$\mathcal{A} = \sum_i C_i A_i \quad (2.1)$$

The C_i are thereby generating vectors, in the color vector space of the amplitude, with coefficients A_i . For pure n -gluon tree-level amplitudes the vectors that span the corresponding vector space are in the so called fundamental basis for example given by all color factors $C_\sigma = \text{Tr}(T^{a_{\sigma(1)}} \dots T^{a_{\sigma(n)}})$, where the elements $\sigma \in S_n/Z_n = S_{n-1}$ denote the $(n-1)!$ non-cyclic permutations of the n elements in the set of the adjoint gluon indices. The matrices T_{ij}^a are the generators of the $SU(N_c)$ algebra in the fundamental representation, carrying an adjoint index $a = 1, \dots, N_c^2 - 1$, a fundamental index $i = 1, \dots, N_c$ and an antifundamental index $\bar{j} = 1, \dots, N_c$, and the trace $\text{Tr}(\dots)$ is over the (anti-)fundamental indices, where we have neglected to write the corresponding $SU(N_c)$ coupling constant as well as the proper normalization factor for the moment. Another popular basis for color-decomposition is the so called color-flow basis [108, 97, 31], where summation over a repeated adjoint index is turned into summation over two corresponding (anti-)fundamental indices and all color factors in this double-line notation are given by products of Kronecker deltas with (anti-)fundamental indices only. The partial amplitudes are gauge invariant sets of diagrams, built from color-stripped Feynman rules as given in appendix A. All diagrams in a tree-level partial amplitude can be drawn in planar fashion and have the same color ordering, which means that their corresponding Feynman diagrams contribute to a common color factor, and the same cyclic ordering, which means that their external legs possess the same fixed order in a given cyclic, usually clock-wise, direction around the diagrams. The whole set of diagrams to a given partial amplitude can be constructed efficiently by the help of recurrence relations, which will be described in chapter 4 and especially chapter 4.1.

At the one-loop level we can similarly write

$$\mathcal{A}^{(1)} = \sum_i C_i A_i^{(1)} = \sum_i C_i \sum_j F_{ij} B_j \quad (2.2)$$

where the factors C_i denote color factors again, e.g. strings and traces of fundamental color matrices in the fundamental basis or open and closed strings of Kronecker deltas in the (dual) color-flow basis respectively. The purely kinematical functions $A_i^{(1)}$ are the one-loop partial

amplitudes, which again only depend on the momenta and helicities of the external particles. One-loop partial amplitudes are still gauge invariant sets of diagrams and still color-ordered by definition. However, due to the additional degrees of freedom in the loop, not all the diagrams in a partial one-loop amplitude need to have the same fixed cyclic ordering of the external legs. We can, however, split the one-loop partial amplitudes further into smaller and still gauge invariant subsets of diagrams, i.e. the so called (one-loop) primitive amplitudes B_j , where all the diagrams in a primitive amplitude possess the same fixed cyclic ordering of the external legs. The set of primitive amplitudes is thereby mapped onto the set of one-loop partial amplitudes by a matrix F and one-loop partial amplitudes are then given by linear combinations of primitive amplitudes, where the set of linear equations is usually overcomplete and where the coefficients F_{ij} are simple monomials in the number of colors N_c and the number of active quark flavors n_f in the case of closed fermion loops. Primitive amplitudes with external fermion lines can further be distinguished by the routing of the external fermion lines through the loop, i.e. whether an external fermion turns left or right, with respect to the fermion flow arrow, upon entering the loop. Those sets of right-mover and left-mover diagrams are again gauge invariant subsets. All diagrams in a primitive amplitude can be drawn in planar fashion and be constructed efficiently by the help of one-loop recurrence relations, which will be described in chapter 4.2. The fixed cyclic ordering of the one-loop diagrams ensures that the QCD flavor of each propagator in the loop is uniquely determined, which leads to much more compact expressions where only subsets of the kinematic loop-invariants play a role. The importance of this will become clear in chapter 3.2, where we will derive the subtraction terms for the local virtual subtraction on the level of the primitive amplitudes.

In order to be able to discuss the color decomposition of one-loop QCD amplitudes further we first have to understand certain aspects of the color decomposition of tree-level QCD amplitudes and of the corresponding color flow. This will be described in sections 2.1 to 2.4, before we turn to one-loop color decomposition in section 2.5.

2.1 Tree-Level Color Decomposition

2.1.1 Tree-Level Gluon Amplitudes

Using the fundamental representation of the gauge theory generators, the color decomposition of a tree-level gauge amplitude with n external gluons in the fundamental basis follows more closely from replacing the structure constants, which appear in every non-abelian (three- and four-gluon) vertex, by

2.1 Tree-Level Color Decomposition

$$if^{abc} = 2Tr(T^a[T^b, T^c]) \quad (2.3)$$

which in turn follows from the commutator relation $[T^a, T^b] = if^{abc}T^c$ of the hermitian, traceless fundamental generator matrices T_{ij}^a . Using the Fierz identity for the fundamental $SU(N_c)$ generator matrices

$$T_{ij}^a T_{kl}^a = \frac{1}{2}(\delta_{i\bar{l}}\delta_{k\bar{j}} - \frac{1}{N_c}\delta_{ij}\delta_{k\bar{l}}) \quad (2.4)$$

which is sometimes useful in the form

$$Tr(T^a X)Tr(T^a Y) = \frac{1}{2}(Tr(XY) - \frac{1}{N_c}Tr(X)Tr(Y)) \quad (2.5)$$

or

$$Tr(T^a X T^a Y) = \frac{1}{2}(Tr(X)Tr(Y) - \frac{1}{N_c}Tr(XY)) \quad (2.6)$$

where X and Y are strings of fundamental $SU(N_c)$ generator matrices, and the orthonormalization condition

$$Tr(T^a T^b) = \frac{1}{2}\delta^{ab} \quad (2.7)$$

repeatedly, we finally arrive at the color decomposition for the pure gluon tree-level amplitude, which reads

$$\mathcal{A}_n(1, \dots, n) = g_s^{n-2} \sum_{\sigma \in S_n/Z_n} 2Tr(T^{a_{\sigma(1)}} \dots T^{a_{\sigma(n)}}) A_n(\sigma(1), \dots, \sigma(n)) \quad (2.8)$$

where g_s denotes the $SU(N_c)$ coupling constant and the traces over the products of the fundamental $SU(N_c)$ generator matrices contain all the group theoretical information. The gauge invariant functions $A_n(\sigma(1), \dots, \sigma(n))$ are the color-ordered partial amplitudes and contain all the kinematical information, where the ordered lists $\{1, \dots, n\}$ in the arguments of the partial amplitudes serve as appropriate short-hand notation to denote the momenta and helicities of the n external gluons in the given cyclic ordering. The sum runs over all $(n-1)!$ non-cyclic permutations of the external gluon legs, due to cyclic invariance. The partial amplitudes are built from color-stripped Feynman rules as given in appendix A and can be efficiently constructed with

the help of recurrence relations as will be discussed chapter 4. The resulting set of color-ordered diagrams in one partial amplitude forms thereby a gauge invariant subset. We note that the $-1/N_c$ -term from the Fierz identity vanishes in the pure gluon case at tree-level. In chapter 2.2 we will see that the color factor of the gluon propagator can be written in terms of a $U(N_c)$ -part and a $U(1)$ -part, where we speak of $U(N_c)$ - and $U(1)$ -gluons, and where the $U(1)$ -gluon carries no color information and only couples between quark lines. The above factorization of n -gluon tree-level amplitudes into purely group-theoretical factors $Tr(T^{a_{\sigma(1)}} \dots T^{a_{\sigma(n)}})$ and purely kinematical functions is also known by string theorists, where the group-theory factors are known as Chan-Paton factors [109]. The permutation sum is such that permutations which leave the trace structure invariant, i.e. exactly the cyclic permutations, are not considered and only the non-cyclic permutations are singled out. We can thus keep one external gluon leg fixed, say the first one, and sum over all permutations of the remaining $(n-1)$ gluons

$$\mathcal{A}_n(1, \dots, n) = g_s^{n-2} \sum_{\sigma \in S_{n-1}} 2Tr(T^{a_1} T^{a_{\sigma(2)}} \dots T^{a_{\sigma(n)}}) A_n(1, \sigma(2), \dots, \sigma(n)) \quad (2.9)$$

In a few special cases, i.e. for certain helicity combinations of the external gluons, the n -gluon partial amplitudes take on a particularly simple form, expressed by the Parke-Taylor formulae [102, 98, 8]

$$\begin{aligned} A_n(1^+, 2^+, \dots, n^+) &= 0 \\ A_n(1^+, 2^+, \dots, j^-, \dots, n^+) &= 0 \\ A_n(1^+, 2^+, \dots, j^-, \dots, k^-, \dots, n^+) &= i(\sqrt{2})^{n-2} \frac{\langle jk \rangle^4}{\langle 12 \rangle \dots \langle n1 \rangle} \end{aligned} \quad (2.10)$$

or by flipping the helicities completely

$$\begin{aligned} A_n(1^-, 2^-, \dots, n^-) &= 0 \\ A_n(1^-, 2^-, \dots, j^+, \dots, n^-) &= 0 \\ A_n(1^-, 2^-, \dots, j^+, \dots, k^+, \dots, n^-) &= i(\sqrt{2})^{n-2} \frac{[kj]^4}{[1n][n(n-1)] \dots [21]} \end{aligned} \quad (2.11)$$

where in the equations above the superscripts denote helicities, and the amplitudes with $(n-2)$ gluons of one helicity and two gluons of the other helicity are known as maximal-helicity violating (MHV) amplitudes. The sharp and square brackets denote spinor products between two-component Weyl spinors [124–126]. In general the partial amplitudes can efficiently be

2.1 Tree-Level Color Decomposition

constructed with the help of recurrence relations as will be described in chapter 4, where one can make use of certain identities in order to compute only a small set of partial amplitudes. The $A(1, 2, \dots, n)$ are in general invariant under cyclic permutations of the elements in the set $\{1, 2, \dots, n\}$ and obey further

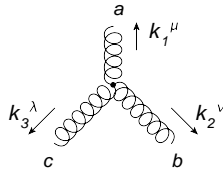
i) the reflective property: $A(n, \dots, 2, 1) = (-1)^n A(1, 2, \dots, n)$ and

ii) the dual Ward identity: $A(1, 2, 3, \dots, n) + A(2, 1, 3, \dots, n) + \dots + A(2, 3, \dots, 1, n) = 0$, also known as the photon decoupling identity or as

iii) the sub-cyclic sum: $\sum_{Z_{n-1}(2, \dots, n)} A(1, 2, \dots, n) = 0$.

The Kleiss–Kuijf relations [100] for multi-gluon amplitudes reduce the necessary set of partial amplitudes further to a set of $(n - 2)!$ linearly independent partial amplitudes, which will be described at the end of section 2.4. Upon the invent of on-shell recursion relations [127] the set of independent amplitudes has been decreased even further, which, however, is not content of this thesis.

A simple example to see how color decomposition works is given by considering the three-gluon vertex, where the usual Feynman rule for the three-gluon vertex is given by



$$\begin{aligned}
 &= g_s f^{abc} [g^{\mu\nu} (k_1 - k_2)^\lambda + g^{\nu\lambda} (k_2 - k_3)^\mu + g^{\lambda\mu} (k_3 - k_1)^\nu] \\
 &= -g_s f^{abc} [g^{\mu\nu} (k_2 - k_1)^\lambda + g^{\nu\lambda} (k_3 - k_2)^\mu + g^{\lambda\mu} (k_1 - k_3)^\nu] \\
 &\equiv -g_s f^{abc} V_3^{\mu\nu\lambda}(k_1, k_2, k_3) \equiv g_s (i f^{abc}) V_{ggg}^{(0)\mu\nu\lambda}(k_1, k_2, k_3)
 \end{aligned} \tag{2.12}$$

where we have defined the purely kinematical function $V_3^{\mu\nu\lambda}(k_1, k_2, k_3)$ and subsequently the color-stripped tree-level three-gluon vertex $V_{ggg}^{(0)\mu\nu\lambda}(k_1, k_2, k_3) = iV_3^{\mu\nu\lambda}(k_1, k_2, k_3)$. If we make the replacement $i f^{abc} = 2Tr(T^a [T^b, T^c])$ this reads

$$\begin{aligned}
 & g_s (if^{abc}) V_{ggg}^{(0)\mu\nu\lambda}(k_1, k_2, k_3) \\
 &= g_s \left[2Tr(T^a T^b T^c) V_{ggg}^{(0)\mu\nu\lambda}(k_1, k_2, k_3) - 2Tr(T^b T^a T^c) V_{ggg}^{(0)\mu\nu\lambda}(k_1, k_2, k_3) \right] \\
 &= g_s \left[2Tr(T^a T^b T^c) V_{ggg}^{(0)\mu\nu\lambda}(k_1, k_2, k_3) + 2Tr(T^b T^a T^c) V_{ggg}^{(0)\nu\mu\lambda}(k_2, k_1, k_3) \right] \\
 &= g_s \sum_{P(1,2)} 2Tr(T^{a_1} T^{a_2} T^{a_3}) V_{ggg}^{(0)\mu_1\mu_2\mu_3}(k_1, k_2, k_3) \\
 &\equiv g_s \sum_{P(1,2)} 2Tr(T^{a_1} T^{a_2} T^{a_3}) A_3^{\mu_1\mu_2\mu_3}(k_1, k_2, k_3) \tag{2.13}
 \end{aligned}$$

where we used the antisymmetry of the color-stripped three-vertex $V_{ggg}^{(0)\mu_1\mu_2\mu_3}(k_1, k_2, k_3)$, when any two of the three legs are exchanged, for the second line and identified $(a, b, c) = (a_1, a_2, a_3)$ and $(\mu, \nu, \lambda) = (\mu_1, \mu_2, \mu_3)$ in the second-to-last line. The sum in the last two lines is over the permutations of the first two legs, which corresponds to the two non-cyclic permutations of the three gluon-legs. In the last line we also identified the color-stripped Feynman rule for the color-stripped tree-level three-gluon vertex with the Born partial amplitude in three-gluon scattering $V_{ggg}^{(0)\mu_1\mu_2\mu_3}(k_1, k_2, k_3) \equiv iV_3^{\mu_1\mu_2\mu_3}(k_1, k_2, k_3) = A_3^{\mu_1\mu_2\mu_3}(k_1, k_2, k_3)$. In a similar fashion we can derive the color-stripped Feynman rule for the color-stripped four-gluon vertex. The Feynman rules for the QCD propagators and the quark-gluon vertex have a simpler color structure and the respective color-stripped Feynman rules are derived by simply stripping off the color factors. All color-stripped Feynman rules are collected in appendix A.

An instructive example for color decomposition in a scattering process is the color decomposition of the amplitude to the process $2g \rightarrow 2g$. In the Feynman diagrammatic picture we have four distinct diagrams that contribute here. These are the diagrams corresponding to the s -, t - and u -channel and the direct four-gluon vertex contribution, shown in figure 2.1. However, there are only three distinct color-stripped diagrams that contribute to a partial amplitude in this process, which are the planar diagrams shown in figure 2.2. Upon summation over the sum of the $(4-1)! = 6$ non-cyclic permutations in four-gluon scattering, taking into account the respective traces of color matrices, as given in equation 2.8, and the antisymmetric properties of the color-stripped Feynman rules with respect to the exchange of any two of the three legs, we gain back the original four full-colored Feynman diagrams upon consideration of the group-theoretical manipulations as given above.

2.1 Tree-Level Color Decomposition

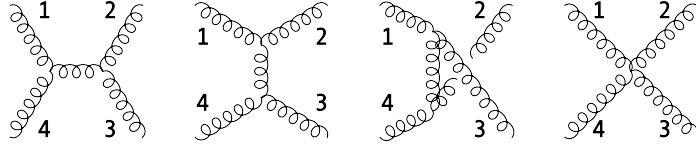


Figure 2.1: The four Feynman diagrams that contribute to four-gluon scattering. In the process $2g \rightarrow 2g$, for example, the particles labeled with 1 and 4 might be taken as incoming, whereas the particles labeled with 2 and 3 might be taken as outgoing. The four diagrams correspond to the s -, t - and u -channel and the direct four-gluon vertex contribution respectively.

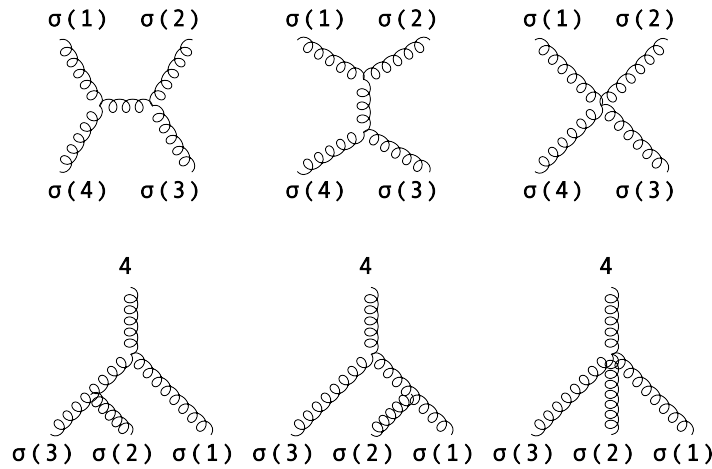


Figure 2.2: Upper row: The three color-stripped diagrams that contribute to a partial amplitude in four-gluon scattering. Lower row: The same color-stripped diagrams depicted in a different fashion, useful for off-shell recursion relations (chapter 4), where we decided to keep the leg number 4 fixed.

2.1.2 Tree-Level Amplitudes with Gluons and Quarks

A similar decomposition holds for n -parton tree-level amplitudes with one external quark-antiquark pair and $(n - 2)$ external gluons. With the same group-theoretical manipulations as above, considering that the usual Feynman rule for the quark-gluon vertex is already proportional to a fundamental color matrix (appendix A), we arrive at

$$\mathcal{A}_n(q_1, 2, \dots, (n - 1), \bar{q}_n) = g_s^{n-2} \sum_{\sigma \in S_{n-2}} (T^{a_{\sigma(2)}} \dots T^{a_{\sigma(n-1)}})_{i_{q_1} \bar{j}_{\bar{q}_n}} \mathcal{A}_n(q_1, \sigma(2), \dots, \sigma(n - 1), \bar{q}_n) \quad (2.14)$$

where the sum runs over all $(n-2)!$ permutations of the external gluon legs. The $-1/N_c$ -term from the Fierz identity is still not apparent. It will become important, however, for the color decomposition of amplitudes with more than one external quark-antiquark pairs. From the above it is evident that we sum over all possible color antennae, which are given by all $(n-2)!$ cyclically different possibilities to radiate the external gluons from the quark line. Remember that (anti-)quarks carry one (anti-)fundamental color index, their color flow is therefore depicted by one fundamental color line, whereas gluons carry one adjoint color index. We introduce the notion of a color antenna, which is a fundamental color line from which gluons can radiate. This fundamental color line coincides in the case of only one external quark-antiquark pair obviously with only the one quark line and has a color-flow arrow assigned, which directs from an antifundamental color index \bar{j} of an antiquark to a fundamental color index i of a quark.

It was noted that supersymmetry can be used to infer various relations for amplitudes with one quark-antiquark pair from the pure gluon amplitudes [128–131, 8]. From the MHV amplitude with $(n-2)$ positive helicities and two negative helicities one can for example infer

$$A_n(q_1^+, 2^+, \dots, j^-, \dots, (n-1)^+, \bar{q}_n^-) = i(\sqrt{2})^{n-2} \frac{\langle j1 \rangle \langle jn \rangle^3}{\langle 12 \rangle \dots \langle n1 \rangle} \quad (2.15)$$

The color decomposition for tree-level amplitudes with n gluons and m distinguishable quark-antiquark pairs in the fundamental basis is well known [113, 97, 31] and reads

$$\begin{aligned} \mathcal{A}_{n+2m} = & \sum_{\sigma \in S_n} \sum_{\{\alpha\}} \sum_{\{n_i\}} C(\{\sigma\}, \{\alpha\}, \{n_i\}) \times \\ & \times A_{n+2m}(q_{i_1}, \sigma_1, \dots, \sigma_{n_1}, \bar{q}_{\bar{j}_{\alpha_1}}; q_{i_2}, \sigma_{n_1+1}, \dots, \sigma_{n_2}, \bar{q}_{\bar{j}_{\alpha_2}}; \dots; q_{i_m}, \sigma_{n_{m-1}+1}, \dots, \sigma_{n_m}, \bar{q}_{\bar{j}_{\alpha_m}}) \end{aligned} \quad (2.16)$$

where we have dropped the coupling constant for the moment and where the $A_{n+2m}(\dots)$ denote the partial amplitudes for n gluons and m quark-antiquark pairs. The notation in the list of arguments is thereby inferred from the corresponding color factors and we thus have a closer look first at the color factors $C(\{\sigma\}, \{\alpha\}, \{n_i\})$, which are given by

$$\begin{aligned} C(\{\sigma\}, \{\alpha\}, \{n_i\}) = \\ \left(\frac{-1}{N_c} \right)^{p_\alpha} (T^{a_{\sigma_1}} \dots T^{a_{\sigma_{n_1}}})_{i_1 \bar{j}_{\alpha_1}} (T^{a_{\sigma_{n_1+1}}} \dots T^{a_{\sigma_{n_2}}})_{i_2 \bar{j}_{\alpha_2}} \dots (T^{a_{\sigma_{n_{m-1}+1}}} \dots T^{a_{\sigma_{n_m}}})_{i_m \bar{j}_{\alpha_m}} \end{aligned} \quad (2.17)$$

2.1 Tree-Level Color Decomposition

The color factors $C(\{\sigma\}, \{\alpha\}, \{n_i\})$ encode all possibilities to distribute n gluons among m color antennae. The sum over σ is thereby over all permutations of the external gluon legs. The sum over $\{n_i\} = \{n_1, \dots, n_m\}$, where $n_m = n$, is over all partitions to distribute n gluons of a certain permutation σ among m color antennae. If there are no fundamental generator matrices in one or more of the brackets above we put Kronecker deltas instead. The sum over $\{\alpha\}$ is over all permutations of antiquark indices, so that each ordered set $\{\alpha\}$ is a permutation of the set $\{\bar{j}\}$. The power p_α is thereby determined by the rank of the permutation $\{\alpha\}$, where the rank is determined in turn by the number of matches between members of the ordered set $\{\bar{j}\}$ and the ordered set $\{\alpha\}$. For the special case that $\{\bar{j}\} = \{\alpha\}$, p_α is given by $p_{\alpha=\bar{j}} \equiv p_{max} = m - 1$. For the cases of all $(m - 1)$ cyclic permutations of $(1, \dots, m)$, p_α is given by $p_{min} = 0$, since the number of matches is zero in these cases. In all other cases p_α is given by the number of matches between $\{\bar{j}\}$ and $\{\alpha\}$, or in other words by the number of times a color antenna coincides with a fermionic line.

The fundamental color lines of the possible antennae in the above color factor can either be congruent with the fermion-flow line of a quark-antiquark pair, where fermionic lines or quark lines always connect an antiquark with index \bar{j}_k to the corresponding quark with index i_k , or it can establish a color connection between an antiquark from one quark-antiquark pair to a quark from another, distinguishable, quark-antiquark pair. For $m > 1$ this results in distinct color disconnected pieces, so called color clusters, where two distinct color clusters are only connected through a so called U(1)-gluon, which does not carry any color information. In that regard p_α counts the number of U(1)-gluons. The U(1)-gluons result from the SU(N_c) Fierz identity and corresponds to the subtraction of a U(1)-piece from its corresponding U(N_c)-piece in any given SU(N_c) theory.

For example denotes $(T^{a_1} \dots T^{a_5})_{i_1 \bar{j}_1}$ a color antenna, where five gluons are radiated from the fundamental color-flow line that connects the antifundamental index from the quark-antiquark pair 1 to the corresponding fundamental index. For three quark-antiquark pairs and n gluons, as another example, the permutations and partitions can be such that we encounter a color factor $(T^{a_1} \dots T^{a_n})_{i_1 \bar{j}_2 \delta_{i_2 \bar{j}_3} \delta_{i_3 \bar{j}_1}$, which indicates that all n gluons are radiated off one color antenna, where the color flow of this particular color antenna is defined to flow from \bar{j}_2 to i_1 , and for those color antennae off which no gluons are radiated we put Kronecker deltas with (anti-)fundamental indices. In the second example none of the color antennae coincide with the fermionic lines, in which case $p_\alpha = p_{min} = 0$. We will discuss further details of color flow in the next section 2.2.

2.2 Color Flow in $SU(N_c)$ Theories

Another and maybe more natural basis to factorize QCD amplitudes into color factors and kinematic factors is the color–flow basis [108, 97, 31]. The color–flow decomposition is based on treating the gluon field as a $(N_c \times N_c)$ –matrix $(A_\mu)_{i\bar{j}}$ in the fundamental representation of the corresponding color space, where $i, \bar{j} = 1, \dots, N_c$, rather than in the adjoint representation as A_μ^a , with $a = 1, \dots, N_c^2 - 1$. We thus trade one adjoint index for a pair of (anti–)fundamental indices to work in a double–line formalism for color flow. The color coefficients in the color–flow decomposition consist thereby of products of Kronecker deltas with (anti–)fundamental indices, rather than of products of fundamental $SU(N_c)$ generator matrices. This allows for a more efficient treatment of the color algebra and also for a more natural interpretation in terms of all possible flows of color through a QCD amplitude. The color–flow basis relies as such on $U(N_c)$ generator matrices rather than on $SU(N_c)$ generator matrices.

In the QCD Lagrangian, as given in the introduction, the quark fields transform under the fundamental representation and the gluon fields under the adjoint representation of $SU(N_c)$, such that local $SU(N_c)$ –invariance is satisfied. The gluon field is thereby usually decomposed in the fundamental representation via

$$(A_\mu)_{i\bar{j}} \propto A_\mu^a T_{i\bar{j}}^a \quad (2.18)$$

and the Lagrangian subsequently rewritten in terms of the adjoint gluon field A_μ^a , which yields the usual Feynman rules that involve the fundamental generator matrices $T_{i\bar{j}}^a$ in the quark–gluon vertex and the structure constants f^{abc} in the three– and four–gluon vertices, which arises from $[T^a, T^b] = if^{abc}T^c$. The QCD Feynman rules are given in appendix A. As we saw above the color decomposition in the fundamental basis is then gained by simply inverting this relation to $if^{abc} = 2Tr(T^a[T^b, T^c])$. It was however noted [97], that the gluon field $(A_\mu)_{i\bar{j}}$ can directly be used in the fundamental representation, which subsequently yields Feynman rules that do not contain any fundamental generator matrices and structure constants, but rather simple Kronecker deltas with (anti–)fundamental color–flow indices. For example is the quark–gluon vertex in this formalism given by

$$\mu_1 = -i \frac{g_s}{\sqrt{2}} \gamma^{\mu_1} \delta_{i_q \bar{j}_1} \delta_{i_1 \bar{j}_q} = \left(\frac{g_s}{\sqrt{2}} \right) \times \left(\begin{array}{c} i_q \\ \leftarrow \quad \leftarrow \quad \leftarrow \\ \leftarrow \quad \leftarrow \quad \leftarrow \\ \bar{j}_q \end{array} \right) \times \left(\begin{array}{c} \bar{j}_1 \\ \leftarrow \quad \leftarrow \\ \leftarrow \quad \leftarrow \\ i_1 \end{array} \right) \times (-i \gamma^{\mu_1}) \quad (2.19)$$

where the arrows in the diagrammatic color-flow rule track the flow of color, defined to flow from an antifundamental index \bar{j} to a fundamental index i . The color-stripped Feynman rule is given by $-i\gamma^{\mu_1}$ and the factor $g_s/\sqrt{2}$ for the coupling constant is usually encoded in the color decomposition formulae.

The decomposition in the color-flow basis can also be retrieved from the fundamental basis by applying a projector $P(a_x) = \sqrt{2}T_{i_x \bar{j}_x}^{a_x}$ onto each fundamental color matrix T^{a_x} in the fundamental basis decomposition formulae, thus converting each adjoint index into a corresponding pair of (anti-)fundamental indices. The three-gluon vertex for example contributes two color flows, which is seen from $iP(a_1)P(a_2)P(a_3)f^{a_1 a_2 a_3} = 2P(a_1)P(a_2)P(a_3)\text{Tr}(T^{a_1}[T^{a_2}, T^{a_3}]) \propto \delta_{i_1 \bar{j}_2} \delta_{i_2 \bar{j}_3} \delta_{i_3 \bar{j}_1} - \delta_{i_1 \bar{j}_3} \delta_{i_3 \bar{j}_2} \delta_{i_2 \bar{j}_1}$, and the four-gluon vertex contributes six color flows. For further reference we derive the color-stripped Feynman rules in appendix A together with their corresponding color-flow rules in the color-flow basis.

One subtlety resides in the consequence for the gluon propagator. In the usual Feynman rules the color part of the gluon propagator is simply given by δ^{ab} , thereby connecting two color indices in the adjoint representation. In the color-flow basis the corresponding color-flow rule is given by

$$\sqrt{2}T_{i_a \bar{j}_a}^a \sqrt{2}T_{i_b \bar{j}_b}^b \delta^{ab} = \delta_{i_a \bar{j}_b} \delta_{i_b \bar{j}_a} - \frac{1}{N_c} \delta_{i_a \bar{j}_a} \delta_{i_b \bar{j}_b} = \begin{array}{c} i_a \\ \leftarrow \quad \leftarrow \\ \leftarrow \quad \leftarrow \\ \bar{j}_a \end{array} \begin{array}{c} \bar{j}_b \\ \leftarrow \quad \leftarrow \\ \leftarrow \quad \leftarrow \\ i_b \end{array} - \frac{1}{N_c} \begin{array}{c} i_a \\ \leftarrow \quad \leftarrow \\ \leftarrow \quad \leftarrow \\ \bar{j}_a \end{array} \begin{array}{c} \bar{j}_b \\ \leftarrow \quad \leftarrow \\ \leftarrow \quad \leftarrow \\ i_b \end{array} \quad (2.20)$$

which indicates two different fundamental color flows. This somewhat more complicated color structure for the gluon propagator, however, is a worthwhile tradeoff and is easily seen from the $SU(N_c)$ Fierz identity in equation 2.4. The second term in equation 2.20 is interpreted as U(1)-gluon, which subtracts one degree of freedom from the $U(N_c)$ color flow in order to gain the correct $SU(N_c)$ -behavior. We can also infer from the above that the U(1)-gluon does not couple to pure gluon interactions but only between quark lines.

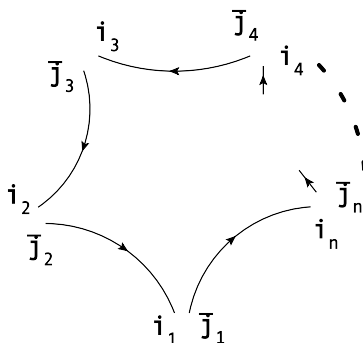


Figure 2.3: Color flow in an n -gluon amplitude. The specific color flow corresponds to $\delta_{i_1\bar{j}_2}\delta_{i_2\bar{j}_3}\dots\delta_{i_n\bar{j}_1}$ for the fixed cyclic ordering $(1, 2, \dots, n)$, i.e. $\sigma = id$. Every pair $(i_k\bar{j}_k)$ corresponds to an external gluon. In such an ordered diagram color flows from an antifundamental index of one pair to the fundamental index of the adjacent pair, i.e. all the corresponding diagrams are planar. The reading direction is always against the color-flow arrow, which corresponds then to the clock-wise ordering of the external legs.

2.2.1 Tree-Level Gluon Amplitudes in the Color-Flow Basis

By using the projector $P(a_x) = \sqrt{2}T_{i_x\bar{j}_x}^{a_x}$ onto each color matrix T^{a_x} , the color decomposition for n -gluon amplitudes in the fundamental basis can be converted into the color-flow basis to read

$$\mathcal{A}_n(1, \dots, n) = \left(\frac{g_s}{\sqrt{2}}\right)^{n-2} \sum_{\sigma \in S_n/Z_n} \delta_{i_{\sigma(1)}\bar{j}_{\sigma(2)}} \delta_{i_{\sigma(2)}\bar{j}_{\sigma(3)}} \dots \delta_{i_{\sigma(n)}\bar{j}_{\sigma(1)}} A_n(\sigma(1), \dots, \sigma(n)) \quad (2.21)$$

The graphical interpretation can be given in terms of color-flow diagrams as shown in figure 2.3. To calculate the corresponding partial amplitude $A_n(1, \dots, n)$, i.e. all the necessary color-ordered diagrams, one deforms the color-flow lines in figure 2.3 in all possible ways. For the case of four gluons this yields the sum of diagrams in figure 2.4, which correspond to the diagrams in figure 2.2. In our notation color flows always from an antifundamental to a fundamental index. For a given fermion line the direction of the color-flow arrows and the direction of the fermion-flow arrows thus always coincide. The preferred reading direction of the color factors from the color-flow diagrams, with respect to the fundamental color indices, is always against the direction of the color-flow arrow. The interpretation of a tree-level partial amplitude is then that of a set of ordered diagrams, whose corresponding Feynman diagrams contribute to a specific color flow. Color ordering and cyclic ordering coincide therefore. The partial amplitudes in the color-flow decomposition have been shown to be the same as in the fundamental color decomposition [97]. The deformation of color-flow lines as shown in figure 2.4 yields exactly the

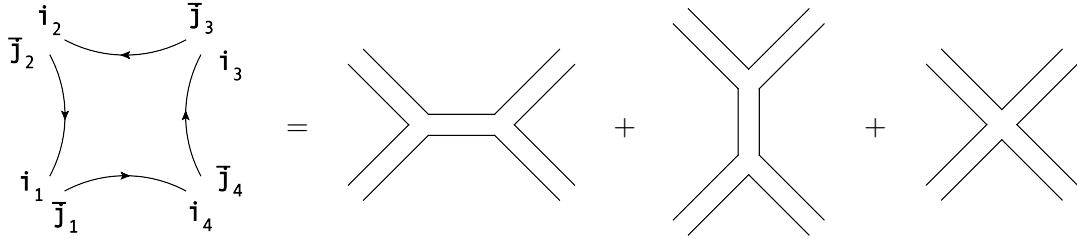


Figure 2.4: Color flow in a four-gluon amplitude. Deforming the color-flow lines in all possible ways, by hooking them together, yields the four color-stripped diagrams that contribute to the corresponding partial amplitude with the fixed cyclic ordering $(1, 2, 3, 4)$, where color double-lines correspond to gluons.

same sum of color-stripped diagrams as we get from the corresponding Berends–Giele recursion relations [98] (see chapter 4). It was also noted [108, 97] that the construction above is similar to the construction of string amplitudes, or dual amplitudes, where each gluon resembles an open string with charge (i_k, \bar{j}_k) [110, 109, 108].

2.2.2 Tree-Level Amplitudes with Gluons and Quarks in the Color-Flow Basis

The color decomposition for $(n - 2)$ external gluons and one quark–antiquark pair in the color-flow basis can again be inferred from the fundamental basis decomposition by applying the appropriate projectors for each adjoint gluon index, as described above, and reads

$$\mathcal{A}_n(q_1, 2, \dots, (n - 1), \bar{q}_n) = \left(\frac{g_s}{\sqrt{2}} \right)^{n-2} \sum_{\sigma \in S_{n-2}} \delta_{i_{q_1} \bar{j}_{\sigma(2)}} \delta_{i_{\sigma(2)} \bar{j}_{\sigma(3)}} \dots \delta_{i_{\sigma(n-1)} \bar{j}_{\bar{q}_n}} \mathcal{A}_n(q_1, \sigma(2), \dots, \sigma(n - 1), \bar{q}_n) \quad (2.22)$$

where the $(n - 2)!$ permutations $\sigma \in S_{n-2}$ are over the $(n - 2)$ external gluon legs. This decomposition resembles the $(n - 1)$ -gluon case if we compare the (q_1, \bar{q}_n) -pair to an external gluon. Again we sum over all possible color antennae, which are given by all $(n - 2)!$ cyclically different possibilities to radiate the external gluons from the quark line, i.e. to attach the corresponding gluon color-flow double-lines to the one fundamental color-flow line between the fundamental and antifundamental indices of the quark and the antiquark respectively, just as describe in the previous section. The $U(1)$ -gluon does still not play a role, since it can only couple between two quark lines.

In the computation of amplitudes with more than one quark–antiquark pair we have to consider the introduction of $U(1)$ –gluons. Gluons that connect two quark lines split into a $U(N_c)$ –piece and a $U(1)$ –piece, as described before in appendix A. In the color–flow basis, where we primarily consider $U(N_c)$ –gluons through the double–line formalism, we thus have to introduce with each $U(N_c)$ –gluon that connects two quark lines an additional $U(1)$ –gluon with an associated factor of $-1/N_c$. This introduces subleading terms in $1/N_c$ in the color decomposition. As an example the color decomposition of an amplitude with two distinguishable quark–antiquark pairs and n gluons reads in the color–flow basis

$$\begin{aligned}
 & \left(\frac{\sqrt{2}}{g_s}\right)^n \mathcal{A}_{n+4}(\bar{q}_1, q_1, \bar{q}_2, q_2, 1, \dots, n,) \\
 &= \sum_{r=0}^n \sum_{\sigma \in S_n} (\delta_{i_{q_1} \bar{j}_{\sigma(1)}} \delta_{i_{\sigma(1)} \bar{j}_{\sigma(2)}} \dots \delta_{i_{\sigma(r)} \bar{j}_{\bar{q}_2}} \delta_{i_{q_2} \bar{j}_{\sigma(r+1)}} \delta_{i_{\sigma(r+1)} \bar{j}_{\sigma(r+2)}} \dots \delta_{i_{\sigma(n)} \bar{j}_{\bar{q}_1}}) \times \\
 & \quad \times A_{n+4}(q_1, \sigma(1, r), \bar{q}_2, q_2, \sigma(r+1, n), \bar{q}_1) \\
 & - \frac{1}{N_c} \sum_{r=0}^n \sum_{\sigma \in S_n} (\delta_{i_{q_1} \bar{j}_{\sigma(1)}} \delta_{i_{\sigma(1)} \bar{j}_{\sigma(2)}} \dots \delta_{i_{\sigma(r)} \bar{j}_{\bar{q}_1}}) (\delta_{i_{q_2} \bar{j}_{\sigma(r+1)}} \delta_{i_{\sigma(r+1)} \bar{j}_{\sigma(r+2)}} \dots \delta_{i_{\sigma(n)} \bar{j}_{\bar{q}_2}}) \times \\
 & \quad \times A_{n+4}(q_1, \sigma(1, r), \bar{q}_1; q_2, \sigma(r+1, n), \bar{q}_2) \tag{2.23}
 \end{aligned}$$

where we have introduced the shorthand notation $\sigma(a, z) = \sigma(a), \dots, \sigma(z)$. We note the two different products of color antennae, indicated by the brackets in the color–flow strings of Kronecker deltas. In the first (leading) term we notice one connected color cluster, in the second (subleading) term we note two color–disconnected color clusters. This coincides with the radiation of the gluons from two different products of color antennae upon the permutation of the antifundamental indices from the antiquarks, just as discussed for the decomposition in the fundamental basis in the previous section, and generalizes accordingly to multiple quark–antiquark pairs. If we were to consider a pure $U(N_c)$ theory, the second term in the above would actually not appear, since the corresponding $U(N_c)$ Fierz identity does not involve the subtraction of a $U(1)$ –term. This will be different for one–loop amplitudes, where even in a pure $U(1)$ theory we can have subleading terms in $1/N_c$.

So far we have always considered distinguishable quark–antiquark pairs. Of course, we also have to consider amplitudes with flavor–like quark–antiquark pairs. These can, however, simply be given by proper antisymmetrization with respect e.g. to the antiquark indices. In the case of an amplitude with two indistinguishable quark–antiquark pairs and one gluon, for example, we then have $A(1_{q_1}, 2_{\bar{q}_1}, 3_{q_1}, 4_{\bar{q}_1}, 5_g) = A(1_{q_1}, 2_{\bar{q}_1}, 3_{q_2}, 4_{\bar{q}_2}, 5_g) - A(1_{q_1}, 4_{\bar{q}_1}, 3_{q_2}, 2_{\bar{q}_2}, 5_g)$, where we remember that the shorthand notation of the arguments denotes external momenta and helicities.

An efficient algorithm that implements the color decomposition for amplitudes with multiple quark–antiquark pairs in the color–flow basis is given in [31], where the quite natural organization in terms of all possible color clusters is used.

2.3 Squared Amplitudes and the Color Matrix

Upon calculating observables the amplitude has to be squared, i.e. multiplied by the adjoint of itself and summed over the external color and spin degrees of freedom. Let us focus on the color decomposition in the fundamental basis again. Upon squaring, and summation over the color degrees of freedom, the color structure of the squared amplitude is collected in a color matrix C_{ij} via

$$|\mathcal{A}|^2 = \sum_{color} \mathcal{A}^\dagger \mathcal{A} = \sum_i \sum_j A_i^\dagger \left(\sum_{color} C_i^\dagger C_j \right) A_j \equiv \sum_i \sum_j A_i^\dagger C_{ij} A_j = \vec{A}^\dagger C \vec{A} \quad (2.24)$$

Specifically in the case for the pure n –gluon amplitude we get

$$|\mathcal{A}_n(1, \dots, n)|^2 = 4g_s^{2(n-2)} \sum_{\sigma_1 \in S_n/Z_n} \sum_{\sigma_2 \in S_n/Z_n} A_{\sigma_1}^\dagger \underbrace{\left(\sum_{color} C_{\sigma_1}^\dagger C_{\sigma_2} \right)}_{\equiv C_{\sigma_1 \sigma_2}} A_{\sigma_2} \quad (2.25)$$

where $C_{\sigma_1 \sigma_2}$ is a $((n-1)! \times (n-1)!)$ –matrix with each entry generally given by a polynomial in the number of colors N_c and where we have chosen a shorthand notation $A_{\sigma_i} = A_n(\sigma(1), \dots, \sigma(n))$. In the case with one pair of external quarks and $(n-2)$ external gluons we get

$$|\mathcal{A}_n(q_1, 2, \dots, (n-1), \bar{q}_n)|^2 = g_s^{2(n-2)} \sum_{\sigma_1 \in S_{n-2}} \sum_{\sigma_2 \in S_{n-2}} A_{\sigma_1}^\dagger \underbrace{\left(\sum_{color} C_{\sigma_1}^\dagger C_{\sigma_2} \right)}_{\equiv C_{\sigma_1 \sigma_2}} A_{\sigma_2} \quad (2.26)$$

with $C_{\sigma_1 \sigma_2}$ a $((n-2)! \times (n-2)!)$ –matrix and the short–hand notation $A_{\sigma_i} = A_n(q_1, \sigma(2), \dots, \sigma(n-1), \bar{q}_n)$. The sum over colors is thereby over the contracted adjoint indices from the external gluons and the contracted (anti–)fundamental indices from the external (anti–)quarks. A fundamental index in the adjoint amplitude A^\dagger turns thereby into an antifundamental index and vice versa, and upon squaring we always contract pairs of fundamental and antifundamental indices which are associated to the same particle ID in the list of particles. The summation over colors can also be cast into a (color summation) projection operator P , which contains a Kronecker

$\delta_{i^\dagger i} = \delta_{\bar{i}\bar{i}}$ or $\delta_{\bar{j}^\dagger \bar{j}} = \delta_{\bar{j}\bar{j}}$ for every contraction of (anti-)fundamental indices from external (anti-)quarks and a Kronecker $\delta^{a^\dagger a} = \delta^{aa}$ for every contraction of adjoint indices from external gluons. As a notational aid we have put daggers as superscripts on those indices that originate from the adjoint amplitude.

Let us have a closer look at the color matrix in the case of one quark–antiquark pair and three gluons, where we denote the fundamental and antifundamental indices of the quark–antiquark pair by \bar{j} and i respectively and the gluon indices simply by 1 to 3. We use lexicographic ordering for the $3! = 6$ permutations and get

$$C = \begin{pmatrix} (123)_{i\bar{j}}^\dagger(123)_{i\bar{j}} & (123)_{i\bar{j}}^\dagger(132)_{i\bar{j}} & \cdots & (123)_{i\bar{j}}^\dagger(321)_{i\bar{j}} \\ (132)_{i\bar{j}}^\dagger(123)_{i\bar{j}} & \ddots & & \vdots \\ \vdots & & \ddots & \vdots \\ (321)_{i\bar{j}}^\dagger(123)_{i\bar{j}} & \cdots & \cdots & (321)_{i\bar{j}}^\dagger(321)_{i\bar{j}} \end{pmatrix} \quad (2.27)$$

where we introduce a shorthand notation $(123)_{i\bar{j}}$ for the (color antenna) string $(T^{a_1}T^{a_2}T^{a_3})_{i\bar{j}}$. Due to the hermitian property of the fundamental color matrices we have $(abc)_{i\bar{j}}^\dagger(abc)_{i\bar{j}} = (cba)_{\bar{j}i}(abc)_{i\bar{j}} = \text{Tr}(T^c T^b T^a T^a T^b T^c) \equiv [cbaabc]$ which, considering the cyclic property of the trace, yields

$$C = \begin{pmatrix} [123321] & [123231] & \cdots & [123123] \\ [132321] & \ddots & & \vdots \\ \vdots & & \ddots & \vdots \\ [321321] & \cdots & \cdots & [321123] \end{pmatrix} \quad (2.28)$$

and in general for one quark–antiquark pair and $(n - 2)$ gluons

$$C = \begin{pmatrix} [12\dots(n-2)(n-2)\dots 21] & \cdots & [12\dots(n-2)12\dots(n-2)] \\ \vdots & \ddots & \vdots \\ [(n-2)\dots 21(n-2)\dots 21] & \cdots & [(n-2)\dots 2112\dots(n-2)] \end{pmatrix} \quad (2.29)$$

where at first glance the number of traces to be calculated is $(n - 2)! \times (n - 2)!$. There are, however, really only $(n - 2)!$ different traces, since due to the pairing of color indices and implicit summation over colors one can always rearrange e.g. $[132321]$ into $[123231]$. The trace factors on the diagonal are for example always the same and given by $[12\dots(n-2)(n-2)\dots 21] =$

2.3 Squared Amplitudes and the Color Matrix

$N_c C_F^{n-2} = N_c ((N_c^2 - 1)/2N_c^2)^{n-2} = N_c (\frac{1}{2}(N_c - 1/N_c))^{n-2}$. As we can see from equation 2.24 consists the computation of the squared matrix element more or less of the computation of the color matrix and the computation of kinematic vectors, which contain the partial amplitudes. The partial amplitudes have thereby to be evaluated for each phase-space point in the Monte Carlo integration to a given process. In contrast to that it suffices to evaluate the color matrix to a given process, since it is independent of the kinematical information, only once right at the beginning of the corresponding computation.

In general the color matrix consists of non-vanishing diagonal and non-diagonal terms, where each is given by a polynomial in the number of colors N_c . The diagonal entries contain thereby terms which are leading in N_c compared to the non-diagonal entries, which are subleading. The color factors in the diagonal terms multiply the products of partial amplitudes with their adjoint equivalents of the same cyclic ordering in the external legs. The non-diagonal terms multiply interference terms between partial amplitudes and adjoint partial amplitudes of different cyclic orderings in the external legs. In the large- N_c or leading color limit all non-diagonal terms vanish and only the leading terms in the diagonal entries survive. Thus only the non-interference terms survive and the color decomposition of the squared amplitude factorizes into a sum over squares

$$|\mathcal{A}|^2 = \left| \sum_i C_i A_i \right|^2 \xrightarrow{\text{large-}N_c} \sum_i |C_i A_i|^2 = \sum_{\sigma_i} C_{\sigma_i \sigma_i} A_{\sigma_i}^\dagger A_{\sigma_i} \quad (2.30)$$

Tree-level computations for many particles in the final state can nowadays be efficiently carried through in full color [132, 31, 133, 134]. In order to simplify the more intense higher order computations, especially for multi-parton final states, however, one can approximate the results by considering only the leading color terms, which form the dominant contributions to the final results. For systems with a Bose symmetry we can further simplify the computational effort. Since the phase-space integration is symmetric under permutation of the outgoing gluons we may simply consider only one of the cyclically ordered amplitudes with a specific cyclic ordering in the gluon legs, which reduces the set of cyclically ordered amplitudes that need to be computed dramatically, and instead multiply by an appropriate factorial factor $\propto (n-x)!$, where $(n-x)$ is the number of gluons, or $\propto (n-1)!$ in the case of pure n -gluon amplitudes [135, 136, 73].

Upon squaring and summing over colors in the color-flow basis we would naively count for N_c^2 color degrees of freedom per external gluon instead of $(N_c^2 - 1)$, since in the color-flow basis the sum over colors is a sum over contracted (anti-)fundamental indices instead of contracted adjoint indices. We have to correct for this, which we do by simply subtracting the $-1/N_c$ -term

in the color summation projection operator for each external gluon

$$P_{g_k} = \delta_{i_k \bar{v}_k} \delta_{j_k \bar{j}_k} - \frac{1}{N_c} \delta_{j_k \bar{v}_k} \delta_{i_k \bar{j}_k} \quad (2.31)$$

which is easily seen from converting to the color-flow basis and subsequent use of the Fierz identity as discussed before

$$\delta_k^{a^\dagger a} \longrightarrow \sqrt{2} T_{i_k \bar{j}_k}^{a_k \dagger} \sqrt{2} T_{i_k \bar{j}_k}^{a_k} \delta_k^{a^\dagger a} = 2 T_{j_k \bar{v}_k}^{a_k} T_{i_k \bar{j}_k}^{a_k} \delta_k^{a_k a_k} = \delta_{j_k \bar{j}_k} \delta_{i_k \bar{v}_k} - \frac{1}{N_c} \delta_{j_k \bar{v}_k} \delta_{i_k \bar{j}_k} \quad (2.32)$$

The second term, which corresponds to the U(1)-gluon, does not play a role in squaring pure gluon amplitudes, since the U(1)-gluon does not couple to the gluonic interactions. This means that we can naively sum over the U(N)-indices in this case, i.e. $P_{g_k} = \delta_{i_k \bar{v}_k} \delta_{j_k \bar{j}_k}$ in the case of amplitudes which have only gluons as external particles. This is different for squaring amplitudes that involve $m \geq 1$ external quark-antiquark pairs.

In summary: For a quark with fundamental index i and corresponding antifundamental index \bar{i} from the side of the adjoint amplitude we use $P_{q_k} = \delta_{i_k \bar{v}_k}$. For an antiquark with antifundamental index \bar{j} and corresponding fundamental index j from the side of the adjoint amplitude we use $P_{\bar{q}_k} = \delta_{j_k \bar{j}_k}$. For a gluon with indices $(i\bar{j})$ and a corresponding set of indices $(j\bar{v})$ from the side of the adjoint amplitude and in the case of a U(N) theory we can use $P_{g_k} = \delta_{i_k \bar{v}_k} \delta_{j_k \bar{j}_k}$. For a corresponding gluon in an SU(N) theory we use in general $P_{g_k} = \delta_{i_k \bar{v}_k} \delta_{j_k \bar{j}_k} - \frac{1}{N_c} \delta_{j_k \bar{v}_k} \delta_{i_k \bar{j}_k}$. The total projector P is then given by the product of the projectors for all external particles, which inserted yields the correct summation over colors. The color matrix, which was introduced before, is then simply

$$C_{\sigma_1 \sigma_2} \equiv C_{\sigma_1}^\dagger P C_{\sigma_2} \quad (2.33)$$

where the color summation is implicit in the (color summation) projection operator. Squaring and summing over colors in the color-flow basis will result in an expansion in the number of colors N_c , where the leading terms are given by the squares of color flows of the same permutation and lead to leading monomials in N_c

$$(\delta_{i_1 \bar{j}_2} \delta_{i_2 \bar{j}_3} \dots \delta_{i_n \bar{j}_1})^\dagger \delta_{i_1 \bar{j}_2} \delta_{i_2 \bar{j}_3} \dots \delta_{i_n \bar{j}_1} = N_c^n \quad (2.34)$$

and the subleading terms, interference terms of different permutations, yield monomials in

2.3 Squared Amplitudes and the Color Matrix

N_c^{n-2a} , with $a = \text{integer}$, quite in contrast to the decomposition in the fundamental basis, where we have polynomials rather than monomials.

In the application of the projection operator to project the color space of the non-adjoint matrix element onto the color space of the adjoint matrix element and at the same time contracting the (anti-)fundamental indices, and thereby squaring and summing over colors, we have to consider the full $SU(N_c)$ -projector $P_{g_k} = \delta_{i_k \bar{i}_k} \delta_{j_k \bar{j}_k} - \frac{1}{N_c} \delta_{j_k \bar{i}_k} \delta_{i_k \bar{j}_k}$ for the external gluons. This will lead to an expansion in $1/N_c$ already in the projected amplitude, dropping the factor for the coupling constant for the moment, which reads [97]

$$\begin{aligned}
P_q P_{g_1} \dots P_{g_n} P_{\bar{q}} A_{n+2}(q, 1, \dots, n, \bar{q}) &= \sum_{\sigma \in S_n} \delta_{i_q \bar{j}_{\sigma(1)}} \delta_{i_{\sigma(1)} \bar{j}_{\sigma(2)}} \dots \delta_{i_{\sigma(n)} \bar{j}_{\bar{q}}} A_{n+2}(q, \sigma(1), \dots, \sigma(n), \bar{q}) \\
&+ \left(-\frac{1}{N_c} \right) \sum_{\sigma \in S_n} \delta_{i_q \bar{j}_{\sigma(1)}} \dots \delta_{i_{\sigma(n-1)} \bar{j}_{\bar{q}}} \delta_{i_{\sigma(n)} \bar{j}_{\sigma(n)}} A_{n+2}((q, \sigma(1), \dots, \sigma(n-1), \bar{q}, \sigma(n)) \\
&+ \left(-\frac{1}{N_c} \right)^2 \frac{1}{2!} \sum_{\sigma \in S_n} \delta_{i_q \bar{j}_{\sigma(1)}} \dots \delta_{i_{\sigma(n-2)} \bar{j}_{\bar{q}}} \delta_{i_{\sigma(n-1)} \bar{j}_{\sigma(n-1)}} \delta_{i_{\sigma(n)} \bar{j}_{\sigma(n)}} \times \\
&\quad \times A_{n+2}(q, \sigma(1), \dots, \sigma(n-2), \bar{q}, \sigma(n-1), \sigma(n)) \\
&+ \dots + \left(-\frac{1}{N_c} \right)^n \delta_{i_q \bar{j}_{\bar{q}}} \delta_{i_{\sigma(1)} \bar{j}_{\sigma(1)}} \dots \delta_{i_{\sigma(n)} \bar{j}_{\sigma(n)}} A_{n+2}(q, \bar{q}, \sigma(1), \dots, \sigma(n)) \quad (2.35)
\end{aligned}$$

where the partial amplitudes in the subleading terms in $1/N_c$ can be computed as linear combinations of the partial amplitudes in the leading term. These subleading tree-level amplitudes correspond to amplitudes with $(n-k)$ $U(N_c)$ -gluons and k $U(1)$ -gluons. The different terms contain each a factor of $1/k!$ because in the permutations the terms that differ only by an exchange of $U(1)$ -gluons are identical. There are hence $n!/k!$ different permutations in the terms with k $U(1)$ -gluons, and thus there is also only a single term in the last line with n $U(1)$ -gluons. The sub-leading amplitude with one $U(1)$ -gluon is for example given by

$$\begin{aligned}
A_{n+2}(q, \sigma(1), \dots, \sigma(n-1), \bar{q}, \sigma(n)) &= A_{n+2}(q, \sigma(1), \dots, \sigma(n-1), \sigma(n), \bar{q}) \\
&+ A_{n+2}(q, \sigma(1), \dots, \sigma(n), \sigma(n-1), \bar{q}) \\
&+ \dots + A_{n+2}(q, \sigma(n), \sigma(1), \dots, \sigma(n-1), \bar{q}) \quad (2.36)
\end{aligned}$$

quite in analogy to the decoupling identity, or more generally to the Kleiss-Kuijf relations [100], for the n -gluon tree-level partial amplitudes, where two gluons are kept fix. Subleading tree-level amplitudes with more than one $U(1)$ -gluon can be computed via an appropriate shuffle sum

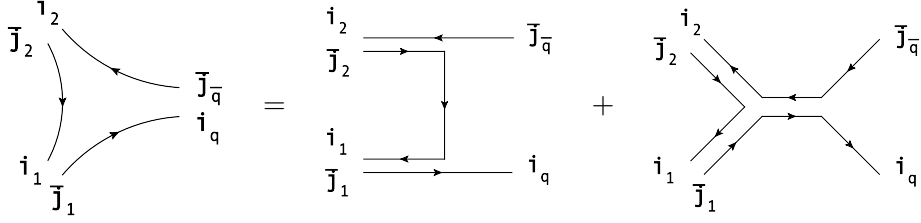


Figure 2.5: The color-stripped diagrams to a partial amplitude with one quark-antiquark pair and two gluons.

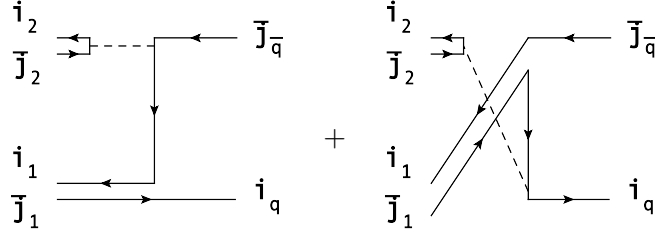


Figure 2.6: The color-stripped diagrams to a subleading partial amplitude $A_{n+2}(q, 1, \bar{q}, 2)$ with one quark-antiquark pair, one $U(N_c)$ -gluon and one $U(1)$ -gluon. The $U(1)$ -gluon is depicted by a dashed line.

over two sets of gluons, one containing the $U(N_c)$ -gluons and one containing the $U(1)$ -gluons, which will be explained in some more detail in the next subsection 2.4. Shuffle relations for subleading amplitudes will become important in the one-loop case as well, which will be discussed in more detail in section 2.5. In [97] it is noted that the direct computation of the subleading partial amplitudes is more efficient than expressing them in terms of linear combinations of the leading partial amplitudes, which is done by simply replacing k of the external $U(N_c)$ -gluons by $U(1)$ -gluons and associated factors of $-1/N_c$.

We show the diagrams that contribute to a partial amplitude with one quark-antiquark pair and two gluons in figure 2.5. We also show the diagrams that contribute to a subleading partial amplitude with one quark-antiquark pair, one $U(N_c)$ -gluon and one $U(1)$ -gluon in figure 2.6. In figure 2.6 the diagrams with the non-abelian vertex, as shown in figure 2.5, cancel when the subleading partial amplitude is computed as linear combination of leading partial amplitudes, due the antisymmetry of the color-stripped three-gluon vertex with respect to the exchange of any two of the three legs. One notes that there is a contribution from a non-planar diagram.

2.4 Gluon Amplitudes in the Adjoint Basis

This is due to the fact that $U(1)$ -gluons can be attached to any quark line without any effect on the color flow, as depicted. The number of Feynman diagrams that contribute to a subleading partial amplitude with k $U(1)$ -gluons grows thus like $k!$. However, we can safely drop those non-planar diagrams, only computing the planar ones, and simply dress the term with a factor $k!$. The projected amplitude from above is then multiplied with the corresponding (non-projected) adjoint amplitude. The role of the subleading terms is then simply to subtract, in each of the external gluons, one of the nine color flows of a $U(N_c)$ -gluon, such that the correct $SU(N_c)$ -behavior is regained.

2.4 Gluon Amplitudes in the Adjoint Basis

Before we turn to one-loop color decomposition we want to discuss another basis for the color decomposition of gluon amplitudes at the tree-level [119]. Instead of using only the generators in the fundamental representation one uses only the generators in the adjoint representation, i.e. matrices $(F^a)_{bc} \equiv if^{abc}$ where the structure constants f^{abc} are exactly the generators of $SU(N_c)$ in the adjoint representation. This reads then

$$\begin{aligned} \mathcal{A}_n^{(0)}(g_1, \dots, g_n) &= (ig_s)^{n-2} \sum_{\sigma \in S_{n-2}} f^{a_1 a_{\sigma(2)} x_1} f^{x_1 a_{\sigma(3)} x_2} \dots f^{x_{n-3} a_{\sigma(n-1)} a_n} A_n^{(0)}(1, \sigma(2), \dots, \sigma(n-1), n) \\ &= g_s^{n-2} \sum_{\sigma \in S_{n-2}} (F^{a_{\sigma(2)}} F^{a_{\sigma(3)}} \dots F^{a_{\sigma(n-1)}})_{a_1 a_n} A_n^{(0)}(1, \sigma(2), \dots, \sigma(n-1), n) \end{aligned} \quad (2.37)$$

where we have included additional superscripts (0) to the amplitudes, to denote their tree-level nature. One notes the structural similarity to the decomposition of a tree-level amplitude with one quark-antiquark pair and $(n-2)$ gluons in equation 2.14, if neglecting the different color basis for the moment. The above decomposition in equation 2.37 uses a set of $(n-2)!$ partial amplitudes, with leg 1 and n held fixed, quite in contrast to the somewhat bigger set of $(n-1)!$ partial amplitudes that is needed in the fundamental decomposition of n -gluon tree-level amplitudes in equation 2.8. This reduced set of partial amplitudes is the same set of linearly independent partial amplitudes as the one which is used in the Kleiss-Kuijff relations [100], which are given by

$$A_n^{(0)}(1, \{\alpha\}, n, \{\beta\}^T) = (-1)^{\#\beta} \sum_{OP\{\alpha\}\{\beta\}} A_n^{(0)}(1, \sigma(\{\alpha\}, \{\beta\}), n) \quad (2.38)$$

where $\{\alpha\} = \{2, \dots, x\}$ and $\#\beta$ is the number of elements in the set $\{\beta\}^T = \{x+1, \dots, n-1\}$.

$OP\{\alpha\}\{\beta\}$ is the ordered product of $\{\alpha\}$ and $\{\beta\} = \{n-1, \dots, x+1\}$, which is the set of all permutations of the elements in the ordered list $\{1, 2, \dots, x, n-1, \dots, x+1, n\}$, with 1 and n held fixed, that preserve the ordering of the $\alpha_i \in \{\alpha\}$ within $\{\alpha\}$ and of the $\beta_i \in \{\beta\}$ within $\{\beta\}$, while allowing for all relative orderings of the α_i with respect to the β_i . $A_n^{(0)}(1, \{\alpha\}, n, \{\beta\}^T)$ denotes the partial amplitude which multiplies the color factor $Tr(T^1 T^{\sigma(2)} \dots T^{\sigma(x)} T^n T^{\sigma(x+1)} \dots T^{\sigma(n-1)})$. The corresponding color flow to $A_n^{(0)}(1, \{\alpha\}, n, \{\beta\}^T)$ is depicted in the upper right of figure 2.7.

The color factor can also be depicted as the one on the lower left in figure 2.7 by virtue of another representation of the three-gluon vertex color-flow diagram, as given in appendix A. We can then associate to the same color factor a partial amplitude as the one depicted by the multiperipheral diagram shown on the lower right in figure 2.7, where we have to include a relative minus sign for every gluon color-flow double-line that is radiated to the left with respect to the color-flow arrow in the associated color-flow diagram, just as explained in appendix A. We can thus express all partial amplitudes to a color factor $Tr(T^1 T^{\sigma(2)} \dots T^{\sigma(x)} T^n T^{\sigma(x+1)} \dots T^{\sigma(n-1)})$ by an appropriate shuffle sum over partial (multiperipheral) amplitudes with gluon 1 and n held fixed at the beginning and the end of the argument list respectively and where the gluon indices of members in the list $\{\sigma(2), \dots, \sigma(x)\}$ and members in the list $\{\sigma(x+1), \dots, \sigma(n-1)\}$ shuffle with respect to each other while keeping the ordering within each list fixed.

One can think of the associated amplitude to $Tr(T^1 T^{\sigma(2)} \dots T^{\sigma(x)} T^n T^{\sigma(x+1)} \dots T^{\sigma(n-1)})$ as one where gluons of one set are radiated to one side of a uniquely given gluon-strand between gluon 1 and n and gluons of the other set to the other side, depicted in the upper left in figure 2.7. The amplitudes $A_n^{(0)}(1, \{\alpha\}, n, \{\beta\}^T)$ must not contain diagrams where gluons from one set connect directly to gluons from the other set via a color-stripped tree-level three- or four-gluon vertex, since those would contribute to a wrong color flow. In the corresponding shuffle sums over the multiperipheral amplitudes these diagrams must therefore cancel. Upon the antisymmetry of the color-stripped three- and four-valent vertices with respect to the exchange of external legs we note that this is indeed the case. In the shuffle sum there is always a diagram with a permutation of two directly connected gluon legs in the cyclic ordering $(\dots, \alpha_i, \beta_i, \dots)$ which cancels another identical diagram but with the two gluon legs exchanged in the cyclic ordering $(\dots, \beta_i, \alpha_i, \dots)$. Similar considerations hold for diagrams with four-gluon vertices. We elaborate on this in more detail also in chapter 3.3. All the diagrams that can be drawn for $A_n^{(0)}(1, \{\alpha\}, n, \{\beta\}^T)$ behave then such as if the gluons in $\{\alpha\}$ and the gluons in $\{\beta\}$ belong to two different gauge groups, i.e. they do not couple. It was shown [119] that equation 2.37 yields the same result as inserting the Kleiss-Kuijff relation of equation 2.38 into

2.5 One-Loop Color Decomposition

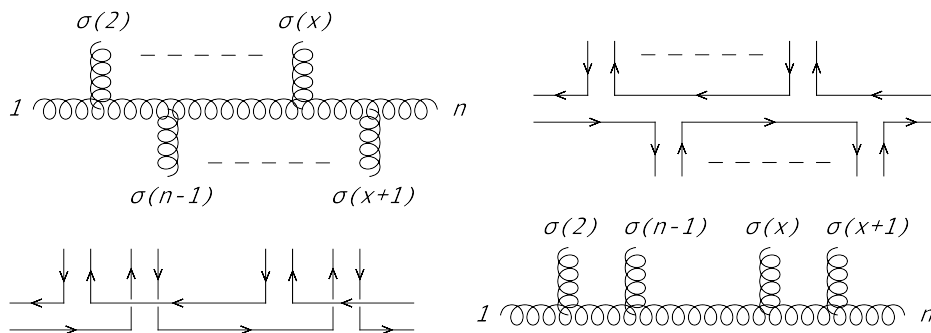


Figure 2.7: Graphical depiction of the multiperipheral basis that can be used in the color decomposition of gluonic amplitudes. In this basis two of the n gluons can be held fixed and the permutations over gluon indices are only over the remaining $(n - 2)$ gluons. In the diagrams the gluons 1 and n form a distinct pair of indices between which a unique gluon-strand can be spanned. From this gluon-strand the other $(n - 2)$ gluons are radiated in $(n - 2)!$ different cyclic orderings.

the fundamental basis color decomposition. Since the basis in equation 2.37 relies directly on the structure constants, which encode both color flows in a three-gluon vertex simultaneously, it is evident that using this basis and the reduced set of associated partial amplitudes suffices for the color decomposition of n -gluon tree-level amplitudes, or generally for any amplitude that involves only gluonic interactions for that matter.

2.5 One-Loop Color Decomposition

After the discussion of color decomposition at the tree-level we will now turn to the discussion of color decomposition at the one-loop level. A first suggestion towards the possible color basis of gauge amplitudes at the one-loop level, by contracting the legs of tree-level amplitudes, was suggested in [113]. In the one-loop sector the literature tells us how to perform the color decomposition for n -gluon amplitudes [114–116, 118, 119] and for gauge amplitudes with n gluons and $m = 1$ quark-antiquark pairs [117], where closed formulae have been given in these cases. For $m > 1$ quark-antiquark pairs little can be found and if, then mostly in the application to specific processes [122, 69, 123] or in reviews [76, 77].

Any one-loop amplitude can as well be decomposed into a purely gauge theoretical part and a purely kinematical part. The agreement between cyclic ordering and color ordering, as given at the tree-level, is thereby not apparent anymore. The basic gauge invariant building blocks are not the partial amplitudes anymore, which are defined to be the kinematical factors that

multiply a specific product of color antennae, but rather the so called primitive amplitudes. Primitive amplitudes are sets of diagrams with the same cyclic ordering of the external legs and are usually represented by corresponding top-level or representative diagrams. The one-loop partial amplitudes are then generically expressed as linear combinations of several primitive amplitudes with different cyclic orderings, i.e. several primitive amplitudes with different cyclic orderings may contribute to the same color coefficient, quite in contrast to the tree-level case. This is naturally expressed as

$$\mathcal{A}^{(1)} = \sum_i C_i A_i^{(1)} = \sum_i C_i \sum_j F_{ij} B_j \quad (2.39)$$

where the $A_i^{(1)}$ are one-loop partial amplitudes to specific color orderings i and the B_j are the primitive amplitudes with specific cyclic orderings j . The matrix F_{ij} states thereby the linear relations, which connect several primitive amplitudes with different cyclic orderings j to a specific color ordering i . For the case of pure n -gluon one-loop amplitudes and one-loop amplitudes with one external quark-antiquark pair and multiple gluons, these relations are known and have been given in closed Formulae [117].

Recently there has been some development towards the decomposition of amplitudes with multiple quark-antiquark pairs [120], which is the formal extension of the ideas in [69, 77]. This new method relies on the intermediate use of Feynman diagrams, to establish the relations between one-loop partial amplitudes and primitive amplitudes, but unfortunately there are no closed all- n formulae at the core of this new method, as in the style of [117] for the $m = 1$ case. Nevertheless is the method very applicable in multi-parton calculations at the one-loop level and has found further application in [123, 73].

We would like to complement the methods for color decomposition at the one-loop level in this regard and introduce a new method, which can be used to derive relations between the partial amplitudes and the primitive amplitudes without the need to use Feynman diagrams and to solve a therefrom intermediately established linear system of equations.

In order to become familiar with one-loop color decomposition we would like to comment on one-loop color decomposition in the case of gluon one-loop amplitudes and one-loop amplitudes with one external quark-antiquark pair and multiple gluons first, in the next two subsections 2.5.1 and 2.5.2. For a more intuitive presentation we will thereby use the expansion in the

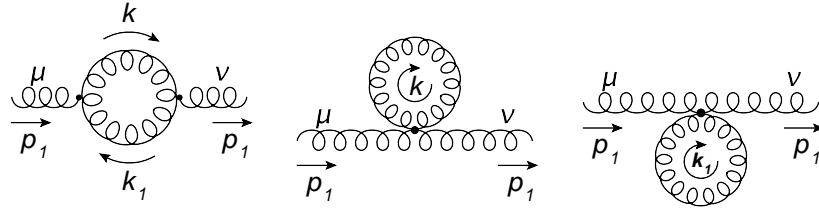


Figure 2.8: The left-most color-stripped diagram represents the top-level or representative diagram to the pure gluonic [1]-part of a one-loop gluon primitive amplitude with two external gluons. We can pinch gluon propagators in the loop in two possible ways in order to get the two color-stripped diagrams on the right. The corresponding primitive amplitude includes then all three color-stripped diagrams.

fundamental basis for the decomposition formulae. To translate this into the color-flow basis, however, one has simply to apply the rules discussed in section 2.2. Subsequently we would like to comment on the method in [120, 73] to color decompose amplitudes with multiple quark-antiquark pairs before we introduce our new method in subsection 2.5.3.

To this end we want to note two things. Firstly: Any one-loop amplitude can generically be separated into a n_f -part, which contains a closed fermion loop, and a mixed part, where the loop contains gluons as well as fermions

$$\mathcal{A}^{(1)} = \mathcal{A}^{(1),[1]} + \mathcal{A}^{(1),[1/2]} \quad (2.40)$$

Here we have chosen a common convention which denotes the n_f -part by a superscript [1/2] and the parts with pure gluonic or mixed particle content in the loop by [1]. In a theory which contains also a scalar particle, we can have pure scalar-loops as well. In the following we will not consider any scalar contributions and we will drop the superscripts (1), denoting the explicit one-loop contribution, for notational simplicity.

Secondly: Each primitive amplitude can be represented uniquely by a respective top-level or representative diagram, with the maximum possible number of propagators in the loop and only three-valent vertices [117, 69, 120]. All other diagrams that contribute to a given primitive amplitude can be constructed from the respective top-level diagram by pinching propagators from the loop and pulling out trees whenever necessary. This is exemplarily shown in figures 2.8 and 2.9. The whole set of diagrams to a primitive amplitude can again be constructed very efficiently with the help of recurrence relations, which will be discussed in chapter 4.

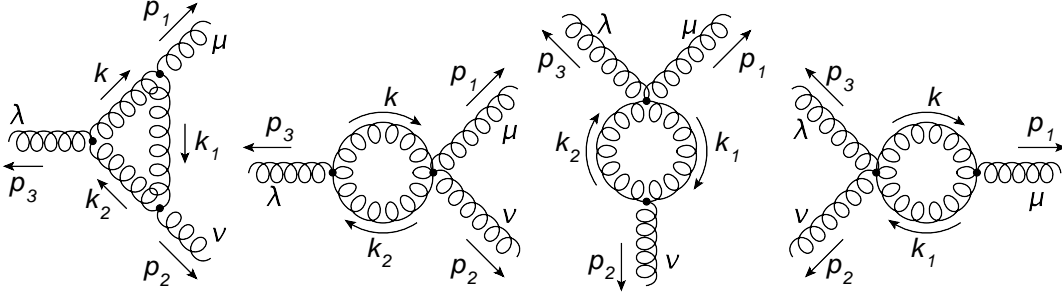


Figure 2.9: The left-most color-stripped diagram represents the top-level or representative diagram to the pure gluonic [1]-part of a one-loop gluon primitive amplitude with three external gluons. In a first step we can pinch gluon propagators in the loop in three possible ways in order to get the three color-stripped diagrams on the right. In subsequent steps each of those three diagrams on the right can further be pinched, which yields diagrams with bubbles and tadpoles on the three legs. The corresponding primitive amplitude includes then all those color-stripped diagrams.

2.5.1 One-Loop Gluon Amplitudes

One-loop color decomposition was first discussed in the context of pure unbroken Yang-Mills theories [114–116], where the connection to super Yang-Mills amplitudes and string amplitudes has been noted. The color decomposition for the n -gluon amplitudes in the fundamental basis, without the n_f -part, is given by

$$\begin{aligned}
 \mathcal{A}_n^{[1]} &= g_s^n \sum_{c=1}^{\lfloor \frac{n}{2} \rfloor - 1} \sum_{\sigma \in S_n / S_{n;c}} \text{Tr}(T^{a_{\sigma(1)}} \dots T^{a_{\sigma(c-1)}}) \text{Tr}(T^{a_{\sigma(c)}} \dots T^{a_{\sigma(n)}}) A_{n;c}^{[1]}(\sigma(1), \dots, \sigma(n)) \\
 &= g_s^n N_c \sum_{\sigma \in S_n / \mathbb{Z}_n} \text{Tr}(T^{a_{\sigma(1)}} \dots T^{a_{\sigma(n)}}) A_{n;1}^{[1]}(\sigma(1), \dots, \sigma(n)) \\
 &\quad + g_s^n \sum_{c=2}^{\lfloor \frac{n}{2} \rfloor - 1} \sum_{\sigma \in S_n / S_{n;c}} \text{Tr}(T^{a_{\sigma(1)}} \dots T^{a_{\sigma(c-1)}}) \text{Tr}(T^{a_{\sigma(c)}} \dots T^{a_{\sigma(n)}}) A_{n;c}^{[1]}(\sigma(1), \dots, \sigma(n))
 \end{aligned} \tag{2.41}$$

Here we have used $\text{Tr}(\mathbb{1}) = N_c$ in the second line, which yields the leading color contributions to the n -gluon amplitude for $c = 1$. The subleading parts are given for $c \geq 2$. The sums are over all partitions to distribute an ordered set of n gluons among the two traces and for each partition over all permutations S_n of the members of the ordered set of n gluons, without the subset $S_{n;c} \subset S_n$ of those permutations that leave the trace structure invariant for that particular partition. This double sum generates clearly all possible distinguishable color flows. The

2.5 One-Loop Color Decomposition

sum over the possible partitions is up to $\lfloor \frac{n}{2} \rfloor - 1$, where $\lfloor x \rfloor$ denotes the greatest integer less or equal to x , and $c = \lfloor \frac{n}{2} \rfloor, \dots, n$ would only generate the same double-trace structure again.

The possible color flows can graphically be depicted by annulus or ring diagrams as shown in figure 2.10, where our convention is such that the inner ring in the color-flow double-ring diagram depicts the first trace and the outer ring the second trace. These double-ring diagrams are gained from tree-level multiperipheral diagrams, described in section 2.2, if we sew together the two gluons 1 and n , which are held fixed in the multiperipheral diagrams, via $\delta^{a_1 a_n}$ or $\delta_{i_1 \bar{j}_n} \delta_{i_n \bar{j}_1}$ in the double-line formalism of the color-flow basis, where the $-1/N_c$ -terms from the Fierz identity cancels for pure gluon interactions. The various partitions and permutations of the double-ring diagram reflect the simple fact that every three-gluon vertex in the respective Feynman diagram contributes with two different color flows (see appendix A), which has of course to be attributed for in the color decomposition formula.

Just as in the case of the multiperipheral diagrams at tree-level, we can also associate at the one-loop level representative diagrams of primitive amplitudes with a certain cyclic ordering to any given color-flow double-ring diagram, by flipping the gluon color double-lines in color-flow double-ring diagrams from the inside to the outside. If we flip the inner gluon color double-lines in the color-flow double-ring diagram on the left of figure 2.10 to the outside and define the first particle in the cyclic ordering to be the gluon with number 1, then this can be related for example to the primitive amplitude $A_{n;c}^{[1]}(1, c, (c-1), (c+1), 3, (c+2), 2, n)$ represented by the diagram with the cyclic ordering $(1, c, (c-1), (c+1), 3, (c+2), 2, n)$ on the right of figure 2.10. However, we also have to take into account all other cyclic orderings that contribute to this color flow. These are given by all permutations of the members of the set $\{1, c, (c-1), (c+1), 3, (c+2), 2, n\}$, with e.g. gluon n held fixed, that preserve the cyclic ordering between the members of the set $\{c-1, \dots, 3, 2, 1\}$ and between the members of the set $\{c, c+1, c+2, \dots, n\}$, while allowing for all relative orderings of the members of one set with respect to the members of the other set. In other words in the color-flow double-ring diagram we can revolve the external gluons associated to the inner ring and the external gluons associated to the outer ring independently as long as we keep the ordering of the gluons within each of the rings fixed. Since the reading direction is always against the color-flow arrow this yields a reversed cyclic ordering of the gluons on the inner ring, if flipped to the outside, with respect to the gluons on the outer ring, as depicted in figure 2.10.

Consider the case for $n = 4$ and $c = 1$, which describes the leading color contribution to $\mathcal{A}_4^{[1]}$.

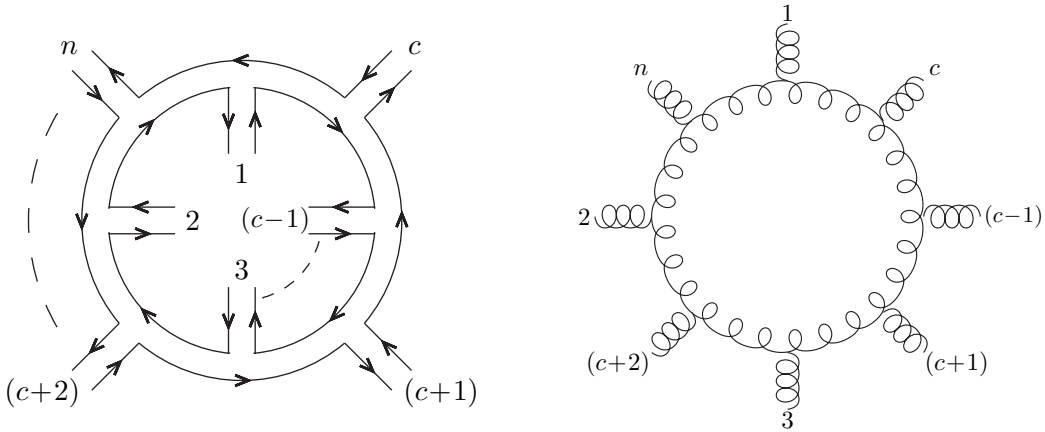


Figure 2.10: Left: Color-flow double-ring diagram associated to $\text{Tr}(T^{a_{\sigma(1)}} \dots T^{a_{\sigma(c-1)}}) \text{Tr}(T^{a_{\sigma(c)}} \dots T^{a_{\sigma(n)}})$ in a purely gluonic one-loop amplitude. The two color rings can be revolved with respect to each other. If we hold gluon n fixed we can revolve or cyclically shuffle the gluon color double-lines on the inner ring with respect to the gluon color double-lines on the outer ring in such a way that each relative position of the gluons from the inner ring with respect to the gluons from the outer ring is generated, while respecting the ordering of the gluons within each ring. If flipped to the outside there are $c - 1$ gluon color double-lines on the closed inner ring which emanate to the left with respect to the color-flow line and generate each a relative minus sign. Right: If we take the specifically depicted ordering of the gluon legs in the left diagram with respect to each other seriously and flip the gluon legs on the inner color ring to the outside, then we can relate this to the top-level representative diagram for the primitive amplitude $A_{n,c}^{[1]}(1, c, (c-1), (c+1), 3, (c+2), 2, n)$. In order to generate all possible diagrams associated to $\text{Tr}(T^{a_{\sigma(1)}} \dots T^{a_{\sigma(c-1)}}) \text{Tr}(T^{a_{\sigma(c)}} \dots T^{a_{\sigma(n)}})$ we have to draw the top-level diagrams for every allowed ordered set of gluon permutations that can be generated from the color-flow double-ring diagram on the left.

2.5 One-Loop Color Decomposition

In this case the color flow is such that in the double-ring color-flow diagram all four gluons are on the outer ring. The inner ring is given by a closed color-flow line, which generates a factor $Tr(\mathbb{1}) = N_c$. With gluon $n = 4$ held fixed all the possible distinguishable color flows that can be generated in the leading color contribution are given by the $(n - 1)! = 3!$ non-cyclic permutations of the external gluon legs. To each of those permutations there exists exactly one primitive amplitude, with a specific cyclic ordering that corresponds exactly to the given color ordering. All diagrams that can be generated by pinching from the associated representative diagram have the same cyclic ordering and contribute to the same color flow. This is different for the subleading contributions for $c \geq 2$.

Assume $n = 4$ and $c = 2$. In that case there is one gluon associated with the inner ring in the color-flow double-ring diagram in figure 2.10 and three gluons associated with the outer ring. Let us assume $\sigma = id$, then the gluon 1 is associated with the inner ring and the gluons 2, ..., 4 are associated with the outer ring. Although $Tr(T^a) = 0$ this will be a worthwhile example to study. One primitive amplitude that corresponds to this color flow is $A_4^{[1]}(1, 2, 3, 4)$, however, with a relative minus sign due to the "flipped" color-flow as explained in appendix A. Our convention will be that every gluon color double-line, if all are flipped to the outside in the respective color-flow double-ring diagram, which is directly radiated to the left with respect to a fundamental color-flow arrow receives a relative minus sign. If we look now at all the diagrams that are generated from the respective top-level diagram we discover for example one diagram, where gluon 1 is directly connected to gluon 4 through a color-stripped tree-level three-gluon vertex in the cyclic order $(\dots, 4, 1, \dots)$. This diagram has obviously the wrong color flow and must be absent from the set of diagrams that multiply the specific color factor at hand. There are two options to exclude this diagram. One option is to explicitly veto the said diagram, which however would leave behind a set of diagrams that is no longer gauge invariant. The other option is to add to the primitive amplitude $A_4^{[1]}(1, 2, 3, 4)$ another primitive amplitude $A_4^{[1]}(2, 3, 1, 4)$ with a different cyclic ordering. If we look at all the diagrams of the other set then, there is one where gluon 1 is again directly connected to gluon 4, this time in the cyclic ordering $(\dots, 1, 4, \dots)$ but otherwise identical. The two diagrams cancel due to the antisymmetry of the color-stripped three-gluon tree-level vertex upon permutation of any two of the three legs. Through the pinching process there might also be a diagram where for example the gluons 1, 2 and 3 are connected via a color-stripped four-gluon vertex in the cyclic ordering $(\dots, 1, 2, 3, \dots)$. These also yield a wrong color flow and need to be canceled by similar diagrams with the cyclic orderings $(\dots, 2, 1, 3, \dots)$ and $(\dots, 2, 3, 1, \dots)$ as seen from the antisymmetry properties of the color-stripped four-gluon vertex (appendix A). If we consider the

sum $A_{4;2}^{[1]}(1, 2, 3, 4) = A_4^{[1]}(1, 2, 3, 4) + A_4^{[1]}(2, 1, 3, 4) + A_4^{[1]}(2, 3, 1, 4)$ we note that all diagrams that contribute to a wrong color flow cancel and we are left with exactly all the diagrams that contribute exclusively to the subleading color factor $Tr(T^1)Tr(T^2T^3T^4)$.

This behavior generalizes trivially in the case of n gluons, where the leading contributions are given by

$$A_{n;1}^{[1]}(1, 2, \dots, n) = A_n^{[1]}(1, 2, \dots, n) \quad (2.42)$$

and the subleading contributions by

$$A_{n;c \geq 2}^{[1]}(1, 2, \dots, c-1; c, c+1, \dots, n) = (-1)^{c-1} \sum_{COP\{\alpha\}\{\beta\}} A_n^{[1]}(1, 2, \dots, n) \quad (2.43)$$

with $\{\alpha\} = \{c-1, \dots, 2, 1\}$ and $\{\beta\} = \{c, c+1, \dots, n\}$. $COP\{\alpha\}\{\beta\}$ is the cyclic ordered product between $\{\alpha\}$ and $\{\beta\}$, also called merging or shuffle, which denotes all permutations of the members in the ordered list $\{1, 2, \dots, n\}$, with n held fixed, that preserve the cyclic ordering of the $\alpha_i \in \{\alpha\}$ within $\{\alpha\}$ and the cyclic order of the $\beta_i \in \{\beta\}$ within $\{\beta\}$, while allowing for all relative orderings of the α_i with respect to the β_i . This is the one-loop equivalent to the Kleiss–Kuijff relations at tree-level. The general rule for diagrams which are not allowed due to wrong color assignment is that members of the set $\{\alpha\}$ and members of the set $\{\beta\}$ may never be directly connected through a color-stripped three- or four-valent vertex. These diagrams cancel exactly in the shuffle sum as described above, since there are always combinations which fulfill the necessary antisymmetry relations of the three- and four-valent vertices.

The subleading part for $c = 2$ can be set to zero due to $Tr(T^a) = 0$, which leads subsequently to

$$\begin{aligned} 0 &= A_{n;2}^{[1]}(1; 2, 3, \dots, n) = - \sum_{COP\{1\}\{2,3,\dots,n\}} A_n^{[1]}(1, 2, \dots, n) \\ &= -A_n^{[1]}(1, 2, \dots, n) - A_n^{[1]}(2, 1, 3, \dots, n) - A_n^{[1]}(2, 3, 1, \dots, n) - \dots - A_n^{[1]}(2, 3, \dots, 1, n) \end{aligned} \quad (2.44)$$

This is just the photon decoupling identity for one-loop n -gluon primitive amplitudes $A_n^{[1]}$, which reads

$$A_n^{[1]}(1, 2, \dots, n) = -A_n^{[1]}(2, 1, 3, \dots, n) - A_n^{[1]}(2, 3, 1, 4, \dots, n) - \dots - A_n^{[1]}(2, 3, 4, \dots, n-1, 1, n) \quad (2.45)$$

Thus, we can express one of the $(n-1)$ primitive amplitudes for a certain gluon permutation σ as linear combination of the other $(n-2)$ primitive amplitudes for that specific gluon permutation.

In order to complete the color decomposition for n -gluon amplitudes we have to consider the n_f -part as well, which is given by

$$\mathcal{A}_n^{[1/2]} = g_s^n n_f \sum_{\sigma \in S_n / \mathbb{Z}_n} \text{Tr}(T^{a_{\sigma(1)}} \dots T^{a_{\sigma(n)}}) A_{n;1}^{[1/2]}(\sigma(1), \dots, \sigma(n)) \quad (2.46)$$

where $A_{n;1}^{[1/2]}(\sigma(1), \dots, \sigma(n))$ contains all diagrams with a closed fermion loop and a cyclic ordering $(\sigma(1), \dots, \sigma(n))$ of the external gluon legs, and S_n / \mathbb{Z}_n denotes all non-cyclic permutations of n gluons that leave the trace invariant. The color flow for the n_f -part is the same as for the leading color part, which can be seen from the fact that only $U(N_c)$ -gluons can couple to the fermion loop. The n_f -part is thus usually accounted for together with the leading color part.

Last but not least we note that the adjoint basis introduced at the end of section 2.4 has also been used for the decomposition of one-loop gluon amplitudes, however only for the non- n_f part [119].

2.5.2 One-Loop Amplitudes with Gluons and One Quark-Antiquark Pair

The color decomposition for QCD amplitudes with one quark-antiquark pair and multiple gluons has been known for a while by now [117]. In contrast to the n -gluon case one of the trace factors, or closed color strings, from the double-trace structure is basically replaced by a color antenna, or open color string, where gluons are radiated between the (anti-)fundamental indices of the external quark-antiquark pair. In [117] the various color factors and associated combinations of primitive amplitudes have been derived by studying the similarities to super Yang-Mills amplitudes with two gluinos and $(n-2)$ gluons. Adjoint representation gluinos, which carry naturally two fundamental color-flow lines can thereby be turned into fundamental representation quarks upon the appropriate removal of one of the color-flow lines. In the process one of the traces cuts open, simply speaking, and the color decomposition is subsequently derived to read

$$\mathcal{A}_n(\bar{q}_1, q_2, g_3, \dots, g_n) = g_s^n \sum_{c=1}^{n-1} \sum_{\sigma \in S_{n-2}/S_{n;c}} Gr_{n;c}(\sigma(3), \dots, \sigma(n)) A_{n;c}(1_{\bar{q}}, 2_q; \sigma(3), \dots, \sigma(n)) \quad (2.47)$$

where

$$Gr_{n;c}(\sigma(3), \dots, \sigma(n)) \equiv Tr(T^{a_{\sigma(3)}} \dots T^{a_{\sigma(c+1)}}) [T^{a_{\sigma(c+2)}} \dots T^{a_{\sigma(n)}}]_{i_2 \bar{j}_1} \quad (2.48)$$

and σ denotes again all permutations of gluon indices such that the trace is left invariant. We normalize again to $Tr(\mathbf{1}) = N_c$ and whenever there is no fundamental generator matrix between the fundamental indices of an open color string we put a Kronecker delta instead. For clarification we note the special cases

$$\begin{aligned} Gr_{n;1}(\sigma(3), \dots, \sigma(n)) &= N_c [T^{a_{\sigma(3)}} \dots T^{a_{\sigma(n)}}]_{i_2 \bar{j}_1} \\ Gr_{n;2}(\sigma(3), \dots, \sigma(n)) &= 0, \quad \text{due to } Tr(T^a) = 0 \\ Gr_{n;n-1}(\sigma(3), \dots, \sigma(n)) &= Tr(T^{a_{\sigma(3)}} \dots T^{a_{\sigma(n)}}) \delta_{i_2 \bar{j}_1} \end{aligned} \quad (2.49)$$

In contrast to the n -gluon case we can now have contributions from $U(1)$ -gluons, if the two ends of a gluon propagator in the loop connect to the same quark line. The partial amplitudes for the leading case ($c = 1$) and the subleading cases ($c \geq 2$), including the n_f -parts, are then for a specific gluon permutation given by

$$A_{n;1}(1_{\bar{q}}, 2_q; 3, \dots, n) = A_n^{L,[1]}(1_{\bar{q}}, 2_q, 3, \dots, n) - \frac{1}{N_c^2} A_n^{R,[1]}(1_{\bar{q}}, 2_q, 3, \dots, n) + \frac{n_f}{N_c} A_n^{L,[1/2]}(1_{\bar{q}}, 2_q, 3, \dots, n) \quad (2.50)$$

and

$$\begin{aligned} A_{n;c \geq 2}(1_{\bar{q}}, 2_q; 3, \dots, c+1; c+2, \dots, n) &= (-1)^{c-1} \sum_{COP\{\alpha\}\{\beta\}} A_n^{L,[1]}(1_{\bar{q}}, 2_q, 3, \dots, n) \\ &+ (-1)^{c-1} \sum_{COP\{\alpha\}\{\beta\}} \left(-\frac{n_f}{N_c} \right) A_n^{R,[1/2]}(1_{\bar{q}}, 2_q, 3, \dots, n) \end{aligned} \quad (2.51)$$

with $\{\alpha\} = \{c+1, \dots, 4, 3\}$ and $\{\beta\} = \{1, 2, c+2, c+3, \dots, n\}$. $COP\{\alpha\}\{\beta\}$ is the cyclic ordered product between $\{\alpha\}$ and $\{\beta\}$, which denotes all permutations of the members of the

2.5 One-Loop Color Decomposition

list $\{1, 2, \dots, n\}$ with 1 held fixed, that preserve the cyclic ordering of the $\alpha_i \in \{\alpha\}$ within $\{\alpha\}$ and the cyclic order of the $\beta_i \in \{\beta\}$ within $\{\beta\}$, while allowing for all relative orderings of the α_i with respect to the β_i . Note that in equation 2.50, which constitutes the leading part, we also find contributions that are formally subleading in $1/N_c$. Since they multiply to the same color–flow string, however, they are usually accounted for together with the real leading color contribution.

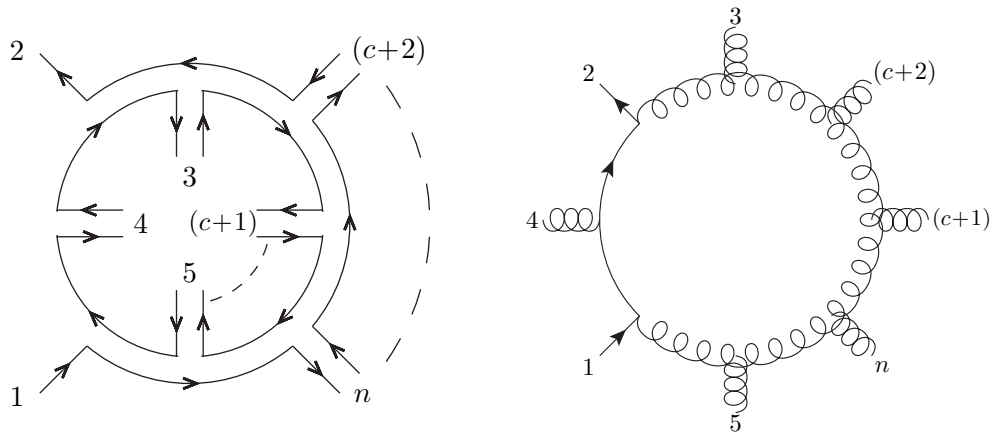


Figure 2.11: Left: Color–flow double–ring diagram associated to $\text{Tr}(T^{a_{\sigma(3)}} \dots T^{a_{\sigma(c+1)}}) [T^{a_{\sigma(c+2)}} \dots T^{a_{\sigma(n)}}]_{i_2 \bar{j}_1}$ in a one–loop amplitude with one quark–antiquark pair. The closed and the open ring can be revolved with respect to each other. If we hold the antiquark 1 fixed we can revolve or shuffle the gluon color double–lines on the inner closed ring with respect to the gluon color double–lines on the outer open arc in such a way that each relative position of the gluons from the closed ring with respect to the gluons from the open arc is generated, while respecting the ordering of the gluons within the closed ring and the ordering of the fermions and the gluons within the arc. If flipped to the outside there are $(c - 1)$ gluon color double–lines on the closed ring which emanate to the left with respect to the color–flow line and generate each a relative minus sign. Right: If we take the specifically depicted ordering of the gluon legs in the left diagram with respect to each other seriously and flip the gluon color double–lines on the inner color ring to the outside, then we can relate this to the representative diagram for the primitive amplitude $A_n^{L,[1]}(1, 4, 2, 3, (c + 2), (c + 1), n, 5)$. In order to generate all possible representative diagrams associated to $\text{Tr}(T^{a_{\sigma(3)}} \dots T^{a_{\sigma(c+1)}}) [T^{a_{\sigma(c+2)}} \dots T^{a_{\sigma(n)}}]_{i_2 \bar{j}_1}$ we have to draw the top–level diagrams for every allowed ordered set of permutations that can be generated from the color–flow double–ring diagram on the left.

It is instructive again to look at the associated color–flow double–ring diagram for the mixed contribution, which will be somewhat different from the one for the n –gluon case but works

essentially in the same way and is shown in figure 2.11. We note that the fermion line which connects \bar{q}_1 and q_2 turns left with respect to the fermion-flow arrow upon entering the loop. A left-router primitive amplitude, denoted by $A^{L,[j]}$, contains thereby all diagrams of the same cyclic ordering where the quark line turns left upon entering the loop, which yields a gauge invariant subset of diagrams. Correspondingly are right-router primitive amplitudes defined as gauge invariant subsets of all the diagrams with a specific cyclic ordering of the external legs and where the fermion lines turn right upon entering the loop. The superscript $[j]$ denotes again the particle content in the loop, where $[1/2]$ denotes the gauge invariant subset of diagrams with a closed fermion loop and $[1]$ denotes the subset of diagrams with only gluons or mixed particle content in the loop, for which we have just described the additional property of fermion-routing. We can have diagrams, where the fermion line is attached to the loop via a tree-level like sub-diagram. In this case we denote the fermion line with routing L if it passes to the left of the loop and with routing R if it passes to the right of the loop with respect to its fermion-flow arrow. In general the primitive amplitudes of different routing information are related to each other by a reflection identity

$$\begin{aligned} A_n^{R/L,[j]}(1_{\bar{q}}, 3, 4, \dots, 2_q, \dots, n-1, n) &= (-1)^{n-2} A_n^{L/R,[j]}(n, n-1, \dots, 2_q, \dots, 4, 3, 1_{\bar{q}}) \\ &= (-1)^{n-2} A_n^{L/R,[j]}(1_{\bar{q}}, n, n-1, \dots, 2_q, \dots, 4, 3) \end{aligned} \quad (2.52)$$

where cyclic invariance has been used in order to keep the antiquark 1 at the first position in the list of arguments.

Concentrating on the non- n_f contribution we can see from figure 2.11 how the leading and the subleading parts come about. The leading contribution for $c = 1$ is given by all those primitive amplitudes that contribute to the color flow string $[T^{a_{\sigma(3)}} \dots T^{a_{\sigma(n)}}]_{i_2 \bar{j}_1}$, where in the associated color-flow double-ring diagrams no gluon color double-line is attached to the closed ring. For a certain gluon permutation σ we have thereby on the one hand the left-router primitive amplitude $A_n^{L,[1]}(1, 2, 3, \dots, n)$, where the factor $Tr(\mathbb{1}) = N_c$ is generated explicitly through the closed fundamental color line of the inner ring. On the other hand, however, there is another class of diagrams which can contribute to the same color-flow string, which is given by the primitive amplitude $A_n^{L,[1]}(1, n, n-1, \dots, 4, 3, 2)$, where the fermion line is still left-routing upon entering the loop but all gluons are now radiated to the left and in reversed order from the fermion line in the corresponding representative diagram. We note that this generates a relative minus sign $(-1)^{n-2}$. If we look at the color flow of this diagram upon replacing the one gluon propagator in the loop by a $U(1)$ -gluon we note that this also generates the color-flow string

2.5 One-Loop Color Decomposition

$[T^{a_{\sigma(3)}} \dots T^{a_{\sigma(n)}}]_{i_2 \bar{j}_1}$ but with a factor $-1/N_c$ instead of a factor N_c in front. Upon factoring out an overall factor N_c and using the reflection identity in equation 2.52 this leads to the contribution proportional to $-1/N_c^2$ in equation 2.50. Similar considerations lead to the n_f -contribution in equation 2.50.

The subleading contribution is similarly explained as in the n -gluon case. Imagine $n = 4$ and $c = 2$, and $\sigma = id$. Then there are three primitive amplitudes that contribute in general to the subleading color factor $Tr(T^3)[T^4]_{i_2 \bar{j}_1}$, i.e. $A_4^{L,[1]}(1, 3, 2, 4) + A_4^{L,[1]}(1, 2, 3, 4) + A_4^{L,[1]}(1, 2, 4, 3)$. Looking at $A_4^{L,[1]}(1, 3, 2, 4)$ we note that the corresponding set of diagrams contains for example a diagram where the gluon 3 is directly connected to the quark 2 via a color-stripped quark-gluon vertex in the cyclic order $(\dots, 3, 2, \dots)$. This diagram contributes obviously to the wrong color flow and needs to be canceled. The cancellation occurs if we add the primitive amplitude $A_4^{L,[1]}(1, 2, 3, 4)$, which contains a diagram where again the gluon 3 is directly connected to the quark 2, this time in the cyclic order $(\dots, 2, 3, \dots)$ but otherwise identical. Upon the antisymmetry of the color-stripped quark-gluon vertex with respect to the exchange of any two of the legs, as explained in appendix A, as well as of the corresponding color-flow rule the two diagrams cancel. In general the same rule holds as does for the n -gluon case, i.e. all diagrams need to cancel that connect members from a set $\{\alpha\}$ and members from a set $\{\beta\}$ directly through a three- or four-valent color-stripped tree-level vertex, where the two sets are simply determined from the closed ring and the open arc respectively. This is exactly fulfilled by the sum $A_4^{L,[1]}(1, 3, 2, 4) + A_4^{L,[1]}(1, 2, 3, 4) + A_4^{L,[1]}(1, 2, 4, 3)$, where all the unwanted diagrams cancel and we are left exactly with all the diagrams that contribute exclusively to the subleading color factor $Tr(T^3)[T^4]_{i_2 \bar{j}_1}$. The generalization for arbitrary n and $c \geq 2$ leads again to the Kleiss-Kuijff type relations of equation 2.51, which expresses one-loop partial amplitudes to specific subleading color-flow strings as linear combinations of several primitive amplitudes with different cyclic orderings. In the case of $c = 2$ we can thereby again derive a decoupling equation, which reads

$$A_4^{L,[1]}(1, 3, 2, 4, \dots, n) = -A_4^{L,[1]}(1, 2, 3, 4, \dots, n) - A_4^{L,[1]}(1, 2, 4, 3, \dots, n) - \dots - A_4^{L,[1]}(1, 2, 4, \dots, n, 3) \quad (2.53)$$

2.5.3 One-Loop Amplitudes with Gluons and Multiple Quark-Antiquark Pairs

The color decomposition for more than one quark-antiquark pair and multiple gluons is rather involved and there is no corresponding closed formula in the modern literature that establishes relations between partial and primitive amplitudes in the style of the above given formulas for

the cases of external gluons only or with one external quark–antiquark pair.

Methods to find relations between cyclically ordered primitive amplitudes and color–ordered one–loop partial amplitudes have been devised by taking the detour of establishing the desired inverted relations for a fixed number of particles by exploring the color factors of appropriately chosen Feynman diagrams and subsequently inverting these relations [69, 77, 120, 123, 73]. We will briefly discuss these methods and then continue to describe an alternative method that comes about without taking this detour via Feynman diagrams and rather relies on classes of double–ring type diagrams and appropriately chosen shuffle relations in each class. The method can be used to establish closed formulae for fixed numbers of distinguishable quark–antiquark pairs but for an arbitrary number of gluons in each case. The case for flavor–like quark–antiquark pairs can be retrieved by proper antisymmetrization as described in chapter 2.2.

First we note that the general color decomposition formula in terms of partial amplitudes is trivially generalized for multiple quark–antiquark pairs, where we can write

$$\begin{aligned}
 \mathcal{A}_n^{(1)}\left(1_{\bar{q}_1}, 2_{q_1}, 3_{\bar{q}_2}, 4_{q_2}, \dots, (2m-1)_{\bar{q}_m}, (2m)_{q_m}; (2m+1), \dots, n\right) = \\
 g_s^n \sum Tr\left(T^{a_{\sigma(2m+1)}}, T^{a_{\sigma(c_1+2m-1)}}\right) \left[T^{a_{\sigma(c_1+2m)}}, T^{a_{\sigma(c_1+c_2+2m-2)}}\right]_{i_{\pi(2)\bar{1}}} \times \dots \\
 \dots \times \left[T^{a_{\sigma(c_1+\dots+c_m+(2m-(m-1)))}}, T^{a_{\sigma(n)}}\right]_{i_{\pi(2m)\bar{J}(2m-1)}} \times \\
 \times A_{n; (c_1, c_m)}^{(1)}\left(\sigma(2m+1, c_1+2m-1); \pi(2_{q_1}), \sigma(c_1+2m, c_1+c_2+2m-2), 1_{\bar{q}_1}; \dots \right. \\
 \left. \dots; \pi((2m)_{q_m}), \sigma(c_1+\dots+c_m+(2m-(m-1))), n), (2m-1)_{\bar{q}_m}\right)
 \end{aligned} \tag{2.54}$$

and where

$$\begin{aligned}
 \sum \equiv \sum_{\substack{c_1=1, n-(2m-1) \\ c_2=1, n-(c_1+2m-2) \\ \vdots \\ c_m=1, n-(c_1+\dots+c_{m-1}+2m-m)}} \sum_{\pi \in P_m} \sum_{\sigma \in S_{n-2m}/S_{(n-2m; c_1)}}
 \end{aligned} \tag{2.55}$$

The indices on the (anti–)quarks denote quark lines between specific quark–antiquark pairs,

which we take as being all distinct for the moment. The shorthand notation (a, z) denotes the list (a, b, \dots, z) . The sums above simply generate all possible distinct products of color antennae that can occur in one-loop QCD amplitudes multiplied by the respective partial amplitudes. The partial amplitudes are again the sets of all those color-stripped diagrams whose corresponding Feynman diagrams give rise to the same color flows or products of color antennae, i.e. all diagrams of the same color ordering. The notation in the list of arguments inside a partial amplitude $A_{n;(j_1, j_m)}^{(1)}(\dots)$ is thereby inferred from the corresponding product of color antennae that it multiplies.

Due to the additional internal degrees of freedom, introduced by the loop, several primitive amplitudes with different cyclic orderings of the external legs may contribute to the same product of color antennae, as we saw for the leading as well as subleading contributions in the case of one quark-antiquark pair or in general for the subleading contributions already in the case of external gluons only. And as in the case for $m = 0$ and $m = 1$ quark-antiquark pairs we want to express the color-ordered partial amplitudes in the case of $m = 2$ quark-antiquark pairs as linear combinations of cyclically ordered one-loop primitive amplitudes. However, for multiple quark-antiquark pairs closed formulae, as in the case for $m = 0$ and $m = 1$ quark-antiquark pairs, have not been given so far in the modern literature.

The primitive amplitudes in this case can be similarly classified by the cyclic ordering of the external legs and the routing information of each fermion line with respect to the loop, i.e. also in the case for multiple quark-antiquark pairs all the diagrams that contribute to a specific primitive amplitude form a gauge invariant subset and have again the same cyclic ordering in the external legs and the same routing of the external fermions with respect to the loop. Primitive amplitudes in this case can again be represented by top-level or representative diagrams, where all external particles are directly attached to the loop and only via three-valent vertices. All other diagrams can then be generated from the representative diagrams by a continuous pinching process and pulling out trees, as described in the introduction to this chapter. In problems with more than one quark-antiquark pair, however, there exist primitive amplitudes, where tree-level parts are branched off at the level of the representative diagram already. These are primitive amplitudes with a representative diagram, where an external fermion line in a specific cyclic ordering and with a specific routing is not allowed to enter the loop and is therefore branched off via a gluon that connects this tree-level part to a fermion line in the loop. In the literature [69, 77, 73] these situations are usually represented by effective "dummy" propagators in those places where no fundamental vertex-propagator combination can be inserted to form a top-level

diagram, such that all the external particles can again directly be attached to the loop through three-valent vertices. We find it useful, however, to resolve the tree-level like sub-diagrams directly and will thus in the following exclusively use the term "representative" diagram instead of "top-level" diagram, due to the misleading nature of the latter.

In one-loop computations it is desirable to use the cyclically ordered primitive amplitudes, because they are gauge invariant and only a subset of the kinematical loop-invariants plays a role. This will be clarified further in chapter 3.2. One thus wants to establish the relations between the one-loop partial amplitudes and the primitive amplitudes. The method which was originally introduced in [69, 77] and later formalized in [120] works thereby as follows. For a specific n -parton one-loop amplitude, with a certain number of distinguishable quark-antiquark pairs, one can generate the set of all one-loop Feynman diagrams $D_i^{(1)}$ by using ones favorite Feynman diagram generator. The respective amplitude can then be written as

$$\mathcal{A}_n^{(1)} = \sum_i D_i^{(1)} \quad (2.56)$$

and upon collecting all the diagrams that give rise to a specific product of color antennae this is further written in the familiar form

$$\mathcal{A}_n^{(1)} = \sum_i D_i^{(1)} = \sum_j C_j A_j^{(1)} \quad (2.57)$$

The partial amplitudes $A_j^{(1)}$ collect thereby all those color-stripped one-loop diagrams $d_k^{(1)}$ whose corresponding Feynman diagrams contribute to the color factors C_j , which reads

$$A_j^{(1)} = \sum_k K_{jk} d_k^{(1)} \quad (2.58)$$

where K is determined by construction. More closely, since the diagrams with four-valent vertices can always be reproduced by pinching from diagrams with three-valent vertices, $A_j^{(1)}$ may contain only those diagrams $d_k^{(1)}$ with only three-valent vertices. In a different step one considers all possible primitive amplitudes, i.e. all possible cyclic orderings. Upon collecting this time all the diagrams to a specific cyclic ordering one can also express the primitive amplitudes B_i in terms of the color-stripped one-loop diagrams $d_j^{(1)}$, which reads

$$B_i = \sum_l L_{il} d_l^{(1)} \quad (2.59)$$

where L is again determined by construction. The partial amplitudes can then be related to the primitive amplitudes by an ansatz

$$A_j^{(1)} = \sum_i Z_{ji} B_i = \sum_i \sum_l Z_{ji} L_{il} d_l^{(1)} \quad (2.60)$$

and since $A_j^{(1)} = \sum_l K_{jl} d_l^{(1)}$ one can finally establish the relations between the partial and the primitive amplitudes by solving the set of linear equations

$$K_{jl} = \sum_i Z_{ji} L_{il} \quad (2.61)$$

for the coefficients Z_{ji} . In general the set of linear equations is overcomplete and only a subset of diagrams is needed in order to establish the desired relations. To determine the relations between the primitive and the partial amplitudes in a given process can be done once right at the beginning of the corresponding computation. Nevertheless one needs to establish, revert and solve a process-dependent set of linear equations.

In contrast to this we would like to introduce a method that does not rely on such a procedure.

The method generates first, for a given set of distinguishable quark–antiquark pairs and no external gluons, the set of all the possible cyclic orderings. These are basically all cyclic orderings where we can draw planar diagrams without any fermion lines crossing each other. This set is overcomplete in the sense that it contains diagrams, which are directly related to each other by a relative sign. Upon removal of those double-copies we gain a set of distinct primitive amplitudes, which we call henceforth cyclic classes, following thereby the already established nomenclature of classes in [69, 77]. Each of these cyclic classes can be represented uniquely by a representative diagram, containing only the external quark–antiquark pairs. By looking at the corresponding color-flow diagrams we note that each of these cyclic classes can thereby contribute to various color flows, which we call color sub-classes henceforth and which is seen by simply considering all possibilities of the internal gluons to be either $U(N_c)$ or $U(1)$. For each such color sub-class in a certain cyclic class we can draw a unique color-flow diagram that, upon potential dressing with external gluon color double-lines, is used in a similar fashion as the color-flow double-ring

diagrams introduced in the subsections 2.5.1 and 2.5.2 above, namely to determine all the possible primitive amplitudes that contribute to a specific product of color antennae by observing all the possible ways that the gluons can "move" on the fundamental color lines in such a diagram. This generates automatically all the needed diagrams to a specific color sub-class, while canceling all other diagrams that would contribute to a wrong color flow.

We give a set of rules to generate the cyclic classes in appendix B and continue right away with an example. Consider a process with two distinct quark-antiquark pairs, (\bar{q}, q) and (\bar{Q}, Q) , with associated particle numbers $(1_{\bar{q}}, 2_q)$ and $(3_{\bar{Q}}, 4_Q)$ respectively. The set of cyclic classes that we choose is thereby depicted by the representative diagrams shown in figure 2.12. Instead of the cyclic classes depicted in b) and c) we could have equally chosen cyclic classes, which are represented by diagrams where the order of the fermions in the tree-part is flipped. These yield the same diagrams up to a sign, due to the antisymmetry of the color-stripped quark-gluon vertex. Upon this observation we could have also chosen cyclic classes where the antiquark 1 is exclusively left-routing with respect to the loop. We decide, however, on the depicted cyclic classes in order to compare some of the results which we will derive with our method to known results in [69, 77].

To each of the cyclic classes in figure 2.12 we can now assign the corresponding color sub-classes represented by color-flow diagrams, where we can assign four color sub-classes to each cyclic class. The color-flow diagrams for the color sub-classes to cyclic class a) and cyclic class a*) are shown in figure 2.13, for cyclic class b) and cyclic class c) in figure 2.14.

For the cyclic class that is needed for the n_f -contribution we choose the one represented by diagram d) in figure 2.15, which has the four associated color sub-classes depicted in the same figure in diagrams I) through IV).

Each QCD one-loop amplitude with n external partons can, as we already noted, be separated according to

$$\mathcal{A}_n^{(1)} = \mathcal{A}_n^{(1),[1]} + \mathcal{A}_n^{(1),[1/2]} \quad (2.62)$$

where now

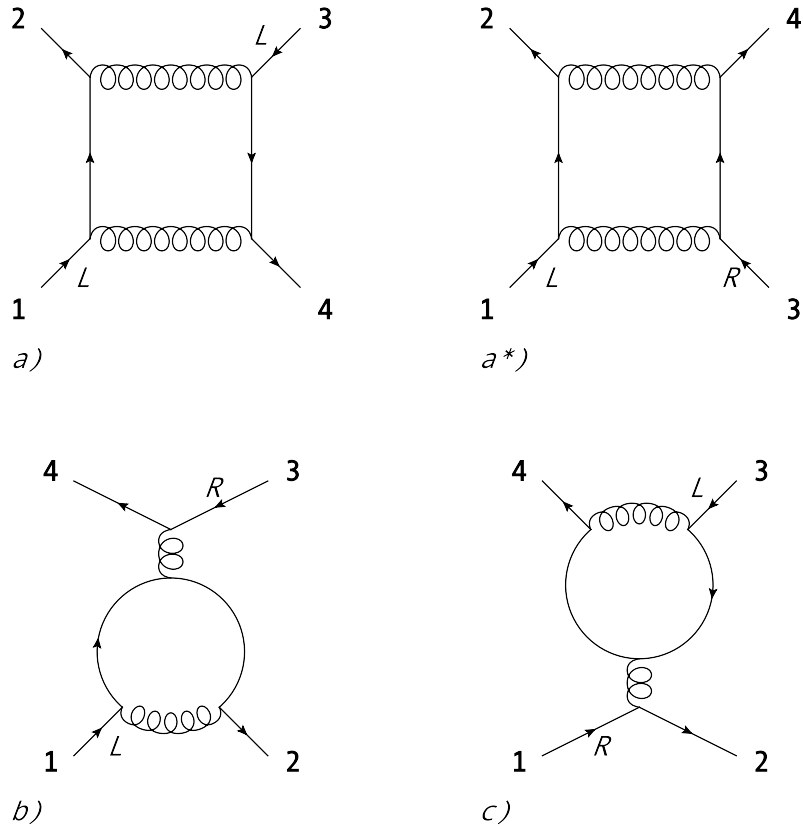


Figure 2.12: Representative color-stripped diagrams to the four different cyclic classes of a one-loop amplitude with two distinguishable quark-antiquark pairs and mixed particle content in the loop. The routing labels of the external fermion lines are made explicit. In class b) and c) we note that one of the fermion lines is connected to the fermion in the loop via a gluon through a tree-like sub-diagram. For the respective cyclic orderings there is no other way to draw planar diagrams without crossing fermion lines, except for double copies where for example the tree-parts are flipped and which only differ then by a relative minus sign.

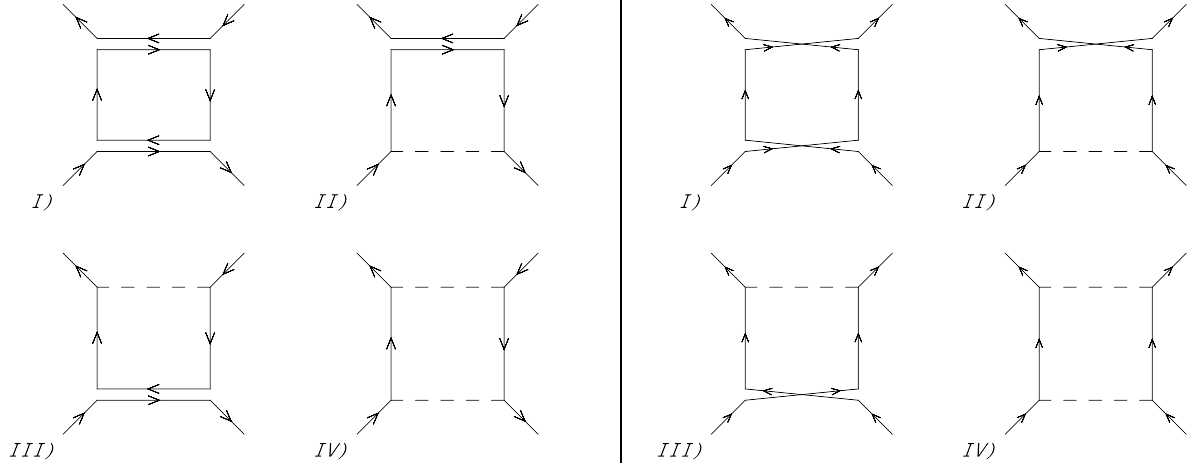


Figure 2.13: Representative color-flow diagrams to the color sub-classes of the cyclic classes a (on the left) and a^* (on the right). We note the non-planar color flow in the first three representative diagrams to the color sub-classes of cyclic class a^* .

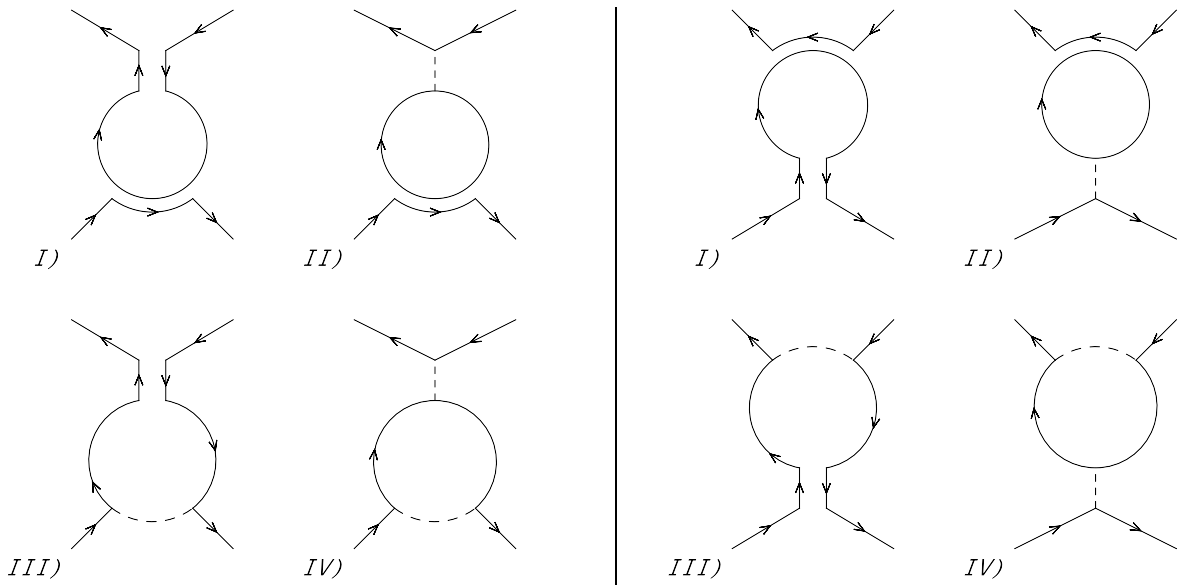


Figure 2.14: Representative color-flow diagrams to the color sub-classes of the cyclic classes b (on the left) and c (on the right). The cyclic classes are best chosen such that the respective color sub-classes do not contain non-planar color flows in those gluons that connect the tree-like sub-diagrams, although it would not make any fundamental difference.

2.5 One-Loop Color Decomposition

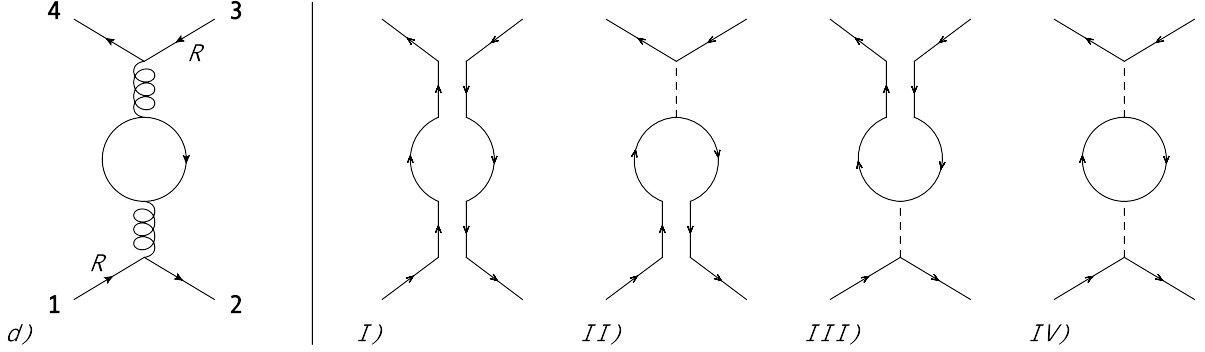


Figure 2.15: Left: Representative color-stripped diagram to the cyclic class of the n_f -contribution of a one-loop amplitude with two distinguishable quark-antiquark pairs. Right: Representative color-flow diagrams to the color sub-classes of the cyclic class d). For simplicity is the cyclic class chosen such that the respective color sub-classes do not contain non-planar color flows in those gluons that connect the tree-like sub-diagrams, although it would not make any fundamental difference to the color decomposition.

$$\mathcal{A}_n^{(1),[j]} = g_s^n \sum_{c \in \text{cyclic classes}} \mathcal{A}^{(1),[j],c} \quad (2.63)$$

and where we will drop the superscript (1) from now on again. Further

$$\mathcal{A}^{[j],c} = \sum_{c_s \in \text{color sub-classes}} \mathcal{A}^{[j],c_s} \quad (2.64)$$

where c_s is an element in the set of all color sub-classes to the cyclic class c . Let us now assume that we want to add a gluon to the two quark-antiquark pairs, in order to derive the color decomposition for $\mathcal{A}(\bar{q}, q, \bar{Q}, Q, g)$, where we assign specific particle labels to each of the partons via $(1_{\bar{q}}, 2_q, 3_{\bar{Q}}, 4_Q, 5_g)$. The cyclic classes that we need are again the ones depicted by the diagrams in figure 2.12 and for the n_f -part by the first diagram in figure 2.15. The associated color sub-classes are again the ones depicted by the diagrams in figures 2.13 and 2.14, and on the right of figure 2.15. Upon dressing the color sub-classes with the one gluon we note six different color-flow strings that may appear, which are

$$\begin{aligned} C_1 &= [T^{a_5}]_{i_4 \bar{j}_1} \delta_{i_2 \bar{j}_3}, & C_2 &= [T^{a_5}]_{i_2 \bar{j}_1} \delta_{i_4 \bar{j}_3}, \\ C_3 &= \delta_{i_4 \bar{j}_1} [T^{a_5}]_{i_2 \bar{j}_3}, & C_4 &= \delta_{i_2 \bar{j}_1} [T^{a_5}]_{i_4 \bar{j}_3}, \\ C_5 &= \delta_{i_4 \bar{j}_1} \delta_{i_2 \bar{j}_3}, & C_6 &= \delta_{i_2 \bar{j}_1} \delta_{i_4 \bar{j}_3} \end{aligned} \quad (2.65)$$

For the start we consider the most simple cyclic class in this case, which is the cyclic class a). The color sub-classes to the cyclic class a) are depicted by the left four color-flow diagrams in figure 2.13 and for each we can associate containers of color antennae products, namely

$$\begin{aligned}
 a_{\text{I}} &\longrightarrow \text{Tr}(\dots) [\dots]_{i_4\bar{j}_1} [\dots]_{i_2\bar{j}_3} \\
 a_{\text{II}} &\longrightarrow \left(-\frac{1}{N_c}\right) [\dots]_{i_4\bar{j}_1} [\dots]_{i_2\bar{j}_3} \\
 a_{\text{III}} &\longrightarrow \left(-\frac{1}{N_c}\right) [\dots]_{i_4\bar{j}_1} [\dots]_{i_2\bar{j}_3} \\
 a_{\text{IV}} &\longrightarrow \left(-\frac{1}{N_c}\right)^2 [\dots]_{i_2\bar{j}_1} [\dots]_{i_4\bar{j}_3}
 \end{aligned} \tag{2.66}$$

Upon filling the containers in all possible ways with the one gluon 5, i.e. considering all possible partitions, we can associate to each of the color sub-classes a_{I} through a_{IV} specific products of color antennae times factors in N_c via

$$\begin{aligned}
 a_{\text{I}} &\longrightarrow \text{Tr}(T^{a_5})C_5, \quad \text{Tr}(\mathbb{1})C_1 = N_c C_1, \quad \text{Tr}(\mathbb{1})C_3 = N_c C_3 \\
 a_{\text{II}} &\longrightarrow \left(-\frac{1}{N_c}\right)C_1, \quad \left(-\frac{1}{N_c}\right)C_3 \\
 a_{\text{III}} &\longrightarrow \left(-\frac{1}{N_c}\right)C_1, \quad \left(-\frac{1}{N_c}\right)C_3 \\
 a_{\text{IV}} &\longrightarrow \left(-\frac{1}{N_c}\right)^2 C_2, \quad \left(-\frac{1}{N_c}\right)^2 C_4
 \end{aligned} \tag{2.67}$$

Of course $\text{Tr}(T^{a_5}) = 0$, but it will be instructive and useful not to drop it for the moment. If we now look at the representative color-flow diagram to the color sub-class a_{I} we can infer four possible cyclic orderings in which we can insert a gluon color double-line in order to contribute to the subleading color factor $\text{Tr}(T^{a_5})C_5$. These are $(1_{\bar{q}}, 5_g, 2_q, 3_{\bar{Q}}, 4_Q)$, $(1_{\bar{q}}, 2_q, 5_g, 3_{\bar{Q}}, 4_Q)$, $(1_{\bar{q}}, 2_q, 3_{\bar{Q}}, 5_g, 4_Q)$ and $(1_{\bar{q}}, 2_q, 3_{\bar{Q}}, 4_Q, 5_g)$, where we have revolved the gluon color double-line on the closed color-flow line quite in analogy to the double-ring diagram in figure 2.11. If flipped to the outside the gluon color double-line is always radiated to the left with respect to the color-flow arrow on the fundamental color-flow line off which it radiates. The associated primitive amplitudes are therefore included with a relative minus sign. The sum of primitive amplitudes that multiplies the color factor $\text{Tr}(T^{a_5})C_5$ is therefore

$$\begin{aligned}
 \text{Tr}(T^{a_5})C_5 \times \left[\right. & - A(1_{\bar{q}}^L, 5_g, 2_q, 3_{\bar{Q}}^L, 4_Q) - A(1_{\bar{q}}^L, 2_q, 5_g, 3_{\bar{Q}}^L, 4_Q) \\
 & \left. - A(1_{\bar{q}}^L, 2_q, 3_{\bar{Q}}^L, 5_g, 4_Q) - A(1_{\bar{q}}^L, 2_q, 3_{\bar{Q}}^L, 4_Q, 5_g) \right]
 \end{aligned} \tag{2.68}$$

where we have included the routing information for each fermion line as superscripts to the antiquark indices. Remember that each primitive amplitude in the above represents a set of color–stripped diagrams, which is obtained by pinching from the respective representative diagram. In each of those sets, however, there are diagrams which do not contribute to the correct color flow. From the representative of $A(1_{\bar{q}}^L, 5_g, 2_q, 3_{\bar{Q}}^L, 4_Q)$, for example, we can generate a diagram where the gluon 5 is directly attached to the quark 2 in the cyclic ordering $(\dots, 5, 2, \dots)$ via a color–stripped quark–gluon tree–level vertex, which looking at the color–flow diagram of color sub–class a_I contributes obviously not to $Tr(T^{a_5})C_5$. There is, however, a corresponding diagram in $A(1_{\bar{q}}^L, 2_q, 5_g, 3_{\bar{Q}}^L, 4_Q)$, but where the gluon 5 is directly attached to the quark 2 in the cyclic ordering $(\dots, 2, 5, \dots)$, which can also never contribute to $Tr(T^{a_5})C_5$. Due to the antisymmetric property of the color stripped quark–gluon vertex with respect to the exchange of any two of the legs, however, this color–stripped diagram cancels the unwanted diagram from $A(1_{\bar{q}}^L, 5_g, 2_q, 3_{\bar{Q}}^L, 4_Q)$. Thus we need $A(1_{\bar{q}}^L, 2_q, 5_g, 3_{\bar{Q}}^L, 4_Q)$ and $A(1_{\bar{q}}^L, 2_q, 3_{\bar{Q}}^L, 4_Q, 5_g)$ in order to cancel all unwanted diagrams in $A(1_{\bar{q}}^L, 5_g, 2_q, 3_{\bar{Q}}^L, 4_Q)$ and $A(1_{\bar{q}}^L, 2_q, 3_{\bar{Q}}^L, 5_g, 4_Q)$. The remaining diagrams in $A(1_{\bar{q}}^L, 2_q, 5_g, 3_{\bar{Q}}^L, 4_Q)$ and $A(1_{\bar{q}}^L, 2_q, 3_{\bar{Q}}^L, 4_Q, 5_g)$ contribute to the correct color flow by virtue of one of the two color flows associated to each tree–level three–gluon Feynman vertex. All vertices and propagators, together with their color–stripped as well as color–flow contributions, are given in appendix A. Note that upon $Tr(T^{a_5}) = 0$ we can infer an identity from equation 2.68, which reads

$$A(1_{\bar{q}}^L, 2_q, 3_{\bar{Q}}^L, 4_Q, 5_g) = -A(1_{\bar{q}}^L, 5_g, 2_q, 3_{\bar{Q}}^L, 4_Q) - A(1_{\bar{q}}^L, 2_q, 5_g, 3_{\bar{Q}}^L, 4_Q) - A(1_{\bar{q}}^L, 2_q, 3_{\bar{Q}}^L, 5_g, 4_Q) \quad (2.69)$$

and which can be used if one wants to minimize the set of primitive amplitudes that have to be computed. The generalization of this to multiple gluons is given by summing over appropriately chosen shuffles of the external partons in the primitive amplitudes, similar to the ones described in equation 2.51. We will give all the necessary relations for $m = 2$ quark–antiquark pairs and an arbitrary number of gluons collectively at the end of this section.

The primitive amplitudes that multiply the other two (leading) color factors in the color sub–class a_I are trivial. For each possibility there is only one meaningful cyclic ordering to attach the gluon 5, which is

$$Tr(\mathbb{1})C_1(+ A(1_{\bar{q}}^L, 2_q, 3_{\bar{Q}}^L, 4_Q, 5_g)) = N_c C_1(+ A(1_{\bar{q}}^L, 2_q, 3_{\bar{Q}}^L, 4_Q, 5_g)) \quad (2.70)$$

and

$$\text{Tr}(\mathbb{1})C_3(+A(1_{\bar{q}}^L, 2_q, 5_g, 3_{\bar{Q}}^L, 4_Q)) = N_c C_3(+A(1_{\bar{q}}^L, 2_q, 5_g, 3_{\bar{Q}}^L, 4_Q)) \quad (2.71)$$

In total we can then write

$$\begin{aligned} \mathcal{A}^{[1],a_I} &= N_c C_1(+A(1_{\bar{q}}^L, 2_q, 3_{\bar{Q}}^L, 4_Q, 5_g)) \\ &\quad + N_c C_3(+A(1_{\bar{q}}^L, 2_q, 5_g, 3_{\bar{Q}}^L, 4_Q)) \end{aligned} \quad (2.72)$$

We proceed in a similar fashion for all the gluon-dressed color sub-classes to the cyclic class a), where for a_{II} we get

$$\begin{aligned} \mathcal{A}^{[1],a_{II}} &= -\frac{1}{N_c} C_1(-A(1_{\bar{q}}^L, 5_g, 2_q, 3_{\bar{Q}}^L, 4_Q) - A(1_{\bar{q}}^L, 2_q, 5_g, 3_{\bar{Q}}^L, 4_Q) - A(1_{\bar{q}}^L, 2_q, 3_{\bar{Q}}^L, 5_g, 4_Q)) \\ &\quad - \frac{1}{N_c} C_3(+A(1_{\bar{q}}^L, 2_q, 5_g, 3_{\bar{Q}}^L, 4_Q)) \end{aligned} \quad (2.73)$$

for a_{III} we get

$$\begin{aligned} \mathcal{A}^{[1],a_{III}} &= -\frac{1}{N_c} C_1(+A(1_{\bar{q}}^L, 2_q, 3_{\bar{Q}}^L, 4_Q, 5_g)) \\ &\quad - \frac{1}{N_c} C_3(-A(1_{\bar{q}}^L, 5_g, 2_q, 3_{\bar{Q}}^L, 4_Q) - A(1_{\bar{q}}^L, 2_q, 3_{\bar{Q}}^L, 5_g, 4_Q) - A(1_{\bar{q}}^L, 2_q, 3_{\bar{Q}}^L, 4_Q, 5_g)) \end{aligned} \quad (2.74)$$

and for a_{IV} we get

$$\begin{aligned} \mathcal{A}^{[1],a_{IV}} &= \left(-\frac{1}{N_c}\right)^2 C_2(-A(1_{\bar{q}}^L, 5_g, 2_q, 3_{\bar{Q}}^L, 4_Q)) \\ &\quad + \left(-\frac{1}{N_c}\right)^2 C_4(-A(1_{\bar{q}}^L, 2_q, 3_{\bar{Q}}^L, 5_g, 4_Q)) \end{aligned} \quad (2.75)$$

The general strategy should be obvious: Gluon color double-lines can revolve freely on closed fundamental color-flow lines in order to generate combinations of cyclic orderings or are bounded to move between the (anti-)fundamental indices of open fundamental color-flow lines. They cannot move on U(1)-lines. We continue with the cyclic class a*), depicted in figure 2.12. Looking at the respective color sub-classes on the right in figure 2.13 we note that this specific cyclic ordering leads to a twisted color-flow of the gluon propagators in the loop. Nevertheless, by inspecting how a gluon color double-line can move in the associated color-flow diagrams, we

2.5 One-Loop Color Decomposition

can determine the necessary linear combinations of primitive amplitudes to each color flow that can be assigned by adding a gluon. This leads then to

$$\begin{aligned}\mathcal{A}^{[1],a_I^*} &= C_2(+A(1,2,5,4,3) + A(1,2,4,5,3) + A(1,2,4,3,5)) \\ &\quad + C_4(-A(1,5,2,4,3) - A(1,2,5,4,3) - A(1,2,4,3,5))\end{aligned}\quad (2.76)$$

$$\begin{aligned}\mathcal{A}^{[1],a_{II}^*} &= -\frac{1}{N_c}C_1(-A(1,5,2,4,3) - A(1,2,5,4,3)) \\ &\quad -\frac{1}{N_c}C_3(+A(1,2,5,4,3) + A(1,2,4,5,3))\end{aligned}\quad (2.77)$$

$$\begin{aligned}\mathcal{A}^{[1],a_{III}^*} &= -\frac{1}{N_c}C_1(+A(1,2,4,5,3) + A(1,2,4,3,5)) \\ &\quad -\frac{1}{N_c}C_3(-A(1,5,2,4,3) - A(1,2,4,3,5))\end{aligned}\quad (2.78)$$

$$\begin{aligned}\mathcal{A}^{[1],a_{IV}^*} &= \left(-\frac{1}{N_c}\right)^2 C_2(-A(1,5,2,4,3)) \\ &\quad + \left(-\frac{1}{N_c}\right)^2 C_4(+A(1,2,4,5,3))\end{aligned}\quad (2.79)$$

with associated routing labels $1\frac{L}{q}$ and $3\frac{R}{Q}$ in the cyclic class a^*). For the cyclic class c) we determine

$$\begin{aligned}\mathcal{A}^{[1],c_I} &= C_2(-A(1,5,4,3,2) - A(1,4,5,3,2) - A(1,4,3,5,2)) \\ &\quad + C_4(+A(1,4,5,3,2))\end{aligned}\quad (2.80)$$

$$\begin{aligned}\mathcal{A}^{[1],c_{II}} &= -\frac{1}{N_c}Tr(\mathbb{1})C_2(+A(1,4,3,2,5)) \\ &\quad -\frac{1}{N_c}Tr(\mathbb{1})C_4(+A(1,4,5,3,2)) \\ &= -C_2(+A(1,4,3,2,5)) \\ &\quad -C_4(+A(1,4,5,3,2))\end{aligned}\quad (2.81)$$

$$\begin{aligned}\mathcal{A}^{[1],c_{\text{III}}} &= -\frac{1}{N_c}C_1(-A(1,5,4,3,2)) \\ &\quad -\frac{1}{N_c}C_3(-A(1,4,3,5,2))\end{aligned}\tag{2.82}$$

$$\begin{aligned}\mathcal{A}^{[1],c_{\text{IV}}} &= \left(-\frac{1}{N_c}\right)^2C_2(+A(1,4,3,2,5)) \\ &\quad + \left(-\frac{1}{N_c}\right)^2C_4(-A(1,5,4,3,2) - A(1,4,3,5,2) - A(1,4,3,2,5))\end{aligned}\tag{2.83}$$

with associated routing labels $1_{\bar{q}}^R$ and $3_{\bar{q}}^L$. In c_{II} we have already omitted the part with $\text{Tr}(T^{a_5})C_6$ due to $\text{Tr}(T^{a_5}) = 0$. Looking at the corresponding linear combination of primitive amplitudes, however, we can again read off the identity

$$0 = -A(1,5,4,3,2) - A(1,4,5,3,2) - A(1,4,3,5,2) - A(1,4,3,2,5)\tag{2.84}$$

One notes that in $\mathcal{A}^{[1],c_{\text{I}}}$ and $\mathcal{A}^{[1],c_{\text{III}}}$ we have not included the cyclic orderings where the gluon 5 is radiated in cyclic order between $2_{\bar{q}}$ and $1_{\bar{q}}$. The respective diagrams are already included in the sets of diagrams that are generated by pinching from the representative diagrams of $A(1,5,4,3,2)$ and $A(1,4,3,5,2)$ respectively. The one-gluon results for the cyclic class b) are derived similarly and since there is no further instructive gain, and we will present the all- n formulae in the case of $m = 2$ quark-antiquark pairs at the end of this section anyway, we will not repeat it here. The n_f -part is derived similarly, by dressing the color-flow representatives of the color sub-classes to the cyclic class d) in figure 2.15 with a gluon, and reads

$$\begin{aligned}\mathcal{A}^{[1],d_{\text{I}}} &= n_f C_1(-A(1,5,4,3,2)) \\ &\quad + n_f C_3(-A(1,4,3,5,2))\end{aligned}\tag{2.85}$$

$$\begin{aligned}\mathcal{A}^{[1],d_{\text{II}}} &= n_f \left(-\frac{1}{N_c}\right)C_2(-A(1,5,4,3,2) - A(1,4,3,5,2) - A(1,4,5,3,2)) \\ &\quad + n_f \left(-\frac{1}{N_c}\right)C_4(+A(1,4,5,3,2))\end{aligned}\tag{2.86}$$

$$\begin{aligned}
 \mathcal{A}^{[1],d_{\text{III}}} &= n_f \left(-\frac{1}{N_c} \right) C_2(+ A(1, 4, 3, 2, 5)) \\
 &+ n_f \left(-\frac{1}{N_c} \right) C_4(- A(1, 5, 4, 3, 2) - A(1, 4, 3, 5, 2) - A(1, 4, 3, 2, 5)) \quad (2.87)
 \end{aligned}$$

$$\begin{aligned}
 \mathcal{A}^{[1],d_{\text{IV}}} &= n_f \left(-\frac{1}{N_c} \right)^2 \text{Tr}(\mathbf{1}) C_2(+ A(1, 4, 3, 2, 5)) \\
 &+ n_f \left(-\frac{1}{N_c} \right)^2 \text{Tr}(\mathbf{1}) C_4(+ A(1, 4, 5, 3, 2)) \\
 &+ n_f \left(-\frac{1}{N_c} \right)^2 \text{Tr}(T^{a_5}) C_6(- A(1, 5, 4, 3, 2) - A(1, 4, 5, 3, 2) \\
 &\quad - A(1, 4, 3, 5, 2) - A(1, 4, 3, 2, 5)) \\
 &= n_f \left(\frac{1}{N_c} \right) C_2(+ A(1, 4, 3, 2, 5)) \\
 &+ n_f \left(\frac{1}{N_c} \right) C_4(+ A(1, 4, 5, 3, 2)) \quad (2.88)
 \end{aligned}$$

with associated routing labels $1_{\bar{q}}^R$ and $3_{\bar{Q}}^R$. Also in this case we find $-A(1, 5, 4, 3, 2) - A(1, 4, 5, 3, 2) - A(1, 4, 3, 5, 2) - A(1, 4, 3, 2, 5) = 0$ again, with which we can rewrite the terms proportional to C_2 and proportional to C_4 in the equations 2.86 and 2.87 respectively, in order to compare to the corresponding results in [69, 77].

We can generalize the above to the case of $(n - 2m)$ gluons. In the following we will give the corresponding expressions for the color sub-classes in the case of the two distinguishable quark-antiquark pairs and $(n - 4)$ gluons.

For $\mathcal{A}^{[1],a_1}$ we write

$$\mathcal{A}^{[1],a_1} = \sum_{\sigma} \sum_{\substack{x=4,\dots,n \\ y=x,\dots,n}} \text{Tr}(T^{\sigma(5)} \dots T^{\sigma(x)}) [T^{\sigma(x+1)} \dots T^{\sigma(y)}]_{i_4 \bar{j}_1} [T^{\sigma(y+1)} \dots T^{\sigma(n)}]_{i_2 \bar{j}_3} A_{(\sigma;x,y)}^{[1],a_1} \quad (2.89)$$

where

$$\begin{aligned}
 A_{(\sigma;x,y)}^{[1],a_I} = & \\
 (-1)^{x-4} \sum_{SCOP\{\alpha\}\{\beta\}} & A(\underbrace{1_{\bar{q}}^L, x_g, (x-1)_g, \dots, 5_g, 2_q, (y+1)_g, (y+2)_g, \dots, n_g, 3_Q^L, 4_Q, (x+1)_g, (x+2)_g, \dots, y_g}_{\{list\}})
 \end{aligned} \tag{2.90}$$

with $\alpha_i \in \{\alpha\} = \{x, x-1, \dots, 5\}$ and $\beta_i \in \{\beta\} = \{1, 2, y+1, y+2, \dots, n, 3, 4, x+1, x+2, \dots, y\}$. Here σ denotes the set of all permutations of gluon indices without those that leave the trace structure invariant. $SCOP\{\alpha\}\{\beta\}$ denotes the semi-cyclic ordered product of $\{\alpha\}$ and $\{\beta\}$, which is the set of all permutations of the members in the ordered list $\{list\}$ with 1 held fixed that preserve the cyclic ordering of the α_i within $\{\alpha\}$ and the ordering of the β_i within $\{\beta\}$, while allowing for all possible relative orderings of the α_i with respect to the β_i .

In the large- N_c limit of all the terms to the amplitude for $m = 2$ quark-antiquark pairs and $(n - 2m)$ gluons the above with $x = 4$ is the only one that contributes. We will comment on this type of contributions for arbitrary m in more detail at the end of this section.

The sum is in general over all possibilities, according to the desired product of color antennae, to move the external gluon color double-lines in the color-flow representatives between the ends of the associated open or closed fundamental color lines. The ordering between those gluons that are attached to one fundamental color line has thereby to be kept, while gluons of different fundamental color lines may shuffle. External quark and/or antiquarks may not be shuffled within one cyclic class. If we flip in a color-flow representative diagram all gluon color double-lines to the outside there are those double lines that are radiated to the right, with respect to the fundamental color line that they radiate from, and those which are radiated to the left. Our convention of assigning the necessary relative signs between primitive amplitudes is such that we add a primitive amplitude with a plus sign if it is included on the basis of a color right-radiator and with a minus sign if it is included on the basis of a color left-radiator. The diagrams within the primitive amplitudes are built from color-stripped Feynman rules, which themselves are defined to be antisymmetric with respect to the exchange of any two legs. In combination this leads then to the necessary cancellations of diagrams that contribute to a wrong color flow for a certain color sub-class and to the inclusion of exactly those diagrams that contribute exclusively to the correct color flow for this specific color sub-class. The color-stripped Feynman rules as well as the corresponding color-flow rules are derived in detail in appendix A.

2.5 One-Loop Color Decomposition

We continue with $\mathcal{A}^{[1],a_{\text{II}}}$ and write

$$\mathcal{A}^{[1],a_{\text{II}}} = \sum_{\sigma} \sum_{x=4,\dots,n} \left(-\frac{1}{N_c}\right) [T^{\sigma(5)} \dots T^{\sigma(x)}]_{i_4 \bar{j}_1} [T^{\sigma(x+1)} \dots T^{\sigma(n)}]_{i_2 \bar{j}_3} A_{(\sigma;x)}^{[1],a_{\text{II}}} \quad (2.91)$$

where

$$A_{(\sigma;x)}^{[1],a_{\text{II}}} = (-1)^{x-4} \sum_{OP\{\alpha\}\{\beta\}} A \left(\underbrace{1_{\bar{q}}, x_g, (x-1)_g, \dots, 5_g, 2_q, (x+1)_g, (x+2)_g, \dots, n_g, 3_{\bar{Q}}, 4_Q}_{\{list\}} \right) \quad (2.92)$$

with $\alpha_i \in \{\alpha\} = \{x, x-1, \dots, 5\}$ and $\beta_i \in \{\beta\} = \{1, 2, x+1, x+2, \dots, n, 3, 4\}$. Here σ denotes the set of all permutations of gluon indices. $OP\{\alpha\}\{\beta\}$ denotes the ordered product of $\{\alpha\}$ and $\{\beta\}$, which is the set of all permutations of the members in the ordered list $\{list\}$ with 1 and 4 held fixed that preserve the ordering of the α_i within $\{\alpha\}$ and the ordering of the β_i within $\{\beta\}$, while allowing for all possible relative orderings of the α_i with respect to the β_i .

$\mathcal{A}^{[1],a_{\text{III}}}$ is given by

$$\mathcal{A}^{[1],a_{\text{III}}} = \sum_{\sigma} \sum_{x=4,\dots,n} \left(-\frac{1}{N_c}\right) [T^{\sigma(5)} \dots T^{\sigma(x)}]_{i_4 \bar{j}_1} [T^{\sigma(x+1)} \dots T^{\sigma(n)}]_{i_2 \bar{j}_3} A_{(\sigma;x)}^{[1],a_{\text{III}}} \quad (2.93)$$

where

$$A_{(\sigma;x)}^{[1],a_{\text{III}}} = (-1)^{n-x} \sum_{OP\{\alpha\}\{\beta\}} A \left(\underbrace{3_{\bar{Q}}, n_g, (n-1)_g, \dots, (x+1)_g, 4_Q, 5_g, 6_g, \dots, x_g, 1_{\bar{q}}, 2_q}_{\{list\}} \right) \quad (2.94)$$

with $\alpha_i \in \{\alpha\} = \{n, n-1, \dots, x+1\}$ and $\beta_i \in \{\beta\} = \{3, 4, 5, 6, \dots, x, 1, 2\}$. Here σ denotes the set of all permutations of gluon indices. $OP\{\alpha\}\{\beta\}$ denotes the ordered product of $\{\alpha\}$ and $\{\beta\}$, which is the set of all permutations of the members in the ordered list $\{list\}$ with 3 and 2 held fixed that preserve the ordering of the α_i within $\{\alpha\}$ and the ordering of the β_i within $\{\beta\}$, while allowing for all possible relative orderings of the α_i with respect to the β_i . After the evaluation of $\sum_{OP\{\alpha\}\{\beta\}}$ the argument list of each primitive amplitude in the above may be cyclically rotated in order to have $1_{\bar{q}}$ at the first position again.

The evaluation of $\mathcal{A}^{[1],a_{\text{IV}}}$ does not involve a non-trivial shuffle and reads

$$\mathcal{A}^{[1],a_{\text{IV}}} = \sum_{\sigma} \sum_{x=4,\dots,n} \left(-\frac{1}{N_c}\right)^2 [T^{\sigma(5)} \dots T^{\sigma(x)}]_{i_2 \bar{j}_1} [T^{\sigma(x+1)} \dots T^{\sigma(n)}]_{i_4 \bar{j}_3} A_{(\sigma;x)}^{[1],a_{\text{IV}}} \quad (2.95)$$

where

$$A_{(\sigma;x)}^{[1],a_{\text{IV}}} = (-1)^{n-4} A(1_{\bar{q}}^L, x_g, (x-1)_g, \dots, 5_g, 2_q, 3_{\bar{Q}}^L, n_g, (n-1)_g, \dots, x_g, 4_Q) \quad (2.96)$$

This ends the evaluation of the cyclic class a). We will now turn to the cyclic class a*), where $\mathcal{A}^{[1],a_{\text{I}}^*}$ is given by

$$\mathcal{A}^{[1],a_{\text{I}}^*} = \sum_{\sigma} \sum_{x=4,\dots,n} [T^{\sigma(5)} \dots T^{\sigma(x)}]_{i_2 \bar{j}_1} [T^{\sigma(x+1)} \dots T^{\sigma(n)}]_{i_4 \bar{j}_3} A_{(\sigma;x)}^{[1],a_{\text{I}}^*} \quad (2.97)$$

where

$$A_{(\sigma;x)}^{[1],a_{\text{I}}^*} = (-1)^{n-x} \sum_{OP\{\alpha\}\{\beta\}\{\gamma\}} A(\underbrace{1_{\bar{q}}^L, n_g, (n-1)_g, \dots, (x+1)_g, 2_q, 4_Q, 5_g, 6_g, \dots, x_g, 3_{\bar{Q}}^R}_{\{list\}}) \quad (2.98)$$

with $\alpha_i \in \{\alpha\} = \{1, 2, 5, 6, \dots, x\}$, $\beta_i \in \{\beta\} = \{n, n-1, \dots, x+1, 4, 3\}$ and $\gamma_i \in \{\gamma\} = \{1, 2, 4, 3\}$. Here σ denotes the set of all permutations of gluon indices. $OP\{\alpha\}\{\beta\}\{\gamma\}$ denotes the set of all shuffles between the members in the ordered list $\{list\}$ that preserve the ordering of the α_i within $\{\alpha\}$, the ordering of the β_i within $\{\beta\}$ and the ordering of the γ_i within $\{\gamma\}$. This is the set of all permutations of the members in the ordered list $\{list\}$, such that the ordering of the fermion indices in the ordered list $\{1, 2, 4, 3\}$ is kept fixed and such that the gluon indices $(n, n-1, \dots, x+1)$ get not shuffled between 4 and 3, but between all other indices, and such that the gluon indices $(5, 6, \dots, x)$ get not shuffled between 1 and 2, but between all other indices.

$\mathcal{A}^{[1],a_{\text{II}}^*}$ is given by

$$\mathcal{A}^{[1],a_{\text{II}}^*} = \sum_{\sigma} \sum_{x=4,\dots,n} \left(-\frac{1}{N_c}\right) [T^{\sigma(5)} \dots T^{\sigma(x)}]_{i_4 \bar{j}_1} [T^{\sigma(x+1)} \dots T^{\sigma(n)}]_{i_2 \bar{j}_3} A_{(\sigma;x)}^{[1],a_{\text{II}}^*} \quad (2.99)$$

where

$$A_{(\sigma;x)}^{[1],a_{\text{II}}^*} = (-1)^{x-4} \sum_{OP\{\alpha\}\{\beta\}\{\gamma\}} A(\underbrace{1_{\bar{q}}^L, x_g, (x-1)_g, \dots, 5_g, 2_q, 4_Q, (x+1)_g, (x+2)_g, \dots, n_g, 3_{\bar{Q}}^R}_{\{list\}}) \quad (2.100)$$

2.5 One-Loop Color Decomposition

with $\alpha_i \in \{\alpha\} = \{1, 2, x+1, x+2, \dots, n\}$, $\beta_i \in \{\beta\} = \{x, x-1, \dots, 5, 4, 3\}$ and $\gamma_i \in \{\gamma\} = \{1, 2, 4, 3\}$. Here σ denotes the set of all permutations of gluon indices. $OP\{\alpha\}\{\beta\}\{\gamma\}$ denotes the set of all shuffles between the members in the ordered list $\{list\}$ with 1 and 3 held fixed that preserve the ordering of the α_i within $\{\alpha\}$, the ordering of the β_i within $\{\beta\}$ and the ordering of the γ_i within $\{\gamma\}$. $\mathcal{A}^{[1],a_{\text{III}}^*}$ is given by

$$\mathcal{A}^{[1],a_{\text{III}}^*} = \sum_{\sigma} \sum_{x=4, \dots, n} \left(-\frac{1}{N_c}\right) [T^{\sigma(5)} \dots T^{\sigma(x)}]_{i_4 \bar{j}_1} [T^{\sigma(x+1)} \dots T^{\sigma(n)}]_{i_2 \bar{j}_3} A_{(\sigma;x)}^{[1],a_{\text{III}}^*} \quad (2.101)$$

where

$$A_{(\sigma;x)}^{[1],a_{\text{III}}^*} = (-1)^{n-x} \sum_{OP\{\alpha\}\{\beta\}\{\gamma\}} A(\underbrace{4_Q, 5_g, 6_g, \dots, x_g, 3_Q^R, 1_{\bar{q}}^L, n_g, (n-1)_g, \dots, (x+1)_g, 2_q}_{\{list\}}) \quad (2.102)$$

with $\alpha_i \in \{\alpha\} = \{4, 3, n, n-1, \dots, x+1\}$, $\beta_i \in \{\beta\} = \{5, 6, \dots, x, 1, 2\}$ and $\gamma_i \in \{\gamma\} = \{1, 2, 4, 3\}$. Here σ denotes the set of all permutations of gluon indices. $OP\{\alpha\}\{\beta\}\{\gamma\}$ denotes the set of all shuffles between the members in the ordered list $\{list\}$ with 4 and 2 held fixed that preserve the ordering of the α_i within $\{\alpha\}$, the ordering of the β_i within $\{\beta\}$ and the ordering of the γ_i within $\{\gamma\}$. After the evaluation of $\sum_{OP\{\alpha\}\{\beta\}}$ the argument list of each primitive amplitude in the above may be cyclically rotated in order to have $1_{\bar{q}}^L$ at the first position again.

$\mathcal{A}^{[1],a_{\text{IV}}^*}$ is given by

$$\mathcal{A}^{[1],a_{\text{IV}}^*} = \sum_{\sigma} \sum_{x=4, \dots, n} \left(-\frac{1}{N_c}\right)^2 [T^{\sigma(5)} \dots T^{\sigma(x)}]_{i_2 \bar{j}_1} [T^{\sigma(x+1)} \dots T^{\sigma(n)}]_{i_4 \bar{j}_3} A_{(\sigma;x)}^{[1],a_{\text{IV}}^*} \quad (2.103)$$

where

$$A_{(\sigma;x)}^{[1],a_{\text{IV}}^*} = (-1)^{x-4} A(1_{\bar{q}}^L, x_g, (x-1)_g, \dots, 5_g, 2_q, 4_Q, (x+1)_g, (x+2)_g, \dots, n_g, 3_Q^R) \quad (2.104)$$

This ends the evaluation of the cyclic class a*) and we can turn to the cyclic class b). $\mathcal{A}^{[1],b_I}$ is thereby given by

$$\mathcal{A}^{[1],b_I} = \sum_{\sigma} \sum_{x=4, \dots, n} [T^{\sigma(5)} \dots T^{\sigma(x)}]_{i_2 \bar{j}_1} [T^{\sigma(x+1)} \dots T^{\sigma(n)}]_{i_4 \bar{j}_3} A_{(\sigma;x)}^{[1],b_I} \quad (2.105)$$

where

$$A_{(\sigma;x)}^{[1],b_I} = (-1)^{n-x} \sum_{OP\{\alpha\}\{\beta\}} A(\underbrace{3_Q^R, n_g, (n-1)_g, \dots, (x+1)_g, 2_q, 5_g, 6_g, \dots, x_g, 1_q^L, 4_Q}_{\{list\}}) \quad (2.106)$$

with $\alpha_i \in \{\alpha\} = \{n, n-1, \dots, x+1\}$ and $\beta_i \in \{\beta\} = \{3, 2, 5, 6, \dots, x, 1, 4\}$. Here σ denotes the set of all permutations of gluon indices. $OP\{\alpha\}\{\beta\}$ denotes the set of all permutations of the members in the ordered list $\{list\}$ with 3 and 4 held fixed that preserve the ordering of the α_i within $\{\alpha\}$ and the ordering of the β_i within $\{\beta\}$, while allowing for all possible relative orderings of the α_i with respect to the β_i . After the evaluation of $\sum_{OP\{\alpha\}\{\beta\}}$ the argument list of each primitive amplitude in the above may be cyclically rotated in order to have 1_q^L at the first position again.

$\mathcal{A}^{[1],b_{II}}$ is given by

$$\mathcal{A}^{[1],b_{II}} = \sum_{\sigma} \sum_{\substack{x=4, \dots, n \\ y=x, \dots, n}} \left(-\frac{1}{N_c}\right) Tr(T^{\sigma(5)} \dots T^{\sigma(x)}) [T^{\sigma(x+1)} \dots T^{\sigma(y)}]_{i_2 \bar{j}_1} [T^{\sigma(y+1)} \dots T^{\sigma(n)}]_{i_4 \bar{j}_3} A_{(\sigma;x,y)}^{[1],b_{II}} \quad (2.107)$$

where

$$A_{(\sigma;x,y)}^{[1],b_{II}} = (-1)^{x-4} \sum_{SCOP\{\alpha\}\{\beta\}} A(\underbrace{1_q^L, x_g, (x-1)_g, \dots, 5_g, 4_Q, (y+1)_g, (y+2)_g, \dots, n_g, 3_Q^R, 2_q, (x+1)_g, (x+2)_g, \dots, y_g}_{\{list\}}) \quad (2.108)$$

with $\alpha_i \in \{\alpha\} = \{x, x-1, \dots, 5\}$ and $\beta_i \in \{\beta\} = \{1, 4, y+1, y+2, \dots, n, 3, 2, x+1, x+2, \dots, y\}$. Here σ denotes the set of all permutations of gluon indices without those that leave the trace structure invariant. $SCOP\{\alpha\}\{\beta\}$ denotes the semi-cyclic ordered product of $\{\alpha\}$ and $\{\beta\}$, which is the set of all permutations of the members in the ordered list $\{list\}$ with 1 held fixed that preserve the cyclic ordering of the α_i within $\{\alpha\}$ and the ordering of the β_i within $\{\beta\}$, while allowing for all possible relative orderings of the α_i with respect to the β_i .

$\mathcal{A}^{[1],b_{III}}$ is given by

2.5 One-Loop Color Decomposition

$$\mathcal{A}^{[1],b_{\text{III}}} = \sum_{\sigma} \sum_{x=4,\dots,n} \left(-\frac{1}{N_c}\right) [T^{\sigma(5)} \dots T^{\sigma(x)}]_{i_4 \bar{j}_1} [T^{\sigma(x+1)} \dots T^{\sigma(n)}]_{i_2 \bar{j}_3} A_{(\sigma;x)}^{[1],b_{\text{III}}} \quad (2.109)$$

where

$$A_{(\sigma;x)}^{[1],b_{\text{III}}} = (-1)^{n-4} A(1_{\bar{q}}^L, x_g, (x-1)_g, \dots, 5_g, 4_Q, 3_Q^R, n_g, (n-1)_g, \dots, (x+1)_g, 2_q) \quad (2.110)$$

$\mathcal{A}^{[1],b_{\text{IV}}}$ is given by

$$\mathcal{A}^{[1],b_{\text{IV}}} = \sum_{\sigma} \sum_{x=4,\dots,n} \left(-\frac{1}{N_c}\right)^2 [T^{\sigma(5)} \dots T^{\sigma(x)}]_{i_2 \bar{j}_1} [T^{\sigma(x+1)} \dots T^{\sigma(n)}]_{i_4 \bar{j}_3} A_{(\sigma;x)}^{[1],b_{\text{IV}}} \quad (2.111)$$

where

$$A_{(\sigma;x)}^{[1],b_{\text{IV}}} = (-1)^{x-4} \sum_{OP\{\alpha\}\{\beta\}} A(\underbrace{1_{\bar{q}}^L, x_g, (x-1)_g, \dots, 5_g, 4_Q, (x+1)_g, (x+2)_g, \dots, n_g, 3_Q^R, 2_q}_{\{list\}}) \quad (2.112)$$

with $\alpha_i \in \{\alpha\} = \{x, x-1, \dots, 5\}$ and $\beta_i \in \{\beta\} = \{1, 4, x+1, x+2, \dots, n, 3, 2\}$. Here σ denotes the set of all permutations of gluon indices. $OP\{\alpha\}\{\beta\}$ denotes the set of all permutations of the members in the ordered list $\{list\}$ with 1 and 2 held fixed that preserve the ordering of the α_i within $\{\alpha\}$ and the ordering of the β_i within $\{\beta\}$, while allowing for all possible relative orderings of the α_i with respect to the β_i .

This ends the evaluation of the cyclic class b) and we can turn to the cyclic class c). $\mathcal{A}^{[1],c_1}$ is thereby given by

$$\mathcal{A}^{[1],c_1} = \sum_{\sigma} \sum_{x=4,\dots,n} [T^{\sigma(5)} \dots T^{\sigma(x)}]_{i_2 \bar{j}_1} [T^{\sigma(x+1)} \dots T^{\sigma(n)}]_{i_4 \bar{j}_3} A_{(\sigma;x)}^{[1],c_1} \quad (2.113)$$

where

$$A_{(\sigma;x)}^{[1],c_1} = (-1)^{x-4} \sum_{OP\{\alpha\}\{\beta\}} A(\underbrace{1_{\bar{q}}^R, x_g, (x-1)_g, \dots, 5_g, 4_Q, (x+1)_g, (x+2)_g, \dots, n_g, 3_Q^L, 2_q}_{\{list\}}) \quad (2.114)$$

with $\alpha_i \in \{\alpha\} = \{x, x-1, \dots, 5\}$ and $\beta_i \in \{\beta\} = \{1, 4, x+1, x+2, \dots, n, 3, 2\}$. Here σ denotes the set of all permutations of gluon indices. $OP\{\alpha\}\{\beta\}$ denotes the set of all permutations of

the members in the ordered list $\{list\}$ with 1 and 2 held fixed that preserve the ordering of the α_i within $\{\alpha\}$ and the ordering of the β_i within $\{\beta\}$, while allowing for all possible relative orderings of the α_i with respect to the β_i .

$\mathcal{A}^{[1],c_{II}}$ is given by

$$\mathcal{A}^{[1],c_{II}} = \sum_{\sigma} \sum_{\substack{x=4,\dots,n \\ y=x,\dots,n}} \left(-\frac{1}{N_c}\right) Tr(T^{\sigma(5)} \dots T^{\sigma(x)}) [T^{\sigma(x+1)} \dots T^{\sigma(y)}]_{i_2 \bar{j}_1} [T^{\sigma(y+1)} \dots T^{\sigma(n)}]_{i_4 \bar{j}_3} A_{(\sigma;x,y)}^{[1],c_{II}} \quad (2.115)$$

where

$$A_{(\sigma;x,y)}^{[1],c_{II}} = (-1)^{x-4} \sum_{SCOP\{\alpha\}\{\beta\}} A \left(\underbrace{1_{\bar{q}}^R, x_g, (x-1)_g, \dots, 5_g, 4_Q, (y+1)_g, (y+2)_g, \dots, n_g, 3_{\bar{Q}}^L, 2_q, (x+1)_g, (x+2)_g, \dots, y_g}_{\{list\}} \right) \quad (2.116)$$

with $\alpha_i \in \{\alpha\} = \{x, x-1, \dots, 5\}$ and $\beta_i \in \{\beta\} = \{1, 4, y+1, y+2, \dots, n, 3, 2, x+1, x+2, \dots, y\}$. Here σ denotes the set of all permutations of gluon indices without those that leave the trace structure invariant. $SCOP\{\alpha\}\{\beta\}$ denotes the semi-cyclic ordered product of $\{\alpha\}$ and $\{\beta\}$, which is the set of all permutations of the members in the ordered list $\{list\}$ with 1 held fixed that preserve the cyclic ordering of the α_i within $\{\alpha\}$ and the ordering of the β_i within $\{\beta\}$, while allowing for all possible relative orderings of the α_i with respect to the β_i .

$\mathcal{A}^{[1],c_{III}}$ is given by

$$\mathcal{A}^{[1],c_{III}} = \sum_{\sigma} \sum_{x=4,\dots,n} \left(-\frac{1}{N_c}\right) [T^{\sigma(5)} \dots T^{\sigma(x)}]_{i_4 \bar{j}_1} [T^{\sigma(x+1)} \dots T^{\sigma(n)}]_{i_2 \bar{j}_3} A_{(\sigma;x)}^{[1],c_{III}} \quad (2.117)$$

where

$$A_{(\sigma;x)}^{[1],c_{III}} = (-1)^{x-4} A \left(1_{\bar{q}}^R, x_g, (x-1)_g, \dots, 5_g, 4_Q, (x+1)_g, (x+2)_g, \dots, n_g, 3_{\bar{Q}}^L, 2_q \right) \quad (2.118)$$

$\mathcal{A}^{[1],c_{IV}}$ is given by

2.5 One-Loop Color Decomposition

$$\mathcal{A}^{[1],c_{\text{IV}}} = \sum_{\sigma} \sum_{x=4,\dots,n} \left(-\frac{1}{N_c}\right)^2 [T^{\sigma(5)} \dots T^{\sigma(x)}]_{i_2 \bar{j}_1} [T^{\sigma(x+1)} \dots T^{\sigma(n)}]_{i_4 \bar{j}_3} A_{(\sigma;x)}^{[1],c_{\text{IV}}} \quad (2.119)$$

where

$$A_{(\sigma;x)}^{[1],c_{\text{IV}}} = (-1)^{n-x} \sum_{OP\{\alpha\}\{\beta\}} A(\underbrace{3_Q^L, n_g, (n-1)_g, \dots, (x+1)_g, 2_q, 5_g, 6_g, \dots, x_g, 1_{\bar{q}}^R, 4_Q}_{\{list\}}) \quad (2.120)$$

with $\alpha_i \in \{\alpha\} = \{n, n-1, \dots, x+1\}$ and $\beta_i \in \{\beta\} = \{3, 2, 5, 6, \dots, x, 1, 4\}$. Here σ denotes the set of all permutations of gluon indices. $OP\{\alpha\}\{\beta\}$ denotes the set of all permutations of the members in the ordered list $\{list\}$ with 3 and 4 held fixed that preserve the ordering of the α_i within $\{\alpha\}$ and the ordering of the β_i within $\{\beta\}$, while allowing for all possible relative orderings of the α_i with respect to the β_i . After the evaluation of $\sum_{OP\{\alpha\}\{\beta\}}$ the argument list of each primitive amplitude in the above may be cyclically rotated in order to have $1_{\bar{q}}^R$ at the first position again.

We can also derive the formula for the n_f -contribution to the amplitude with $m = 2$ quark-antiquark pairs and $(n-4)$ gluons, where $\mathcal{A}^{[1/2],d_{\text{I}}}$ is given by

$$\mathcal{A}^{[1/2],d_{\text{I}}} = \sum_{\sigma} \sum_{x=4,\dots,n} n_f [T^{\sigma(5)} \dots T^{\sigma(x)}]_{i_4 \bar{j}_1} [T^{\sigma(x+1)} \dots T^{\sigma(n)}]_{i_2 \bar{j}_3} A_{(\sigma;x)}^{[1/2],d_{\text{I}}} \quad (2.121)$$

with

$$A_{(\sigma;x)}^{[1/2],d_{\text{I}}} = (-1)^{n-4} A(1_{\bar{q}}^R, x_g, (x-1)_g, \dots, 5_g, 4_Q, 3_Q^R, n_g, (n-1)_g, \dots, (x+1)_g, 2_q) \quad (2.122)$$

$\mathcal{A}^{[1/2],d_{\text{II}}}$ is given by

$$\mathcal{A}^{[1/2],d_{\text{II}}} = \sum_{\sigma} \sum_{x=4,\dots,n} n_f \left(-\frac{1}{N_c}\right) [T^{\sigma(5)} \dots T^{\sigma(x)}]_{i_2 \bar{j}_1} [T^{\sigma(x+1)} \dots T^{\sigma(n)}]_{i_4 \bar{j}_3} A_{(\sigma;x)}^{[1/2],d_{\text{II}}} \quad (2.123)$$

where

$$A_{(\sigma;x)}^{[1/2],d_{\text{II}}} = (-1)^{x-4} \sum_{OP\{\alpha\}\{\beta\}} A(\underbrace{1_{\bar{q}}^R, x_g, (x-1)_g, \dots, 5_g, 4_Q, (x+1)_g, (x+2)_g, \dots, n_g, 3_Q^R, 2_q}_{\{list\}}) \quad (2.124)$$

with $\alpha_i \in \{\alpha\} = \{x, x-1, \dots, 5\}$ and $\beta_i \in \{\beta\} = \{1, 4, x+1, x+2, \dots, n, 3, 2\}$. Here σ denotes the set of all permutations of gluon indices. $OP\{\alpha\}\{\beta\}$ denotes the set of all permutations of the members in the ordered list $\{list\}$ with 1 and 2 held fixed that preserve the ordering of the α_i within $\{\alpha\}$ and the ordering of the β_i within $\{\beta\}$, while allowing for all possible relative orderings of the α_i with respect to the β_i .

$\mathcal{A}^{[1/2],d_{III}}$ is given by

$$\mathcal{A}^{[1/2],d_{III}} = \sum_{\sigma} \sum_{x=4, \dots, n} n_f \left(-\frac{1}{N_c} \right) [T^{\sigma(5)} \dots T^{\sigma(x)}]_{i_2 \bar{j}_1} [T^{\sigma(x+1)} \dots T^{\sigma(n)}]_{i_4 \bar{j}_3} A_{(\sigma;x)}^{[1/2],d_{III}} \quad (2.125)$$

where

$$A_{(\sigma;x)}^{[1/2],d_{III}} = (-1)^{n-x} \sum_{OP\{\alpha\}\{\beta\}} A \left(\underbrace{3_Q^R, n_g, (n-1)_g, \dots, (x+1)_g, 2_q, 5_g, 6_g, \dots, x_g, 1_{\bar{q}}^R, 4_Q}_{\{list\}} \right) \quad (2.126)$$

with $\alpha_i \in \{\alpha\} = \{n, n-1, \dots, x+1\}$ and $\beta_i \in \{\beta\} = \{3, 2, 5, 6, \dots, x, 1, 4\}$. Here σ denotes the set of all permutations of gluon indices. $OP\{\alpha\}\{\beta\}$ denotes the set of all permutations of the members in the ordered list $\{list\}$ with 3 and 4 held fixed that preserve the ordering of the α_i within $\{\alpha\}$ and the ordering of the β_i within $\{\beta\}$, while allowing for all possible relative orderings of the α_i with respect to the β_i .

$\mathcal{A}^{[1/2],d_{IV}}$ is given by

$$\begin{aligned} \mathcal{A}^{[1/2],d_{IV}} = \\ \sum_{\sigma} \sum_{\substack{x=4, \dots, n \\ y=x, \dots, n}} n_f \left(-\frac{1}{N_c} \right)^2 T_r (T^{\sigma(5)} \dots T^{\sigma(x)}) [T^{\sigma(x+1)} \dots T^{\sigma(y)}]_{i_2 \bar{j}_1} [T^{\sigma(y+1)} \dots T^{\sigma(n)}]_{i_4 \bar{j}_3} A_{(\sigma;x,y)}^{[1/2],d_{IV}} \end{aligned} \quad (2.127)$$

where

$$\begin{aligned} A_{(\sigma;x,y)}^{[1/2],d_{IV}} = \\ (-1)^{x-4} \sum_{SCOP\{\alpha\}\{\beta\}} A \left(\underbrace{1_{\bar{q}}^R, x_g, (x-1)_g, \dots, 5_g, 4_Q, (y+1)_g, (y+2)_g, \dots, n_g, 3_Q^R, 2_q, (x+1)_g, (x+2)_g, \dots, y_g}_{\{list\}} \right) \end{aligned} \quad (2.128)$$

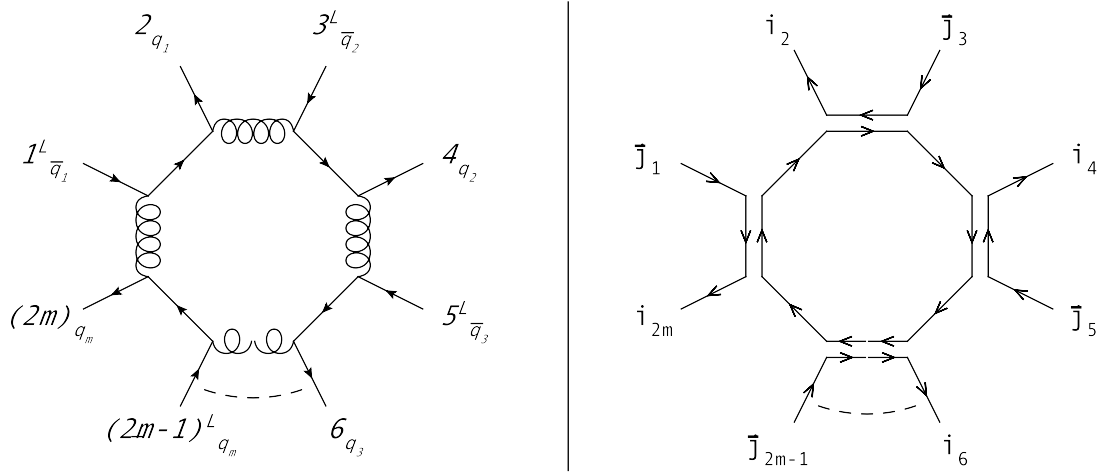


Figure 2.16: Graphical representation of the dominant contribution in an n -parton amplitude with m distinguishable quark-antiquark pairs and $(n - 2m)$ gluons. We show the representative diagram to the corresponding cyclic class on the left and the color-flow representative diagram to the associated color sub-class on the right.

with $\alpha_i \in \{\alpha\} = \{x, x - 1, \dots, 5\}$ and $\beta_i \in \{\beta\} = \{1, 4, y + 1, y + 2, \dots, n, 3, 2, x + 1, x + 2, \dots, y\}$. Here σ denotes the set of all permutations of gluon indices without those that leave the trace structure invariant. $SCOP\{\alpha\}\{\beta\}$ denotes the semi-cyclic ordered product of $\{\alpha\}$ and $\{\beta\}$, which is the set of all permutations of the members in the ordered list $\{list\}$ with 1 held fixed that preserve the cyclic ordering of the α_i within $\{\alpha\}$ and the ordering of the β_i within $\{\beta\}$, while allowing for all possible relative orderings of the α_i with respect to the β_i .

Before we end this chapter we would like to stress one particular contribution that can easily be given in closed form for an n -parton amplitude with m distinguishable quark-antiquark pairs and $(n - 2m)$ gluons, i.e. the leading contribution in the large- N_c limit. The representative diagrams to the respective cyclic class and the associated particular color sub-class that yields the dominant contribution in the large- N_c limit in this amplitude are shown in figure 2.16.

If we dress the color-flow representative diagram on the right in figure 2.16 with $(n - 2m)$ gluons we can easily read off the shuffle relation that yields the correct linear combination of primitive amplitudes. The permutation π in equation 2.54 is thereby such that $\pi(2) = 2m, \pi(4) = 2, \pi(6) = 4, \dots, \pi(2m) = 2m - 2$ and the color factor which is correspondingly multiplied reads

$$\begin{aligned}
 & Tr \left(T^{a_{\sigma(2m+1)}}, T^{a_{\sigma(c_1+2m-1)}} \right) \left[T^{a_{\sigma(c_1+2m)}}, T^{a_{\sigma(c_1+c_2+2m-2)}} \right]_{i_{2m}\bar{j}_1} \times \dots \\
 & \dots \times \left[T^{a_{\sigma(c_1+\dots+c_m+(2m-(m-1)))}}, T^{a_{\sigma(n)}} \right]_{i_{2m-2}\bar{j}_{2m-1}} \times \\
 & \times A_{n;(c_1,c_m)}^{(1)} \left(\sigma(2m+1, c_1+2m-1); (2m)_{q_m}, \sigma(c_1+2m, c_1+c_2+2m-2), 1_{\bar{q}_1}; \dots \right. \\
 & \left. \dots; (2m-2)_{q_{m-1}}, \sigma(c_1+\dots+c_m+(2m-(m-1))), n), (2m-1)_{\bar{q}_m} \right) \quad (2.129)
 \end{aligned}$$

Here σ denotes an element in the set of all permutations of gluon indices without those that leave the trace structure invariant. For notational simplicity we choose a particular permutation, say $\sigma = id$, and give the corresponding expression for $A_{n;(c_1,c_m)}^{(1)}(\dots)$ by

$$\begin{aligned}
 & A_{n;(c_1,c_m)}^{(1)}(\dots) = \\
 & (-1)^{c_1-1} \sum_{SCOP\{\alpha\}\{\beta\}} A \left(\overbrace{1_{\bar{q}_1}^L, (c_1+2m-1)_g, (c_1+2m-2)_g, \dots, (2m+1)_g, 2_{q_1}, (c_1+c_2+2m-1)_g, \dots}^{\{list\}} \right. \\
 & \quad \dots, (c_1+c_2+c_3+2m-3)_g, 3_{\bar{q}_2}^L, 4_{q_2}, \dots, (2m-3)_{\bar{q}_{m-1}}^L, (2m-2)_{q_{m-1}}, \\
 & \quad (c_1+\dots+c_m+2m-(m-1))_g, \dots, n_g, (2m-1)_{\bar{q}_m}^L, (2m)_{q_m}, (c_1+2m)_g, \dots \\
 & \quad \left. \dots, (c_1+c_2+2m-2)_g \right) \quad (2.130)
 \end{aligned}$$

with $\alpha_i \in \{\alpha\} = \{c_1+2m-1, c_1+2m-2, \dots, 2m+1\}$ and $\beta_i \in \{\beta\} = \{1, 2, c_1+c_2+2m-1, \dots, c_1+c_2+c_3+2m-3, 3, 4, \dots, 2m-3, 2m-2, c_1+\dots+c_m+2m-(m-1), \dots, n, 2m-1, 2m, c_1+2m, \dots, c_1+c_2+2m-2\}$. $SCOP\{\alpha\}\{\beta\}$ denotes the semi-cyclic ordered product of $\{\alpha\}$ and $\{\beta\}$, which is the set of all permutations of the members in the ordered list $\{list\}$ with 1 held fixed that preserve the cyclic ordering of the α_i within $\{\alpha\}$ and the ordering of the β_i within $\{\beta\}$, while allowing for all possible relative orderings of the α_i with respect to the β_i .

From figure 2.16 it is obvious that the contributions in equation 2.130, if taken into account for every possible gluon permutation in σ , are the dominant contributions for an amplitude with m quark–antiquark pairs and $(n-2m)$ gluons due to the explicit factor N_c that is generated in only those contributions.

Chapter 3

Virtual Subtraction Method

As discussed in the introduction, in section 1.4, the computation of perturbative higher-order effects to the hard scattering matrix elements involves the complication of divergent contributions. The subtraction method can thereby be used to handle these divergent contributions properly in the computation of infrared safe observables. In Catani–Seymour dipole subtraction an insertion operator \mathbf{I} is thereby defined, which contains all the explicit poles in the dimensional regularization parameter ε , and when combined with the virtual part $\int O_{n-2} d\sigma^V$ the explicit poles cancel. As was further discussed can this procedure as well be extended to the virtual part, which enables therefore the numerical evaluation of $\int O_{n-2} d\sigma^V$, quite in contrast to the commonly used methods which rely on rather traditional methods based on Feynman diagrams or on more modern methods based on generalized unitarity and cut-techniques. The numerical method presents thereby an efficient way to evaluate one-loop contributions with a rather large number of external particles. We will briefly introduce the commonly used methods, and also give an introduction to the numerical approach, in the section 3.4. More details on the direct numerical contour deformation for the computation of jet rates in electron–positron annihilation will be given in chapter 5.2.

It was already discussed in section 1.4 that, in order to be able to perform the one-loop integral numerically, i.e. safely integrating over the physical four dimensions of loop-momentum space, we need to subtract any existing divergences locally off the one-loop integrand of the virtual contributions. We therefor extend the subtraction method for many-leg calculations to the virtual contributions by introducing local virtual subtraction terms on the level of the one-loop integrand. The local virtual subtraction terms are thereby practically derived on the amplitude level, where

$$d\sigma^V = 2\text{Re}(\mathcal{A}_n^{(0)*} \mathcal{A}_n^{(1)}) d\phi_{n-2} \quad \text{and} \quad \mathcal{A}_n^{(1)} = \mathcal{A}_{bare}^{(1)} + \mathcal{A}_{CT} = \int \frac{d^4k}{(2\pi)^4} \mathcal{G}_{bare}^{(1)} + \mathcal{A}_{CT} \quad (3.1)$$

and thus the subtraction terms are introduced on the level of the bare one-loop integrand $\mathcal{G}_{bare}^{(1)}$ via

$$\mathcal{A}_n^{(1)} = \int \frac{d^4k}{(2\pi)^4} \left[\mathcal{G}_{bare}^{(1)} - \mathcal{G}_{UV}^{(1)} - \mathcal{G}_{soft}^{(1)} - \mathcal{G}_{coll}^{(1)} \right] + \left[\mathcal{A}_{CT} + \mathcal{A}_{UV}^{(1)} + \mathcal{A}_{soft}^{(1)} + \mathcal{A}_{coll}^{(1)} \right] \quad (3.2)$$

with $\mathcal{A}_x^{(1)} \equiv S_\varepsilon^{-1} \mu^{2\varepsilon} \int \frac{d^Dk}{(2\pi)^D} \mathcal{G}_x^{(1)}$, where $x = soft, coll, UV$ and $D = 4 - 2\varepsilon$ in dimensional regularization. $S_\varepsilon = (4\pi)^\varepsilon e^{-\varepsilon\gamma_E}$ is the typical volume factor in dimensional regularization, with γ_E the Euler–Mascheroni constant, and μ the typical mass scale in dimensional regularization. Further details on the integration are given in appendix E. We define the three finite contributions in equation 1.21 by

$$\langle O \rangle^{NLO} \equiv \langle O \rangle_{real}^{NLO} + \langle O \rangle_{virtual}^{NLO} + \langle O \rangle_{insertion}^{NLO} \quad (3.3)$$

where the various terms are given by

$$\langle O \rangle_{real}^{NLO} = \int_{n-1} \left(O_{n-1} d\sigma^R - O_{n-2} d\sigma^A \right) \quad (3.4)$$

and

$$\langle O \rangle_{virtual}^{NLO} = 2 \int d\phi_{n-2} \text{Re} \int \frac{d^4k}{(2\pi)^4} \left[\mathcal{A}_n^{(0)*} (\mathcal{G}_{bare}^{(1)} - \mathcal{G}_{UV}^{(1)} - \mathcal{G}_{soft}^{(1)} - \mathcal{G}_{coll}^{(1)}) \right] O_{n-2} \quad (3.5)$$

which is free of IR and UV poles and can be integrated in four dimensions. The integration over the loop momentum k can thereby be performed together with the phase-space integration in one single $(3n-6)$ -dimensional Monte Carlo integration at $(d\phi_{n-2}, d^4k)$, where we have $(3n-10)$ integration dimensions from the $(n-2)$ -particle final-state phase-space integration and four integration dimensions from the one-loop integration. Since in any Monte Carlo integration the error scales like $1/\sqrt{N}$, where N is the number of Monte Carlo evaluations, but regardless of the dimensionality of the integration region, this can be done efficiently and there is no need to evaluate the one-loop integral separately for each phase-space point. We will further discuss the numerical one-loop integration and the Monte Carlo method in section 3.4 as well as in chapter 5.2 and appendix H.

Further

$$\langle O \rangle_{insertion}^{NLO} = \int_{n-2} O_{n-2} \left(d\sigma_{CT}^V + \int_{loop} d\sigma^L + d\sigma^C + \int_1 d\sigma^A \right) = \int d\phi_{n-2} O_{n-2} (\mathbf{L} + \mathbf{I} + \mathbf{K} + \mathbf{P}) \otimes d\sigma^B \quad (3.6)$$

where all the IR poles from the integrated real emission contributions and the initial state collinear subtraction term are contained in the dipole insertion operator \mathbf{I} . The dipole insertion operators \mathbf{K} and \mathbf{P} do not have any poles and pose no problem in the numerical integration [27, 87]. We further defined a new insertion operator \mathbf{L} by

$$\mathbf{L} \otimes d\sigma^B \equiv 2Re[\mathcal{A}_n^{(0)*}(\mathcal{A}_{CT} + \mathcal{A}_{UV}^{(1)} + \mathcal{A}_{soft}^{(1)} + \mathcal{A}_{coll}^{(1)})]d\phi_{n-2} \quad (3.7)$$

which is UV finite and cancels the IR poles of the dipole insertion operator \mathbf{I} . We will further comment on the dipole insertion operator and on the one-loop insertion operator in the next section 3.1. Our local virtual subtraction terms will be derived on the level of primitive one-loop amplitudes, which have been discussed in chapter 2, where the soft and collinear subtraction terms can be defined directly on the primitive amplitude level, which will be discussed in section 3.2.1, and the UV subtraction term is derived via local counterterms to ordered color-stripped propagator and vertex corrections, and subsequent use of recurrence relations, which will be discussed in section 3.2.2 and chapter 4.3 respectively.

3.1 Pole Structure of QCD Amplitudes

For QCD amplitudes the pole structure in the dimensional regularization parameter ε is well known. The poles are either of IR or of UV origin. In massless QCD for example the poles of a bare one-loop n -parton amplitude are after integration given by [137, 138, 87]

$$\mathcal{A}_{bare}^{(1)} = \frac{\alpha_s}{4\pi} \frac{e^{\varepsilon\gamma_E}}{\Gamma(1-\varepsilon)} \left[\frac{(n-2)\beta_0}{2} \frac{1}{\varepsilon} + \sum_i \sum_{i \neq j} \mathbf{T}_i \mathbf{T}_j \left(\frac{1}{\varepsilon^2} + \frac{\gamma_i}{\mathbf{T}_i^2} \frac{1}{\varepsilon} \right) \left(\frac{-2p_i p_j}{\mu^2} \right)^{-\varepsilon} \right] \mathcal{A}_n^{(0)} + \mathcal{O}(\varepsilon^0) \quad (3.8)$$

where α_s denotes the strong coupling constant, γ_E the Euler–Mascheroni constant, μ the mass scale in dimensional regularization, $\Gamma(\dots)$ the Euler Gamma function and ε the dimensional regularization parameter. As given in the introduction $\beta_0 = (\frac{11}{3}N_c - \frac{2}{3}n_f)$, where n_f is the number of active quark flavors in the fundamental representation and N_c the number of colors in the

3.1 Pole Structure of QCD Amplitudes

underlying $SU(N_c)$ gauge theory, i.e. $N_c = 3$ for QCD. The constants γ_i are determined by either $\gamma_q = \gamma_{\bar{q}} = \frac{2}{3}C_F$, with $C_F = (N_c^2 - 1)/2N_c = \frac{1}{2}(N_c - 1/N_c)$, or $\gamma_g = \frac{1}{2}\beta_0$. The color charge operators \mathbf{T}_i are essentially either given in their adjoint representation if^{abc} if i is a gluon or in their fundamental representation T_{ij}^a if i is a (anti-)quark [26]. Therefore $\mathbf{T}_i^2 = C_A = N_c$ if $i = \text{gluon}$ and $\mathbf{T}_i^2 = C_F$ if $i = (\text{anti-})\text{quark}$.

The poles in the bare one-loop parton amplitude are either canceled by the one-loop counterterm $\mathcal{A}_{CT}^{(1)}$, which is for the massless one-loop n -parton amplitude generically given by

$$\mathcal{A}_{CT}^{(1)} = -\frac{\alpha_s}{4\pi} \frac{e^{\varepsilon\gamma_E}}{\Gamma(1-\varepsilon)} \frac{(n-2)\beta_0}{2\varepsilon} \mathcal{A}_n^{(0)} \quad (3.9)$$

or by the real emission contributions integrated over the unresolved one-particle phase-space, which is given in massless QCD by the dipole insertion operator [26, 87]

$$\mathbf{I} = \frac{\alpha_s}{4\pi} \frac{e^{\varepsilon\gamma_E}}{\Gamma(1-\varepsilon)} \sum_i \sum_{i \neq j} \mathbf{T}_i \mathbf{T}_j \left(-\frac{1}{\varepsilon^2} - \frac{\gamma_i}{\mathbf{T}_i^2} \frac{1}{\varepsilon} + \frac{\pi^2}{3} - \frac{\gamma_i}{\mathbf{T}_i^2} - \frac{K_i}{\mathbf{T}_i^2} \right) \left(\frac{|2p_i p_j|}{\mu^2} \right)^{-\varepsilon} + \mathcal{O}(\varepsilon) \quad (3.10)$$

with $K_q = K_{\bar{q}} = \frac{7}{2}C_F - \frac{\pi^2}{6}C_F$ and $K_g = \frac{67}{18}C_A - \frac{\pi^2}{6}C_A - \frac{5}{9}n_f$. These poles, as discussed before, will cancel when combined with the insertion operator \mathbf{L} from the integrated virtual subtraction terms. Remember that in the virtual insertion operator \mathbf{L} the UV poles between the counterterm from usual UV renormalization and the integrated total UV subtraction term are canceled, and the remaining pole structure is only due to the integrated soft and collinear virtual subtraction terms.

We note that after integration, the soft and collinear poles of a bare primitive one-loop amplitude with massless partons are given by [27, 139, 140, 93]

$$A_{bare}^{(1)} = \frac{\alpha_s}{4\pi} \frac{e^{\varepsilon\gamma_E}}{\Gamma(1-\varepsilon)} \sum_{i \in I_g} \left[\left(\frac{2}{\varepsilon^2} \right) \left(\frac{-2p_i p_{i+1}}{\mu^2} \right)^{-\varepsilon} + \frac{2}{\varepsilon} (S_i + S_{i+1}) \right] A_i^{(0)} + \mathcal{O}(\varepsilon^0) \quad (3.11)$$

where the set I_g contains the gluon propagators in the loop and symmetry factors have been introduced, with $\mathcal{S}_i = \mathcal{S}_q = \mathcal{S}_{\bar{q}} = 1$ for external (anti-)quarks and $\mathcal{S}_i = \mathcal{S}_g = \frac{1}{2}$ for external gluons. $A_i^{(0)}$ is a Born partial amplitude, whose corresponding set of tree-level diagrams is gained upon removing the gluon propagator i from the set of diagrams in $A^{(1)}$. This will be further discussed in section 3.2.1.

Let us focus a little more on the pole structure due to UV contributions. In the limit of large loop-momentum k the one-loop integral is generically proportional to $\int d^4k |k|^{a-2n}$. The integrated result will thus be of order $\mathcal{O}(|k|^{a+4-2n})$, which is formally UV divergent for $(a + 4 - 2n) \geq 0$ and in turn determines the local degree of divergence. In QCD we encounter only logarithmic ($a - 2n = -4$), linear ($a - 2n = -3$) and quadratic ($a - 2n = -2$) local UV divergences at the one-loop level, which correspond to propagator and vertex corrections. After integration we are left with the logarithmic UV divergences, i.e. in dimensional regularization in the form of a pole factor which is proportional to a single logarithm of mass scales, while the terms that cause higher divergent powers cancel. In analytic computations usually only the leading logarithmic UV divergent terms are thus taken care of, where renormalization tells us that this can be done by subtracting appropriately chosen counterterms. Further details can be found in standard textbooks and lecture notes, for example [141, 142, 75].

The one-loop UV counterterm to renormalize the massive quark propagator is thereby derived from the quark self-energy diagram to be

$$-i\Sigma(p)_{ij}^{CT} = 2g_s^2 C_F \delta_{ij} \frac{i}{(4\pi)^2} (\not{p} - 4m_t) \frac{1}{\varepsilon} \quad (3.12)$$

where p is the momentum and m_t the mass of the quark. The explicit pole factor in the dimensional regularization parameter ε originates thereby from the UV singular regions. If we remove the color part, where $C_F \delta_{ij} = \frac{1}{2}(N_c - \frac{1}{N_c})\delta_{ij}$ and thus $-i\Sigma(p)_{ij}^{CT} = g_s^2 (N_c - \frac{1}{N_c}) \delta_{ij} \frac{i}{(4\pi)^2} (\not{p} - 4m_t) \frac{1}{\varepsilon}$, this leaves the one-loop counterterm to renormalize the massive color-stripped quark propagator, according to chapter 2 and appendix A, to be

$$-i\Sigma(p)^{CT} = \frac{i}{(4\pi)^2} (\not{p} - 4m_t) \frac{1}{\varepsilon} \quad (3.13)$$

Our interest in the color-stripped renormalized Born propagators and vertices originates in the fact that we will derive the subtraction terms and perform the numerical integration on the level of color-stripped primitive amplitudes, which will become more apparent in the next section 3.2.

The one-loop UV counterterm to renormalize the gluon propagator is derived from the gluon self-energy diagram with a gluon loop, including the necessary ghost contributions, and from the gluon self-energy diagram with a quark loop. The gluonic contribution is thereby given through

3.1 Pole Structure of QCD Amplitudes

$$i\Pi_{\mu\nu,lc}^{CT,ab}(p) = g_s^2 f^{acd} f^{bcd} \frac{i}{(4\pi)^2} \left(\frac{10}{3}\right) (g_{\mu\nu} p^2 - p_\mu p_\nu) \frac{1}{\varepsilon} \quad (3.14)$$

and the fermionic contribution through

$$i\Pi_{\mu\nu,nf}^{CT,ab}(p) = 2g_s^2 T_r(T^a T^b) \frac{i}{(4\pi)^2} \left(-\frac{4}{3}\right) (g_{\mu\nu} p^2 - p_\mu p_\nu) \frac{1}{\varepsilon} \quad (3.15)$$

where p is the momentum of the gluon. If we remove the color parts this leaves us again with the respective color–stripped counterterms

$$i\Pi_{\mu\nu,lc}^{CT}(p) = \frac{i}{(4\pi)^2} \left(\frac{10}{3}\right) (g_{\mu\nu} p^2 - p_\mu p_\nu) \frac{1}{\varepsilon} \quad (3.16)$$

and

$$i\Pi_{\mu\nu,nf}^{CT}(p) = \frac{i}{(4\pi)^2} \left(-\frac{4}{3}\right) (g_{\mu\nu} p^2 - p_\mu p_\nu) \frac{1}{\varepsilon} \quad (3.17)$$

The one–loop UV counterterm to renormalize the quark–gluon vertex is derived from two contributions, the leading color vertex correction which involves a three–gluon coupling and the subleading color vertex correction. The leading color contributions is thereby given through

$$\Gamma_{i\bar{j},lc}^{CT,a\mu} = g_s^2 T_{i\bar{j}}^a \frac{i}{(4\pi)^2} (3C_A) \gamma^\mu \frac{1}{\varepsilon} = g_s^2 N_c T_{i\bar{j}}^a \frac{i}{(4\pi)^2} 3\gamma^\mu \frac{1}{\varepsilon} \quad (3.18)$$

the subleading color contribution through

$$\Gamma_{i\bar{j},sc}^{CT,a\mu} = g_s^2 T_{i\bar{j}}^a \frac{i}{(4\pi)^2} (-C_A + 2C_F) \gamma^\mu \frac{1}{\varepsilon} = g_s^2 \frac{1}{N_c} T_{i\bar{j}}^a \frac{i}{(4\pi)^2} (-1) \gamma^\mu \frac{1}{\varepsilon} \quad (3.19)$$

If we remove the color parts this leaves us again with the respective color–stripped counterterms

$$\Gamma_{lc}^{CT,\mu} = \frac{i}{(4\pi)^2} 3\gamma^\mu \frac{1}{\varepsilon} \quad (3.20)$$

and

$$\Gamma_{sc}^{CT,\mu} = \frac{i}{(4\pi)^2} (-1) \gamma^\mu \frac{1}{\varepsilon} \quad (3.21)$$

The computation of the quark and gluon self-energies defines as usual also the one-loop quark field renormalization constant $Z_2 = 1 + \frac{2g_s^2}{(4\pi)^2} C_F(-\frac{1}{\epsilon})$ and the one-loop gluon field renormalization constant $Z_3 = 1 + \frac{g_s^2}{(4\pi)^2} (4C_A - 2\beta_0)(-\frac{1}{\epsilon})$, where $4C_A - 2\beta_0 = -\frac{10}{3}N_c + \frac{4}{3}n_f$. The one-loop renormalization constant for the strong coupling parameter is usually given by $Z_{g_s} = 1 + \frac{g_s^2}{(4\pi)^2} (-\beta_0)\frac{1}{\epsilon}$.

The counterterms to the vertex corrections can now also be derived from the renormalization constants. The one-loop counterterm to the quark-gluon vertex can thereby be derived from $(1 - Z_{g_2} Z_3^{1/2} Z_2)(T_{ij}^a i\gamma^\mu) = (T_{ij}^a i\gamma^\mu) \frac{g_s^2}{(4\pi)^2} (3N_C - \frac{1}{N_C})\frac{1}{\epsilon}$. The one-loop counterterm to the three-gluon vertex can be derived from $(1 - Z_{g_2} Z_3^{3/2})V_{ggg}^{(0),\mu\nu\lambda,abc}(p_1, p_2, p_3) = \frac{g_s^2}{(4\pi)^2} (\frac{4}{3}n_f - \frac{4}{3}N_C)\frac{1}{\epsilon} V_{ggg}^{(0),\mu\nu\lambda,abc}(p_1, p_2, p_3)$. The one-loop counterterm to the four-gluon vertex can be derived from $(1 - Z_{g_s}^2 Z_3^{4/2})V_{gggg}^{(0),\mu\nu\lambda\rho,abcd} = \frac{g_s^2}{(4\pi)^2} (\frac{4}{3}n_f + \frac{2}{3}N_C)\frac{1}{\epsilon} V_{gggg}^{(0),\mu\nu\lambda\rho,abcd}$. If we again separate off the color degrees of freedom, as described in appendix A, we are left with the counterterms to the color-stripped three- and four-gluon vertices, which read

$$V_{ggg,lc}^{CT,\mu\nu\lambda}(p_1, p_2, p_3) = \frac{iV_3^{\mu\nu\lambda}(p_1, p_2, p_3)}{(4\pi)^2} \left(-\frac{4}{3}\right) \frac{1}{\epsilon} \quad (3.22)$$

$$V_{ggg,nf}^{CT,\mu\nu\lambda}(p_1, p_2, p_3) = \frac{iV_3^{\mu\nu\lambda}(p_1, p_2, p_3)}{(4\pi)^2} \left(\frac{4}{3}\right) \frac{1}{\epsilon} \quad (3.23)$$

and

$$V_{gggg,lc}^{CT,\mu\nu\lambda\rho} = \frac{iV_4^{\mu\nu\lambda\rho}}{(4\pi)^2} \left(\frac{2}{3}\right) \frac{1}{\epsilon} \quad (3.24)$$

$$V_{gggg,nf}^{CT,\mu\nu\lambda\rho} = \frac{iV_4^{\mu\nu\lambda\rho}}{(4\pi)^2} \left(\frac{4}{3}\right) \frac{1}{\epsilon} \quad (3.25)$$

respectively.

In our direct numerical approach we are interested, however, in the local UV behaviour of the integrand. We need to consider all terms that behave locally like $\mathcal{O}(1/|k|^2)$, $\mathcal{O}(1/|k|^3)$ and $\mathcal{O}(1/|k|^4)$, which correspond to quadratic, linear and logarithmic divergences respectively. These terms need to be taken care of on the level of the integrand already, in order to enable the numerical evaluation. What we thus aim for is a method for local one-loop renormalization, which

3.1 Pole Structure of QCD Amplitudes

can be used in numerical approaches to one-loop integration. As described above, we will devise UV subtraction terms that subtract the divergent terms locally off the bare integrand, so that all the terms of order $\mathcal{O}(1/k^2)$, $\mathcal{O}(1/k^3)$ and $\mathcal{O}(1/k^4)$ will be absent in the subtracted integrand and it will locally behave at worst as $\mathcal{O}(1/|k|^5)$ for $|k| \rightarrow \infty$. To this end we derive local UV counterterms for the color-stripped QCD vertex and propagator corrections. Upon integration these local counterterms yield the same results as the counterterms for the color-stripped QCD vertex and propagator corrections that we have just discussed. Since these are all proportional to their respective Born level counterparts, the sum of all integrated local UV counterterms will be proportional to the corresponding Born amplitude. This means in turn that the total local UV subtraction term will yield the same pole structure upon integration as $\mathcal{A}_{CT}^{(1)}$.

The totally subtracted integrand $[\mathcal{G}_{bare}^{(1)} - \mathcal{G}_{coll}^{(1)} - \mathcal{G}_{soft}^{(1)} - \mathcal{G}_{UV}^{(1)}]$ includes no terms anymore which give rise to IR or UV divergences and starts with $\mathcal{O}(1/|k|^5)$ for $|k| \rightarrow \infty$. When we add back the integrated subtraction terms, on the other hand, the one-loop insertion operator \mathbf{L} , which is defined by

$$\mathcal{A}^{(0)*} \mathbf{L} \mathcal{A}^{(0)} = 2Re \mathcal{A}^{(0)*} (\mathcal{A}_{CT}^{(1)} + \mathcal{A}_{soft}^{(1)} + \mathcal{A}_{coll}^{(1)} + \mathcal{A}_{UV}^{(1)}) \quad (3.26)$$

and in massless QCD for example given by [87]

$$\mathbf{L} = \frac{\alpha_s \exp(\varepsilon \gamma_E)}{2\pi \Gamma(1-\varepsilon)} Re \left[\sum_i \sum_{j \neq i} \mathbf{T}_i \mathbf{T}_j \frac{1}{\varepsilon^2} \left(\frac{-2p_i \cdot p_j}{\mu_s^2} \right)^{-\varepsilon} - \sum_i \frac{\gamma_i}{\varepsilon} \left(\frac{\mu_{UV}^2}{\mu_s^2} \right)^{-\varepsilon} - \frac{(n-2)}{2} \beta_0 \log \frac{\mu_{UV}^2}{\mu_s^2} \right] \quad (3.27)$$

which is free of any UV poles, yields in combination with the dipole insertion operator \mathbf{I} [87]

$$\begin{aligned} \mathbf{I} + \mathbf{L} = \frac{\alpha_s}{2\pi} Re \left[\sum_i \sum_{j \neq i} \mathbf{T}_i \mathbf{T}_j \left(\frac{\gamma_i}{\mathbf{T}_i^2} \log \frac{|2p_i p_j|}{\mu_{UV}^2} - \frac{\pi^2}{2} \theta(2p_i p_j) \right) \right. \\ \left. + \sum_i \left(\gamma_i + K_i - \frac{\pi^2}{3} \mathbf{T}_i^2 \right) - \frac{(n-2)}{2} \beta_0 \log \frac{\mu_{UV}^2}{\mu_s^2} \right] \quad (3.28) \end{aligned}$$

which is completely free of any IR or UV poles and can thus be integrated numerically over the $(n-2)$ -particle final-state phase-space in the insertion part. The numerical one-loop integration of $[\mathcal{G}_{bare}^{(1)} - \mathcal{G}_{coll}^{(1)} - \mathcal{G}_{soft}^{(1)} - \mathcal{G}_{UV}^{(1)}]$ will be performed in combination with the $(n-2)$ -particle final-state phase-space integration in the virtual part. The necessary numerical deformation of the loop-integration contour into the complex space, in order to escape the remaining on-

shell poles of the loop-propagators, will be discussed in section 3.4 chapter 5.2. The recursive construction of the integrand to the bare primitive amplitude and the corresponding total local UV subtraction term will be discussed in chapter 4.

3.2 Virtual Subtraction Terms

Remember from chapter 2, especially chapter 2.5, that any QCD one-loop amplitude can be decomposed into color factors multiplying kinematical factors, which can be written as

$$\mathcal{A}^{(1)} = \sum_i C_i A_i^{(1)} = \sum_i C_i \sum_j F_{ij} B_j \quad (3.29)$$

where the factors C_i denote the color factors and the purely kinematical functions $A_i^{(1)}$ are the one-loop partial amplitudes, which are further expressed as linear combination of cyclically ordered one-loop primitive amplitudes B_j . The primitive amplitudes are defined to be gauge invariant sets of diagrams, built from color-stripped Feynman rules, with a fixed cyclic ordering in the external legs and a definite routing of the external fermion legs through the loop. We further separated the contributions with a mixed particle content, i.e. fermions and gluons, or only gluons in the loop from the contributions with closed fermion loops.

Our subtraction terms will be derived on the level of the primitive amplitudes. The cyclic ordering ensures thereby that the QCD flavour of each propagator in the loop is uniquely determined, which leads to a much more compact expression where only a subset of the kinematic loop-invariants plays a role. We stress that using gauge invariant primitive amplitudes is crucial to our method, since gauge invariance and the fixed cyclic ordering of the corresponding sets of diagrams are necessary ingredients in the determination of the local virtual subtraction terms. Furthermore suffer gauge invariant terms less from numerical instabilities. Remember that each primitive amplitude can be represented uniquely by a representative diagram, as discussed in chapter 2.5, and that all other diagrams which contribute to a primitive amplitude can be generated from the representative diagrams by pinching propagators and pulling out trees. Such a representative diagram to a generic primitive amplitude is shown in figure 3.1. The corresponding one-loop integral to such a generic bare primitive amplitude, with n external legs, is written as

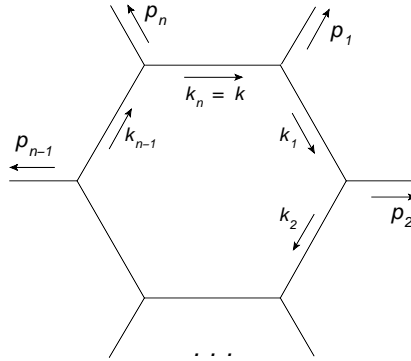


Figure 3.1: Representative diagram to a generic bare primitive one-loop integrand. All external four-momenta are defined as outgoing and the internal loop-momentum is defined in clock-wise direction, where $k_j \equiv k - \sum_{l=1}^j p_l$. The cyclic ordering is defined in clock-wise direction as well.

$$A_{bare}^{(1)} = \int \frac{d^4 k}{(2\pi)^4} G_{bare}^{(1)}, \quad \text{with} \quad G_{bare}^{(1)} = P_a(k, \{p_j\}, \{m_j\}) \prod_{j=1}^n \frac{1}{(k_j^2 - m_j^2) + i\delta} \quad (3.30)$$

where we use $k_j \equiv k - \sum_{l=1}^j p_l$ and the $+i\delta$ -prescription tells us in which direction to deform the integration contour. We will drop the $+i\delta$ from now on. $P_a(k, \{p_j\}, \{m_j\})$ is a polynomial of degree a in the loop momentum k , which generally depends on the external momenta $\{p_j\}$ and on the masses $\{m_j\}$ of the particles in the loop.

The integral becomes singular for $|k| \rightarrow \infty$ if $(4 + a - 2n) \geq 0$. In QCD the corresponding UV divergent diagrams are in general those which correspond to one-loop propagator or vertex corrections. In order to perform the necessary one-loop integration by numerical means we need to subtract those terms which are the source to the UV divergences on the level of the integrand, as discussed in the last section. This can be done by simply expanding the corresponding integrand in the limit of large loop-momentum and subsequently considering only those terms which are locally UV divergent. This has been done before on a Feynman diagrammatic basis [92]. We introduce a method to devise local UV counterterms to propagator and vertex corrections, which can be used to recursively construct a total local UV subtraction term, such that they can be used together with a suitable method to deform the loop integration contour in the numerical one-loop integration. This will be discussed in great detail in subsection 3.2.2.

There are soft divergences for $k \sim q_i$ (or equivalently for $k_i \sim 0$), where $q_i = \sum_{l=1}^i p_l$, if $p_i^2 = m_{i-1}^2$, $m_i = 0$ and $p_{i+1}^2 = m_{i+1}^2$, which we infer from

$$\frac{1}{(k_{i-1}^2 - m_{i-1}^2)(k_i^2 - m_i^2)(k_{i+1}^2 - m_{i+1}^2)} \xrightarrow{k \sim q_i} \frac{1}{(p_i^2 - m_{i-1}^2)(-m_i^2)(p_{i+1}^2 - m_{i+1}^2)} \quad (3.31)$$

where all three denominators in the above become singular simultaneously for the given kinematical setup. There are collinear divergences for $k \sim q_i - xp_i = q_{i-1} + (1-x)p_i$ (or equivalently for $k_i \sim -xp_i$ or $k_{i-1} \sim (1-x)p_i$) if $p_i^2 = 0$, $m_{i-1} = 0$ and $m_i = 0$, which we infer from

$$\frac{1}{(k_{i-1}^2 - m_{i-1}^2)(k_i^2 - m_i^2)} \xrightarrow{k_{i-1} \parallel k_i \parallel p_i} \frac{1}{((1-x)^2 p_i^2 - m_{i-1}^2)(x^2 p_i^2 - m_i^2)} \quad (3.32)$$

where the two denominators in the above become singular simultaneously for the given kinematical setup. In order to perform the necessary one-loop integration by numerical means, we also need to subtract the terms, which are the source to the soft and collinear divergences, locally on the level of the integrand. The corresponding local soft and collinear subtraction terms will be given in the following subsection 3.2.1.

3.2.1 Local Soft and Collinear Subtraction Terms

The thesis at hand has not been concerned with the derivation of the soft and collinear subtraction terms. We will therefore only discuss the necessary basics in this section and refer the reader to [93, 87] for further details.

The soft singular structures, as mentioned above, arise in a setup where a massless particle is exchanged between two on-shell particles. The corresponding diagrammatic setup is depicted in figure 3.2. The collinear singular structures, as mentioned above, arise in a setup where a massless on-shell particle is attached between two massless propagators. The corresponding diagrams are depicted in figure 3.3.

To build the respective soft and collinear subtraction terms to the bare primitive one-loop integrand we have to consider all those diagrams with a gluon at position i and sum over all conceivable positions i . This has been done on a Feynman diagrammatic basis in [92]. It has been shown, however, that one can formulate the subtraction terms for the soft and collinear singularities in a generic multi-parton amplitude directly on the level of the primitive amplitudes [93], which opened the door to the efficient direct numerical implementation based on recurrence relations. The expressions for the soft and collinear subtraction terms are thereby given by

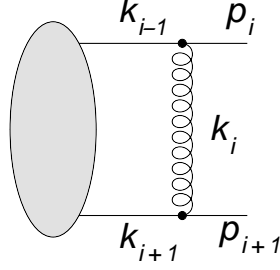


Figure 3.2: Diagrammatic setup, which leads to soft singularities. The two on-shell particles are either gluons, (massive) quarks or both.

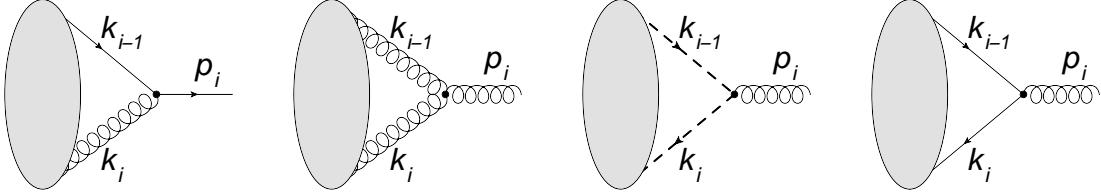


Figure 3.3: Diagrammatic setup, which leads potentially to collinear singularities. The $g \rightarrow$ ghost ghost and the $g \rightarrow qq$ splittings, however, vanish in the collinear limit. Only the $q \rightarrow qg$ and the $g \rightarrow gg$ splittings have a non-vanishing contribution in the collinear limit.

$$G_{soft}^{(1)} = 4i \sum_{j \in I_g} \frac{p_j p_{j+1}}{k_{j-1}^2 k_j^2 k_{j+1}^2} A_j^{(0)} \quad (3.33)$$

and

$$G_{coll}^{(1)} = -2i \sum_{j \in I_g} \left(\frac{\mathcal{S}_j g_{UV}(k_{j-1}^2, k_j^2)}{k_{j-1}^2 k_j^2} + \frac{\mathcal{S}_{j+1} g_{UV}(k_j^2, k_{j+1}^2)}{k_j^2 k_{j+1}^2} \right) A_j^{(0)} \quad (3.34)$$

where the set I_g contains the gluon propagators in the loop and symmetry factors have been introduced, with $\mathcal{S}_i = \mathcal{S}_q = \mathcal{S}_{\bar{q}} = 1$ if the outgoing line i corresponds to a (anti-)quark and $\mathcal{S}_i = \mathcal{S}_g = \frac{1}{2}$ if the outgoing line corresponds to a gluon. $A_j^{(0)}$ is a Born partial amplitude, whose corresponding set of tree-level diagrams is gained upon removing the gluon propagator j from the diagrams in the one-loop primitive amplitude. More explicitly, if we take the set of diagrams which have the gluon propagator j and if we remove from each diagram of this set the said propagator, we obtain a set of diagrams which, after removing multiple copies of identical diagrams, forms the Born partial amplitude $A_j^{(0)}$ [87]. In some cases the removal of such gluons j can give rise to subleading tree-level partial amplitudes, which we will discuss briefly in section

3.3.

We further introduce the function g_{UV} to regularize artificially introduced UV divergences through the $\mathcal{O}(1/|k|^4)$ -behavior in $G_{coll}^{(1)}$. This function has to suppress the collinear subtraction term in the UV region at least by

$$\lim_{k_{i-1}||k_i} g_{UV}(k_{i-1}^2, k_i^2) = 1 \text{ and } \lim_{k \rightarrow \infty} g_{UV}(k_{i-1}^2, k_i^2) = \mathcal{O}(1/|k|) \quad (3.35)$$

There are many possible choices, of which one is given through $g_{UV}(k_{i-1}^2, k_i^2) = 1 - \frac{k_{i-1}^2 k_i^2}{(k-Q)^2 - \mu_{UV}^2}$. In section 5.1 we introduce suppression functions g_{UV} , which contain an even higher power in $((k-Q)^2 - \mu_{UV}^2)^{-1}$ and lead to a better dampening in UV critical regions. The four-vector Q and the mass scale μ_{UV}^2 are arbitrary parameters for the moment, which can be chosen such as to improve the numerical stability upon integration.

The given virtual soft and collinear subtraction terms are formulated directly on the amplitude level, where they match the soft and collinear limits of the corresponding bare primitive one-loop integrand and are proportional to the corresponding Born level amplitude. They are simple and therefore ideally suited for a numerical implementation. They further yield simple results upon analytic integration, which are again proportional to the corresponding Born level amplitude and read

$$S_\varepsilon^{-1} \mu_s^{2\varepsilon} \int \frac{d^D k}{(2\pi)^D} G_{soft}^{(1)} = \frac{-1}{(4\pi)^2} \frac{\exp(\varepsilon\gamma_E)}{\Gamma(1-\varepsilon)} \sum_{j \in I_g} \frac{2}{\varepsilon^2} \left(\frac{-2p_j p_{j+1}}{\mu_s^2} \right)^{-\varepsilon} A_j^{(0)} + \mathcal{O}(\varepsilon) \quad (3.36)$$

and

$$S_\varepsilon^{-1} \mu_s^{2\varepsilon} \int \frac{d^D k}{(2\pi)^D} G_{coll}^{(1)} = \frac{-1}{(4\pi)^2} \frac{\exp(\varepsilon\gamma_E)}{\Gamma(1-\varepsilon)} \sum_{j \in I_g} \frac{2}{\varepsilon} (\mathcal{S}_j + \mathcal{S}_{j+1}) \left(\frac{\mu_{uv}^2}{\mu_s^2} \right)^{-\varepsilon} A_j^{(0)} + \mathcal{O}(\varepsilon) \quad (3.37)$$

which match the pole structure of the dipole insertion term in the dimensional regularization parameter ε for a primitive amplitude in massless QCD (see equation 3.11). The IR subtraction terms for the massive case $m_i \neq 0$ have also been derived, where the soft subtraction term for massive QCD reads

$$G_{soft}^{(1)} = 4i \sum_{j \in I_g} \frac{p_j p_{j+1}}{(k_{j-1}^2 - m_{j-1}^2) k_j^2 (k_{j+1}^2 - m_{j+1}^2)} A_j^{(0)} \quad (3.38)$$

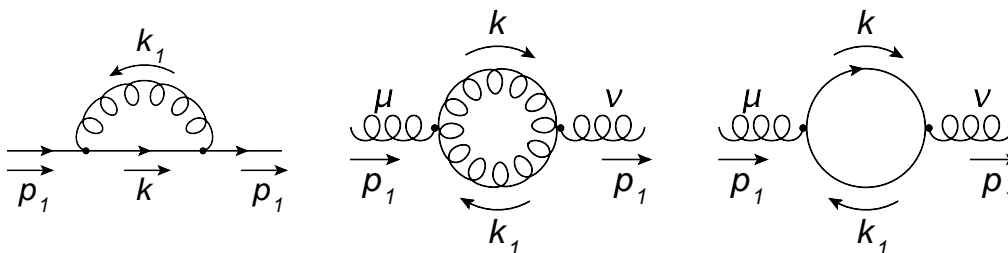


Figure 3.4: Representative diagrams to the various color-stripped ordered propagator corrections.

which integrates to

$$S_\varepsilon^{-1} \mu_s^{2\varepsilon} \int \frac{d^D k}{(2\pi)^D} G_{soft}^{(1)} = \frac{-1}{(4\pi)^2} \frac{\exp(\varepsilon\gamma_E)}{\Gamma(1-\varepsilon)} \sum_{j \in I_g} C((p_j + p_{j+1})^2, m_{j-1}^2, m_{j+1}^2, \mu^2) A_j^{(0)} + \mathcal{O}(\varepsilon) \quad (3.39)$$

The functions $C(s, m_1^2, m_2^2, \mu)$ are given in [93, 87] and will not be repeated here. There is no collinear singularity in the case of a massive external (anti-)quark. For a massive modification of $G_{coll}^{(1)}$ it is therefore sufficient to set $\mathcal{S}_i = \mathcal{S}_q = \mathcal{S}_{\bar{q}} = 0$ in this case. A proof for the soft and collinear subtraction terms on the amplitude level has been given in [93, 87] and will also not be repeated here.

3.2.2 Local UV Subtraction Terms / Local UV Renormalization

We also need to find a subtraction term in order to subtract the UV divergences locally off the integrand to our bare primitive one-loop amplitude. In contrast to the soft and collinear subtraction terms, which are defined directly on the level of the primitive amplitude, the derivation of the UV subtraction term is twofold. We repeat that in QCD the UV divergent one-loop diagrams are exactly those which correspond to propagator and vertex corrections. These are one-loop corrections to the quark and gluon propagators as well as to the quark-gluon, three-gluon and four-gluon vertices. The representative diagrams to the corresponding color-stripped ordered propagator and vertex corrections are shown in figure 3.4 and 3.5 respectively.

For those representative diagrams we can derive local counterterms in the UV limit. These local counterterms are calculated once, i.e. they are process independent and can then be used, in a second step, to recursively build a total local UV subtraction term, which approximates the bare primitive one-loop amplitude in the UV regions of loop-momentum space. The recursive construction of the total UV subtraction term will be discussed in chapter 4.3. In the following

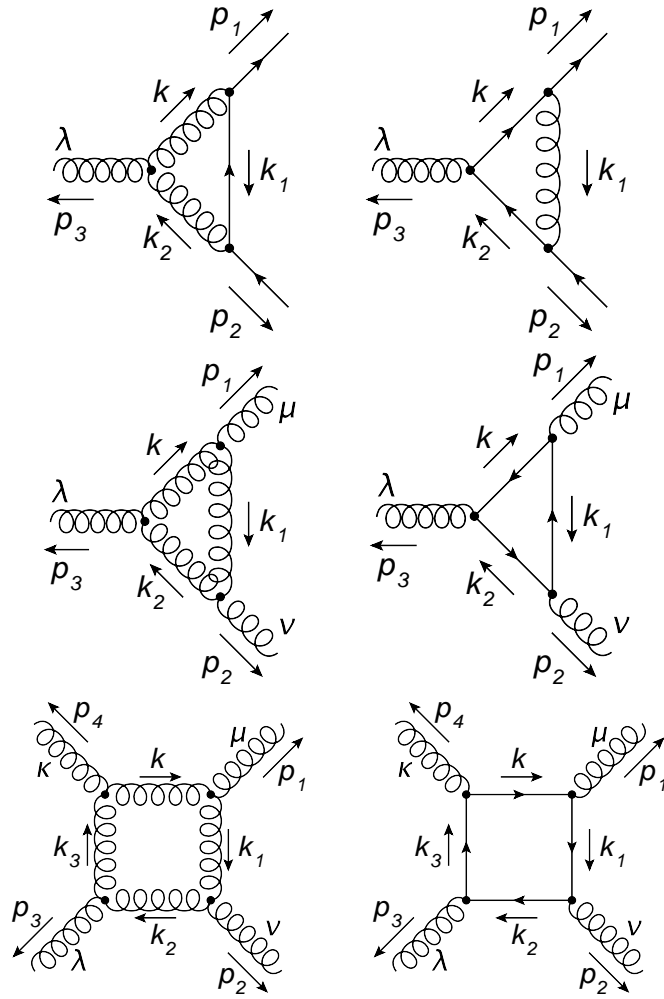


Figure 3.5: Representative diagrams to the various color-stripped ordered vertex corrections.

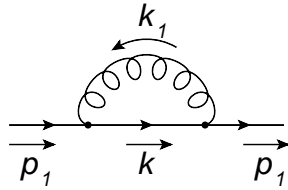


Figure 3.6: One-loop diagram to the color-stripped ordered quark propagator correction.

we will discuss how to explicitly derive all the local UV counterterms to the color-stripped ordered one-loop propagator and vertex corrections.

Each local counterterm, to a given propagator or vertex correction, may consist of several parts, depending whether there are contributions which are leading or subleading in the number of colors N_c , or whether there are contributions from closed fermion loops, generally denoted as n_f -contributions. We will briefly describe the various contributions. A more detailed account is given in appendix C.

There is only one diagram that contributes to the quark propagator correction, which is shown in figure 3.6. For the gluon propagator correction we have to consider the diagrams of figure 3.7. Here we note one diagram with a closed fermion loop, which contributes to the n_f -part of the gluon propagator correction and is gauge independent from the other diagrams, which contribute to the leading color part of the gluon propagator correction and consist of the representative gluon "bubble" diagram, the corresponding ghost "bubble" diagrams, and also those diagrams which are allowed by one-time pinching gluon propagators from the representative gluon "bubble" diagram in all possible ways.

The inclusion of the pinched diagrams at this point in the derivation of the UV counterterms ensures that all UV divergent contributions are correctly taken into account in the recursive construction of the total UV subtraction term to the bare primitive one-loop amplitude.

The correction to the quark-gluon vertex consists of two diagrams, where the first is leading in color and the second is subleading in color. These are shown in figure 3.8.

All necessary diagrams to derive the local UV counterterms to the three- and four-gluon vertices are shown in the figures 3.9 and 3.10 respectively, where we distinguish again the diagrams that contribute to the respective n_f -parts from all the necessary diagrams that contribute to the

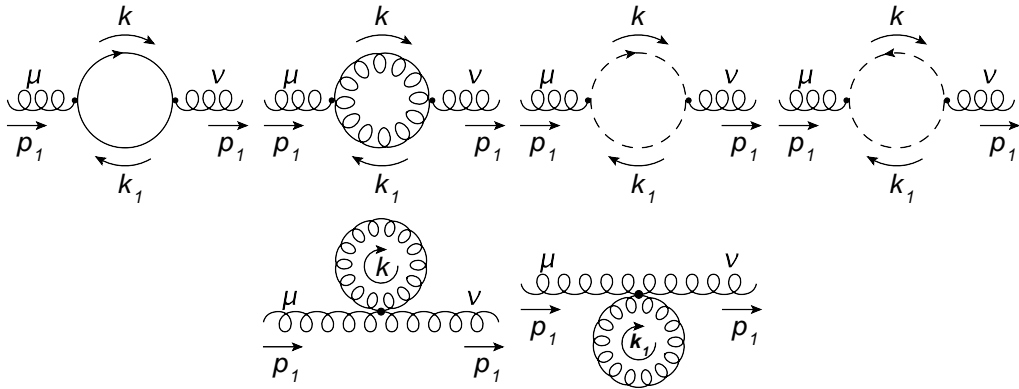


Figure 3.7: One-loop diagrams to the ordered color-stripped gluon propagator correction. The first diagram contributes to the n_f -part, all other diagrams contribute to the leading color part.

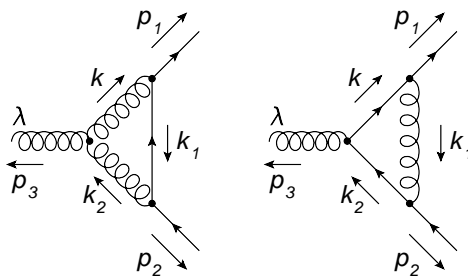


Figure 3.8: One-loop diagrams to the ordered color-stripped quark-gluon vertex correction. The first diagram contributes to the leading color part and the second diagram to the subleading color part.

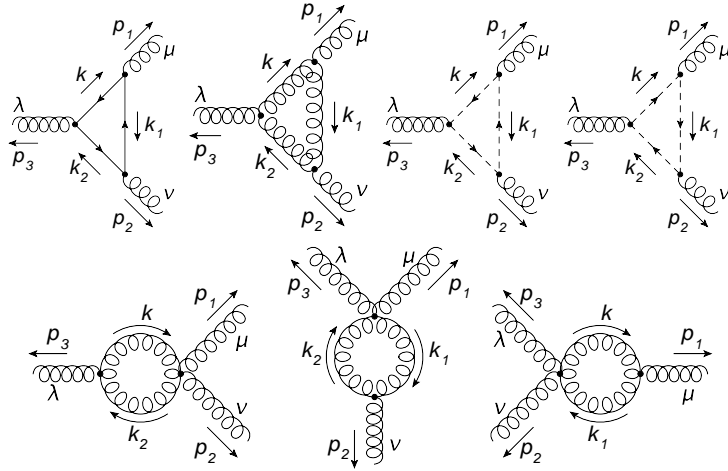


Figure 3.9: One-loop diagrams to the ordered color-stripped three-gluon vertex correction. The first diagram contributes to the n_f -part, all other diagrams contribute to the leading color part.

respective leading color parts.

We will call the collection of all diagrams to a given propagator or vertex correction, as discussed above, a graph G . The integrand of such an ordered bare one-loop graph G with n_G external legs, and therefore a set of n_G outgoing four-momenta, and n_G internal masses in the loop on the representative level, is written as

$$g_{n_G,a}^G(k, \{p_j\}, \{m_j\}) \equiv P_a^G(k, \{p_j\}, \{m_j\}) \prod_{j=1}^{n_G} \frac{1}{(k_j^2 - m_j^2)} \quad (3.40)$$

where we dropped the $+i\delta$ -prescription in the denominator and used $k_j \equiv k - \sum_{l=1}^j p_l$. Here $P_a^G(k, \{p_j\}, \{m_j\})$ is a polynomial of degree a in the loop momentum k , which differs somewhat from the notation for the one-loop integrals in appendix E and which generally depends on the external momenta $\{p_j\}$ and on the masses $\{m_j\}$ of the particles in the loop, subject to the given graph G . The algebraic reductions to simplify $P_a^G(k, \{p_j\}, \{m_j\})$ are done in general D dimensions, where the four-dimensional trace for the Dirac gamma matrices is used as commonly accepted. The integrand $g_{n_G,a}^G(k, \{p_j\}, \{m_j\})$ is therefore of degree $(a - 2n_G)$ in the loop momentum k . Depending on G , i.e. which type of correction is given, we are faced with different (leading) local degrees of UV divergence. Simple power counting in k yields a local quadratic UV divergence for the gluon self-energy, local linear UV divergences for the quark self-energy and the three-gluon vertex correction, and local logarithmic UV divergences for the quark-gluon

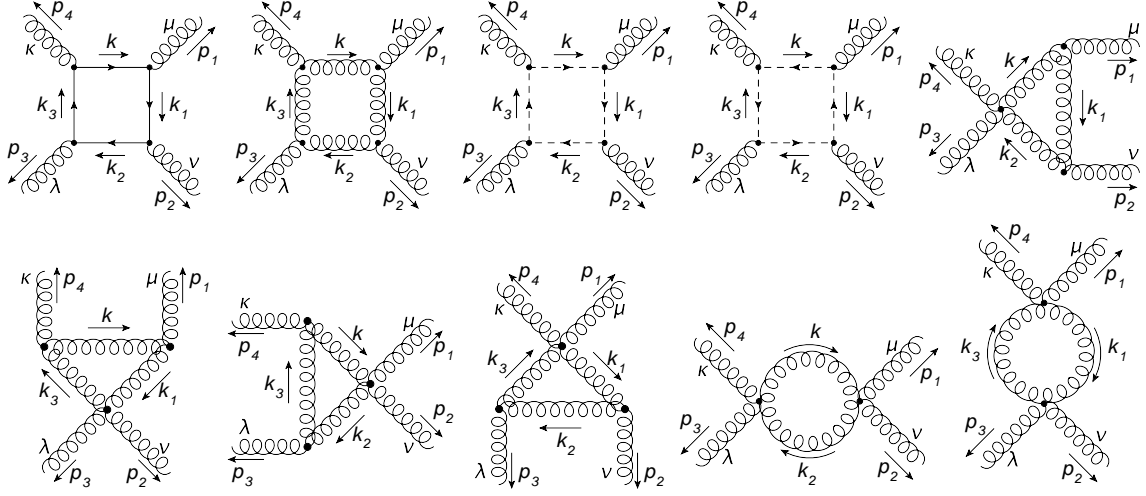


Figure 3.10: One-loop diagrams to the ordered color-stripped four-gluon vertex correction. The first diagram contributes to the n_f -part, all other diagrams contribute to the leading color part.

and the four-gluon vertex corrections. The integrands are built from color-stripped Feynman rules, as given in appendix A, and the corresponding expressions are given in appendix C.

As discussed before, the strategy is now to devise a set of local UV counterterms that match the UV behaviour of these UV divergent graphs locally, in order to carry out the UV subtraction already at the level of the integrand. To this end we expand the integrand $g_{n_G,a}^G(k, \{p_j\}, \{m_j\})$ in the limit of large loop-momentum k and subsequently only keep those terms that are of $\mathcal{O}(1/|k|^2)$, $\mathcal{O}(1/|k|^3)$ and $\mathcal{O}(1/|k|^4)$. More precisely, we shift the loop-momentum $k \rightarrow \bar{k} = k - Q$, where Q is an arbitrary four-vector, and expand around a new UV propagator of the form $(\bar{k}^2 - \mu_{UV}^2)^{-1}$, where we introduce a new additional mass scale μ_{UV} . The expansion for a single propagator reads thereby

$$\frac{1}{((k-p)^2 - m^2)} = \frac{1}{(\bar{k}^2 - \mu_{UV}^2)} \left\{ 1 + \frac{2\bar{k} \cdot (p-Q)}{\bar{k}^2 - \mu_{UV}^2} - \frac{(p-Q)^2 - m^2 + \mu_{UV}^2}{\bar{k}^2 - \mu_{UV}^2} + \frac{(2\bar{k} \cdot (p-Q))^2}{(\bar{k}^2 - \mu_{UV}^2)^2} \right\} + \mathcal{O}(1/|\bar{k}|^5) \quad (3.41)$$

After the expansion the singularities of every integrand $g_{n_G,a}^G(k, \{p_j\}, \{m_j\})$ will then be determined only by powers of the one UV propagator $(\bar{k}^2 - \mu_{UV}^2)^{-1}$, i.e. they will be located on the surface of a single cone described by $\bar{k}^2 - \mu_{UV}^2 = 0$. The integration of the associated terms will thus be simplified. In general we get

$$g_{n_G,a}^G(\bar{k}, Q, \{p_j\}, \{m_j\}) \equiv \frac{P_a^G(\bar{k}, Q, \{p_j\}, \{m_j\})}{(\bar{k}^2 - \mu_{UV}^2)^{n_G}} \left\{ \sum_{m=0}^{\infty} \frac{U_m(\bar{k}, Q, \{p_j\}, \{m_j\})}{(\bar{k}^2 - \mu_{UV}^2)^m} \right\} \quad (3.42)$$

where $P_a^G(\bar{k}, Q, \{p_j\}, \{m_j\})$ is now a polynomial of degree a in the shifted loop-momentum \bar{k} and $U_m(\bar{k}, Q, \{p_j\}, \{m_j\})$ a polynomial of degree m in \bar{k} . The arbitrary four-vector Q and the newly introduced mass scale μ_{UV}^2 can be chosen to our will, even complex valued, since the outcome of the computation will not depend on one or the other. We will choose those parameters such as to enhance the numerical stability of our one-loop integral, which will be discussed further in section 3.4 and especially in chapter 5.2. The local UV counterterms will be chosen such that the integrated results are independent of Q . Every summand is now of degree $(a - 2n_G - m)$ in \bar{k} . We define the truncated expansion by

$$g_{n_G,a}^{G,\ell_G}(\bar{k}, Q, \{p_j\}, \{m_j\}) \equiv \frac{P_a^G(\bar{k}, Q, \{p_j\}, \{m_j\})}{(\bar{k}^2 - \mu_{UV}^2)^{n_G}} \left\{ \sum_{m=0}^{\ell_G} \frac{U_m(\bar{k}, Q, \{p_j\}, \{m_j\})}{(\bar{k}^2 - \mu_{UV}^2)^m} \right\} \quad (3.43)$$

and choose the expansion limit ℓ_G such that $(4 + a - 2n - m) \geq 0$, i.e. $(4 + a - 2n - \ell_G) = 0$ or $(4 - \ell_G = 2n - a)$. We note that ℓ_G depends as such on the local degree of UV divergence of G . If we want to truncate the expansion such that the result only subtracts terms of $\mathcal{O}(1/|k|^2)$, $\mathcal{O}(1/|k|^3)$ and $\mathcal{O}(1/|k|^4)$ we can choose $\ell_G = 0$ if G is (locally) logarithmic divergent, $\ell_G = 1$ if G is linearly divergent and $\ell_G = 2$ if G is quadratically divergent.

The UV divergent parts of $g_{n_G,a}^{G,\ell_G}(\bar{k}, Q, \{p_j\}, \{m_j\})$ match now exactly the UV divergent parts of $g_{n_G,a}^G(k, \{p_j\}, \{m_j\})$. Integration of $g_{n_G,a}^{G,\ell_G}(\bar{k}, Q, \{p_j\}, \{m_j\})$ in dimensional regularization thus yields in general

$$S_\varepsilon^{-1} \mu^{2\varepsilon} \int \frac{d^D \bar{k}}{(2\pi)^D} g_{n_G,a}^{G,\ell_G}(\bar{k}, Q, \{p_j\}, \{m_j\}) = C^{G,(0)}(\{p_j\}, \{m_j\}) \left(\frac{1}{\varepsilon} - \log\left(\frac{\mu_{uv}^2}{\mu^2}\right) \right) + R^{G,\ell_G}(\{p_j\}, \{m_j\}) + \mathcal{O}(\varepsilon) \quad (3.44)$$

where $C^{G,(0)}(\{p_j\}, \{m_j\})$ takes on the typical form of the corresponding renormalized color-ordered Born level propagator or vertex function and $R^{G,\ell_G}(\{p_j\}, \{m_j\})$ is a finite remainder, which depends on G and the truncation of the UV expansion. The explicit pole factors in $1/\varepsilon$ are the typical pole factors of one-loop integrals which originate in the UV singular regions.

We would like to choose our local UV counterterms, as mentioned before, such that after

the integration the pole part and the finite part have the same factor of proportionality, i.e. $C^{G,(0)}(\{p_j\}, \{m_j\})$, and the additional finite remainder $R^{G,\ell_G}(\{p_j\}, \{m_j\})$ vanishes. This ensures that the sum of all integrated local counterterms to the bare primitive one-loop amplitude is proportional to the corresponding color-ordered Born level amplitude, which is important for the recursive construction of a total (local) UV subtraction term from the local UV counterterms. To this end we subtract a locally finite version of $R^{G,\ell_G}(\{p_j\}, \{m_j\})$ from $g_{n_G,a}^{G,\ell_G}(\bar{k}, Q, \{p_j\}, \{m_j\})$ and define

$$g_{n_G,a}^{G,\ell_G,UV}(\bar{k}, Q, \{p_j\}, \{m_j\}) = g_{n_G,a}^{G,\ell_G}(\bar{k}, Q, \{p_j\}, \{m_j\}) - \frac{-2\mu_{UV}^2 R^{G,\ell_G}(\{p_j\}, \{m_j\})}{(\bar{k}^2 - \mu_{UV}^2)^3} \quad (3.45)$$

We note that $S_\varepsilon^{-1} \mu^{2\varepsilon} \int d^D \bar{k} (\bar{k}^2 - \mu_{UV}^2)^{-3} = -\frac{1}{2\mu_{UV}^2} (1 + \mathcal{O}(\varepsilon)) = \text{finite}$, which finally leads upon integration to

$$S_\varepsilon^{-1} \mu^{2\varepsilon} \int \frac{d^D \bar{k}}{(2\pi)^D} g_{n_G,a}^{G,\ell_G,UV}(\bar{k}, Q, \{p_j\}, \{m_j\}) = C^{G,(0)}(\{p_j\}, \{m_j\}) \left(\frac{1}{\varepsilon} - \log\left(\frac{\mu_{uv}^2}{\mu^2}\right) \right) + \mathcal{O}(\varepsilon) \quad (3.46)$$

where we observe that the only finite part in the integrated result is now proportional to the pole part, with $C^{G,(0)}(\{p_j\}, \{m_j\})$ as factor of proportionality.

In practice the expansion for large \bar{k} follows from

$$\begin{aligned} g_{n_G,a}^G(k, \{p_j\}, \{m_j\}) &= P_a^G(k, \{p_j\}, \{m_j\}) \prod_{j=1}^{n_G} \frac{1}{(k_j^2 - m_j^2)} \\ &= \frac{P_a^G(\bar{k}, Q, \{p_j\}, \{m_j\})}{(\bar{k}^2 - \mu_{UV}^2)^{n_G}} \prod_{j=1}^{n_G} \frac{1}{\left(\frac{(Q_j^2 - m_j^2) + \mu_{UV}^2}{(k^2 - \mu_{UV}^2)} + \frac{2\bar{k} \cdot Q_j}{(k^2 - \mu_{UV}^2)} + 1 \right)} \end{aligned} \quad (3.47)$$

where $k_j^2 = (\bar{k} + Q_j)^2$ and $Q_j = Q - q_j = Q - (p_1 + \dots + p_j)$, and from the expansion

$$\begin{aligned} \frac{1}{a_j x^2 + b_j x + 1} &= 1 + x^1(-b_j) + x^2(-a_j + b_j^2) + x^3(2a_j b_j - b_j^3) + x^4(a_j^2 - 3a_j b_j^2 + b_j^4) \\ &\quad + x^5(-3a_j^2 b_j + 4a_j b_j^3 - b_j^5) + x^6(-a_j^3 + 6a_j^2 b_j^2 - 5a_j b_j^4 + b_j^6) + \mathcal{O}(x^7) \end{aligned} \quad (3.48)$$

with $a_j = \frac{(Q_j^2 - m_j^2) + \mu_{UV}^2}{(k^2 - \mu_{UV}^2)}$ and $b_j = \frac{2\bar{k} \cdot Q_j}{(k^2 - \mu_{UV}^2)}$. In the practical application we expand the integrand

3.2 Virtual Subtraction Terms

$g_{n_G,a}^G(k, \{p_j\}, \{m_j\})$ up to a high enough power in \bar{k} and throw away every term that is of order $\mathcal{O}(\bar{k}^{-n_{fin}})$ for $n_{fin} \geq 5$.

As an example consider the self-energy correction to the massless quark propagator. Here we have $P_a^G(k, \{p_j\}, \{m_j\}) = (-1)\gamma^\mu \not{k} \gamma_\mu = 2 \not{k}(1-\varepsilon)$, with $D = 4-2\varepsilon$ in dimensional regularization and where we have performed the algebraic reduction in general D dimensions. In this case $a = 1$ and $\{m_j\} = (m_1, m_2 = m_0 \equiv m) = (0, 0)$. The product of denominators is simply $1/(k^2 k_1^2)$, with $k_2 = k_0 \equiv k$, so $n = 2$. This yields for the integrand

$$\begin{aligned} & \frac{P_a^G(\bar{k}, Q, \{p_j\}, \{m_j\})}{(\bar{k}^2 - \mu_{UV}^2)^{n_G}} \prod_{j=1}^{n_G} \frac{1}{\left(\frac{(Q_j^2 - m_j^2) + \mu_{UV}^2}{(\bar{k}^2 - \mu_{UV}^2)} + \frac{2\bar{k} \cdot Q_j}{(\bar{k}^2 - \mu_{UV}^2)} + 1\right)} \\ &= \frac{2(\bar{k} + Q)(1-\varepsilon)}{(\bar{k}^2 - \mu_{UV}^2)^2} \prod_{j=1}^2 \frac{1}{\left(\frac{(Q_j^2 - m_j^2) + \mu_{UV}^2}{(\bar{k}^2 - \mu_{UV}^2)} + \frac{2\bar{k} \cdot Q_j}{(\bar{k}^2 - \mu_{UV}^2)} + 1\right)} \end{aligned} \quad (3.49)$$

$(\mathcal{O}(1/\bar{k}^3) + \mathcal{O}(1/\bar{k}^4))$

where we note that we need the expansion of the product function only up to order $\mathcal{O}(1/|\bar{k}|)$ if we want to match only up to the singular $\mathcal{O}(1/|\bar{k}|^4)$ -behavior. So, using the above expansion in equation 3.48 each bracket in the denominator of the product function has to be expanded up to order $\mathcal{O}(x)$, which corresponds to order $\mathcal{O}(1/|\bar{k}|)$. In total the expansion yields

$$\begin{aligned} & \frac{2(\bar{k} + Q)(1-\varepsilon)}{(\bar{k}^2 - \mu_{UV}^2)^2} (1 + x(-b_1 - b_2) + \mathcal{O}(x^2)) \\ &= \frac{2(\bar{k} + Q)(1-\varepsilon)}{(\bar{k}^2 - \mu_{UV}^2)^2} \left(1 + \left(-\frac{2\bar{k} \cdot Q_1}{(\bar{k}^2 - \mu_{UV}^2)} - \frac{2\bar{k} \cdot Q_2}{(\bar{k}^2 - \mu_{UV}^2)}\right) + \mathcal{O}(1/\bar{k}^2)\right) \\ &= \underbrace{\frac{2(1-\varepsilon)(\bar{k} + Q)}{(\bar{k}^2 - \mu_{UV}^2)^2}}_{\mathcal{O}(1/\bar{k}^3) + \mathcal{O}(1/\bar{k}^4)} + \underbrace{\frac{-4(1-\varepsilon)(\bar{k} \cdot Q + \bar{k} \cdot Q_1) \bar{k}}{(\bar{k}^2 - \mu_{UV}^2)^3}}_{\mathcal{O}(1/\bar{k}^4)} + \underbrace{\frac{-4(1-\varepsilon) Q(\bar{k} \cdot Q + \bar{k} \cdot Q_1)}{(\bar{k}^2 - \mu_{UV}^2)^3}}_{\mathcal{O}(1/\bar{k}^5)} \\ &= \frac{2(1-\varepsilon)(\bar{k} + Q)}{(\bar{k}^2 - \mu_{UV}^2)^2} + \frac{-4(1-\varepsilon)(\bar{k} \cdot Q + \bar{k} \cdot Q_1) \bar{k}}{(\bar{k}^2 - \mu_{UV}^2)^3} + \mathcal{O}(1/\bar{k}^5) \end{aligned} \quad (3.50)$$

with $b_2 = b_0 \equiv b$ and $Q_2 = Q_0 \equiv Q$. We also see that even if we had considered the massive case it would have made no difference in the expansion since the dependence on the masses only enters with the coefficients a_j in equation 3.48, which does not play a role if we expand only up

to order $\mathcal{O}(x)$. Hence, we can also use the approximate initial expression in equation C.3, in appendix C, for the massive case in this expansion. Integration upon $S_\varepsilon^{-1}\mu^{2\varepsilon} \int \frac{d^D \bar{k}}{(2\pi)^D}$, where the necessary integral equations can be found in appendix E, yields

$$\frac{i}{(4\pi)^2} \left[(p_\perp - 4m_t) \left(\frac{1}{\varepsilon} - \log \frac{\mu_{UV}^2}{\mu^2} \right) - p_\perp \right] + \mathcal{O}(\varepsilon) \quad (3.51)$$

and we note the additional finite remainder to be $R^{G, \ell_G}(\{p_j\}, \{m_j\}) = -p_\perp$. Further, the local form of the corresponding counterterm to the massive quark propagator with mass m_t , already subtracting the additional finite remainder, is for example given by

$$g_{2,1}^{qq, \ell_{qq}=1, UV}(\bar{k}, Q, p_1, m_t) = \left[\frac{-4(1-\varepsilon)(\bar{k} \cdot Q + \bar{k} \cdot Q_1)\bar{k} + 2\mu_{UV}^2(-p_\perp + 2m_t)}{(\bar{k}^2 - \mu_{UV}^2)^3} + \frac{2(1-\varepsilon)(\bar{k} + Q) - 2(2-\varepsilon)m_t}{(\bar{k}^2 - \mu_{UV}^2)^2} \right] \quad (3.52)$$

and upon integration this yields

$$\begin{aligned} -i\Sigma_{UV}^{(1)} &= S_\varepsilon^{-1}\mu^{2\varepsilon} \int \frac{d^D \bar{k}}{(2\pi)^D} g_{2,1}^{qq, \ell_{qq}=1, UV}(\bar{k}, Q, p_1, m_t) \\ &= \frac{i}{(4\pi)^2} \left[(p_\perp - 4m_t) \left(\frac{1}{\varepsilon} - \log \frac{\mu_{UV}^2}{\mu^2} \right) \right] + \mathcal{O}(\varepsilon) \end{aligned} \quad (3.53)$$

where from equation 3.13 in section 3.1 we know that this is the correct expression for the renormalized massive color-ordered Born level quark propagator.

The results, local as well as integrated, for all other local UV counterterms to the color-stripped ordered propagator and vertex corrections are given in appendix D. The individual local UV counterterms $g_{n,a}^{G, \ell_G, UV}(\bar{k}, Q, \{p_j\}, \{m_j\}, \ell)$, for propagators and vertices, can now be used to recursively construct a total local UV subtraction term $G_{UV}^{(1)}$ to the bare primitive integrand $G_{bare}^{(1)}$ of a given primitive one-loop amplitude, which will be further discussed in chapter 4.3.

The summation limits ℓ_G , as chosen above, yield a situation where $G_{bare}^{(1)} - G_{UV}^{(1)} \propto \mathcal{O}(1/|k|^5)$. However, our experience shows that, in order to further improve the numerical stability in the UV, it is worthwhile to choose the summation limits ℓ_G such that $G_{bare}^{(1)} - G_{UV}^{(1)} \propto \mathcal{O}(1/|k|^7)$. This will be further discussed in the chapter 5.1.

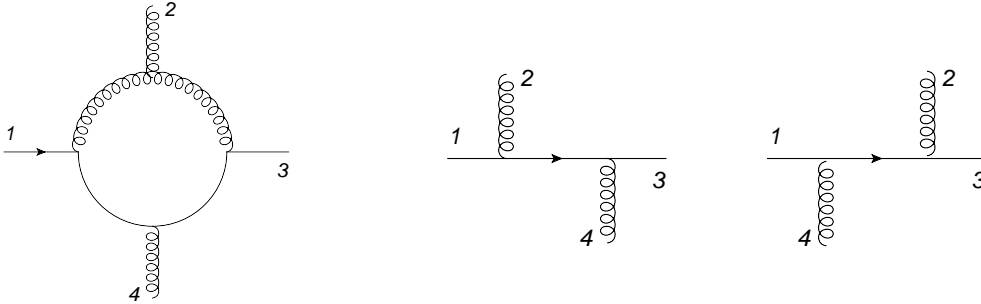


Figure 3.11: *Left: Representative diagram to a four-parton primitive amplitude with one quark-antiquark pair and the cyclic ordering $(1_{\bar{q}}, 2_g, 3_q, 4_g)$. Right: Removing for example the gluon loop-propagator k_1 in all the diagrams in the set $A^{(1)}(1_{\bar{q}}, 2_g, 3_q, 4_g)$, subsequently removing double-copies, leads to the two depicted tree-level diagrams.*

3.3 Remarks

Remember that in the formula for the infrared subtraction terms we sum over all indices $j \in I_g$, where the set I_g denotes the set of indices j , for which the propagator j in the loop corresponds to a gluon. In other words, a primitive amplitude which has soft or collinear divergences must have at least one loop propagator which corresponds to a gluon. If we take the subset of diagrams which have the loop propagator j and if we remove from each diagram of this subset said propagator, we then obtain a set of tree-level diagrams which form the Born partial amplitude $A_j^{(0)}$. Equations 3.33 and 3.34 approximate the integrand of a primitive one-loop QCD amplitude in all soft and collinear limits, where the approximation is given by simple scalar two- and three-point functions, multiplied by the corresponding Born partial amplitude $A_j^{(0)}$.

Consider now the following situation in figure 3.11, where we have one external quark-antiquark pair and $n = 2$ external gluons. In all the pinched diagrams to the representative one-loop diagram on the left of figure 3.11 we can remove for example the propagator k_1 , which in the representative diagram connects between the external partons 1 and 2. This leaves us with a set of tree-level diagrams, and upon the removal of identical diagrams this leaves us with the two diagrams on the right of figure 3.11. If we look closer we note that these diagrams do not contain a three-gluon vertex. The associated tree-level partial amplitude is a subleading tree-level partial amplitude $A^{(0)}(1_{\bar{q}}, 2_g, 3_q, 4_g)$ with the same cyclic order $(1_{\bar{q}}, 2_g, 3_q, 4_g)$ as the corresponding primitive one-loop amplitude.

If we add the leading partial amplitudes $A^{(0)}(1_{\bar{q}}, 2_g, 4_g, 3_q)$ and $A^{(0)}(1_{\bar{q}}, 4_g, 2_g, 3_q)$ we are also

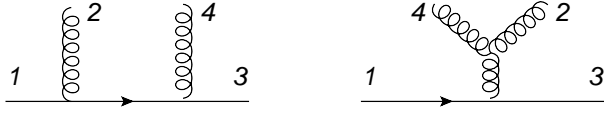


Figure 3.12: Diagrams contributing to the leading partial amplitude $A^{(0)}(1_{\bar{q}}, 2_g, 4_g, 3_q)$.

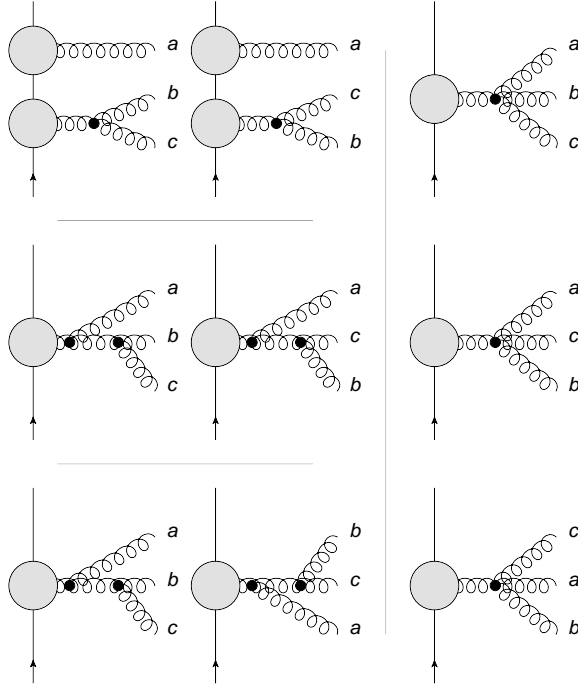


Figure 3.13: Due to the antisymmetric nature of the color-stripped three- and four-valent vertices certain combinations of diagrams cancel each other.

left with the diagrams on the right in figure 3.11. Due to the antisymmetric nature of the color-stripped three-gluon vertex, with respect to exchange of any two of the three legs, the diagrams which contain a three-gluon vertex cancel, since in one the three-gluon vertex appears in the ordering $(\dots, 2, 4, \dots)$ and in the other in the ordering $(\dots, 4, 2, \dots)$. We have to consider, though, that in each of the tree-level diagrams in figure 3.11 one of the gluons is radiated to the left with respect to the fermion flow, so $A^{(0)}(1_{\bar{q}}, 2_g, 3_q, 4_g) = -A^{(0)}(1_{\bar{q}}, 2_g, 4_g, 3_q) - A^{(0)}(1_{\bar{q}}, 4_g, 2_g, 3_q)$. The appropriate generalization to one quark-antiquark pair and $(n - 2)$ gluons is simply given by the Kleiss-Kuijf relations in equation 2.38, if we replace the gluon 1 and the gluon n with \bar{q} and q respectively, which was also noted towards equation 2.36.

Let us examine the general case for the above a little closer. As we infer from chapter 2.4, the subleading partial amplitudes can be written in terms of leading partial amplitudes, which reads

$$A^{(0)}(\bar{q}, \underbrace{g_1, \dots, g_m}_{\{\alpha\}}, q, \underbrace{g_{m+1}, \dots, g_{n-2}}_{\{\beta\}^T}) = (-1)^{\#\beta} \sum_{OP\{\alpha\}\{\beta\}} A^{(0)}(\bar{q}, g_1, \dots, g_m, \underbrace{g_{n-2}, \dots, g_{m+1}}_{\{list\}}, q) \quad (3.54)$$

where $\{\alpha\} = \{g_1, \dots, g_m\}$, $\{\beta\} = \{g_{n-2}, \dots, g_{m+1}\}$ and $\#\beta$ denotes the number of elements in the set $\{\beta\}$. $OP\{\alpha\}\{\beta\}$ denotes the ordered product, also shuffle, between $\{\alpha\}$ and $\{\beta\}$, which is the set of all permutations of the members in the ordered list $\{list\}$, with \bar{q} held fixed, that preserve the ordering of the $\alpha_i \in \{\alpha\}$ within $\{\alpha\}$ and the ordering of the $\beta_i \in \{\beta\}$ within $\{\beta\}$, while allowing for all relative orderings of the α_i with respect to the β_i .

In the shuffle sum each diagram of $A^{(0)}(\bar{q}, \dots, a, b, \dots, q)$ with a three-valent vertex in the cyclic ordering (\dots, a, b, \dots) has an identical counterpart from the amplitude $A^{(0)}(\bar{q}, \dots, b, a, \dots, q)$ with the reversed ordering (\dots, b, a, \dots) . However, these counterparts cancel each other due to the antisymmetric nature of the color-stripped three-valent vertex. For the four-valent vertices that appear we have a similar situation. In the sum over shuffles the four-valent vertices appear always in combinations (\dots, c, a, b, \dots) , (\dots, a, c, b, \dots) and (\dots, a, b, c, \dots) . Also these combinations cancel each other due to the antisymmetric nature of the color-stripped four-valent vertex. A representation of contributions that cancel each other is shown in figure 3.13, where the gray "blobs" represent further underlying arbitrary interactions, but the same for all contributions that cancel each other. The contributions that cancel each other are thereby figuratively clustered. Considering all the possible shuffles for a given subleading tree-level partial amplitude in equation 3.54 and summing them up we are left only with non-abelian interactions between gluons of the same sets, but all non-abelian interactions between gluons from different sets are absent. In a sense the gluons from the two sets behave as if they belonged to different gauge groups respectively.

As we saw in chapter 2.5.3, for problems with more than one quark-antiquark pair we can have primitive amplitudes, whose representative diagrams contain tree-level like sub-diagrams. These are diagrams where for a specific cyclic ordering one of the fermion lines is not allowed to enter the loop. Such a situation is depicted if we pinch from the diagram in figure 3.1 for example the loop-propagator k_n . This leaves a tree-level like sub-diagram where the fermion line between p_1 and p_n is attached to the loop via a branch, which is attached itself between the loop-propagators k_{n-1} and k_1 . We note that the subtraction terms for the corresponding primitive amplitude can nevertheless be applied, where we simply remove the propagator k_n

from the set I_g of gluon propagators in the loop.

Further remarks concerning the renormalization scheme independence and the locality of the soft and collinear subtraction terms have been given in [87].

3.4 One-Loop Integration

We want to give a brief overview on one-loop techniques. Except for the integrals that are needed for the analytical integration of the local UV counterterms, this thesis was not concerned with the matter of the actual (numerical) one-loop integration. We will thus only give a short overview on the standard techniques. Plenty of references can be found in the literature [33–51] and [52–70, 67, 71–73]. Further comprehensive overviews can be found in [8, 74–77]. We will also give a brief introduction to the numerical method, which was elaborated on in more detail in [87, 91].

In appendix E we have explained how to solve scalar integrals of the generic form $I_{n,a}(A) \equiv \int d^D k (k^2)^a (k^2 - A + i\delta)^{-n}$, where Feynman's $+i\delta$ -prescription tells us how to regulate the on-shell poles at $k^2 = A$, by deforming the integration contour into complex space. Considering $a = 0$ for the moment, we have in general however scalar integrals of the form

$$I_{n,0}(\{p_i\}, \{m_i\}) \equiv \int d^D k \prod_{i=1}^n \frac{1}{(k_i^2 - m_i^2 + i\delta)} \quad (3.55)$$

with $k_i \equiv k - q_i$, where $q_i \equiv p_1 + \dots + p_i$, and $k_n = k$ due to momentum conservation of the outgoing external four-momenta p_i . These are the scalar one-loop n -point functions with arbitrary masses m_i in each one-loop propagator. For $n = 1$, $n = 2$ or $n = 3$ we have for example a scalar tadpole, bubble or triangle diagram respectively with arbitrary masses. The $+i\delta$ -regulators in the denominator tell us in which direction the poles in the complex k_0 -plane have to be shifted, or equivalently in which direction the integration contour has to be deformed, in order for the integral to be well-defined. In contrast to the example in appendix E, however, we have now multiple poles in different locations in the complex k_0 -plane, since for $n > 1$ the denominators are not given in a quadratic form in the integration variable anymore. This is usually solved by introducing Feynman parameters, where we turn the product over denominators into a sum at the cost of introducing additional integrals by using the identity

$$\prod_{i=1}^n \frac{1}{(P_i)^{\nu_i}} = \frac{\Gamma(\nu)}{\prod_{i=1}^n \Gamma(\nu_i)} \int_0^1 \left(\prod_{i=1}^n dx_i x_i^{\nu_i-1} \right) \frac{\delta(1 - \sum_{i=1}^n x_i)}{\left(\sum_{i=1}^n x_i P_i \right)^\nu} \quad (3.56)$$

where the x_i are the Feynman parameters and $\nu = \nu_1 + \dots + \nu_n$. We have dropped the $+i\delta$ -prescription for the moment. In the case of the massless three-point function for example, already evaluating one integral by the delta-function, this results in

$$\frac{1}{k_1^2 k_2^2 k_3^2} = 2 \int_0^1 dx_1 \int_0^{1-x_1} dx_2 \frac{1}{(x_1 k_1^2 + x_2 k_2^2 + (1-x_1-x_2)k_3^2)^3} \quad (3.57)$$

Quadratic completion in the denominator and interchanging the integrals leads finally to

$$\begin{aligned} I_{3,0}(\{p_i\}, \{0\}) &= 2 \int_0^1 dx_1 \int_0^{1-x_1} dx_2 \int d^D k \frac{1}{(x_1 k_1^2 + x_2 k_2^2 + (1-x_1-x_2)k_3^2 + i\delta')^3} \\ &= 2 \int_0^1 dx_1 \int_0^{1-x_1} dx_2 \int d^D k' \frac{1}{(k'^2 - A' + i\delta')^3} = 2 \int_0^1 dx_1 \int_0^{1-x_1} dx_2 I_{3,0}(A'(x_1, x_2)) \end{aligned} \quad (3.58)$$

with $k' = k - x_1 q_1 - x_2 q_2$ and $A' = (x_1 q_1 + x_2 q_2)^2 - x_1 q_1^2 - x_2 q_2^2$. We see that we have now only one common pole in the complex k'_0 -plane which is regulated by a $+i\delta'$ -prescription. We note also, however, that this pole comes with a power of 3 in the denominator.

An alternative parametrization is the introduction of Schwinger parameters. In this approach every propagator is replaced by the identity

$$\frac{1}{P} = \frac{(-1)^\nu}{\Gamma(\nu)} \int_0^\infty dx x^{\nu-1} e^{xP} \quad (3.59)$$

where x is now a Schwinger parameter. For the example of the denominator in the massless three-point integrals this means $(k_1^2 k_2^2 k_3^2)^{-1} = - \int \int \int dx_1 dx_2 dx_3 \exp(x_1 k_1^2 + x_2 k_2^2 + x_3 k_3^2)$, with the three integration boundaries $\in (0, \infty)$. In general we can have tensor integrals of the form

$$I_{n,a}(\{p_i\}, \{m_i\})^{\alpha_1 \dots \alpha_{2a}} = \int d^D k \frac{k^{\alpha_1} \dots k^{\alpha_{2a}}}{\prod_{i=1}^n (k_i^2 - m_i^2 + i\delta)^n} \quad (3.60)$$

where the numerator of the integrand is of tensor rank $2a$ in the loop-momentum k . Without going into further details it can be shown by algebraic reduction, by virtue of Lorentz invariance and by the symmetry properties of the integrals in the algebraically reduced system, that these tensor integrals can always be related to linear combinations of the scalar integrals $I_{n,0}(\{p_i\}, \{m_i\})$, which is formally known by the terminus "tensor reduction". It turns out further that scalar integrals with more than four external legs can actually be expressed by linear combinations of scalar integrals with no more than four external legs, which means in total that all appearing one-loop integrals can be calculated through algebraic reduction and knowledge of an integral basis with only up to four different types of scalar integrals. The price which one has to pay upon using tensor reduction, however, are the introduction of inverse Gram determinants. Gram determinants are the determinants of the Gram matrices $G_{ij} = 2q_i q_j$, where q_i has been defined above. In the tensor reduction of the tensor three-point integral with rank two, for example, we encounter the Gram determinant $|G| \propto p_1^2 p_2^2 - (p_1 \cdot p_2)^2$, which tends to zero in a phase-space region where p_1 and p_2 become collinear. The inverse Gram determinants thus lead to a singular behavior in such phase-space regions, and this problem becomes more annoying with larger numbers of external legs. Several solutions based on different reduction schemes or expansion around small Gram determinants in critical regions have been proposed. One solution, which falls in a different class, is the direct numerical integration. We will discuss this method in a bit.

First we would like to turn to another method, which is based on unitarity and has been used quite successfully throughout the last years in the computation of many cutting-edge processes, and we only want to give a brief overview on the general strategy. As we discussed above we can reduce all appearing one-loop integrals to a linear combination of a basis set of four scalar integrals. This means that in a massless theory, for example, a one-loop amplitude can also be written as

$$A_n^{(1)} = \sum_i c_i I_2^{(i)} + \sum_{i,j} c_{ij} I_3^{(ij)} + \sum_{i,j,k} c_{ijk} I_4^{(ijk)} + R \quad (3.61)$$

where the I_2 , I_3 and I_4 are the scalar two-, three- and four-point integrals respectively. The scalar one-point integral would appear in addition if we would consider a massive theory. R is

a so called rational term, which is a finite remainder that appears in dimensional regularization when poles of order $\mathcal{O}(1/\varepsilon)$ or $\mathcal{O}(1/\varepsilon^2)$ in the dimensional regularization parameter ε hit terms of order $\mathcal{O}(\varepsilon)$ or $\mathcal{O}(\varepsilon^2)$. The rational terms cannot be determined naively in four-dimensional calculations. The basis set of all integrals $\{I_2^{(i)}, I_3^{(ij)}, I_4^{(ijk)}\}$ is obtained from pinching and is known in advance. All that is left is to determine the coefficients c_i, c_{ij}, c_{ijk} and the rational term R . Cut techniques are thereby based on the unitarity of the S-matrix and relate with the help of the Cutkosky rules the imaginary part of a one-loop amplitude to the imaginary part of a phase-space integral over the product of tree-level amplitudes and propagators associated with the cuts between the tree-level amplitudes. One can then reconstruct a one-loop amplitude uniquely by knowing only its imaginary parts and thereby cut-construct a one-loop amplitude by all possible ways that the associated one-loop diagram can be cut into tree-level parts, except for the so called cut-free pieces. These cannot be detected by cut-techniques and have to be determined by an expansion in the dimensional regularization parameter ε . The cut-free piece corresponds then to the rational term at order $\mathcal{O}(\varepsilon^0)$. Upon evaluation of the cuts one determines the coefficients $c_{i\dots}$ in equation 3.61.

Let us now turn to the numerical method. In the previous sections we have determined local subtraction terms, which ensure that the integration over the loop-momentum yields a finite result and can therefore be performed in finite four dimension. There is, however, still the possibility that some of the loop-propagators can go on-shell for certain real values of the loop-momentum, which leads to a complex pole structure in the complex k_0 -plane. As we have seen in the above and in the simple example in appendix E this can be regulated by deforming the integration contour into the complex plane, which works fine if the contour is not too tightly pinched between the poles and may thus not be deformed. This implies that the integration should be done over a region of real dimension four in complex space \mathbb{C}^4 .

There are many possibilities to deform the integration contour correctly into complex space, such that the poles are avoided, but only a few are suited for an efficient Monte Carlo integration such that the resulting contours are constructed algorithmically in a process-independent way and lead to small Monte Carlo errors. Many techniques have been studied during the past years, where basically three methods became apparent. One is to introduce a Feynman or Schwinger parametrization, solve the integral over the loop-momentum analytically, and only compute the remaining Feynman or Schwinger parameter integrals numerically by complex deformation. Another one is to introduce a Feynman or Schwinger parametrization and then solve all the resulting integrals numerically by complex contour deformation. Within these methods the defi-

nition of the integration contours is straightforward, even for the massive case, since as we have seen after the Feynman parametrization the singularities are for fixed external momenta and Feynman parameters localized only on a single cone. However, as we have also seen this single pole is raised to a high power in the denominator, which grows with the number of external legs and is an artifact of the Feynman parametrization. After an analytic Feynman parameter integration this high power will be lowered down, however, since we resort to numerical integration can be a source for large Monte Carlo errors [87].

The third option is to consider the direct deformation of the loop integration contour, without the additional introduction of Feynman or Schwinger parametrization. This method yields smaller Monte Carlo errors, the definition of the integration contour however is not as straightforward anymore, which prevented the application to the massive case for some time. The method was initially studied in multi-photon amplitudes [82] and then extended to be used in more sophisticated processes [91]. Only recently it has become clear that the direct contour deformation can also be applied efficiently to the massive case [88] and even to multi-loop problems [89]. We want to introduce the direct contour deformation here briefly, while discussing some efficiency improvements in the application to the process $e^+e^- \rightarrow jets$ in chapter 5.2.

The integral over the subtracted integrand looks roughly as follows

$$I = \int \frac{d^4k}{(2\pi)^4} [G_{bare}^{(1)} - G_{soft}^{(1)} - G_{coll}^{(1)} - G_{UV}^{(1)}] = \int \frac{d^4k}{(2\pi)^4} \frac{R(k)}{\prod_{j=1}^n (k_j^2 - m_j^2)} \quad (3.62)$$

with $R(k) = P(k) - \frac{P_{UV}(k)}{(k^2 - \mu_{UV}^2)^{n_{UV}}} \prod_{j=1}^n (k_j^2 - m_j^2)$. $P(k)$ and $P_{UV}(k)$ are polynomials in k , whereby the second term proportional to $P_{UV}(k)$ results from the UV subtraction term and parts of the collinear subtraction term and $P(k)$ from the soft subtraction term and parts of the collinear subtraction term. In an improved version of the subtraction terms, which we will discuss in the application to the process $e^+e^- \rightarrow jets$ in chapter 5.2, also parts of the soft subtraction term will contribute to $P_{UV}(k)$. $R(k)$ is thus a rational function in k with poles that are only localized on the surface of a single cone with $(\bar{k}^2 - \mu_{UV}^2)^{n_{UV}} = 0$. For the part proportional to $P_{UV}(k)$ it suffices to choose μ_{UV}^2 large enough on the negative imaginary axis, such that $Re(\mu_{UV}^2) = 0$ and $Im(\mu_{UV}^2) < 0$, which thus always ensures $(\bar{k}^2 - \mu_{UV}^2)^{n_{UV}} \neq 0$. We are left with all the poles on the surfaces of the cones j with $(k_j^2 - m_j^2) = 0$. To this end we promote the loop-momentum to a complex four-vector by setting

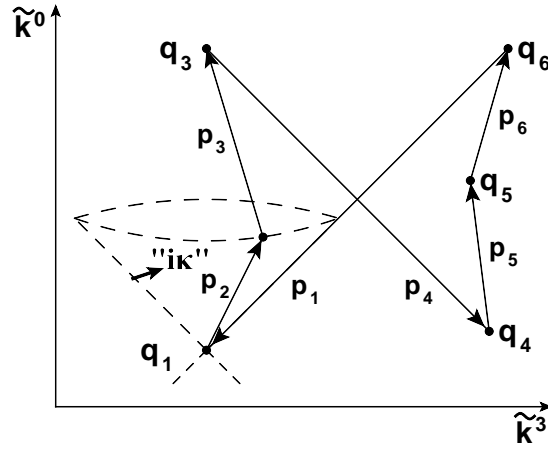


Figure 3.14: The plane with zero- and three-component of loop-momentum space. Depicted are the origins of the light cones q_i and the forward light cone which originates in q_1 . The external four-momenta connect thereby the origins of the light cones via $p_i = q_i - q_{i-1}$. The deformation vector κ is chosen such that it directs towards the interior of a light cones whenever the loop-momentum comes close to a singular point on the surface of this light cone. Whenever the loop-momentum hits one of the lines $p_i = q_i - q_{i-1}$ the singularity is pinched and a deformation is impossible.

$$k = \tilde{k} + i\kappa(\tilde{k}) \quad (3.63)$$

where \tilde{k}^μ contains only the real components and $\kappa^\mu(\tilde{k})$ only the imaginary components. The \tilde{k} -depending choice of the deformation vector κ is thereby crucial to the numerical efficiency. The integral assumes then the form

$$I = \int \frac{d^4\tilde{k}}{(2\pi)^4} \det \left[\frac{\partial k^\mu}{\partial \tilde{k}^\nu} \right] \frac{R(k(\tilde{k}))}{\prod_{j=1}^n (\tilde{k}_j^2 - m_j^2 - \kappa(\tilde{k})^2 + 2i\tilde{k}_j \cdot \kappa(\tilde{k}))} \quad (3.64)$$

where we note the imaginary part in the denominator. Feynman's $+i\delta$ -prescription instructs us now to construct the deformation vector κ such that

$$\tilde{k}_j^2 - m_j^2 = 0 \quad \longrightarrow \quad \tilde{k} \cdot \kappa(\tilde{k}) \geq 0 \quad (3.65)$$

where the equal sign holds if the singularities are pinched. We consider the massless case, where the singularities lie on the surfaces of the cones described by $\tilde{k}_j^2 = (\tilde{k} - q_j)^2 = 0$, with origins at q_1, \dots, q_n . Such a situation is depicted in figure 3.14 for $n = 6$.

$\tilde{k}_j \cdot \kappa(\tilde{k}) > 0$ can be interpreted as κ pointing towards the interior of the cone j . To see this one defines a set of points $\tilde{k} + \lambda\kappa$, with $0 < \lambda \ll 1$. Points inside the light cone are time-like, i.e. $(\tilde{k} - q_j + \lambda\kappa)^2 > 0$. Expansion to first order in λ and setting $(\tilde{k} - q_j)^2 = 0$ yields

$$2\lambda\kappa \cdot (\tilde{k} - q_j) > 0 \tag{3.66}$$

Note that $\tilde{k}_j \cdot \kappa = 0$ corresponds to κ being tangential to the light cone. We can parametrize the connecting line segments, corresponding to $p_j = q_j - q_{j-1}$, between the points q_j by $q_j - xp_j$ for $0 \leq x \leq 1$. If we introduce this parametrization to the deformed denominator in equation 3.64 we note that no deformation is possible for \tilde{k} being on such a line segment. These pinch singularities coincide with the soft ($x = 0, 1$) and collinear ($0 < x < 1$) singularities and are already taken care of by our local soft and collinear subtraction terms. The construction of the deformation vector has been outline in great detail in [83, 91] for massless amplitudes and will not be given here. A construction of the deformation vector for the massive case has also recently been given in [88]. We will elaborate a bit more on the construction of the deformation vector for the application to the process $e^+e^- \rightarrow jets$ in chapter 5.2, where we will discuss how to extend the construction in the massless case and how to choose the arbitrary four-vector Q and the UV mass μ_{UV}^2 in order to enhance the numerical efficiency.

Chapter 4

Recursive Relations

The sets of diagrams to cyclically ordered color-stripped amplitudes, as described in chapter 2, can be constructed efficiently with the help of recurrence relations. For our purposes we use Berends-Giele type recursions on ordered color-stripped off-shell currents, first discussed for tree-level amplitudes [98, 99, 101, 113, 31] and later extended to the one-loop case [50, 51, 91]. Off-shell recursion relations relate thereby currents with one off-shell leg and multiple on-shell legs to "smaller" off-shell currents with fewer on-shell legs.

Other recursive techniques have been studied in the literature, which either use a color-dressed version of the Berends-Giele relations [143, 144] or are based on on-shell amplitudes [127, 145]. For practical purposes the Berends-Giele type off-shell recursion relations offer a good agreement between speed and applicability [146].

The idea is best illustrated with a brief example for a vectorial three-valent toy model, where the tree-level recursion can be depicted graphically as in figure 4.1. The off-shell leg is hereby denoted by the label $(n + 1)$ on both sides of the equation and a specific cyclic ordering $(m, \dots, n, n + 1)$ is noted. On the left hand side we note the $(n + 1 - m)$ on-shell legs connected to the shaded blob, whereas on the right hand side we resolve the shaded blob by following the off-shell leg into the blob and accounting for all possibilities to connect the $(n + 1 - m)$ on-shell legs via smaller off-shell currents to the remaining two legs of the three-valent vertex. If we start for $m = 1$ and follow through with the recursion until it terminates we get a set of diagrams, which contains exactly all those diagrams that contribute to the associated partial amplitude with the given cyclic ordering of the external $(n + 1)$ legs. In formula it reads

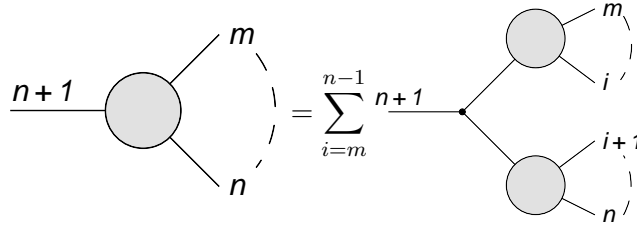


Figure 4.1: Recursive tree-level relation for a vectorial three-valent toy model. Straight lines denote vector bosons.

$$\begin{aligned}
 J_{\alpha}^{(0)}(p_m^{\lambda_m}, \dots, p_n^{\lambda_n}) &\equiv J_{\alpha}^{(0)}(m, \dots, n) = \frac{-ig_{\alpha\mu}}{P(m, \dots, n)^2} \times \\
 &\times \sum_{i=m}^{n-1} V_{ggg}^{(0)\mu\nu\rho}(-P(m, \dots, n), P(m, \dots, i), P(i+1, \dots, n)) J_{\nu}^{(0)}(m, \dots, i) J_{\rho}^{(0)}(i+1, \dots, n) \quad (4.1)
 \end{aligned}$$

where momentum conservation is understood and $P(i, \dots, j) = \sum_{l=i}^j p_l$, for $i \leq j$, or $P(m, m-1) = 0$. If not stated otherwise the external momenta p_l are always directed outwards and the color-stripped three-valent vertex $V_{ggg}^{(0)\mu\nu\rho}$ is given in appendix A. The number of arguments of a given off-shell current $J_{\mu}^{(0)}(i, \dots, j)$ accounts for the number of connected on-shell legs, the argument list itself is an appropriate shorthand notation for the set of the associated external momenta and helicities. The recursion terminates with the off-shell one-current $J_{\mu}^{(0)}(l) \equiv \varepsilon_{\mu}(p_l, q)$ which has one on-shell leg l , where $\varepsilon_{\mu}(p_l, q)$ is the polarization vector of particle l with momentum p_l and an arbitrary light-like reference momentum q .

The associated $(n+1)$ -particle partial tree-level amplitude is obtained from the off-shell current with n on-shell legs, by putting the $(n+1)$ th leg on-shell, which is formally done by multiplying with the inverse of the off-shell propagator and contracting with the respective polarization vector, which reads

$$A^{(0)}(1, \dots, n+1) = \varepsilon^{\mu}(p_{n+1}, q) i P(1, \dots, n)^2 J_{\mu}^{(0)}(1, \dots, n) \Big|_{P(1, \dots, n) = -p_{n+1}} \quad (4.2)$$

Since for massless on-shell particles $p_l^2 = 0$ we have also $P(1, \dots, n)^2 = 0$. To prevent division by zero the propagator $P(1, \dots, n)^2$ in equation 4.2 and for $m = 1$ in equation 4.1 is simply dropped for practical purposes in the numerical implementation.

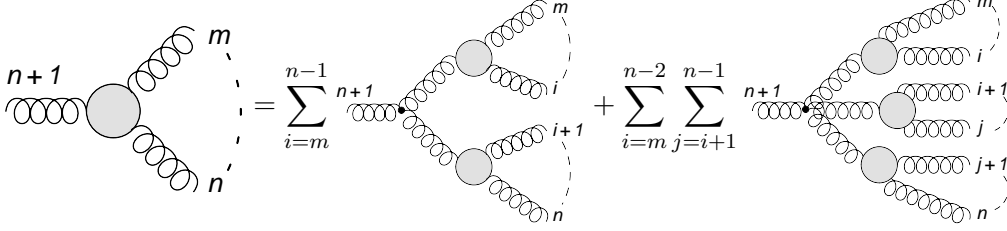


Figure 4.2: Recursive tree-level relation for a pure gluon off-shell current. Curly lines denote gluons.

We will briefly discuss the recursive relations for QCD tree-level off-shell currents in section 4.1 before we continue with the one-loop recursions in section 4.2. The total UV subtraction term to a given primitive one-loop amplitude can also be constructed by recursive means, which will be discussed in section 4.3. We will conclude this chapter, by discussing some numerical checks regarding the recursive interplay between the one-loop construction and the UV construction, in section 4.4.

4.1 Tree-Level Recurrence Relations

The recursion relation for pure gluon tree-level off-shell currents are depicted in figure 4.2, where the label $(n + 1)$ denotes the off-shell leg again and in formula it reads

$$\begin{aligned}
 J_{\alpha}^{(0)}(m, \dots, n) &= \frac{-i g_{\alpha\mu}}{P(m, \dots, n)^2} \times \\
 &\times \left[\sum_{i=m}^{n-1} V_{ggg}^{(0)\mu\nu\rho}(-P(m, \dots, n), P(m, \dots, i), P(i+1, \dots, n)) J_{\nu}^{(0)}(m, \dots, i) J_{\rho}^{(0)}(i+1, \dots, n) \right. \\
 &\left. + \sum_{i=m}^{n-2} \sum_{j=i+1}^{n-1} V_{gggg}^{(0)\mu\nu\rho\sigma} J_{\nu}^{(0)}(m, \dots, i) J_{\rho}^{(0)}(i+1, \dots, j) J_{\sigma}^{(0)}(j+1, \dots, n) \right] \quad (4.3)
 \end{aligned}$$

where the color-stripped three- and four-gluon vertices, $V_{ggg}^{(0)\mu\nu\rho}$ and $V_{gggg}^{(0)\mu\nu\rho\sigma}$ respectively, are given in appendix A. Except for the additional part with the color-stripped four-gluon vertex this corresponds to the case of the three-valent toy model above, where the recursion terminates again with $J_{\mu}^{(0)}(l) \equiv \varepsilon_{\mu}(p_l, q)$.

The associated $(n + 1)$ -gluon partial tree-level amplitude is retrieved from the n -gluon tree-level off-shell current again by putting the off-shell leg on-shell and contracting with the respective

4.1 Tree-Level Recurrence Relations

polarization vector

$$A^{(0)}(1, \dots, n+1) = \varepsilon^\mu(p_{n+1}, q) i P(1, \dots, n)^2 J_\mu^{(0)}(1, \dots, n) \Big|_{P(1, \dots, n) = -p_{n+1}} \quad (4.4)$$

We can infer certain symmetry properties for the ordered gluon off-shell currents from the symmetry properties of the associated partial amplitudes as given in chapter 2.1. Although the off-shell current with n on-shell legs is thereby not invariant under cyclic permutations of $(1, 2, \dots, n)$ anymore, we can infer

i) from the reflective property that $J_\mu^{(0)}(1, 2, \dots, n) = (-1)^{n+1} J_\mu^{(0)}(n, \dots, 2, 1)$, and

ii) from the dual Ward identity that

$$J_\mu^{(0)}(1, 2, 3, \dots, n) + J_\mu^{(0)}(2, 1, 3, \dots, n) + \dots + J_\mu^{(0)}(2, 3, \dots, 1, n) + J_\mu^{(0)}(2, 3, \dots, n, 1) = 0,$$

iii) which can be recast in the form of the sub-cyclic identity as

$$\sum_{Z_n(1, 2, \dots, n)} J_\mu^{(0)}(1, 2, \dots, n) = 0.$$

Similar recurrence relations hold for the case of one quark-antiquark pair, where we distinguish between quark and antiquark off-shell currents. Pictorially these are given in figure 4.3 and in formula they read

$$\begin{aligned} \bar{U}^{(0)}(m_q, m+1, \dots, n) = \\ \left[\sum_{i=m}^{n-1} \bar{U}^{(0)}(m_q, m+1, \dots, i) \Gamma^{(0)\mu} J_\mu^{(0)}(i+1, \dots, n) \right] \frac{i [\not{p}_{m_q} + \not{P}(m+1, \dots, n)]}{[p_{m_q} + P(m+1, \dots, n)]^2} \end{aligned} \quad (4.5)$$

$$\begin{aligned} V^{(0)}(m, \dots, n-1, n_{\bar{q}}) = \\ \frac{i [-\not{P}(m, \dots, n-1) + \not{p}_{n_{\bar{q}}}]}{[P(m, \dots, n-1) + p_{n_{\bar{q}}}]^2} \left[\sum_{i=m}^{n-1} \Gamma^{(0)\mu} J_\mu^{(0)}(m, \dots, i) V^{(0)}(i+1, \dots, n-1, n_{\bar{q}}) \right] \end{aligned} \quad (4.6)$$

where $\bar{U}^{(0)}(m_q, m+1, \dots, n)$ and $V^{(0)}(m, \dots, n-1, n_{\bar{q}})$ denote the tree-level recursions for quark and antiquark off-shell currents respectively, and the recursions terminate with $J_\mu^{(0)}(l) \equiv \varepsilon_\mu(p_l, q)$ and with $\bar{U}^{(0)}(m_q) = \bar{u}(p_{m_q})$ or $V^{(0)}(n_{\bar{q}}) = v(p_{n_{\bar{q}}})$ respectively, where $\bar{u}(p_{m_q})$ and $v(p_{n_{\bar{q}}})$ represent quark and antiquark spinors respectively. The color-stripped tree-level quark-gluon vertex $\Gamma^{(0)\mu}$, where the gluon is radiated to the right with respect to the fermion flow, is given in appendix A. Note that in tree-level problems we can arrange the cyclic ordering always such

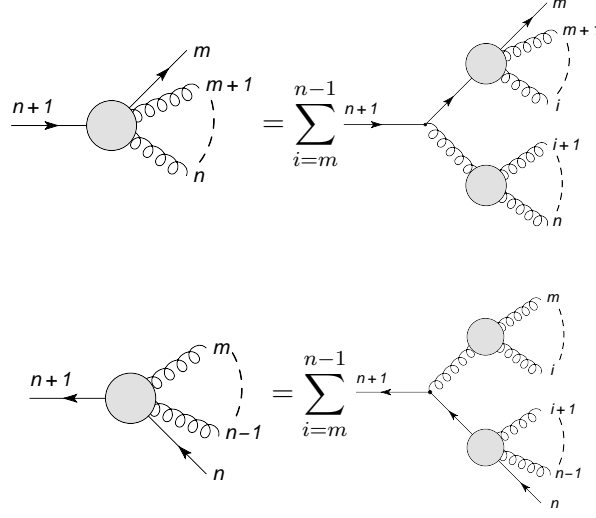


Figure 4.3: Recursive relations for tree-level quark (top) and antiquark (bottom) off-shell currents respectively. Curly lines denote gluons, straight lines with a fermion arrow denote fermions. In the quark current the on-shell fermion is a quark, in the antiquark current the on-shell fermion is an antiquark.

that gluons are radiated off quark lines to the right with respect to the fermion flow arrow. This infers especially that in the cyclic ordering in clock-wise direction an antiquark is always followed directly by its corresponding quark.

Note that in the above $\bar{U}^{(0)}$ and $V^{(0)}$ are matrices in Dirac space, which means that their position with respect to the quark-gluon vertex and the quark or antiquark propagators matters. The corresponding partial amplitudes are recovered from the quark or antiquark off-shell currents by

$$\begin{aligned}
 & A^{(0)}(1_q, 2, \dots, n-1, n_{\bar{q}}) \\
 &= \bar{U}^{(0)}(1_q, 2, \dots, n-1)(-i)[\not{p}_{1_q} + \not{P}(2, \dots, n-1)]v(p_{n_{\bar{q}}})|_{p_{1_q} + P(2, \dots, n-1) = -p_{n_{\bar{q}}}} \quad (4.7)
 \end{aligned}$$

$$= \bar{u}(p_{1_q})(-i)[-\not{P}(2, \dots, n-1) + \not{p}_{n_{\bar{q}}}]V^{(0)}(2, \dots, n-1, n_{\bar{q}})|_{P(2, \dots, n-1) + p_{n_{\bar{q}}} = -p_{1_q}} \quad (4.8)$$

We can use the above building blocks in order to construct the tree-level amplitude for the process $e^+e^- \rightarrow q, g, \dots, g, \bar{q}$, i.e. for the process $e^+e^- \rightarrow jets$ in the leading color approximation. For $\#_{jets} = (n-2)$ the amplitudes for the respective photon or Z-boson channels are thereby given by

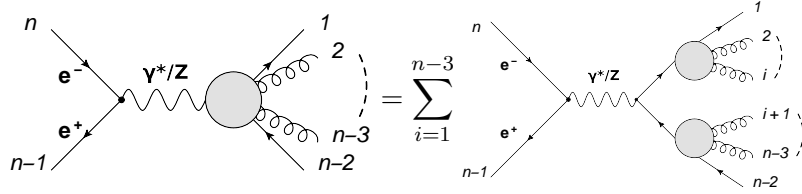


Figure 4.4: Tree-level amplitude to $e^+e^- \rightarrow (n-2)$ jets in the leading color approximation. We choose the leptons as incoming.

$$\begin{aligned}
 A_{\gamma/Z}^{(0)}(1_q, 2_g, \dots, (n-3)_g, (n-2)_{\bar{q}}, (n-1)_l, n_{\bar{l}}) = \\
 \sum_{i=1}^{n-3} \bar{U}^{(0)}(1_q, 2, \dots, i) V_{qq\gamma/Z}^{(0)\mu} V^{(0)}(i+1, \dots, (n-3), (n-2)_{\bar{q}}) J_{\mu}^{(0)EW}((n-1)_l, n_{\bar{l}}) \quad (4.9)
 \end{aligned}$$

where $V_{qq\gamma/Z}^{\mu}$ denotes the electroweak quark–photon or quark–Z–boson vertex, which can be found in many textbooks, and $J_{\mu}^{(0)EW}((n-1)_l, n_{\bar{l}})$ is the electroweak off-shell current, where the off-shell leg is chosen to be the appropriate photon/Z–boson off-shell propagator. If we choose the center-of-mass energy to be m_Z^2 , with m_Z the mass of the Z–boson, we have to use the appropriate propagator for an unstable particle with a denominator of the form $p^2 - m_Z^2 + im_Z\Gamma$, which can be found as well in many textbooks. We choose the leptons as incoming. The process is depicted in figure 4.4.

The recursion relations for multiple quark–antiquark pairs are a little bit more involved. An efficient algorithm to generate all possible color–ordered tree–level diagrams for processes with multiple quark–antiquark pairs, in conjunction with color decomposition in the color–flow basis, has been described in [31].

4.2 One-loop Recurrence Relations

Algorithms for the recursive construction of one–loop amplitudes have been discussed on several occasions [51, 50], where we make use of Berends–Giele type recursion relations for ordered one–loop off–shell currents [91]. These yield sets of diagrams, which are exactly the sets of cyclically ordered diagrams to the corresponding primitive amplitudes. In one–loop recursions one can make use of tree–level recursions with two off–shell legs by means of cutting open one propaga-

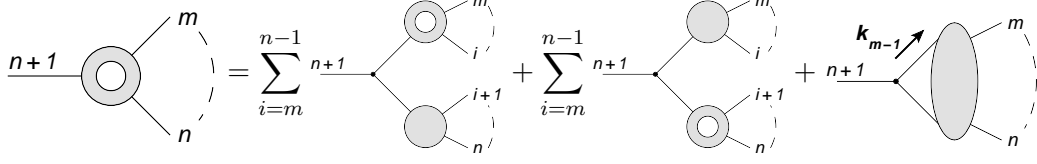


Figure 4.5: Recursive one-loop relation for a vectorial three-valent toy model. Straight lines denote vector bosons. In the third term we note the direct one-loop contribution.

tor in the loop [91]. In this regard should tree-level currents with two off-shell legs essentially behave as tree-level currents with one off-shell leg and one additional on-shell leg. We thus expect the scaling behavior in CPU time with respect to the number of legs for the one-loop recursions to behave essentially as for the tree-level recursions, which was indeed observed [90]. The concept of cutting open loop-propagators has also recently been discussed by others, in the context of Feynman diagrams [147].

The idea is again drafted best for a toy model with a single vector field and a single three-valent vertex. We can work out the recursive relations for the unintegrated off-shell currents of cyclically ordered primitive one-loop amplitudes in this toy model, where the recursion is depicted graphically in figure 4.5 and the label $(n + 1)$ denotes the off-shell leg again. In the first two terms on the right hand side we follow the off-shell leg, in tree-level like fashion, into the blob and account for all possibilities to connect the $(n - m)$ on-shell legs via smaller unintegrated one-loop off-shell currents to the remaining two legs of the color-stripped three-valent tree-level vertex. In the third term on the right, which we call the direct one-loop contribution, the three-valent vertex connects to the two adjacent edges of a loop. In formula this reads

$$\begin{aligned}
 J_{\alpha}^{(1)}(m, \dots, n) &= \frac{-ig_{\alpha\mu}}{P(m, \dots, n)^2} \times \\
 &\times \left[\sum_{i=m}^{n-1} V_{ggg}^{(0)\mu\nu\rho}(-P(m, \dots, n), P(m, \dots, i), P(i+1, \dots, n)) J_{\nu}^{(1)}(m, \dots, i) J_{\rho}^{(0)}(i+1, \dots, n) \right. \\
 &+ \sum_{i=m}^{n-1} V_{ggg}^{(0)\mu\nu\rho}(-P(m, \dots, n), P(m, \dots, i), P(i+1, \dots, n)) J_{\nu}^{(0)}(m, \dots, i) J_{\rho}^{(1)}(i+1, \dots, n) \\
 &\left. + V_{ggg}^{(0)\mu\nu\rho}(-P(m, \dots, n), k_{m-1}, -k_n) K_{\nu\rho}(m, \dots, n; k_{m-1}) \right] \quad (4.10)
 \end{aligned}$$

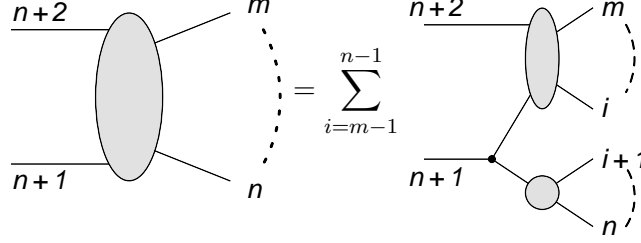


Figure 4.6: Recursive tree-level relation for an off-shell current with two off-shell legs in a vectorial three-valent toy model. Straight lines denote vector bosons and the labels $(n+1)$ and $(n+2)$ denote the two off-shell legs.

where $k_i = k - \sum_{l=1}^i p_l$ and with $k_0 \equiv k$, according to the conventions in chapter 3.2. $K_{\nu\rho}$ in the third term on the right hand side denotes an auxiliary ordered tree-level off-shell current with two off-shell legs, where the upper off-shell leg carries the loop momentum k_{m-1} according to our convention. We will discuss this term further below. Except for the direct one-loop contribution, the recursion terminates with the unintegrated one-loop one-current $J_\mu^{(1)}(l)$, which corresponds to a self-energy correction on an external leg and is thus set to zero, or with the usual tree-level one-current $J_\mu^{(0)}(l) \equiv \varepsilon_\mu(p_l, q)$. The integrand to the associated primitive one-loop amplitude is then retrieved in the same way as in the tree-level case by

$$G_{bare}^{(1)}(1, \dots, n+1) = \varepsilon^\mu(p_{n+1}, q) i P(1, \dots, n)^2 J_\mu^{(1)}(1, \dots, n) \Big|_{P(1, \dots, n) = -p_{n+1}} \quad (4.11)$$

Here we put the off-shell leg on-shell again. Care has thus to be taken when a self-energy correction appears on this off-shell leg, which has then to be set to zero as well.

The recursion relation for the auxiliary tree-level off-shell current with two off-shell legs is graphically depicted in figure 4.6. In formula the recursion relation for the tree-level two-leg off-shell current reads

$$\begin{aligned} K_{\mu\alpha}(m, \dots, n; q) &= \frac{-ig_{\alpha\nu}}{(q - P(m, \dots, n))^2} \times \\ &\times \sum_{i=m-1}^{n-1} K_{\mu\lambda}(m, \dots, i; q) V_{gg}^{(0)\nu\lambda\kappa}(q - P(m, \dots, n), -q + P(m, \dots, i), P(i+1, \dots, n)) J_\kappa^{(0)}(i+1, \dots, n) \end{aligned} \quad (4.12)$$

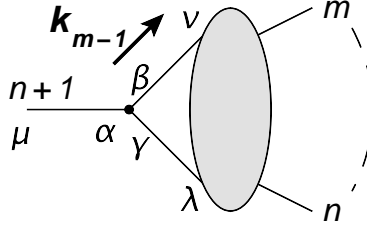


Figure 4.7: Direct one-loop contribution to the recursive one-loop off-shell current in a vectorial three-valent toy model. Straight lines denote vector bosons and the label $(n + 1)$ denotes the off-shell leg of the one-loop off-shell current. Lorentz indices are explicitly shown.

where q denotes the incoming off-shell four-momentum on the off-shell leg with label $(n + 2)$ and the outgoing off-shell four-momentum on leg $(n + 1)$ is fixed by $q - P(m, \dots, n)$. The recursion of $K_{\mu\nu}$ terminates with the two-leg off-shell current $K_{\mu\nu}(m, m - 1; q)$ with no additional on-shell leg, which is just an off-shell propagator given by $K_{\mu\nu}(m, m - 1; q) = \frac{-ig_{\mu\nu}}{q^2}$, and with the tree-level one-currents $J_\mu^{(0)}(l)$.

In the third term on the right hand side of equation 4.10 above we notice the contraction of the auxiliary two-leg off-shell current with two legs of the three-valent vertex, which describes the connection of the three-valent vertex to two adjacent edges of the loop in the direct one-loop contribution as shown in figure 4.7. One could in principle define the two legs on the right of the three-valent vertex as one tensorial object, in which case the coupling of the three-valent vertex to the two-leg off-shell current would be given by a tensor product on the corresponding Lorentz indices. This is numerically cumbersome and we seek for a more efficient way, which is given by simply cutting open one propagator in the loop. We thereby use an explicit decomposition of the metric tensor $g_{\beta\nu}$ in the upper loop-propagator in figure 4.7 into two sets of four-vectors $\{a^{[l]}\}$ and $\{b^{[l]}\}$, such that $g_{\beta\nu} = \sum_l a_\beta^{[l]} b_\nu^{[l]}$, where l runs from 1 to 4 and the indices β and ν on the four-vectors $a_\beta^{[l]}$ and $b_\nu^{[l]}$ denote their four components respectively.

We thus split the upper off-shell leg in figure 4.7 into a part that couples to the Lorentz index β of the three-valent vertex and a part that couples to the Lorentz index ν of the two-leg off-shell current. This will translate $V_{ggg}^{(0)\alpha\beta\gamma} K_{\beta\gamma} = V_{ggg}^{(0)\alpha\beta\gamma} g_{\beta\nu} g_{\gamma\lambda} K^{\nu\lambda}$ into a sum over vector multiplications $\sum_l V_{ggg}^{[l]\alpha\gamma} K_\gamma^{[l]} \equiv V_{ggg}^{(0)\alpha\beta\gamma} a_\beta^{[l]} b_\nu^{[l]} g_{\gamma\lambda} K^{\nu\lambda}$, or in simple terms will cut open the loop. The third term on the right hand side of equation 4.10 can then be rewritten into

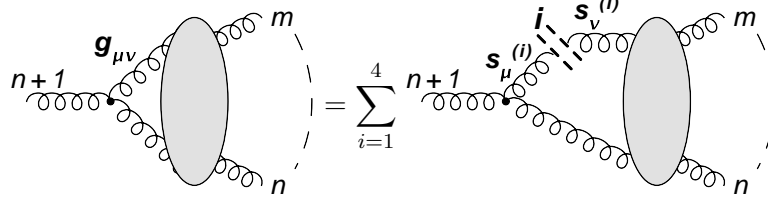


Figure 4.8: Cutting a gluon propagator in the loop. One replaces the tensor structure of the upper gluon leg by a sum over four (pseudo-)polarizations.

$$\frac{-ig_{\alpha\mu}}{P(m, \dots, n)^2} \left[\sum_{l=1}^4 V_{ggg}^{[l]\mu\rho}(-P(m, \dots, n), k_{m-1}, -k_n) K_\rho^{[l]}(m, \dots, n; k_{m-1}) \right] \quad (4.13)$$

where $V_{ggg}^{[l]\mu\rho}(-P(m, \dots, n), k_{m-1}, -k_n) \equiv V_{ggg}^{(0)\mu\nu\rho}(-P(m, \dots, n), k_{m-1}, -k_n) a_\nu^{[l]}$ and the associated two-leg off-shell current $K_\rho^{[l]}(m, \dots, n; k_{m-1})$ can be recursively calculated via

$$\begin{aligned} K_\rho^{[l]}(m, \dots, n; q) &= \frac{-ig_{\rho\lambda}}{(q - P(m, \dots, n))^2} \times \\ &\times \sum_{i=m-1}^{n-1} V_{ggg}^{(0)\lambda\sigma\tau}(q - P(m, \dots, n), -q + P(m, \dots, i), P(i+1, \dots, n)) K_\sigma^{[l]}(m, \dots, i; q) J_\tau(i+1, \dots, n) \end{aligned} \quad (4.14)$$

where the recursion terminates with $K_\mu^{[l]}(m, m-1; q) = \frac{-ib_\mu^{[l]}}{q^2}$. For the two four-vectors one can simply choose $g_{\mu\nu} = \sum_{l=1}^4 a_\mu^{[l]} b_\nu^{[l]} = \sum_{l=1}^4 s_\mu^{[l]} s_\nu^{[l]}$, with the four standard (pseudo-)polarizations $s_\mu^{[1]} = (1, 0, 0, 0)$, $s_\mu^{[2]} = (0, -i, 0, 0)$, $s_\mu^{[3]} = (0, 0, -i, 0)$ and $s_\mu^{[4]} = (0, 0, 0, -i)$. An alternative set of four-vectors is given in appendix F. This cut-prescription is of course used as well if we cut open a gluon propagator in the loop, as depicted in figure 4.8.

If, on the other hand, the propagator we wish to cut open corresponds to a massless quark line, as it appears in one-loop quark or antiquark off-shell currents, we have to replace the momentum \not{k} in the numerator of the quark or antiquark propagator by

$$\not{k} = \not{k}^b + \frac{k^2}{2k \cdot q} \not{q}, \quad \text{with } k^b = k - \frac{k^2}{2k \cdot q} q \quad (4.15)$$

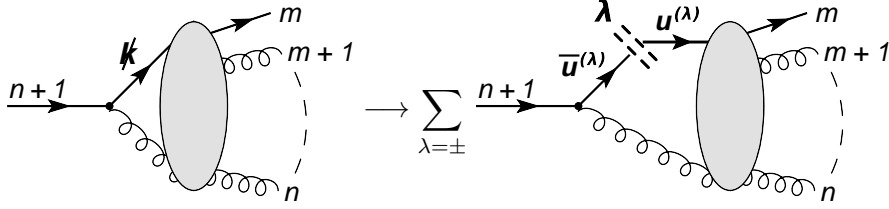


Figure 4.9: Cutting a quark propagator in the loop. One replaces the tensor structure of the quark leg by a sum over polarizations.

where q is a light-like reference momentum and k^b is light-like by construction. The light-like momenta k^b and q can then be replaced by a sum over polarizations

$$k^b = \sum_{\lambda=\pm} u(k^b, \lambda) \bar{u}(k^b, \lambda) \quad \text{and} \quad \not{q} = \sum_{\lambda=\pm} u(q, \lambda) \bar{u}(q, \lambda) \quad (4.16)$$

which is depicted schematically in figure 4.9. The extension to massive propagators is straightforward and further details are given in [91, 145].

We also have to cut open ghost-loops, as they appear in the gluon one-loop off-shell currents, which is rather simple since the ghosts are scalar particles and the corresponding propagators do not contain any non-trivial tensor structures that need to be replaced by any polarization sums. A complete collection of recursive relations to compute the integrand $G_{bare}^{(1)}$ of QCD one-loop primitive amplitudes in the leading color approximation is given in appendix F. We shall stop the discussion at this point and turn to the recursive construction of the total UV subtraction term $G_{UV}^{(1)}$.

4.3 UV Recurrence Relations

The recursive construction of $G_{bare}^{(1)}$ ensures the correct incorporation of all necessary one-loop diagrams in the integrand of a given bare primitive amplitude. Similarly ensures the recursive construction of $G_{UV}^{(1)}$ the correct incorporation of all necessary local UV counterterms to a given primitive amplitude on the integrand level.

We will again draft the idea with the help of the three-valent toy model from before. The recursion relation that generates the total unintegrated UV subtraction term to a given primitive

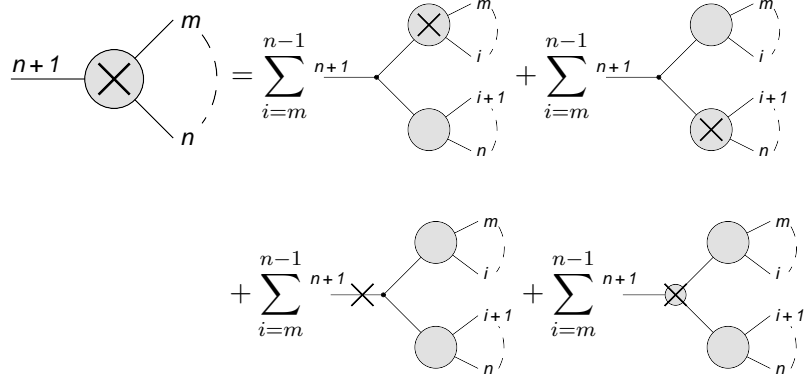


Figure 4.10: Recursive UV relation for a vectorial three-valent toy model. Straight lines denote vector bosons. Crosses denote local UV counterterms.

amplitude, in the three-valent toy model, from the local UV counterterms is depicted in figure 4.10. In the first two terms on the right hand side we follow the off-shell leg, in tree-level like fashion, into the blob and account for all possibilities to connect the $(n - m)$ on-shell legs via smaller unintegrated UV off-shell currents to the remaining two legs of the three-valent vertex. In the third and fourth term on the right, which we call the direct UV contributions, we replace the vector propagator and the three-valent vertex in the toy model by their corresponding local UV counterterms respectively. In formula this reads

$$\begin{aligned}
 J_{\alpha}^{(1)UV}(m, \dots, n) &= \frac{-ig_{\alpha\mu}}{P(m, \dots, n)^2} \times \\
 &\times \left[\sum_{i=m}^{n-1} V_{ggg}^{(0)\mu\nu\rho}(-P(m, \dots, n), P(m, \dots, i), P(i+1, \dots, n)) J_{\nu}^{(1)UV}(m, \dots, i) J_{\rho}^{(0)}(i+1, \dots, n) \right. \\
 &+ \sum_{i=m}^{n-1} V_{ggg}^{(0)\mu\nu\rho}(-P(m, \dots, n), P(m, \dots, i), P(i+1, \dots, n)) J_{\nu}^{(0)}(m, \dots, i) J_{\rho}^{(1)UV}(i+1, \dots, n) \\
 &+ g_{gg}^{UV, \ell_{gg}, \mu\beta}(\bar{k}, Q_{m-1}, P(m, \dots, n), \mu_{UV}) \frac{-ig_{\beta\gamma}}{P(m, \dots, n)^2} \times \\
 &\quad \times \sum_{i=m}^{n-1} V_{ggg}^{(0)\gamma\nu\rho}(-P(m, \dots, n), P(m, \dots, i), P(i+1, \dots, n)) J_{\nu}^{(0)}(m, \dots, i) J_{\rho}^{(0)}(i+1, \dots, n) \\
 &\left. + \sum_{i=m}^{n-1} g_{ggg, UV}^{UV, \ell_{ggg}, \mu\nu\rho}(\bar{k}, Q_{m-1}, P(m, \dots, i), P(i+1, \dots, n), \mu_{UV}) J_{\nu}^{(0)}(m, \dots, i) J_{\rho}^{(0)}(i+1, \dots, n) \right]
 \end{aligned} \tag{4.17}$$

where $g_{gg}^{UV,\ell_{gg},\mu\beta}(\dots)$ in the third term on the right hand side and $g_{ggg,UV}^{UV,\ell_{ggg},\mu\nu\rho}(\dots)$ in the fourth term on the right hand side denote the local (unintegrated) UV counterterms to the vector propagator and the three-valent vertex respectively. Those correspond to the local UV counterterms for the leading color gluon propagator and leading color three-gluon vertex as given in appendix D.

Regarding the dependence of $g_{gg}^{UV,\ell_{gg},\mu\beta}(\dots)$ and $g_{ggg,UV}^{UV,\ell_{ggg},\mu\nu\rho}(\dots)$ on the arbitrary four-vector Q : As we saw in the construction of the one-loop recursion, the general dependence on the loop-momentum is on the shifted loop-momentum $k_{m-1} = k - q_{m-1}$, with $q_i = \sum_{l=1}^i p_l$. In the computation of the local UV counterterms, however, we expanded around the UV propagator $(\bar{k} - \mu_{UV}^2)^{-1}$ with $\bar{k} = k - Q$. Since the integrated results are independent of the arbitrary four-vector Q we can choose to keep the momentum \bar{k} fixed upon shifting of the loop-momentum $k_{m-1} = k - q_{m-1}$ by simply balancing the shift through the arbitrary four-vector Q and thus have $\bar{k} = k - Q = k_{m-1} - Q_{m-1}$, with $Q_{m-1} = Q - q_{m-1}$.

A complete collection of UV recursion relations in QCD and for the process $e^+e^- \rightarrow jets$, for usage in the leading color approximation, is given in appendix G.

4.4 Cross-Checking the Recursive Interplay

We need to check whether the implemented recursive constructions of the bare one-loop integrand and the total unintegrated UV subtraction term play along well.

In the figures 4.11, 4.12 and 4.13 we plot $|2Re(A^{(0)*}G^{(1)})|$ vs. a UV scaling parameter λ_{UV} , where the summation over helicities has been performed and where we scale a fixed value for the loop-momentum according to $\bar{k} = k - Q_{fixed} = \lambda_{UV}\bar{k}_{fixed}$. The plots are for the processes $0 \rightarrow n$ gluons, $e^+e^- \rightarrow 3 jets$ and $e^+e^- \rightarrow 4 jets$ respectively, for a fixed region in the final-state phase-space. A description of the necessary phase-space sampling is included in appendix H.

For the processes $e^+e^- \rightarrow 3$ and $4 jets$ we use the leading color approximation, i.e. $e^+e^- \rightarrow q\bar{q} + 1$ and $2 gluons$ respectively, where the kinematical setup has been described in appendix F and appendix G. The unsubtracted total integrands in gray show all a local UV divergent behavior. The UV subtracted total integrands in red/blue, however, fall off like $1/|\bar{k}|^5$, which is clearly UV finite.

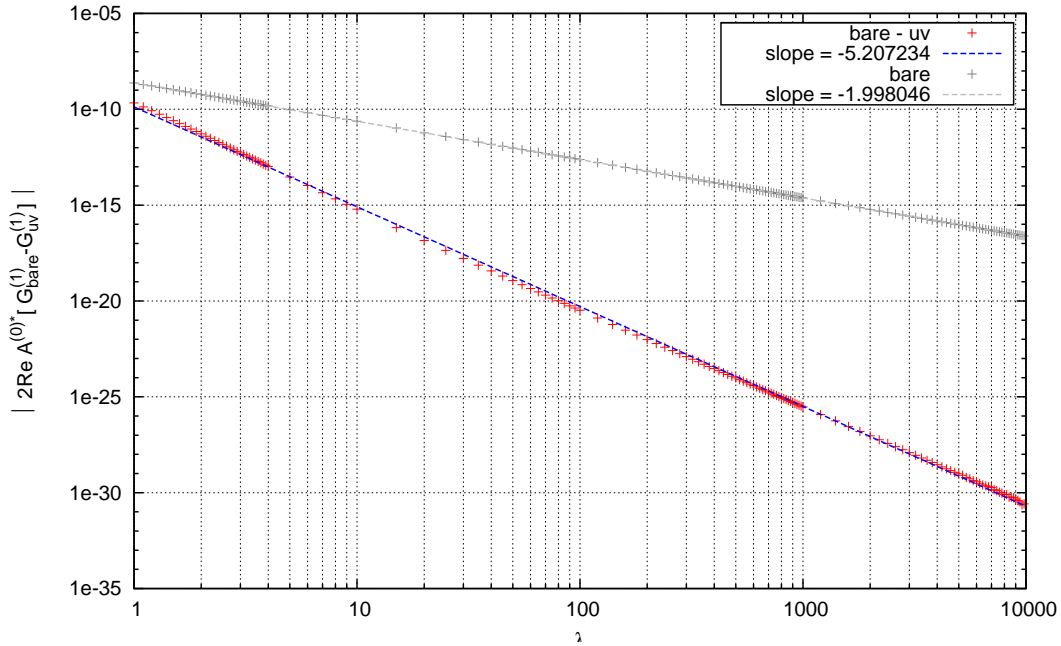


Figure 4.11: Helicity summed integrand for a 7-gluon one-loop amplitude. The unsubtracted total integrand in gray falls off like $1/|\bar{k}|^2$, which leads to UV divergences upon integration. The UV subtracted total integrand in red/blue, however, falls off like $1/|\bar{k}|^5$, which is clearly UV finite.

Looking more closely on these plots, we notice that the unsubtracted integrand for the process $e^+e^- \rightarrow q\bar{q} + 2 \text{ gluons}$ falls off like $1/|\bar{k}|^2$, whereas the unsubtracted integrand for the process $e^+e^- \rightarrow q\bar{q} + 1 \text{ gluon}$ falls off like $1/|\bar{k}|^3$. This reflects the fact that in the process $e^+e^- \rightarrow q\bar{q} + 2 \text{ gluons}$ the UV behavior is dominated by the quadratic UV behavior of the one-loop correction to the gluon propagator. In the process $e^+e^- \rightarrow q\bar{q} + 1 \text{ gluon}$ the one-loop correction to the gluon propagator is not expected to appear and the UV behavior is dominated by a linear UV behavior.

In anticipation of chapter 5.1 we can use improved UV counterterms in the recursive construction as well, where improved means that these local UV counterterms also subtract out the local $1/|k|^5$ - and $1/|k|^6$ -behavior from some parts of the integrand in order to have a better numerical behavior in phase-space regions with small two-particle invariants. We can then perform similar checks, of which one is shown in figure 4.14 for the process $e^+e^- \rightarrow 3 \text{ jets}$ in the leading color approximation. Here we have chosen a final-state phase-space point, where the first and the second jet have a small two-particle invariant. A brief description of how to generate such a phase-space point is given in appendix H.

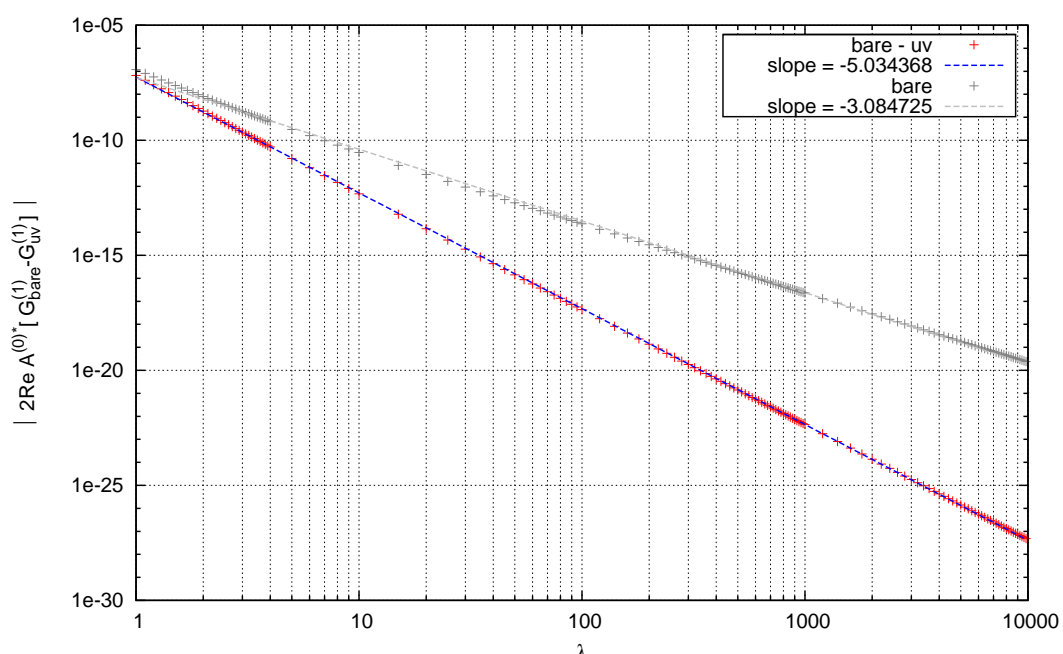


Figure 4.12: Helicity summed integrand for the one-loop QCD correction to the process $e^+e^- \rightarrow q\bar{q} + 1$ gluons. The unsubtracted total integrand in gray falls off like $1/|\bar{k}|^3$, which leads to UV divergences upon integration. The UV subtracted total integrand in red/blue, however, falls off like $1/|\bar{k}|^5$, which is clearly UV finite.

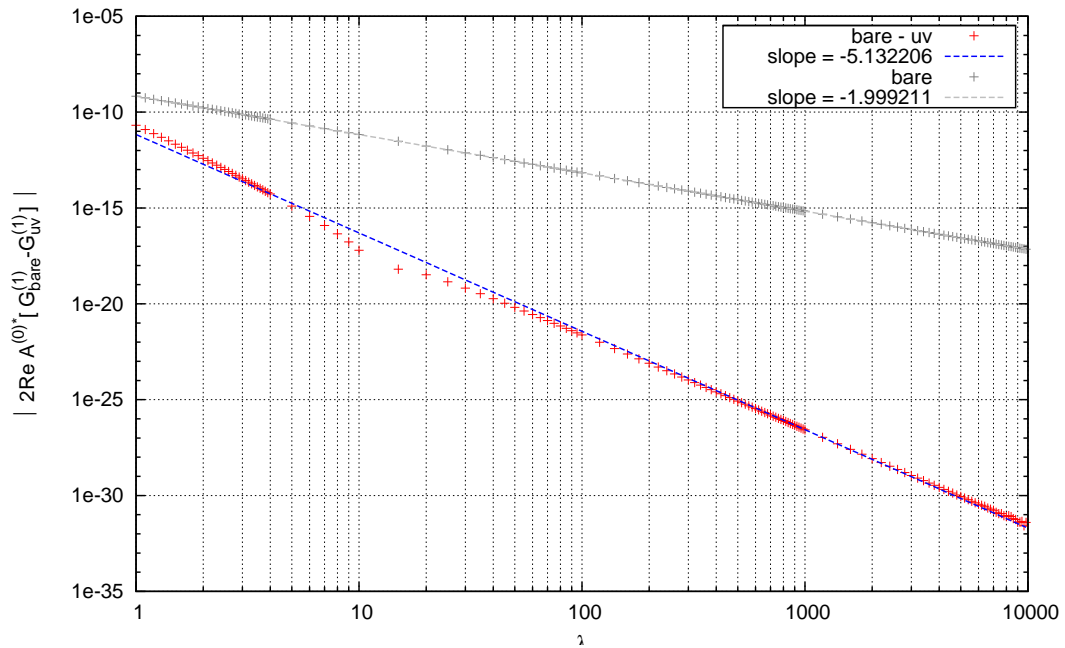


Figure 4.13: Helicity summed integrand for the one-loop QCD correction to the process $e^+e^- \rightarrow q\bar{q} + 2$ gluons. The unsubtracted total integrand in gray falls off like $1/|\bar{k}|^2$, which leads to UV divergences upon integration. The UV subtracted total integrand in red/blue, however, falls off like $1/|\bar{k}|^5$, which is clearly UV finite.

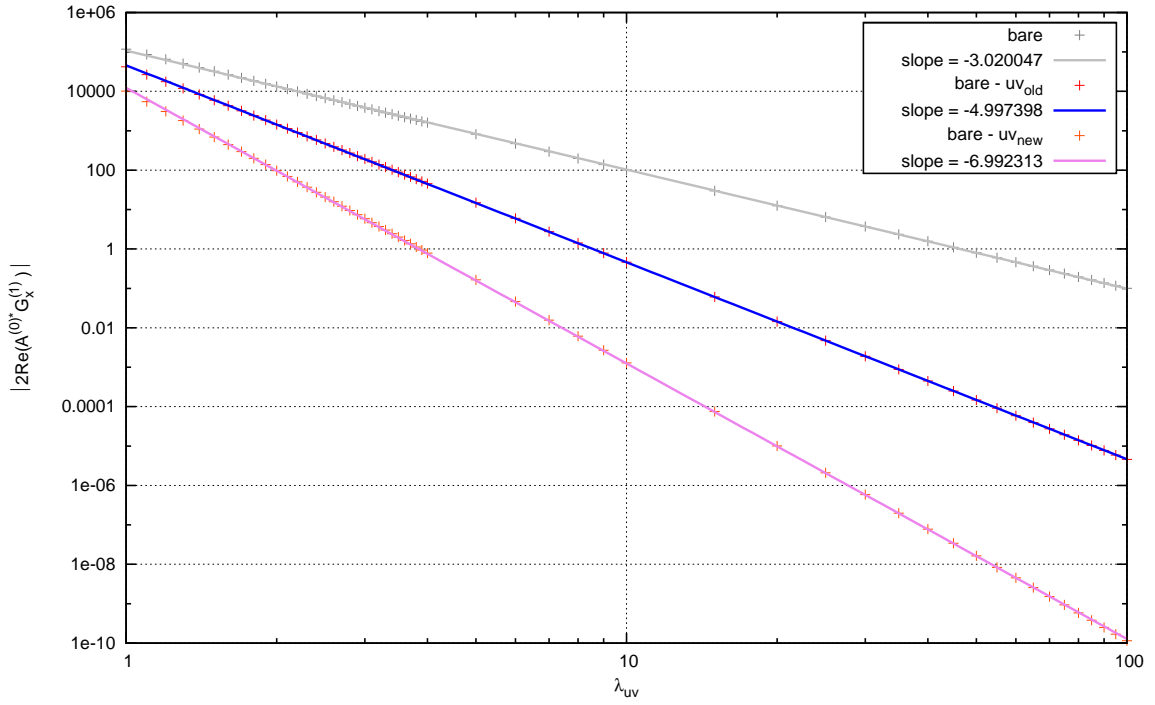


Figure 4.14: The plot shows the helicity summed $|2\text{Re}(A^{(0)*}G^{(1)})|$ vs. a UV scaling parameter λ_{UV} for $e^+e^- \rightarrow 3$ jets, in leading color approximation, where we scale a fixed value for the loop-momentum according to $\bar{k} = k - Q_{fixed} = \lambda_{UV}\bar{k}_{fixed}$. The unsubtracted total integrand (upper fit in gray) grows locally like $1/|\bar{k}|^3$, which leads to UV divergences upon integration. The (standard) UV subtracted total integrand (middle fit in blue) grows like $1/|\bar{k}|^5$, which is clearly UV finite. The (improved) UV subtracted total integrand (lower fit in pink), which contains those local UV counterterms that also subtract the $1/|\bar{k}|^5$ - and $1/|\bar{k}|^6$ -behavior, grows like $1/|\bar{k}|^7$.

Chapter 5

Application to Jet Rates in Electron–Positron Annihilation

Before we comment on the explicit results for the jet rates in electron–positron annihilation in section 5.3, we want to discuss further optimizations to the subtraction terms and the numerical integration in the sections 5.1 and 5.2 respectively.

5.1 Optimization of the Virtual Subtraction Terms in the UV

Up to now we have subtracted only those terms from our integrand which show a $\mathcal{O}(1/|k|^4)$ –behavior at maximum. This leaves us with a UV subtracted integrand that shows a leading $\mathcal{O}(1/|k|^5)$ –behavior for large loop–momentum, which leads formally to a UV finite integral. It turns out, however, that the UV regions contribute significantly to the overall numerical error, where we encounter large oscillations in our integrand in those UV regions where it is likely to have small two–particle invariants. The leading $\mathcal{O}(1/|k|^5)$ –terms are of the generic form

$$\int \frac{d^4k}{(2\pi)^4} \frac{\bar{k} \cdot X}{(\bar{k}^2 - \mu_{UV}^2)^3} \quad (5.1)$$

where X is a four–vector independent of k . This term integrates formally to zero between $|k| \rightarrow -\infty$ and $|k| \rightarrow +\infty$. At the level of the integrand, however, the term is oscillating, where the integrand changes sign under $\bar{k} \leftrightarrow -\bar{k}$. As long as the magnitudes of such oscillations are small, compared to the finite terms after the integration, they pose no threat in a Monte Carlo integration. Our experience shows, unfortunately, that the terms of order $\mathcal{O}(1/|k|^5)$ and $\mathcal{O}(1/|k|^6)$ in our integrands are not small though. Their magnitude is enhanced whenever an

external invariant approaches the jet resolution, which is most likely the case for two-particle invariants.

For a better dampening in the UV critical regions we thus need to have a look at the UV counterterms for the propagators and the three-valent vertices, and modify them such that the UV subtracted integrand shows a leading $\mathcal{O}(1/|k|^7)$ -behavior in the corresponding terms. To this end we extend the local UV counterterms for the propagators and the three-valent vertices to include also terms of order $\mathcal{O}(1/|\bar{k}|^5)$ and $\mathcal{O}(1/|\bar{k}|^6)$.

We are not aiming for a leading behavior of order $\mathcal{O}(1/|k|^7)$ of the complete integrand, since for one this is not necessary to achieve the sufficient numerical stability, and for the second if one would like to do that consequently one would not only have to improve the four-valent vertex in that regards but also introduce new local UV counterterms to effective five- and six-valent vertices as shown in figure 5.1. From a certain point of view this is not a problem, one would, however, also have to modify the respective recursion relations in chapter 4 accordingly.

We have already discussed the general strategy of the UV expansion in the previous section. However, instead of throwing away every term in the expanded integrands to the propagators and the three-valent vertices that is of order $\mathcal{O}(1/|\bar{k}|^5)$ and higher, we keep terms of order $\mathcal{O}(1/|\bar{k}|^5)$ and $\mathcal{O}(1/|\bar{k}|^6)$ and throw away every term of the order $\mathcal{O}(1/|\bar{k}|^7)$ and higher for large loop-momentum in the expanded integrands to the propagators and the three-valent vertices.

One notes that, since we are only adding terms here that lead to finite results after the integration the actual pole parts after the integration will not change. The integrated result is thus only afflicted by a change in the finite remainder $R^{G,\ell_G}(\{p_j\}, \{m_j\})$. As we have stated above the finite remainder depends for every graph G on the truncation limit ℓ_G , or in other words on the local degree of divergence, but for the two- and three-point functions we now choose ℓ_G basically to be larger by a value of 2 compared to before. In order not to spoil our improvements we absorb the finite remainder by dressing it with $\frac{6\mu_{UV}^4 R}{(k^2 - \mu_{UV}^2)^4}$ and not with $\frac{-2\mu_{UV}^2 R}{(k^2 - \mu_{UV}^2)^3}$, where $S_\varepsilon^{-1} \mu^{2\varepsilon} \int d^D \bar{k} (\bar{k}^2 - \mu_{UV}^2)^{-4} = \frac{1}{6\mu_{UV}^4} (1 + \mathcal{O}(\varepsilon)) = finite$. The resulting expressions for the modified local UV counterterms to the propagators and three-valent vertices have been implemented in a C++ library. They are rather long and will not be stated here, but can be obtained by systematically following the above introduced method in chapter 3.2.2. Further are all needed integral identities, to calculate the resulting higher rank integrals analytically, given in appendix E.

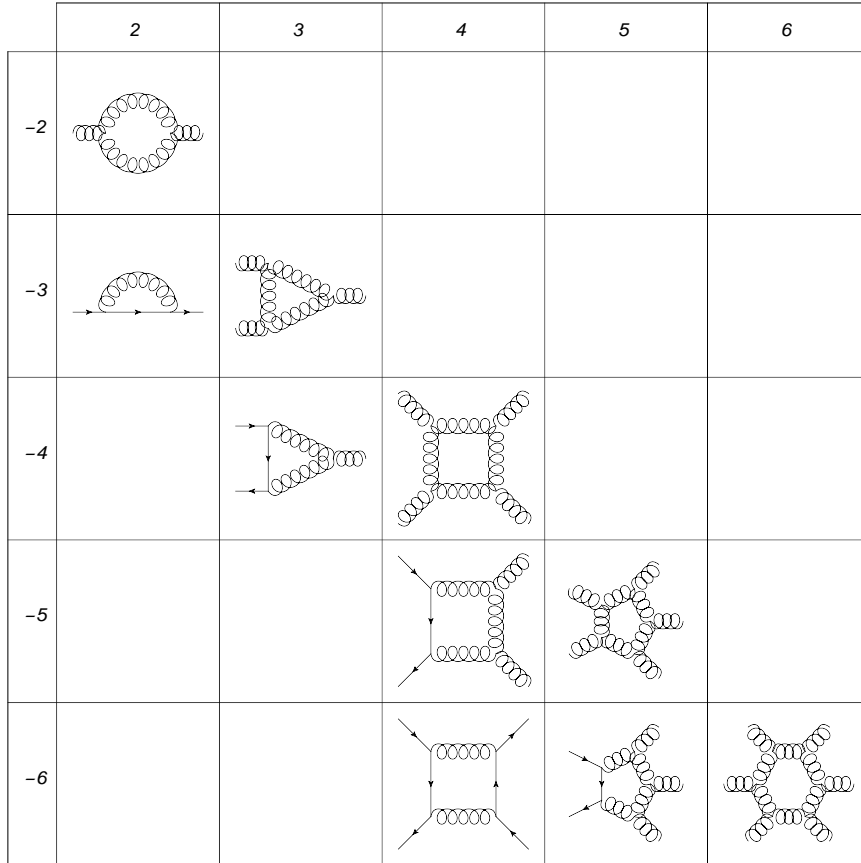


Figure 5.1: Shown are all the ordered one-loop diagrams up to a leading local behavior of order $1/|k|^6$ for $|k| \rightarrow \infty$. The columns show thereby all diagrams with the same number x of external particles, the rows show all diagrams with the same leading behavior in $|k|^y$ from $|k|^{-2}$ down to $|k|^{-6}$. The figure is taken from [91].

5.1 Optimization of the Virtual Subtraction Terms in the UV

We need to remark though, that the UV improved n_f -part of the local UV counterterm to the gluon propagator acquires a mass dependence at the higher order in $1/|\bar{k}|$, compared to the non-improved version in appendix D. The same holds for the n_f -part of the local UV counterterm to the three-gluon vertex. The UV improved local UV counterterm to the quark-gluon vertex acquires a mass dependence and additional dependences on the external momenta. Remember that the local UV counterterm to the four-gluon vertex does not receive an improvement.

We also need to dress the two- and three-point functions of the soft and collinear subtraction terms respectively with an additional suppressions in the UV region. This is done by expanding the typical soft and collinear denominators around the UV propagator in the same manner as described in section 3.2.2. The modified soft subtraction term reads thereby

$$\begin{aligned} G_{soft}^{(1)} &= i \sum_{j \in I_g} 4p_j \cdot p_{j+1} \left[\frac{1}{k_{j-1}^2 k_j^2 k_{j+1}^2} - \frac{1}{(\bar{k}^2 - \mu_{UV}^2)^3} \right] A_j^{(0)} \\ &= i \sum_{j \in I_g} \frac{4p_j \cdot p_{j+1}}{k_{j-1}^2 k_j^2 k_{j+1}^2} g_{soft}^{UV}(k_{j-1}^2, k_j^2, k_{j+1}^2) A_j^{(0)} \end{aligned} \quad (5.2)$$

where

$$g_{soft}^{UV}(k_{j-1}^2, k_j^2, k_{j+1}^2) = \left[1 - \frac{k_{j-1}^2 k_j^2 k_{j+1}^2}{(\bar{k}^2 - \mu_{UV}^2)^3} \right] \quad (5.3)$$

with

$$\lim_{k_j \rightarrow 0} g_{soft}^{UV}(k_{j-1}^2, k_j^2, k_{j+1}^2) = 1, \quad \lim_{|k| \rightarrow \infty} g_{soft}^{UV}(k_{j-1}^2, k_j^2, k_{j+1}^2) = \mathcal{O}(1/|k|) \quad (5.4)$$

This yields upon integration

$$\begin{aligned} S_\varepsilon^{-1} \mu^{2\varepsilon} \int \frac{d^D k}{(2\pi)^D} G_{soft}^{(1)} &= -\frac{1}{(4\pi)^2} \frac{e^{\varepsilon\gamma_E}}{\Gamma(1-\varepsilon)} \times \\ &\times \sum_{j \in I_g} \left[\frac{2}{\varepsilon^2} \left(\frac{-2p_j \cdot p_{j+1}}{\mu^2} \right)^{-\varepsilon} + \underbrace{\Gamma(1-\varepsilon)\Gamma(1+\varepsilon) \frac{2p_j \cdot p_{j+1}}{\mu_{UV}^2} \left(\frac{\mu_{UV}^2}{\mu^2} \right)^{-\varepsilon}}_{\frac{2p_j \cdot p_{j+1}}{\mu_{UV}^2} (1 + \mathcal{O}(\varepsilon))} \right] A_j^{(0)} \end{aligned} \quad (5.5)$$

where we see that, as expected, nothing changed in the pole parts and only finite terms are added. The modified collinear subtraction term reads

$$G_{coll}^{(1)} = i \sum_{j \in I_g} (-2) \left[\frac{S_j g_{coll}^{UV}(k_{j-1}^2, k_j^2)}{k_{j-1}^2 k_j^2} + \frac{S_{j+1} g_{coll}^{UV}(k_j^2, k_{j+1}^2)}{k_j^2 k_{j+1}^2} \right] A_j^{(0)} \quad (5.6)$$

where

$$\begin{aligned} g_{coll}^{UV}(k_{j-1}^2, k_j^2) &= \left(1 - \frac{k_{j-1}^2 k_j^2}{(\bar{k}^2 - \mu_{UV}^2)^2} \right) \\ &+ (k_{j-1}^2 k_j^2) \left(- \frac{2\bar{k} \cdot \bar{q}_{j-1} + 2\bar{k} \cdot \bar{q}_j}{(\bar{k}^2 - \mu_{UV}^2)^3} + \frac{\bar{q}_{j-1}^2 + \bar{q}_j^2 + 2\mu_{UV}^2}{(\bar{k}^2 - \mu_{UV}^2)^3} \right. \\ &\quad \left. - \frac{(2\bar{k} \cdot \bar{q}_{j-1})^2 + (2\bar{k} \cdot \bar{q}_j)^2 + (2\bar{k} \cdot \bar{q}_{j-1})(2\bar{k} \cdot \bar{q}_j)}{(\bar{k}^2 - \mu_{UV}^2)^4} \right) \end{aligned} \quad (5.7)$$

with

$$\lim_{k_j || p_j} g_{coll}^{UV}(k_{j-1}^2, k_j^2) = 1, \quad \lim_{|k| \rightarrow \infty} g_{coll}^{UV}(k_{j-1}^2, k_j^2) = \mathcal{O}(1/|k|^3) \quad (5.8)$$

This yields upon integration

$$\begin{aligned} S_\varepsilon^{-1} \mu^{2\varepsilon} \int \frac{d^D k}{(2\pi)^D} G_{coll}^{(1)} &= - \frac{1}{(4\pi)^2} \frac{e^{\varepsilon\gamma_E}}{\Gamma(1-\varepsilon)} \times \\ &\times \sum_{j \in I_g} \left[\frac{2}{\varepsilon} (S_j + S_{j+1}) \left(\frac{\mu_{UV}^2}{\mu^2} \right)^{-\varepsilon} \right. \\ &\quad \left. + 2\Gamma(1-\varepsilon)\Gamma(1+\varepsilon) \left(S_j \left(1 + \frac{p_j^2}{6\mu_{UV}^2} \right) + S_{j+1} \left(1 + \frac{p_{j+1}^2}{6\mu_{UV}^2} \right) \right) \left(\frac{\mu_{UV}^2}{\mu^2} \right)^{-\varepsilon} \right] A_j^{(0)} \\ &= - \frac{1}{(4\pi)^2} \frac{e^{\varepsilon\gamma_E}}{\Gamma(1-\varepsilon)} \sum_{j \in I_g} \left[2 \left(\frac{1}{\varepsilon} + \underbrace{\Gamma(1-\varepsilon)\Gamma(1+\varepsilon)}_{1+\mathcal{O}(\varepsilon^2)} \right) (S_j + S_{j+1}) \underbrace{\left(\frac{\mu_{UV}^2}{\mu^2} \right)^{-\varepsilon}}_{1+\mathcal{O}(\varepsilon)} \right] A_j^{(0)} \end{aligned} \quad (5.9)$$

for $p_j^2 = p_{j+1}^2 = 0$ and where we note again that only finite terms have been added. As usual $\bar{k} \equiv k - Q$, $\bar{q}_j \equiv q_j - Q$, $k_j \equiv k - q_j$, $q_j \equiv \sum_{i=1}^j p_i$ and $D \equiv 4 - 2\varepsilon$ with $|\varepsilon| \ll 1$. $S_\varepsilon \equiv (4\pi)^\varepsilon e^{-\varepsilon\gamma_E}$, where γ_E denotes the Euler–Mascheroni constant and μ denotes the typical mass scale in dimensional regularization.

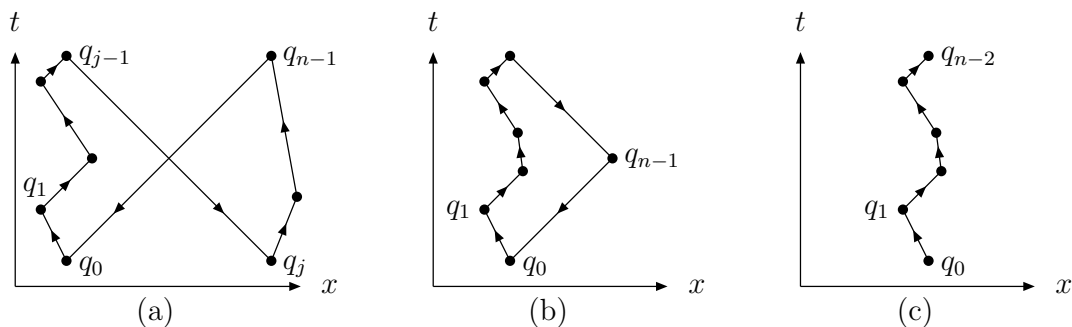


Figure 5.2: The plane with time- and one space-component of the loop-momentum space. Depicted are the origins of the light cones q_i . The external four-momenta connect thereby the origins of the light cones via $p_i = q_i - q_{i-1}$. Diagram (a) shows the setup in a generic primitive amplitude with n external legs. Diagram (b) depicts a situation where the two incoming particles are adjacent. Diagram (c) draws the picture for electron-positron annihilation, where the poles due to q_{n-1} are absent. The figures are taken from [91].

5.2 Direct One-Loop Contour Deformation for the Process $e^+e^- \rightarrow jets$

As we discussed at the end of chapter 3.4 we have to deform the loop-momentum into complex space in order to be able to integrate the finite subtracted integrand. The situation in the loop-momentum space is depicted again in figure 5.2.

We want to elaborate a little bit more on the direct contour deformation for the case of $e^+e^- \rightarrow jets$. The thesis at hand has not been concerned directly with the corresponding algorithm, which is why we only comment on those parts which are necessary to understand the actual optimization for this process. We refer to the discussion in [91] for any further details that are not mentioned here. The situation corresponds to the case shown in diagram (c) of figure 5.2, where the particles n and $(n-1)$ couple through an intermediate photon or Z -boson to the loop and we are left with a single strand in loop-momentum space. We define thereby an interior region by the intersection of the interior of the backward light cone from q_{n-2} with the interior of the forward light cone from q_0 and an exterior region, which is simply the complement to the interior region. Our integral looks in this case as follows

$$I = \int \frac{d^4k}{(2\pi)^4} [G_{bare}^{(1)} - G_{soft}^{(1)} - G_{coll}^{(1)} - G_{UV}^{(1)}] = \int \frac{d^4k}{(2\pi)^4} \frac{R(k)}{\prod_{j=0}^{n-2} (k_j^2 - m_j^2)} = \int \frac{d^4k}{(2\pi)^4} G(k) \quad (5.10)$$

We can split the integral into an exterior and an interior part

$$\begin{aligned} I &= I_{ext} + I_{int} = \int \frac{d^4k}{(2\pi)^4} f_{UV}(k) G(k) + \int \frac{d^4k}{(2\pi)^4} (1 - f_{UV}(k)) G(k) \\ &= \int \frac{d^4k}{(2\pi)^4} G_{ext}(k) \quad + \int \frac{d^4k}{(2\pi)^4} G_{int}(k) \end{aligned} \quad (5.11)$$

where we choose

$$f_{UV}(k) = \prod_{j=0}^{n-2} \frac{k_j^2 - m_j^2}{\bar{k}^2 - \mu_{UV}^2} \quad (5.12)$$

Since $f_{UV}(k)$ is a meromorphic function of k , with poles only at $(\bar{k}^2 - \mu_{UV}^2) = 0$, this splitting is clearly holomorphic in k and we can evaluate I_{ext} and I_{int} along different contours. For I_{ext} we note, as mentioned before, that setting μ_{UV}^2 large enough on the imaginary axis suffices already to ensure $(\bar{k}^2 - \mu_{UV}^2) \neq 0$. However to improve the numerical stability we choose a simple contour deformation for I_{ext} , where

$$k = \tilde{k} + i\kappa(\tilde{k}) \quad (5.13)$$

with

$$\kappa^\mu(\tilde{k}) = g_{\mu\nu}(\tilde{k}^\nu - Q^\nu) \quad (5.14)$$

We thus have $\bar{k}^2 - \mu_{UV}^2 = 2i(\tilde{k} - Q) \circ (\tilde{k} - Q) - \mu_{UV}^2$, where $a \circ b$ denotes the Euclidean scalar product between the four-vectors a and b , which is always positive. Choosing μ_{UV}^2 purely imaginary with $Im(\mu_{UV}^2) < 0$ and without further deformation ensures that the imaginary part of $(\bar{k}^2 - \mu_{UV}^2)$ is always positive but constant along the cone $\bar{k}^2 = 0$. Choosing the additional deformation in equation 5.14 though we make sure that the UV propagator $(\bar{k}^2 - \mu_{UV}^2)^{-1}$ falls always off like $1/|\tilde{k}|^2$ for $|\tilde{k}| \rightarrow \infty$, which enhances the numerical stability in the exterior region further. The Jacobian of the deformation is simply given by $\det[\partial k^\mu / \partial \tilde{k}^\nu] = -4i$.

Regarding the interior region we note that

$$(1 - f_{UV}(k)) = \frac{1}{(\bar{k}^2 - \mu_{uv}^2)^{n-1}} \left\{ (k^2)^{n-2} 2k \cdot \left[\sum_{j=0}^{n-2} q_j - (n-1)Q \right] + \mathcal{O}(k^{2n-4}) \right\} \quad (5.15)$$

Choosing the arbitrary four-vector Q such that $Q = \frac{1}{(n-1)} \sum_{j=0}^{n-2} q_j$ cancels the leading order in k in equation 5.15 and $G_{int}(k)$ will drop with two additional powers of $1/|k|$ for $|k| \rightarrow \infty$. $G_{int}(k)$ show thus a good ultraviolet behavior but has a more complicated infrared structure. For the contour deformation for I_{int} we have to consider the poles around

$$k_j^2 - m_j^2 = 0 \text{ for } 0 \leq j \leq n-2 \quad (5.16)$$

or in the massless case around $k_j^2 = 0$ for $0 \leq j \leq n-2$. The contour deformation along the lines of [83] is therefor chosen, with additional modifications to protect the UV behavior. A more detailed account of the parameters of the deformation for I_{int} is given in [91].

In combination with the improvements to the subtraction terms we can summarize that the integrand $G_{ext}(k)$ falls off like $|k|^{-7}$ in terms corresponding to n -point functions with $n \leq 3$ and like $|k|^{-5}$ in terms corresponding to n -point functions with $n \geq 4$. The integrand $G_{int}(k)$ falls off like $|k|^{-9}$ in terms corresponding to n -point functions with $n \leq 3$ and like $|k|^{-7}$ in terms corresponding to n -point functions with $n \geq 4$. In addition we can further improve the leading UV behavior of all those terms with an odd power in $|k|^{-1}$, by the method of antithetic variates, by always sampling $-\bar{k}$ and \bar{k} together, which reduces the leading behavior down to the next lower even power in $|k|^{-1}$.

Even though we will not give a detailed account of the parameters of the deformation of I_{int} here we want to discuss briefly a further technique, which enhances the Monte Carlo efficiency through a dedicated sampling and is based on the division of the interior region into sub-channels. Consider our integral in the interior region after deformation, which can simply be written as

$$I_{int} = \int \frac{d^4 \tilde{k}}{(2\pi)^4} f(\tilde{k}) \quad (5.17)$$

and the line segments in loop-momentum space, which are parametrized by

$$\tilde{k} = q_j + x(q_{j+1} - q_j) \text{ for } 0 \leq x \leq 1 \text{ and } 0 \leq j \leq n-3 \quad (5.18)$$

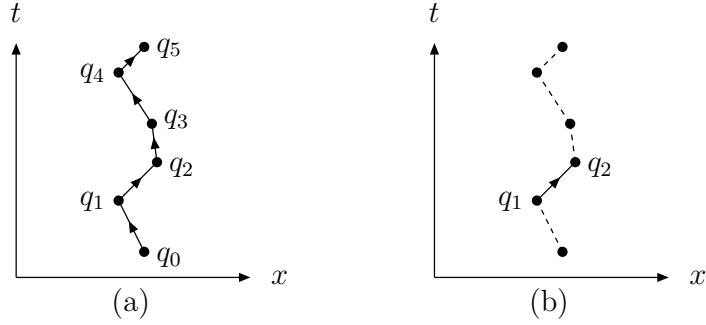


Figure 5.3: The plane with time- and one space-component of the loop-momentum space. Depicted are the origins of the light cones q_i . The external four-momenta connect thereby the origins of the light cones via $p_i = q_i - q_{i-1}$. Diagram (a) draws the picture for electron-positron annihilation, where the poles due to q_{n-1} are absent. For the interior region we divide the integral into $(n - 2)$ sub-channels, such that each line segment i corresponds to a specific sub-channel. Diagram (b) shows this situation, where we have picked out the specific line segment from q_1 to q_2 . The figures are taken from [91].

which is depicted in diagram (a) of figure 5.3. We can now split the integral into several sub-channels, such that each line segment corresponds to a separate channel, which reads

$$I_{int} = \sum_{i=0}^{n-3} \int \frac{d^4 \tilde{k}}{(2\pi)^4} w(\tilde{k}) f(\tilde{k}) \quad (5.19)$$

where we choose the weights, such that $w_i \geq 0$ and $\sum_{i=0}^{n-3} w_i = 1$, by

$$w_i(\tilde{k}) = \frac{(|k_i^2| |k_{i+1}^2|)^{-2}}{\sum_{j=0}^{n-3} (|k_j^2| |k_{j+1}^2|)^{-2}} \quad (5.20)$$

This division into sub-channels is not holomorphic in k and we use the same contour deformation for all channels. However, the weights behave such that

$$\lim w_i = 1 \quad \text{if} \quad \tilde{k} \rightarrow q_i + xp_{i+1} \quad (5.21)$$

$$\lim w_i = 0 \quad \text{if} \quad \tilde{k} \rightarrow q_j + xp_{j+1}, \quad i \neq j \quad (5.22)$$

which ensures that in each sub-channel there is only one critical line segment as depicted in diagram (b) of figure 5.3. This means that we can parametrize each sub-channel differently,

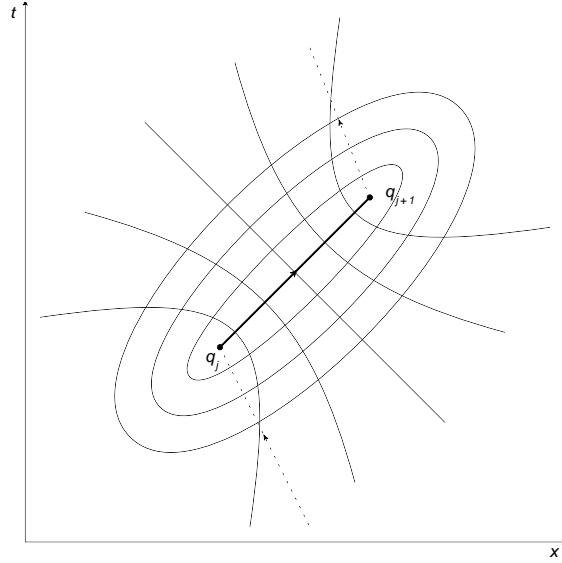


Figure 5.4: We can parametrize each sub-channel by a generalization of elliptical coordinates to four dimensions. Shown is the situation for the j th sub-channel in the t - x -plane of the loop-momentum space. The line segment corresponds to a zero value for the general elliptic radial coordinate. The figure is taken from [96].

where we choose the generalization of elliptical coordinates to four dimensions. The coordinate system of each sub-channel j is thereby chosen such that the origin of this coordinate system corresponds to the line segment that connects q_j and q_{j+1} . This is depicted in figure 5.4 for the sub-channel j .

We can put such an elliptical coordinate system in \mathbb{R}^4 around each critical line segment such that for each sub-channel j

$$\tilde{k} = q_j + \frac{1}{2}p_{j+1} + R_3 \cdot R_2 \cdot R_1 \tilde{k}' \quad (5.23)$$

where

$$\tilde{k}' = \frac{1}{2}|p_{j+1}| \begin{pmatrix} \cosh(\rho) \cos(\xi) \\ \sinh(\rho) \sin(\xi) \cos(\theta) \\ \sinh(\rho) \sin(\xi) \sin(\theta) \cos(\phi) \\ \sinh(\rho) \sin(\xi) \sin(\theta) \sin(\phi) \end{pmatrix} \quad (5.24)$$

with $\rho \in [0, \infty[$, ξ and $\theta \in [0, \pi]$ and $\phi \in [0, 2\pi]$ the parameters of the elliptical coordinate

system. R_3 , R_2 and R_1 are appropriately chosen rotation matrices in four dimensions to orient the elliptical coordinate system correctly around the chosen critical line segment. A more comprehensive account on the loop–momentum sampling for I_{ext} and I_{int} is given in [91].

For the moment we only want to stress that we can reduce the Monte Carlo error in each sub-channel drastically with the method of antithetic variates and upon the following observations: The integrand has a periodic behavior in ϕ . Combining the evaluations at ϕ and $(\phi + \pi) \bmod(2\pi)$ therefore averages out these oscillations. In addition, the integrand is for $\rho \rightarrow 0$ strongly peaked and antisymmetric around $\theta = \pi/2$. Evaluating the integrand at θ and $(\pi - \theta)$ averages out this behavior. Furthermore we evaluate the integrand always with the values \tilde{k}' and $(-\tilde{k}')$, which improves the UV behavior.

5.3 Jet Rates in Electron–Positron Annihilation in the Leading Color Approximation

As a proof of concept we applied our method to the computation of jet rates in electron–positron annihilation [90], where we use the exclusive Durham jet algorithm [148] to define the jets. A comprehensive overview on jet algorithms in electron–positron annihilation can be found in [13]. The corresponding clustering algorithm is thereby defined as follows

- i) To start with a value for the resolution parameter y_{cut} is assigned.
- ii) For each pair (p_k, p_l) of final–state particles the corresponding resolution parameter y_{kl} is computed according to

$$y_{kl} = \frac{2 \min(E_k^2, E_l^2)(1 - \cos \theta_{kl})}{Q^2} \quad (5.25)$$

where E_k and E_l are the energies of the particles k and l , and θ_{kl} is the angle between \vec{p}_k and \vec{p}_l . Q is the center–of–mass energy.

- iii) For all y_{kl} the smallest value $y_{ij} = \min\{y_{kl}\}$ is considered. If $y_{ij} < y_{cut}$ then the associated pair (p_i, p_j) is combined into a jet, which has a combined momentum $p_m = p_{ij}$ according to the E –scheme:

$$E_{ij} = E_i + E_j \quad \text{and} \quad \vec{p}_{ij} = \vec{p}_i + \vec{p}_j \quad (5.26)$$

which conserves energy and momentum, but $p_{ij}^2 \neq 0$ for massless particles i and j .

iv) Repeat steps ii) and iii) until all pairs fulfill $y_{mn} > y_{cut}$.

The production rate for n -jet events, or short jet rate, in electron–positron annihilation is defined as the ratio between the n -jet cross section and the total hadronic cross section σ_{tot} [90]

$$\bar{R}_n(\mu) = \frac{\sigma_{n-jet}(\mu)}{\sigma_{tot}(\mu)} = \left(\frac{\alpha_s}{2\pi}\right)^{n-2} \bar{A}_n(\mu) + \left(\frac{\alpha_s}{2\pi}\right)^{n-1} \bar{B}_n(\mu) + \mathcal{O}(\alpha_s^n) \quad (5.27)$$

where μ is the renormalization scale and we have given the perturbative expansion of the jet rate in α_s . In practice we compute the ratio with respect to the LO hadronic cross section σ_0

$$R_n(\mu) = \frac{\sigma_{n-jet}(\mu)}{\sigma_0(\mu)} = \left(\frac{\alpha_s}{2\pi}\right)^{n-2} A_n(\mu) + \left(\frac{\alpha_s}{2\pi}\right)^{n-1} B_n(\mu) + \mathcal{O}(\alpha_s^n) \quad (5.28)$$

The relations between A_n, B_n and \bar{A}_n, \bar{B}_n are then obtained from the perturbative expansion of the total hadronic cross section

$$\sigma_{tot}(\mu) = \sigma_0(\mu) \left(1 + \frac{3}{2} C_F \frac{\alpha_s}{2\pi} + \mathcal{O}(\alpha_s^2)\right) \quad (5.29)$$

and read

$$\bar{A}_n = A_n \quad \text{and} \quad \bar{B}_n = B_n - \frac{3}{2} C_F A_n \quad (5.30)$$

where it is sufficient to calculate \bar{A}_n and \bar{B}_n at a fixed scale μ_0 , which we can take to be the center-of-mass energy $\mu_0 = Q$, and the scale variation can be determined from the renormalization group equation, as given in equation 1.5 in the introduction, to read

$$\bar{A}_n(\mu) = \bar{A}_n(\mu_0) \quad \text{and} \quad \bar{B}_n(\mu) = \bar{B}_n(\mu_0) + \frac{(n-2)}{2} \beta_0 \ln\left(\frac{\mu^2}{\mu_0^2}\right) \bar{A}_n(\mu_0) \quad (5.31)$$

The computation of the amplitudes in the leading color approximation is thereby reflected in an expansion of A_n and B_n in the number of colors N_c by

$$A_n = N_c \left(\frac{N_c}{2}\right)^{n-2} \left(A_{n,lc} + \mathcal{O}(1/N_c)\right) \quad \text{and} \quad B_n = N_c \left(\frac{N_c}{2}\right)^{n-1} \left(B_{n,lc} + \mathcal{O}(1/N_c)\right) \quad (5.32)$$

The NLO jet rate coefficients in the leading color approximation $B_{n,lc}$ for two, three and four jets are compared to known analytic results [122, 13], which is shown in figures 5.5, 5.6 and 5.7 where excellent agreement is observed. Results for five, six and seven jets have been calculated

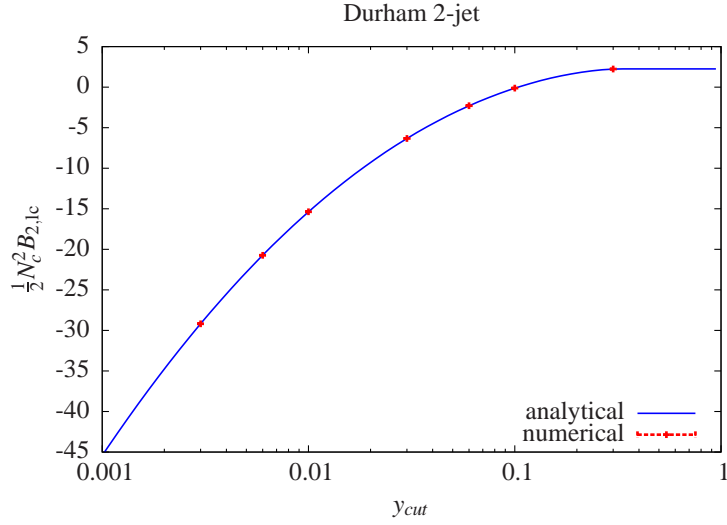


Figure 5.5: NLO leading color jet rate coefficient vs. y_{cut} . Comparison of the numerically computed two-jet rate for selected values of y_{cut} (red) to known analytic results (blue). The Monte Carlo errors are almost invisible. The figure is taken from [90].

and are given for several values of y_{cut} in table 5.1. The results for six and seven jets are new [90] and involve for the first time the computation of a one-loop eight-point integral in the determination of a physics observable. We choose the center-of-mass energy to be equal to the mass of the Z-boson $Q = m_Z$ and use five massless quark flavors $n_f = 5$ in the computation.

Regarding the computational performance we have plotted the CPU time which is needed for one evaluation of the Born contribution, the insertion contribution and the virtual contribution (see chapter 3) as a function of the number n of jets. We note that the insertion contribution is almost as fast as the Born contribution, which is to be expected since the insertion contribution includes only Born amplitudes times some logarithms. For all contributions, including the virtual contribution, the scaling behavior with the number of legs behaves very moderate and scales asymptotically as n^4 , which is shown in figure 5.8. More details can be found in [90, 91].

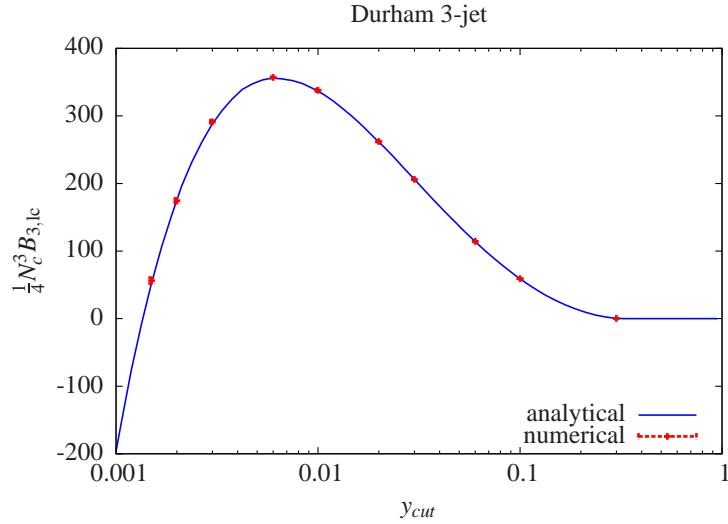


Figure 5.6: NLO leading color jet rate coefficient vs. y_{cut} . Comparison of the numerically computed three-jet rate for selected values of y_{cut} (red) to known analytic results (blue). The Monte Carlo errors are almost invisible. The figure is taken from [90].

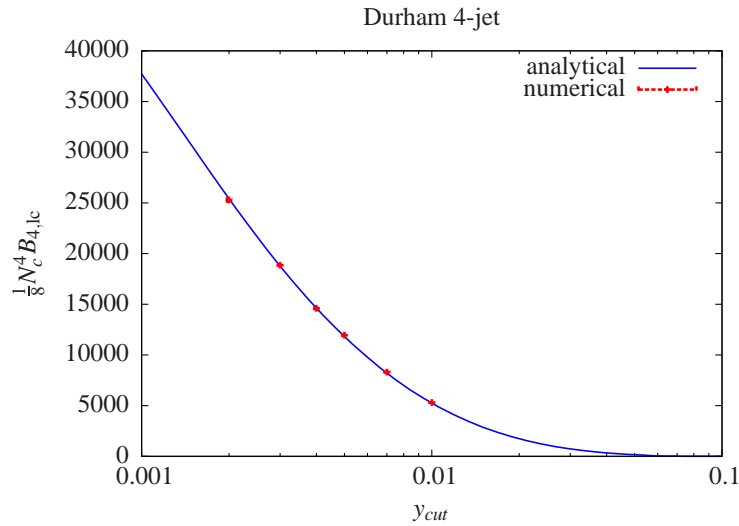


Figure 5.7: NLO leading color jet rate coefficient vs. y_{cut} . Comparison of the numerically computed four-jet rate for selected values of y_{cut} (red) to known analytic results (blue). The Monte Carlo errors are almost invisible. The figure is taken from [90].

y_{cut}	$\frac{N_c^4}{8} A_{5,\text{lc}}$	$\frac{N_c^5}{16} B_{5,\text{lc}}$
0.002	$(5.0529 \pm 0.0004) \cdot 10^3$	$(4.275 \pm 0.006) \cdot 10^5$
0.001	$(1.3291 \pm 0.0001) \cdot 10^4$	$(1.050 \pm 0.026) \cdot 10^6$
0.0006	$(2.4764 \pm 0.0002) \cdot 10^4$	$(1.84 \pm 0.15) \cdot 10^6$
y_{cut}	$\frac{N_c^5}{16} A_{6,\text{lc}}$	$\frac{N_c^6}{32} B_{6,\text{lc}}$
0.001	$(1.1470 \pm 0.0002) \cdot 10^5$	$(1.46 \pm 0.04) \cdot 10^7$
0.0006	$(2.874 \pm 0.002) \cdot 10^5$	$(3.88 \pm 0.18) \cdot 10^7$
y_{cut}	$\frac{N_c^6}{32} A_{7,\text{lc}}$	$\frac{N_c^7}{64} B_{7,\text{lc}}$
0.0006	$(2.49 \pm 0.08) \cdot 10^6$	$(5.4 \pm 0.3) \cdot 10^8$

Table 5.1: NLO leading color jet rate coefficients to the five-, six- and seven-jet rates for selected values of y_{cut} . The relative Monte Carlo errors for the seven-jet rate results are comparatively small if one considers that the evaluation took about five days on a cluster with about 200 standard CPU cores. The table is taken from [90].

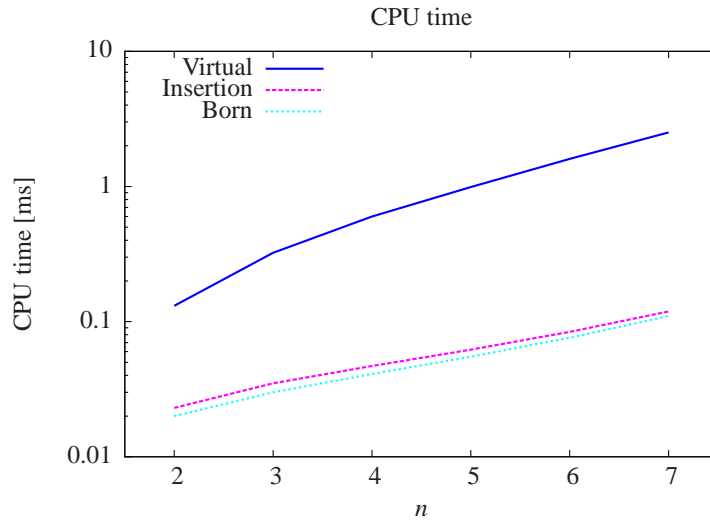


Figure 5.8: CPU time which is required for one evaluation of the Born contribution (cyan), the insertion contribution (pink) and the virtual contribution (blue) as a function of the number n of jets. The times are measured on one standard CPU core. The figure is taken from [90].

Chapter 6

Conclusions and Outlook

In the era of LHC physics it is important to have fast and accurate tools to carry out high precision QCD calculations. Since experiments at the LHC are faced with high QCD jet rates, one needs to be able to predict this large QCD background with the utmost accuracy in order to be able to find new physics on top of it. The large number on radiated partons, to be expected at energies typical for the LHC, calls for fast and reliable techniques to compute higher-than-leading order processes with many particles in the final state. Numerical Monte Carlo calculations are natural candidates to implement such techniques, where of special interest these days are numerical calculations at the NLO level.

One approach to the automated evaluation of collider observables at NLO has been presented here, which puts focus especially on the numerical evaluation of the virtual part of the calculation, i.e. integrating the one-loop integrals by means of Monte Carlo integration, and on the efficient construction of the necessary ingredients by recursive off-shell relations. The numerical integration is thereby only possible if the integrand is locally free of any terms that lead to soft, collinear or UV poles. Regarding this matter we have concentrated especially on the development of a local UV renormalization, with local UV counterterms to QCD propagators and vertices at its heart. Together with the associated recursive UV relations they yield a powerful tool to renormalize any QCD one-loop integrand on a local level, which is important in numerical approaches to one-loop integration. We have further devised recursive one-loop relations, based on cutting open loop-propagators and tree-level off-shell currents with two off-shell legs. We have shown that the recursive UV construction and the recursive one-loop construction behave as expected. We have further shown that the numerical method, including all subtraction terms, recursive components and a direct numerical deformation of the one-loop integration contour

in complex space can be used efficiently in the calculation of a physics observable, where we calculated the NLO coefficients to jet rates in electron–positron annihilation, in the large– N_c limit. The development of the local virtual soft and collinear subtraction terms and the direct numerical deformation of the one–loop integration contour have thereby not been part of this thesis, but have been discussed as well in order to complete the picture.

It has been shown recently, that the direct contour deformation can also be used in the massive case and even be applied to multi–loop problems. In this regard we want to stress, that one might want to extend the local UV subtraction to higher–loop integrands as well. The adopted strategy in the development of the local one–loop UV subtraction could therefore in principle be extrapolated to the pure UV divergences in the two–loop case for a start. The deduction of the associated recursive constructions should be straightforward.

In order to apply the technique further and finally to hadron induced processes we note that we can in principle use the existing components of the calculation for the process $e^+e^- \rightarrow jets$ in leading color approximation in order to calculate observables for the process $pp \rightarrow Z + jets$ in leading color approximation, by applying simple crossing relations. The inclusion of initial–state radiation should not pose a threat concerning the pole cancellation, since our subtraction terms are formulated such that they generically approximate the soft and collinear behavior of any one–loop QCD amplitude locally, and the integrated soft and collinear subtraction terms always cancel the explicit soft and collinear poles from the corresponding dipole insertion operator. One has to think, however, of an efficient way to generate the necessary phase–space in this case, where many solutions exist already in the literature.

The second–to–next step would be to implement the existing calculations also for the full color case. In this regard the thesis at hand was greatly concerned with the associated matter of color management in one–loop QCD amplitudes, especially for multiple external quark–antiquark pairs and an arbitrary number of gluons. We have thereby introduced a new method which can be used to find closed formulae that express color–ordered partial one–loop amplitudes as linear combinations of cyclically ordered one–loop primitive amplitudes, without using Feynman diagrams in an intermediate step. It was realized that we can use the information about the color antennae structure of certain classes to determine the content of primitive amplitudes to a specific partial amplitude. Up to now the method can be used to determine the appropriate shuffle sums over the primitive amplitudes for a specific number of quark–antiquark pairs and an arbitrary number of gluons, i.e. to determine the all– n formula for a specific m , where n

denotes the number of gluons and m the number of quark–antiquark pairs. The formalization to a more algorithmic language will be the content of a future publication. We have studied those contributions which dominate QCD amplitudes in the large- N_c limit for an arbitrary number of quark–antiquark pairs and an arbitrary number of gluons and have derived a closed all- n –all- m formula for this special case. The extension of this case to higher-loop QCD amplitudes should be possible.

As a last outlook we would like to mention that it was thought about an extension of the Les Houches Event file format, which can be used as interface of the output of a hard matrix element calculation to a parton shower, to our NLO calculations. A first output of our calculation of NLO jet rates in electron–positron annihilation has been written to Les Houches Event files and is ready to be used. A more comprehensive approach, however, would be to directly interface or include our numerical routines into existing general purpose Monte Carlo event generators. We will leave a corresponding investigation for future discussion.

Appendix A

QCD Feynman Rules

In this appendix we collect the necessary Feynman rules that are needed in the computation of one-loop QCD amplitudes. We present them in their full color-dressed form, in Feynman gauge, as well as in a factorized form, where the separation between color and kinematic degrees of freedom becomes apparent. For the color parts we also state the representation in the double-line formalism.

If not stated otherwise all external four-momenta are defined to be outgoing. Energy and momentum conservation are understood. Hence $\sum_i p_i = 0$, where the sum runs over all outgoing external four-momenta p_i . Incoming and outgoing external lines in a Feynman diagram are as usual given by the polarization vectors and spinors of the respective incoming and outgoing partons, as can be found in any standard textbook.

Upon the calculation of one-loop diagrams we perform an additional integration over the loop-momentum via $\int \frac{d^4 k}{(2\pi)^4}$, where we choose dimensional regularization in order to regularize the integral via $S_\varepsilon^{-1} \mu^{2\varepsilon} \int \frac{d^D k}{(2\pi)^D}$, where $D = 4 - 2\varepsilon$ with $|\varepsilon| \ll 1$ and μ the typical regularization (mass) scale in dimensional regularization. For every closed fermion loop we thereby need to include an additional minus sign, due to Fermion statistics.

A.1 Propagators

The gluon propagator is given by

A.1 Propagators

$$\begin{aligned}
\begin{array}{c} a \\ \text{-----} \\ \mu \quad \leftarrow k \quad \nu \\ \text{-----} \\ b \end{array} &= \frac{-ig_{\mu\nu}}{k^2} \times \delta^{ab} \hat{=} \frac{-ig_{\mu\nu}}{k^2} \times (\delta_{i_a \bar{j}_b} \delta_{i_b \bar{j}_a} - \frac{1}{N_c} \delta_{i_a \bar{j}_a} \delta_{i_b \bar{j}_b}) \\
&= \begin{array}{c} \text{-----} \\ \mu \quad \leftarrow k \quad \nu \\ \text{-----} \end{array} \times \left(\begin{array}{c} i_a \quad \leftarrow \quad \bar{j}_b \\ \bar{j}_a \quad \rightarrow \quad i_b \\ - \frac{1}{N_c} \begin{array}{c} i_a \\ \bar{j}_a \end{array} \begin{array}{c} \rightarrow \quad \bar{j}_b \\ \leftarrow \quad i_b \end{array} \end{array} \right) \quad (A.1)
\end{aligned}$$

where we have dropped the $+i\delta$ -prescription in the denominator of the propagator, and where we have applied the projector $\sqrt{2}T_{i_a \bar{j}_a}^a \sqrt{2}T_{i_b \bar{j}_b}^b$ onto δ^{ab} and subsequently used the Fierz identity, which has a normalization of $\frac{1}{2}$ in our convention, in order to convert the color part to the color-flow double-line notation as described in chapter 2.2. The second part in the color-flow rules is interpreted as U(1)-gluon, which vanishes in purely gluonic interactions and only couples between quark lines.

The quark propagator is given by

$$\begin{array}{c} i \\ \text{-----} \\ \leftarrow k \\ \text{-----} \\ j \end{array} = i \frac{\not{k} + m}{k^2 - m^2} \times \delta_{i\bar{j}} = \begin{array}{c} \text{-----} \\ \leftarrow k \\ \text{-----} \end{array} \times \begin{array}{c} i \\ \text{-----} \\ \leftarrow k \\ \text{-----} \\ j \end{array} \quad (A.2)$$

where m denotes the mass of the quark. For massless quark-flavors, in the high-energy limit, we simply set $m = 0$.

The ghost propagator is given by

$$\begin{aligned}
\begin{array}{c} a \\ \text{-----} \\ \leftarrow k \\ \text{-----} \\ b \end{array} &= \frac{i}{k^2} \times \delta^{ab} \hat{=} \frac{i}{k^2} \times (\delta_{i_a \bar{j}_b} \delta_{i_b \bar{j}_a} - \frac{1}{N_c} \delta_{i_a \bar{j}_a} \delta_{i_b \bar{j}_b}) \\
&= \text{-----} \times \left(\begin{array}{c} i_a \quad \leftarrow \quad \bar{j}_b \\ \bar{j}_a \quad \rightarrow \quad i_b \\ - \frac{1}{N_c} \begin{array}{c} i_a \\ \bar{j}_a \end{array} \begin{array}{c} \rightarrow \quad \bar{j}_b \\ \leftarrow \quad i_b \end{array} \end{array} \right) \quad (A.3)
\end{aligned}$$

The second term in the color-flow rule actually vanishes because there exists no quark-ghost interaction. Since we are working in Feynman gauge, we need to include ghost loops in our one-loop calculations. Just as for closed fermion loops we need to include an additional minus sign for every ghost loop.

A.2 Vertices

The quark–gluon vertex is given by

$$\begin{aligned}
\begin{array}{c} i \\ \nearrow \\ \text{---} \\ \searrow \\ j \end{array} & \begin{array}{c} a \\ \text{---} \\ \mu \end{array} = -ig_s \gamma^\mu T_{ij}^a = (-i\gamma^\mu) \times (+g_s T_{ij}^a) \\
& \hat{=} (-i\gamma^\mu) \times \left(+\frac{g_s}{\sqrt{2}} \delta_{i\bar{j}a} \delta_{i_a\bar{j}} \right) = \begin{array}{c} \text{---} \\ \mu \end{array} \times \begin{array}{c} i \\ \uparrow \\ \text{---} \\ \downarrow \\ \bar{j} \\ \uparrow \\ j \end{array} \begin{array}{c} \bar{j}_a \\ \text{---} \\ i_a \end{array} \quad (\text{A.4})
\end{aligned}$$

where g_s denotes the QCD coupling constant, γ^μ the Dirac matrices and T_{ij}^a the generators of $SU(N_c)$ in the fundamental representation, where in QCD $N_c = 3$. We have again used a projector $\sqrt{2}T_{i_a\bar{j}_a}^a$ onto T_{ij}^a and the Fierz identity in order to convert to the color–flow formalism, the $-1/N_c$ –term is thereby not taken into account but has to be remembered either in an internal gluon propagator upon connecting two quark lines or in squaring the amplitude if the depicted gluon is an external one, as described in chapter 2.2. The color–stripped quark–gluon vertex is thereby defined by $\Gamma^{(0)\mu} = -i\gamma^\mu$. Although we depict the color–flow rule in the double–line notation we also provide for the gluon the corresponding index in the adjoint representation within the color–flow vertex diagram. For our purposes, i.e. to track the flow of color within one–loop diagrams, it is useful to also have another factorization of the quark–gluon vertex into the color–stripped and color–flow contributions

$$\begin{aligned}
\begin{array}{c} i \\ \nearrow \\ \text{---} \\ \searrow \\ j \end{array} & \begin{array}{c} a \\ \text{---} \\ \mu \end{array} = -ig_s \gamma^\mu T_{ij}^a = (+i\gamma^\mu) \times (-g_s T_{ij}^a) \\
& \hat{=} (+i\gamma^\mu) \times \left(-\frac{g_s}{\sqrt{2}} \delta_{i\bar{j}a} \delta_{i_a\bar{j}} \right) = \begin{array}{c} \text{---} \\ \mu \end{array} \times \begin{array}{c} i \\ \uparrow \\ \text{---} \\ \downarrow \\ \bar{j} \\ \uparrow \\ j \end{array} \begin{array}{c} \bar{j}_a \\ \text{---} \\ i_a \end{array} \quad (\text{A.5})
\end{aligned}$$

and we have thus defined the difference between left– and right–radiating gluons, in the color–stripped rule with respect to the fermion–flow arrow, as well as in the color–flow rule with respect to the color–flow arrow on the single fundamental line. We have therefore antisymmetrized the

$$V_{ggg}^{(0)\mu_1\mu_2\mu_3}(k_1, k_2, k_3) \equiv iV_3^{\mu_1\mu_2\mu_3}(k_1, k_2, k_3) \quad (\text{A.8})$$

as well as the color-flow rule. We note that the color-stripped three-gluon vertex is thus also antisymmetric in the exchange of any two of the three legs. For our purposes to track the flow of color within one-loop diagrams it is useful again to have another factorization of the three-gluon vertex into the color-stripped and color-flow contributions.

$$\left(\begin{array}{c} \text{a} \\ \text{c} \xrightarrow{i_c} \text{b} \\ \text{c} \xleftarrow{j_c} \text{b} \end{array} \right) - \left(\begin{array}{c} \text{a} \\ \text{c} \xrightarrow{j_c} \text{b} \\ \text{c} \xleftarrow{i_c} \text{b} \end{array} \right) \quad (\text{A.9})$$

In the above we kept the cyclic order of the three legs fixed, compared to the previous formula, but therefore defined an antisymmetric color-flow rule, were we define the difference in the three-gluon color-flow vertex for one of the gluon color double-lines to be radiated from either one of the color-flow lines in the respectively remaining color-flow between the other two gluons. In accordance with the similar redefinition for the quark-gluon vertex, we assign a relative minus sign if the one gluon color double-line is radiated to the left with respect to the single color-flow line that it originates from.

The four-gluon vertex is given by

$$\begin{aligned} &= -ig_s^2 [f^{abe} f^{cde} (g^{\mu\lambda} g^{\nu\rho} - g^{\mu\rho} g^{\nu\lambda}) + f^{ace} f^{bde} (g^{\mu\nu} g^{\rho\lambda} - g^{\mu\rho} g^{\nu\lambda}) \\ &\quad + f^{ade} f^{bce} (g^{\mu\nu} g^{\rho\lambda} - g^{\mu\lambda} g^{\nu\rho})] \\ &= g_s^2 [(if^{abe})(if^{cde})i(g^{\mu\lambda} g^{\nu\rho} - g^{\mu\rho} g^{\nu\lambda}) + (if^{ace})(if^{bde})i(g^{\mu\nu} g^{\rho\lambda} - g^{\mu\rho} g^{\nu\lambda}) \\ &\quad + (if^{ade})(if^{bce})i(g^{\mu\lambda} g^{\nu\rho} - g^{\mu\nu} g^{\lambda\rho})] \quad (\text{A.10}) \end{aligned}$$

Using $if^{abc} = 2Tr(T^a[T^b, T^c])$ and the Fierz identity again, noting that all $-1/N_c$ -terms cancel, we can express the products of structure constants as

$$(if^{abe})(if^{cde}) = 2[Tr(T^a T^b T^c T^d) - Tr(T^a T^b T^d T^c) - Tr(T^b T^a T^c T^d) + Tr(T^b T^a T^d T^c)] \quad (\text{A.11})$$

which can be used to rewrite the four-gluon vertex, upon sorting for the various traces of generator matrices and identification of $(a, b, c, d) = (a_1, a_2, a_3, a_4)$ and $(\mu, \nu, \lambda, \rho) = (\mu_1, \mu_2, \mu_3, \mu_4)$, into

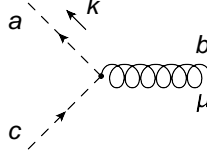
$$\begin{aligned}
\begin{array}{c} d \\ k_4^\rho \\ \swarrow \\ \text{---} \\ \searrow \\ c \\ k_3^\lambda \end{array} & \begin{array}{c} a \\ k_1^\mu \\ \swarrow \\ \text{---} \\ \searrow \\ b \\ k_2^\nu \end{array} &= 2g_s^2 \sum_{P(2,3,4)} Tr(T^{a_1} T^{a_2} T^{a_3} T^{a_4}) \times i(2g^{\mu_1 \mu_3} g^{\mu_2 \mu_4} - g^{\mu_1 \mu_4} g^{\mu_2 \mu_3} - g^{\mu_1 \mu_2} g^{\mu_3 \mu_4}) \\
& \hat{=} \frac{g_s^2}{2} \sum_{P(2,3,4)} \delta_{i_1 \bar{j}_2} \delta_{i_2 \bar{j}_3} \delta_{i_3 \bar{j}_4} \delta_{i_4 \bar{j}_1} \times i(2g^{\mu_1 \mu_3} g^{\mu_2 \mu_4} - g^{\mu_1 \mu_4} g^{\mu_2 \mu_3} - g^{\mu_1 \mu_2} g^{\mu_3 \mu_4}) \\
& = \frac{g_s^2}{2} \sum_{P(2,3,4)} \begin{array}{c} a_4 \bar{j}_4 \\ i_4 \\ \swarrow \\ \text{---} \\ \searrow \\ a_3 i_3 \\ \bar{j}_3 \end{array} \begin{array}{c} \bar{j}_1 a_1 \\ i_1 \\ \swarrow \\ \text{---} \\ \searrow \\ i_2 a_2 \\ \bar{j}_2 \end{array} \times \begin{array}{c} k_4^\rho \\ \swarrow \\ \text{---} \\ \searrow \\ k_2^\nu \\ k_3^\lambda \end{array} \end{array} \quad (\text{A.12})
\end{aligned}$$

where we have defined the color-flow rule and the color-stripped four-gluon vertex is defined as

$$\begin{array}{c} k_4^\rho \\ \swarrow \\ \text{---} \\ \searrow \\ k_2^\nu \\ k_3^\lambda \end{array} \begin{array}{c} k_1^\mu \\ \swarrow \\ \text{---} \\ \searrow \end{array} \equiv V_{gggg}^{(0)\mu\nu\lambda\rho} \equiv iV_4^{\mu\nu\lambda\rho} \equiv i[2g^{\mu\lambda} g^{\nu\rho} - g^{\mu\nu} g^{\lambda\rho} - g^{\mu\rho} g^{\nu\lambda}] \quad (\text{A.13})$$

We do not need to rewrite the color-flow rule in the four-gluon vertex for the purpose of tracking the flow of color in one-loop diagrams, since color-stripped as well as color-flow representative (top-level) diagrams, which are thereby used, are defined to include only the three-valent vertices.

It remains the ghost-gluon vertex, which we need in the calculation of ghost loops and which is given by



$$\begin{aligned}
&= g_s f^{abc} k^\mu = g_s (i f^{abc}) (-i k^\mu) = g_s 2 \text{Tr}(T^a [T^b, T^c]) (-i k^\mu) \\
&= g_s 2 \text{Tr}(T^a T^b T^c) (-i k^\mu) - g_s \text{Tr}(T^a T^c T^b) (-i k^\mu) \\
&= g_s 2 \text{Tr}(T^a T^b T^c) (-i k^\mu) + g_s \text{Tr}(T^a T^c T^b) (+i k^\mu) \\
&\doteq \frac{g_s}{\sqrt{2}} \delta_{i_a \bar{j}_b} \delta_{i_b \bar{j}_c} \delta_{i_c \bar{j}_a} (-i k^\mu) + \frac{g_s}{\sqrt{2}} \delta_{i_a \bar{j}_c} \delta_{i_c \bar{j}_b} \delta_{i_b \bar{j}_a} (+i k^\mu)
\end{aligned} \tag{A.14}$$

which resembles of course the decomposition of the three-gluon vertex with respect to the permutation of two of the three legs. In order to have the same symmetric form in the sum, we had to shift the minus sign in the second term into the kinematic part, which thus defines also here the difference in the color-stripped Feynman rule of the ghost-gluon vertex depending on whether the gluon is radiated to the left or to the right with respect to the fermion flow arrow, quite in analogy to the quark-gluon vertex. The right-radiating type contributes thereby with $V_{ghg}^{(0)\mu}(k) = -i k^\mu$, the left-radiating type with $-V_{ghg}^{(0)\mu}(k) = +i k^\mu$. In the last line we have again converted to the double-line formalism by applying the necessary projector to each generator matrix T^{a_i} and using the Fierz identity. The $-1/N_c$ -terms vanish here for the same reason as already explained for the ghost propagator.

Appendix B

Generating Cyclic Classes

In this appendix we give a prescription how to generate all cyclic classes that are needed in the color decomposition of QCD n -parton one-loop amplitudes with m distinguishable quark-antiquark pairs and $(2m - n)$ gluons. The cyclic classes consist thereby of all possible cyclic orderings of the fermion indices.

Consider the ordered list of particle numbers $\{1_{\bar{q}_1}, 2_{q_1}, 3_{\bar{q}_2}, 4_{q_2}, \dots, (2m-1)_{\bar{q}_m}, (2m)_{q_m}\}$, with distinguishable quark-antiquark pairs (q_k, \bar{q}_k) for $k = 1, \dots, m$, which only contains quark labels. Each quark line k has in addition an associated routing label L for left-routing or R for right-routing. We also assign to each quark line k an additional auxiliary loopness label that indicates whether the quark line k participates in the loop or is attached in a tree-like sub-diagram to another quark line in the loop. The loopness label takes on values in the set $\{0, 1\}$ or $\{tree, loop\}$ and helps us to create a set of rules in order to generate all cyclic classes. Each fermion has thus assigned a specific particle type of a certain flavor, routing and loopness, for example $\bar{1}_k^{Lloop}$ for an antiquark with particle number 1 of a distinct flavor k , routing label L and loopness label $loop$. So, *routing* and *loopness* are properties assigned to specific quark lines.

In order to find all possible cyclic orderings or cyclic classes we first permute all particles in the given list of particle numbers, which consists of the quark labels only. To prevent double-copies due to cyclic invariance we decide to hold the particle number $1_{\bar{q}_1}$ fixed in its position in the ordered list of particle numbers. This generates all non-cyclic $(2m - 1)!$ permutations of the $2m$ fermions. To prevent double copies due to flipping over the diagrams, which would also flip over all routing labels, we also keep the routing of particle $1_{\bar{q}_1}$ fixed as $1_{\bar{q}_1}^L$, so that quark $1_{\bar{q}_1}^L$ is held is fixed in position and routing. All other fermions can be of routing L and R , where quarks and

antiquarks of the same quark line have of course the same routing label. For every permutation of the non-cyclic $(2m - 1)!$ permutations of the $2m$ fermions there are thus 2^{m-1} possibilities to assign combinations of routing labels. In addition, for each of those, there are 2^m possibilities to assign different combinations of loopness labels. This generates $(2m - 1)! \times 2^{2m-1}$ different proto-cyclic classes. Now we have to figure out which of those proto-cyclic classes are actually allowed, and then which of the allowed ones can be dropped because they are double-copies. This will then generate the set of cyclic classes.

Let us state a set of rules that can generate the set of allowed proto-cyclic classes. For each of the $(2m - 1)! \times 2^{2m-1}$ different proto-cyclic classes we have to go through the following considerations:

- a) Sequences with alternating quark line labels are not allowed, since crossing quark lines are not allowed. A sequence $(\dots, i_{\bar{q}_1}, j_{\bar{q}_2}, k_{q_1}, l_{q_2}, \dots)$ would thus be not be allowed. Also a sequence $(\dots, 1, 2, 1, 2, 3, 3, \dots)$, where the numbers give quark-line labels for the moment, is not allowed. However, $(\dots, 1, 2, 2, 1, 3, 3, \dots)$ would be allowed. Which means that encapsulated quark line combinations are in principal allowed, depending however on the preceding and/or following particle type, its quark-line label and its routing label.
- b) We may devise a set of further rules, that helps us in determining which specific particle combinations, considering all the given properties, are allowed and which are not. In principle, looking only at particle type, quark-line label and routing label, it is possible to determine whether a certain cyclic ordering is allowed or not, and which of the quark lines participate in tree-like sub-diagrams in the respective representative diagram. We introduce the auxiliary loopness label to each of the particles, since this allows us to devise such a set of rules in such a fashion that it is applicable to two successive fermions in the cyclic ordering, where we choose clock-wise reading direction, in the sense that by stating that a certain fermion of specific particle type, and with specific quark-line label, routing label and loopness label is allowed to follow another fermion of specific particle type, quark line label, routing label and loopness label. Such a sequential set of rules can then easily be implemented in a computer program. We have collected such a set of rules in table B.1, where green checkmarks denote allowed possibilities for the successive fermion and red crosses denote non-allowed possibilities. If at one point for example we have a quark with quark-line label k at hand, which is left-routing and participating in the loop, then the successive fermion may not be a left-routing quark with a different quark-line label, no matter whether it participates in the loop or not. The first particle in the list, which

Fermion at hand							
q_k^L loop	\bar{q}_k^L loop	q_k^R loop	\bar{q}_k^R loop	q_k^L tree	\bar{q}_k^L tree	q_k^R tree	\bar{q}_k^R tree
↓	↓	↓	↓	↓	↓	↓	↓
Possibly successive fermions (✓ = allowed, ✗ = not allowed)							
\bar{q}_k^L loop ✓	q_k^L loop ✓	\bar{q}_k^R loop ✓	q_k^R loop ✓	\bar{q}_k^L tree ✗	q_k^L tree ✓	\bar{q}_k^R tree ✓	q_k^R tree ✗
$q_{l \neq k}^L$ loop ✗ tree ✗	$q_{l \neq k}^L$ loop ✗ tree ✗	$q_{l \neq k}^L$ loop ✗ tree ✗	$q_{l \neq k}^L$ loop ✗ tree ✗	$q_{l \neq k}^L$ loop ✓ tree ✓	$q_{l \neq k}^L$ loop ✗ tree ✗	$q_{l \neq k}^L$ loop ✗ tree ✗	$q_{l \neq k}^L$ loop ✓ tree ✓
$\bar{q}_{l \neq k}^L$ loop ✓ tree ✓	$\bar{q}_{l \neq k}^L$ loop ✗ tree ✓	$\bar{q}_{l \neq k}^L$ loop ✗ tree ✓	$\bar{q}_{l \neq k}^L$ loop ✓ tree ✓	$\bar{q}_{l \neq k}^L$ loop ✓ tree ✓	$\bar{q}_{l \neq k}^L$ loop ✗ tree ✓	$\bar{q}_{l \neq k}^L$ loop ✗ tree ✓	$\bar{q}_{l \neq k}^L$ loop ✓ tree ✓
$q_{l \neq k}^R$ loop ✓ tree ✓	$q_{l \neq k}^R$ loop ✗ tree ✓	$q_{l \neq k}^R$ loop ✗ tree ✓	$q_{l \neq k}^R$ loop ✓ tree ✓	$q_{l \neq k}^R$ loop ✓ tree ✓	$q_{l \neq k}^R$ loop ✗ tree ✓	$q_{l \neq k}^R$ loop ✗ tree ✓	$q_{l \neq k}^R$ loop ✓ tree ✓
$\bar{q}_{l \neq k}^R$ loop ✗ tree ✗	$\bar{q}_{l \neq k}^R$ loop ✗ tree ✗	$\bar{q}_{l \neq k}^R$ loop ✗ tree ✗	$\bar{q}_{l \neq k}^R$ loop ✗ tree ✗	$\bar{q}_{l \neq k}^R$ loop ✓ tree ✓	$\bar{q}_{l \neq k}^R$ loop ✗ tree ✗	$\bar{q}_{l \neq k}^R$ loop ✗ tree ✗	$\bar{q}_{l \neq k}^R$ loop ✓ tree ✓

Table B.1: Sequential set of rules, which allows the determination of the allowed proto-cyclic classes for one-loop amplitudes with m quark-antiquark pairs. Green checkmarks denote allowed possibilities for the successive fermion and red crosses denote non-allowed possibilities.

is always $1_{q_1}^L$ has of course to be compatible as successor of the last particle in the list. A certain permutation is only accepted if all successions in its list of particles are allowed. We order the assignment of the loopness labels thereby such that for a specific permutation of particle types, with specific quark-line and routing labels, we always start to read the one assignment with the maximal number of particles participating in the loop. If this one is accepted than we have found the (top-level) representative to a cyclic class where all particles participate in the loop and we can stop. If it is not accepted then we probe all the possibilities where one quark-antiquark pair has a loopness label *tree*. If one of those is accepted than we have found the representative to a cyclic class where all particles but one quark-antiquark pair participate in the loop. Etc. This eliminates particle configurations as given in diagram a) of figure B.1, which can be generated, however, from pinching representative diagrams as the one shown in diagram b) of figure B.1.

These rules for example disallow configurations like the one shown in diagram a) and b) of figure B.2. They also give us the correct cyclic class representatives in the case that one fermion line does not enter the loop because it is "blocked" by another, as shown in diagram a) of figure B.3.

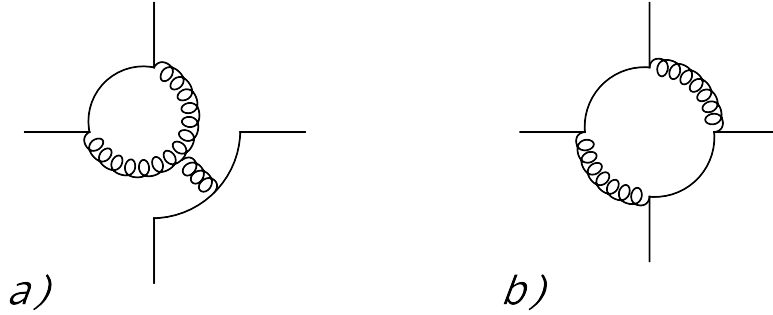


Figure B.1: The diagram on the left can be generated by pinching of the diagram on the right. With our ordering in the assignment of the loopness label the diagram on the right is always generated first and the cyclic class therefore found.

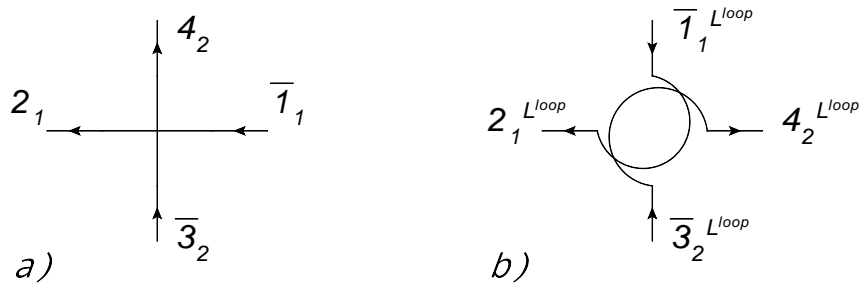


Figure B.2: Depiction of cyclic configurations which are not allowed.

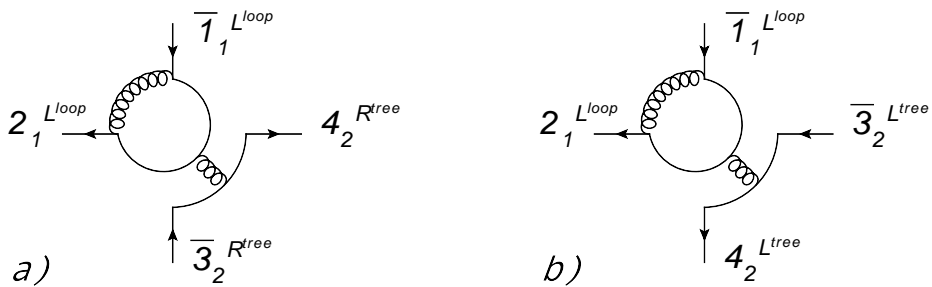


Figure B.3: Color-stripped diagrams that represent cyclic orderings with a tree-part in the representative diagrams, where a) and b) are equal up to a relative sign due to the antisymmetry of the color-stripped quark-gluon vertex.

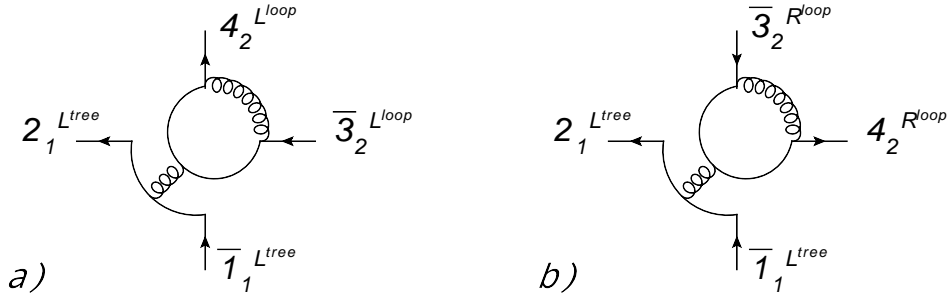


Figure B.4: Color-stripped diagrams that represent cyclic orderings with a tree-part in the representative diagrams, where a) and b) are equal up to a relative sign due to the antisymmetry of the color-stripped quark-gluon vertex.

Now we have to remove those allowed proto-cyclic classes which are double-copies of others. In those representatives with tree-level like sub-diagrams the tree-parts may be flipped with respect to the loop-part. Up to a sign the color-stripped diagrams a) and b) in figure B.3 for example are the same. Exploring diagram b) in figure B.3 we note that the corresponding color-flow representative would have a twisted gluon color double-line if the tree-connecting gluon would be assigned $U(N_c)$ in its color flow, as explained in the caption to figure 2.14. We thus always exclude such diagrams. Another identity of diagrams that arises if we flip the tree-parts with respect to the loop-part is shown in figure B.4, where the color-stripped diagrams a) and b) are again the same up to a sign.

There can also be tree-parts inside tree-parts with respect to the cyclic ordering, as depicted by the color-stripped diagrams in figure B.5. These present double-copies of each other if the gluon that connects from the loop-part to the tree-part and the gluon that connects between the two tree-parts are assigned $U(N_c)$ in one of the corresponding color sub-classes, since the respective diagrams to the specific color assignment can be produced by pinching representatives of the sorts as shown in a1) and b1) in figure B.6, which produce the pinched diagrams shown in a2) and b2) in the same figure respectively. If the gluon that connects between the loop-part and the tree-part is assigned $U(1)$ in another of the corresponding color sub-classes, however, we need to keep this particular cyclic ordering.

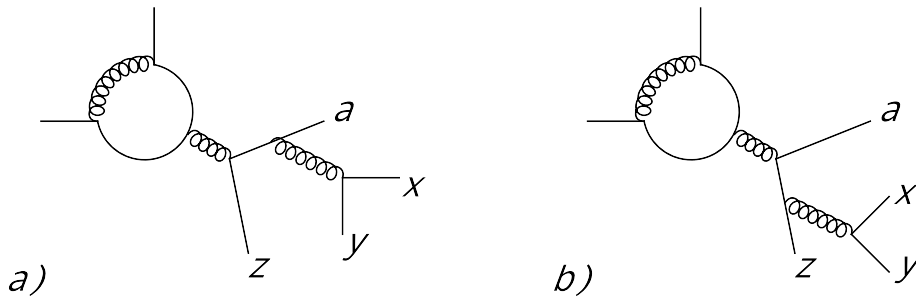


Figure B.5: Cyclic ordering where a quark-antiquark pair is enclosed within another distinguishable quark-antiquark pair with respect to the cyclic direction. The two diagrams can be generated from each other by pinching.

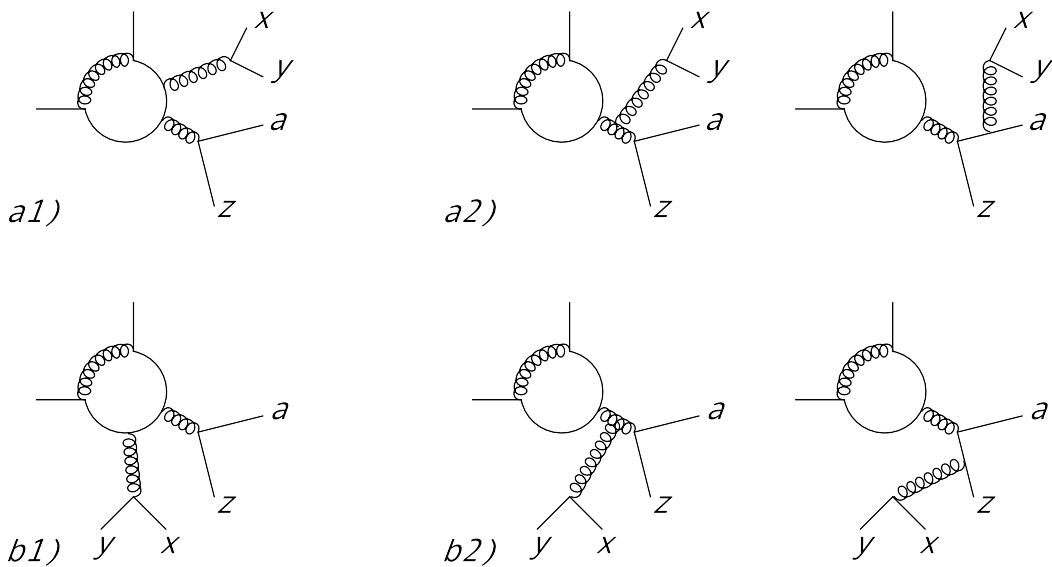


Figure B.6: When the two tree-connecting gluons in figure B.5 are assigned $U(N_c)$ in color then the corresponding diagrams can be generated by pinching from the diagrams in a1) and b1). The resulting diagrams are shown in a2) and b2) respectively.

Appendix C

UV Divergent Ordered One–Loop Diagrams in QCD

In this appendix we collect the integrand expressions for those ordered one–loop diagrams in QCD from which the local UV counterterms to the bare primitive integrands are derived. The integrands are built from the color–stripped Feynman rules as given in appendix A and have to be expanded around the UV propagator $(\bar{k}^2 - \mu_{UV}^2)^{-1}$, as discussed in chapter 3.2.2. The one–loop integrals are written as D –dimensional integrals in dimensional regularization, where the necessary rules and conventions are given in appendix E. Factors of (-1) and i have already been factored out.

The ordered one–loop self–energy correction to the quark propagator, which is linearly UV divergent, is given by

$$-i\Sigma^{(1)} \equiv \begin{array}{c} \text{diagram: quark line with gluon loop} \\ \text{momenta: } \vec{p}_1, \vec{k}, \vec{p}_1, \vec{k}_1 \end{array} = S_\epsilon^{-1} \mu^{2\epsilon} \int \frac{d^D k}{(2\pi)^D} (-1) \frac{\gamma^\mu \not{k} \gamma_\mu}{k^2 k_1^2} \quad (\text{C.1})$$

If we take the quark to be massive the self–energy correction is given by

$$-i\Sigma^{(1)} \equiv \begin{array}{c} \text{diagram: quark line with gluon loop} \\ \text{momenta: } \vec{p}_1, \vec{k}, \vec{p}_1, \vec{k}_1 \end{array} = S_\epsilon^{-1} \mu^{2\epsilon} \int \frac{d^D k}{(2\pi)^D} (-1) \frac{\gamma^\mu (\not{k} + m_q) \gamma_\mu}{(k^2 - m_q^2) k_1^2} \quad (\text{C.2})$$

If we consider to expand the corresponding local UV counterterm only up to $\mathcal{O}(1/|\bar{k}|^4)$ the following expression suffices

$$-i\Sigma^{(1)} \equiv \begin{array}{c} \text{---} \xrightarrow{p_1} \text{---} \\ \text{---} \xrightarrow{k} \text{---} \\ \text{---} \xrightarrow{p_1} \text{---} \end{array} = S_\varepsilon^{-1} \mu^{2\varepsilon} \int \frac{d^D k}{(2\pi)^D} (-1) \frac{\gamma^\mu (\not{k} + m_q) \gamma_\mu}{k^2 k_1^2} \quad (\text{C.3})$$

The n_f -part of the ordered one-loop self-energy correction to the gluon propagator, which is quadratically UV divergent, is given by

$$i\Pi_{nf}^{(1)\mu\nu} \equiv \begin{array}{c} \text{---} \xrightarrow{p_1} \text{---} \\ \text{---} \xrightarrow{k} \text{---} \\ \text{---} \xrightarrow{p_1} \text{---} \end{array} = S_\varepsilon^{-1} \mu^{2\varepsilon} \int \frac{d^D k}{(2\pi)^D} (-1) \frac{\text{Tr}[\gamma^\mu \not{k} \gamma^\nu \not{k}]}{k^2 k_1^2} \quad (\text{C.4})$$

and the leading color part by

$$i\Pi_{lc}^{(1)\mu\nu} \equiv \begin{array}{c} \text{---} \xrightarrow{p_1} \text{---} \\ \text{---} \xrightarrow{k} \text{---} \\ \text{---} \xrightarrow{p_1} \text{---} \end{array} + \begin{array}{c} \text{---} \xrightarrow{p_1} \text{---} \\ \text{---} \xrightarrow{k} \text{---} \\ \text{---} \xrightarrow{p_1} \text{---} \end{array} + \begin{array}{c} \text{---} \xrightarrow{p_1} \text{---} \\ \text{---} \xrightarrow{k} \text{---} \\ \text{---} \xrightarrow{p_1} \text{---} \end{array} \\ + \begin{array}{c} \text{---} \xrightarrow{p_1} \text{---} \\ \text{---} \xrightarrow{k} \text{---} \\ \text{---} \xrightarrow{p_1} \text{---} \end{array} + \begin{array}{c} \text{---} \xrightarrow{p_1} \text{---} \\ \text{---} \xrightarrow{k} \text{---} \\ \text{---} \xrightarrow{p_1} \text{---} \end{array} \quad (\text{C.5})$$

where

$$\begin{array}{c} \text{---} \xrightarrow{p_1} \text{---} \\ \text{---} \xrightarrow{k} \text{---} \\ \text{---} \xrightarrow{p_1} \text{---} \end{array} = S_\varepsilon^{-1} \mu^{2\varepsilon} \int \frac{d^D k}{(2\pi)^D} \frac{V_3^{\mu\gamma}{}_\alpha(-p_1, k, -k_1) V_3^\alpha{}_\gamma{}^\nu(k_1, -k, p_1)}{k^2 k_1^2} \quad (\text{C.6})$$

$$\begin{array}{c} \text{---} \xrightarrow{p_1} \text{---} \\ \text{---} \xrightarrow{k} \text{---} \\ \text{---} \xrightarrow{p_1} \text{---} \end{array} = S_\varepsilon^{-1} \mu^{2\varepsilon} \int \frac{d^D k}{(2\pi)^D} (-1) \frac{k^\mu k_1^\nu}{k^2 k_1^2} \quad (\text{C.7})$$

$$\begin{aligned}
\text{Diagram (C.8)} &= S_\varepsilon^{-1} \mu^{2\varepsilon} \int \frac{d^D k}{(2\pi)^D} (-1) \frac{k_1^\mu k_1^\nu}{k^2 k_1^2} \quad (\text{C.8})
\end{aligned}$$

$$\begin{aligned}
\text{Diagram (C.9)} &= S_\varepsilon^{-1} \mu^{2\varepsilon} \int \frac{d^D k}{(2\pi)^D} \frac{V_4^{\mu\kappa\nu}}{k^2} \quad (\text{C.9})
\end{aligned}$$

$$\begin{aligned}
\text{Diagram (C.10)} &= S_\varepsilon^{-1} \mu^{2\varepsilon} \int \frac{d^D k}{(2\pi)^D} \frac{V_4^{\mu\nu\kappa}}{k_1^2} \quad (\text{C.10})
\end{aligned}$$

The subleading color part of the ordered one-loop correction to the quark–gluon vertex, which is logarithmically UV divergent, is given by

$$\begin{aligned}
\Gamma_{sc}^{(1)\lambda} &\equiv \text{Diagram (C.11)} = S_\varepsilon^{-1} \mu^{2\varepsilon} \int \frac{d^D k}{(2\pi)^D} (-1) \frac{\gamma^\mu \not{k} \gamma^\lambda k_2^\nu \gamma_\mu}{k^2 k_1^2 k_2^2} \quad (\text{C.11})
\end{aligned}$$

and the leading color part by

$$\begin{aligned}
\Gamma_{lc}^{(1)\lambda} &\equiv \text{Diagram (C.12)} = S_\varepsilon^{-1} \mu^{2\varepsilon} \int \frac{d^D k}{(2\pi)^D} \frac{\gamma^\mu k_1^\nu \gamma^\lambda V_{3\nu\mu}^\lambda(-k_2, p_3, k)}{k^2 k_1^2 k_2^2} \quad (\text{C.12})
\end{aligned}$$

The n_f –part of the ordered one-loop correction to the three-gluon vertex, which is linearly UV divergent, is given by

$$V_{ggg,nf}^{(1)\mu\nu\lambda}(p_1, p_2, p_3) \equiv \text{Diagram} = S_\varepsilon^{-1} \mu^{2\varepsilon} \int \frac{d^D k}{(2\pi)^D} \frac{\text{Tr}[\gamma^\mu \not{k} \gamma^\lambda \not{k}_2 \not{k}_1 \gamma^\nu \not{k}_1]}{k^2 k_1^2 k_2^2} \quad (\text{C.13})$$

and the leading color part by

$$V_{ggg,lc}^{(1)\mu\nu\lambda}(p_1, p_2, p_3) \equiv \text{Diagram 1} + \text{Diagram 2} + \text{Diagram 3} + \text{Diagram 4} + \text{Diagram 5} + \text{Diagram 6} \quad (\text{C.14})$$

where

$$\text{Diagram} = S_\varepsilon^{-1} \mu^{2\varepsilon} \int \frac{d^D k}{(2\pi)^D} \frac{V_3^{\mu\alpha\tau}(p_1, k_1, -k) V_{3\alpha}^{\nu\gamma}(-k_1, p_2, k_2) V_{3\gamma}^{\lambda}(-k_2, p_3, k)}{k^2 k_1^2 k_2^2} \quad (\text{C.15})$$

$$\text{Diagram} = S_\varepsilon^{-1} \mu^{2\varepsilon} \int \frac{d^D k}{(2\pi)^D} \frac{k^\mu k_2^\lambda k_1^\nu}{k^2 k_1^2 k_2^2} \quad (\text{C.16})$$

$$= S_\varepsilon^{-1} \mu^{2\varepsilon} \int \frac{d^D k}{(2\pi)^D} \frac{k_1^\mu k^\lambda k_2^\nu}{k^2 k_1^2 k_2^2} \quad (\text{C.17})$$

$$= S_\varepsilon^{-1} \mu^{2\varepsilon} \int \frac{d^D k}{(2\pi)^D} \frac{V_4^{\mu\nu\beta\alpha} V_{3\beta}^\lambda V_{\alpha}^\nu(-k_2, p_3, k)}{k^2 k_2^2} \quad (\text{C.18})$$

$$= S_\varepsilon^{-1} \mu^{2\varepsilon} \int \frac{d^D k}{(2\pi)^D} \frac{V_4^{\mu\alpha\delta\lambda} V_{3\alpha}^\nu V_{\delta}^\nu(-k_1, p_2, k_2)}{k_1^2 k_2^2} \quad (\text{C.19})$$

$$= S_\varepsilon^{-1} \mu^{2\varepsilon} \int \frac{d^D k}{(2\pi)^D} \frac{V_3^{\mu\alpha\delta}(p_1, k_1, -k) V_{4\alpha}^{\nu\lambda\delta}}{k^2 k_1^2} \quad (\text{C.20})$$

Remember that every left-radiator ghost-gluon vertex receives a relative minus sign, as describe in appendix A. In diagrams with an odd number of such vertices this makes of course a difference. A relative minus sign in the second ghost-loop diagram in equation C.17 relative to the first ghost-loop diagram in equation C.16 has therefore to be considered.

The n_f -part of the ordered one-loop correction to the four-gluon vertex, which is logarithmically UV divergent, is given by

$$V_{gggg, nf}^{(1)\mu\nu\lambda\kappa} \equiv \int \frac{d^D k}{(2\pi)^D} (-1) \frac{\text{Tr}[\gamma^\mu k \gamma^\kappa k_\beta \gamma^\lambda k_2 \gamma^\nu k_\lambda]}{k^2 k_1^2 k_2^2 k_3^2} \quad (\text{C.21})$$

and the leading color part by

$$\begin{aligned}
V_{gggg,lc}^{(1)\mu\nu\lambda\kappa} \equiv & \text{[Diagram 1]} + \text{[Diagram 2]} + \text{[Diagram 3]} \\
& + \text{[Diagram 4]} + \text{[Diagram 5]} + \text{[Diagram 6]} + \text{[Diagram 7]} \\
& + \text{[Diagram 8]} + \text{[Diagram 9]}
\end{aligned} \tag{C.22}$$

where

$$\begin{aligned}
& \text{[Diagram 1]} = \\
& S_\epsilon^{-1} \mu^{2\epsilon} \int \frac{d^D k}{(2\pi)^D} \frac{V_3^{\mu\alpha\phi}(p_1, k_1, -k) V_{3\phi}^{\sigma\kappa}(k, -k_3, p_4) V_{3\sigma}^{\delta\lambda}(k_3, -k_2, p_3) V_{3\delta\alpha}{}^\nu(k_2, -k_1, p_2)}{k^2 k_1^2 k_2^2 k_3^2}
\end{aligned} \tag{C.23}$$

$$\begin{aligned}
& \text{[Diagram 2]} = S_\epsilon^{-1} \mu^{2\epsilon} \int \frac{d^D k}{(2\pi)^D} (-1) \frac{k_1^\mu k_2^\nu k_3^\lambda k^\kappa}{k^2 k_1^2 k_2^2 k_3^2}
\end{aligned} \tag{C.24}$$

$$= S_\varepsilon^{-1} \mu^{2\varepsilon} \int \frac{d^D k}{(2\pi)^D} (-1) \frac{k_1^\nu k_2^\lambda k_3^\kappa k^\mu}{k^2 k_1^2 k_2^2 k_3^2} \quad (\text{C.25})$$

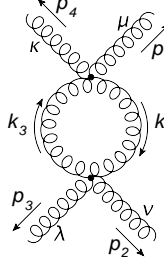
$$= S_\varepsilon^{-1} \mu^{2\varepsilon} \int \frac{d^D k}{(2\pi)^D} \frac{V_3^{\mu\alpha\tau}(p_1, k_1, -k) V_{4\tau}^{\rho\lambda\kappa} V_{3\rho\alpha}^\nu(k_2, -k_1, p_2)}{k^2 k_1^2 k_2^2} \quad (\text{C.26})$$

$$= S_\varepsilon^{-1} \mu^{2\varepsilon} \int \frac{d^D k}{(2\pi)^D} \frac{V_3^{\mu\alpha\tau}(p_1, k_1, -k) V_{4\alpha}^{\nu\lambda\gamma} V_{3\gamma}^\kappa(-k_3, p_4, k)}{k^2 k_1^2 k_3^2} \quad (\text{C.27})$$

$$= S_\varepsilon^{-1} \mu^{2\varepsilon} \int \frac{d^D k}{(2\pi)^D} \frac{V_4^{\mu\nu\beta\alpha} V_{3\beta}^{\lambda\rho}(-k_2, p_3, k_3) V_{3\rho}^\kappa(-k_3, p_4, k)}{k^2 k_2^2 k_3^2} \quad (\text{C.28})$$

$$= S_\varepsilon^{-1} \mu^{2\varepsilon} \int \frac{d^D k}{(2\pi)^D} \frac{V_4^{\mu\alpha\tau\kappa} V_{3\alpha}^{\nu\gamma}(-k_1, p_2, k_2) V_{3\gamma}^\lambda(-k_2, p_3, k_3)}{k_1^2 k_2^2 k_3^2} \quad (\text{C.29})$$

$$= S_\varepsilon^{-1} \mu^{2\varepsilon} \int \frac{d^D k}{(2\pi)^D} \frac{V_4^{\mu\nu\beta\alpha} V_{4\alpha\beta}^{\lambda\kappa}}{k^2 k_2^2} \quad (\text{C.30})$$



$$k_3 \text{ (loop) } k_1 = S_\varepsilon^{-1} \mu^{2\varepsilon} \int \frac{d^D k}{(2\pi)^D} \frac{V_4^{\mu\alpha\rho\kappa} V_{4\alpha}{}^{\nu\lambda}{}_\rho}{k_1^2 k_3^2} \quad (\text{C.31})$$

For those cases where we want the local UV counterterms to subtract only terms up to $\mathcal{O}(1/|\bar{k}|^4)$ we give the series expansions for the corresponding denominators according to the required local degrees of UV divergence, which are reflected in the truncation parameter ℓ respectively

$$\frac{1}{k^2} \Big|_{\mathcal{O}(\bar{k}^{-2})}^{\ell=0} = \frac{1}{(\bar{k}^2 - \mu_{UV}^2)} \quad (\text{C.32})$$

$$\frac{1}{k^2} \Big|_{\mathcal{O}(\bar{k}^{-3})}^{\ell=1} = \frac{1}{(\bar{k}^2 - \mu_{UV}^2)} \left(1 + \frac{-2\bar{k}\cdot Q}{(\bar{k}^2 - \mu_{UV}^2)} \right) \quad (\text{C.33})$$

$$\frac{1}{k^2} \Big|_{\mathcal{O}(\bar{k}^{-4})}^{\ell=2} = \frac{1}{(\bar{k}^2 - \mu_{UV}^2)} \left(1 + \frac{-2\bar{k}\cdot Q}{(\bar{k}^2 - \mu_{UV}^2)} + \left(\frac{-\mu_{UV}^2 - Q\cdot Q}{(\bar{k}^2 - \mu_{UV}^2)} + \frac{4(\bar{k}\cdot Q)^2}{(\bar{k}^2 - \mu_{UV}^2)^2} \right) \right) \quad (\text{C.34})$$

$$\frac{1}{k_1^2} \Big|_{\mathcal{O}(\bar{k}^{-2})}^{\ell=0} = \frac{1}{(\bar{k}^2 - \mu_{UV}^2)} \quad (\text{C.35})$$

$$\frac{1}{k_1^2} \Big|_{\mathcal{O}(\bar{k}^{-3})}^{\ell=1} = \frac{1}{(\bar{k}^2 - \mu_{UV}^2)} \left(1 + \frac{-2\bar{k}\cdot Q_1}{(\bar{k}^2 - \mu_{UV}^2)} \right) \quad (\text{C.36})$$

$$\frac{1}{k_1^2} \Big|_{\mathcal{O}(\bar{k}^{-4})}^{\ell=2} = \frac{1}{(\bar{k}^2 - \mu_{UV}^2)} \left(1 + \frac{-2\bar{k}\cdot Q_1}{(\bar{k}^2 - \mu_{UV}^2)} + \left(\frac{-\mu_{UV}^2 - Q_1\cdot Q_1}{(\bar{k}^2 - \mu_{UV}^2)} + \frac{4(\bar{k}\cdot Q_1)^2}{(\bar{k}^2 - \mu_{UV}^2)^2} \right) \right) \quad (\text{C.37})$$

$$\frac{1}{k^2 k_1^2} \Big|_{\mathcal{O}(\bar{k}^{-4})}^{\ell=0} = \frac{1}{(\bar{k}^2 - \mu_{UV}^2)^2} \quad (\text{C.38})$$

$$\frac{1}{k^2 k_1^2} \Big|_{\mathcal{O}(\bar{k}^{-5})}^{\ell=1} = \frac{1}{(\bar{k}^2 - \mu_{UV}^2)^2} \left(1 + \frac{-2\bar{k}\cdot Q - 2\bar{k}\cdot Q_1}{(\bar{k}^2 - \mu_{UV}^2)} \right) \quad (\text{C.39})$$

$$\begin{aligned} \frac{1}{k^2 k_1^2} \Big|_{\mathcal{O}(\bar{k}^{-6})}^{\ell=2} &= \frac{1}{(\bar{k}^2 - \mu_{UV}^2)^2} \left(1 + \frac{-2\bar{k}\cdot Q - 2\bar{k}\cdot Q_1}{(\bar{k}^2 - \mu_{UV}^2)} \right. \\ &\quad \left. + \left(\frac{-2\mu_{UV}^2 - Q\cdot Q - Q_1\cdot Q_1}{(\bar{k}^2 - \mu_{UV}^2)} + \frac{4(\bar{k}\cdot Q)^2 + 4(\bar{k}\cdot Q_1)^2 + 4(\bar{k}\cdot Q)(\bar{k}\cdot Q_1)}{(\bar{k}^2 - \mu_{UV}^2)^2} \right) \right) \end{aligned} \quad (\text{C.40})$$

$$\frac{1}{k^2 k_2^2} \Big|_{\mathcal{O}(\bar{k}^{-4})}^{\ell=0} = \frac{1}{(\bar{k}^2 - \mu_{UV}^2)^2} \quad (\text{C.41})$$

$$\frac{1}{k^2 k_2^2} \Big|_{\mathcal{O}(\bar{k}^{-5})}^{\ell=1} = \frac{1}{(\bar{k}^2 - \mu_{UV}^2)^2} \left(1 + \frac{-2\bar{k} \cdot Q - 2\bar{k} \cdot Q_2}{(\bar{k}^2 - \mu_{UV}^2)} \right) \quad (\text{C.42})$$

$$\frac{1}{k_1^2 k_2^2} \Big|_{\mathcal{O}(\bar{k}^{-4})}^{\ell=0} = \frac{1}{(\bar{k}^2 - \mu_{UV}^2)^2} \quad (\text{C.43})$$

$$\frac{1}{k_1^2 k_2^2} \Big|_{\mathcal{O}(\bar{k}^{-5})}^{\ell=1} = \frac{1}{(\bar{k}^2 - \mu_{UV}^2)^2} \left(1 + \frac{-2\bar{k} \cdot Q_1 - 2\bar{k} \cdot Q_2}{(\bar{k}^2 - \mu_{UV}^2)} \right) \quad (\text{C.44})$$

$$\frac{1}{k^2 k_1^2 k_2^2} \Big|_{\mathcal{O}(\bar{k}^{-6})}^{\ell=0} = \frac{1}{(\bar{k}^2 - \mu_{UV}^2)^3} \quad (\text{C.45})$$

$$\frac{1}{k^2 k_1^2 k_2^2} \Big|_{\mathcal{O}(\bar{k}^{-7})}^{\ell=1} = \frac{1}{(\bar{k}^2 - \mu_{UV}^2)^3} \left(1 + \frac{-2\bar{k} \cdot Q - 2\bar{k} \cdot Q_1 - 2\bar{k} \cdot Q_2}{(\bar{k}^2 - \mu_{UV}^2)} \right) \quad (\text{C.46})$$

$$\frac{1}{k^2 k_1^2 k_3^2} \Big|_{\mathcal{O}(\bar{k}^{-6})}^{\ell=0} = \frac{1}{(\bar{k}^2 - \mu_{UV}^2)^3} \quad (\text{C.47})$$

$$\frac{1}{k^2 k_1^2 k_3^2} \Big|_{\mathcal{O}(\bar{k}^{-7})}^{\ell=1} = \frac{1}{(\bar{k}^2 - \mu_{UV}^2)^3} \left(1 + \frac{-2\bar{k} \cdot Q - 2\bar{k} \cdot Q_1 - 2\bar{k} \cdot Q_3}{(\bar{k}^2 - \mu_{UV}^2)} \right) \quad (\text{C.48})$$

$$\frac{1}{k^2 k_2^2 k_3^2} \Big|_{\mathcal{O}(\bar{k}^{-6})}^{\ell=0} = \frac{1}{(\bar{k}^2 - \mu_{UV}^2)^3} \quad (\text{C.49})$$

$$\frac{1}{k^2 k_2^2 k_3^2} \Big|_{\mathcal{O}(\bar{k}^{-7})}^{\ell=1} = \frac{1}{(\bar{k}^2 - \mu_{UV}^2)^3} \left(1 + \frac{-2\bar{k} \cdot Q - 2\bar{k} \cdot Q_2 - 2\bar{k} \cdot Q_3}{(\bar{k}^2 - \mu_{UV}^2)} \right) \quad (\text{C.50})$$

$$\frac{1}{k_1^2 k_2^2 k_3^2} \Big|_{\mathcal{O}(\bar{k}^{-6})}^{\ell=0} = \frac{1}{(\bar{k}^2 - \mu_{UV}^2)^3} \quad (\text{C.51})$$

$$\frac{1}{k_1^2 k_2^2 k_3^2} \Big|_{\mathcal{O}(\bar{k}^{-7})}^{\ell=1} = \frac{1}{(\bar{k}^2 - \mu_{UV}^2)^3} \left(1 + \frac{-2\bar{k} \cdot Q_1 - 2\bar{k} \cdot Q_2 - 2\bar{k} \cdot Q_3}{(\bar{k}^2 - \mu_{UV}^2)} \right) \quad (\text{C.52})$$

$$\frac{1}{k^2 k_1^2 k_2^2 k_3^2} \Big|_{\mathcal{O}(\bar{k}^{-8})}^{\ell=0} = \frac{1}{(\bar{k}^2 - \mu_{UV}^2)^4} \quad (\text{C.53})$$

$$\frac{1}{k^2 k_1^2 k_2^2 k_3^2} \Big|_{\mathcal{O}(\bar{k}^{-9})}^{\ell=1} = \frac{1}{(\bar{k}^2 - \mu_{UV}^2)^4} \left(1 + \frac{-2\bar{k} \cdot Q - 2\bar{k} \cdot Q_1 - 2\bar{k} \cdot Q_2 - 2\bar{k} \cdot Q_3}{(\bar{k}^2 - \mu_{UV}^2)} \right) \quad (\text{C.54})$$

where $\bar{k} \equiv k - Q$, $k_i \equiv k - \sum_{j=1}^i p_j$ and $Q_i \equiv Q - \sum_{j=1}^i p_j$. Expansion is around small $\frac{1}{(k^2 - \mu_{UV}^2)}$, where the general prescription has been given in chapter 3.2.2. After applying the expansions to equations C.1 through C.31 and power counting in \bar{k} only the non-finite terms, i.e. terms of up to order $\mathcal{O}(1/|\bar{k}|^4)$, are being kept.

For diagrams that are logarithmic UV divergent the expansions of the form $\frac{1}{k^2 k_1^2 \dots k_n^2} \Big|_{\mathcal{O}(\bar{k}^{-2n})}^{\ell=0}$ suffice in order to cancel the UV divergences. For diagrams that are linear UV divergent the expansions of the form $\frac{1}{k^2 k_1^2 \dots k_n^2} \Big|_{\mathcal{O}(\bar{k}^{-2n-1})}^{\ell=1}$ suffice in order to cancel the UV divergences. For diagrams that are quadratic UV divergent the expansions of the form $\frac{1}{k^2 k_1^2 \dots k_n^2} \Big|_{\mathcal{O}(\bar{k}^{-2n-2})}^{\ell=2}$ suffice in order to cancel the UV divergences.

Appendix D

Local UV Counterterms to Ordered One-Loop QCD Corrections

In this appendix we collect the expressions for the unintegrated local UV counterterms as well as the corresponding analytically integrated results. The analytic one-loop integration is performed in dimensional regularization. The given results for the local UV counterterms are for the case when we only want to subtract terms up to a local $\mathcal{O}(1/|\bar{k}|^4)$ -behavior. These results have been obtained by the methods described in chapter 3.2.2. The expressions in appendix C have been expanded, algebraically reduced and subsequently integrated by an implementation of the algebraic and integral identities in appendix E in the algebraic manipulation program FORM [149].

The result for the local counterterm to the quark propagator correction with quark-mass m_t reads

$$\begin{aligned}
 g_{2,1}^{qq,\ell_{qq}=1,UV}(\bar{k}, Q, p_1, m_t, \mu_{UV}) &\equiv g_{qq}^{UV,\ell_{qq}=1}(\bar{k}, Q, p_1, m_t, \mu_{UV}) = \\
 &+ \frac{1}{(\bar{k}^2 - \mu_{UV}^2)^3} \left[-4(1 - \varepsilon)(\bar{k} \cdot Q + \bar{k} \cdot Q_1)\bar{k} + 2\mu_{UV}^2(-p_1 + 2m_t) \right] \\
 &+ \frac{1}{(\bar{k}^2 - \mu_{UV}^2)^2} \left[+2(1 - \varepsilon)(\bar{k} + Q) - 2(2 - \varepsilon)m_t \right]
 \end{aligned} \tag{D.1}$$

wherein we note the subtraction to avoid the additional finite remainder as described in chapter 3.2.2, which reads in this case

$$R_{qq}^{UV, \ell_{qq}=1}(p_1, m_t) = -p_\lambda + 2m_t \quad (\text{D.2})$$

Upon integration this yields

$$-i\Sigma^{(1)UV}(p_1, m_t, \mu_{UV}/\mu) = S_\varepsilon^{-1} \mu^{2\varepsilon} \int \frac{d^D \bar{k}}{(2\pi)^D} g_{qq}^{UV, \ell_{qq}=1}(\bar{k}, Q, p_1, m_t, \mu_{UV}) \quad (\text{D.3})$$

$$= \frac{i}{(4\pi)^2} \left[(p_\lambda - 4m_t) \left(\frac{1}{\varepsilon} - \log \frac{\mu_{UV}^2}{\mu^2} \right) \right] + \mathcal{O}(\varepsilon) \quad (\text{D.4})$$

The result for the local counterterm to the n_f -part of the gluon propagator correction reads

$$\begin{aligned} g_{2,2}^{gg, \ell_{gg}=2, UV, nf}(\bar{k}, Q, p_1, \mu_{UV}) &\equiv g_{gg, nf}^{UV, \ell_{gg}=2, \mu\nu}(\bar{k}, Q, p_1, \mu_{UV}) = \\ &+ \frac{1}{(\bar{k}^2 - \mu_{UV}^2)^4} \left[-32\bar{k}^\mu \bar{k}^\nu ((\bar{k} \cdot Q)^2 + (\bar{k} \cdot Q_1)^2 + (\bar{k} \cdot Q)(\bar{k} \cdot Q_1)) \right] \\ &+ \frac{1}{(\bar{k}^2 - \mu_{UV}^2)^3} \left[+8g^{\mu\nu} ((\bar{k} \cdot Q)^2 + (\bar{k} \cdot Q_1)^2) + 8\bar{k}^\mu \bar{k}^\nu (Q^2 + Q_1^2 + 2\mu_{UV}^2) \right] \\ &+ \frac{1}{(\bar{k}^2 - \mu_{UV}^2)^3} \left[+8(\bar{k} \cdot Q + \bar{k} \cdot Q_1)(\bar{k}^\mu (\bar{k}^\nu + Q^\nu + Q_1^\nu) + \bar{k}^\nu (\bar{k}^\mu + Q^\mu + Q_1^\mu)) \right] \\ &+ \frac{1}{(\bar{k}^2 - \mu_{UV}^2)^2} \left[-4(\bar{k}^\mu (\bar{k}^\nu + Q^\nu + Q_1^\nu) + Q^\mu Q_1^\nu) \right] + [\mu \leftrightarrow \nu] \\ &+ \frac{1}{(\bar{k}^2 - \mu_{UV}^2)^2} \left[+4g^{\mu\nu} (Q \cdot Q_1 - Q^2 - Q_1^2 - \bar{k} \cdot Q - \bar{k} \cdot Q_1 - \mu_{UV}^2) \right] \\ &+ \frac{1}{(\bar{k}^2 - \mu_{UV}^2)} \left[+4g^{\mu\nu} \right] \end{aligned} \quad (\text{D.5})$$

wherein

$$R_{gg, nf}^{UV, \ell_{gg}=2, \mu\nu} = 0 \quad (\text{D.6})$$

In the above expression there exists a local term, though, which is also proportional to $\frac{2\mu_{UV}^2}{(k^2 - \mu_{UV}^2)^3}$. This term is not of the type that leads to an additional finite remainder, since it also comes with a local factor of $8\bar{k}^\mu \bar{k}^\nu$ in the numerator and hence does not lead to a finite integrated term.

Upon integration this yields

$$\begin{aligned}
i\Pi_{nf}^{(1)UV,\mu\nu}(p_1, \mu_{UV}/\mu) &= S_\varepsilon^{-1} \mu^{2\varepsilon} \int \frac{d^D \bar{k}}{(2\pi)^D} g_{gg,nf}^{UV,\ell_{gg}=2,\mu\nu}(\bar{k}, Q, p_1, \mu_{UV}) \\
&= \frac{i}{(4\pi)^2} \left[\left(-\frac{4}{3}\right) (g^{\mu\nu} p_1^2 - p_1^\mu p_1^\nu) \left(\frac{1}{\varepsilon} - \log \frac{\mu_{UV}^2}{\mu^2}\right) \right] + \mathcal{O}(\varepsilon)
\end{aligned} \tag{D.7}$$

The result for the local counterterm to the leading color part of the gluon propagator correction reads

$$\begin{aligned}
g_{2,2}^{gg,\ell_{gg}=2,UV,lc}(\bar{k}, Q, p_1, \mu_{UV}) &\equiv g_{gg,lc}^{UV,\ell_{gg}=2,\mu\nu}(\bar{k}, Q, p_1, \mu_{UV}) = \\
&+ \frac{1}{(\bar{k}^2 - \mu_{UV}^2)^4} \left[+ 32(1 - \varepsilon) \bar{k}^\mu \bar{k}^\nu ((\bar{k} \cdot Q)^2 + (\bar{k} \cdot Q_1)^2 + (\bar{k} \cdot Q)(\bar{k} \cdot Q_1)) \right] \\
&+ \frac{1}{(\bar{k}^2 - \mu_{UV}^2)^3} \left[- 8(1 - \varepsilon) \bar{k}^\mu \bar{k}^\nu (2\mu_{UV}^2 + 2\bar{k} \cdot Q + 2\bar{k} \cdot Q_1 + Q^2 + Q_1^2) \right] \\
&+ \frac{1}{(\bar{k}^2 - \mu_{UV}^2)^3} \left[+ 2\mu_{UV}^2 \left(\frac{2}{3}(g^{\mu\nu} p_1^2 - p_1^\mu p_1^\nu)\right) \right] \\
&+ \frac{1}{(\bar{k}^2 - \mu_{UV}^2)^3} \left[- 8(1 - \varepsilon) \bar{k}^\mu (Q^\nu + Q_1^\nu) (\bar{k} \cdot Q + \bar{k} \cdot Q_1) \right] + [\mu \leftrightarrow \nu] \\
&+ \frac{1}{(\bar{k}^2 - \mu_{UV}^2)^3} \left[- 8(1 - \varepsilon) g^{\mu\nu} ((\bar{k} \cdot Q)^2 + (\bar{k} \cdot Q_1)^2) \right] \\
&+ \frac{1}{(\bar{k}^2 - \mu_{UV}^2)^2} \left[+ 4(1 - \varepsilon) (\bar{k}^\mu \bar{k}^\nu + \bar{k}^\mu Q^\nu + \bar{k}^\mu Q_1^\nu) \right] + [\mu \leftrightarrow \nu] \\
&+ \frac{1}{(\bar{k}^2 - \mu_{UV}^2)^2} \left[- 2(1 + \varepsilon) (Q^\mu Q^\nu + Q_1^\mu Q_1^\nu) + (6 - 2\varepsilon) (Q^\mu Q_1^\nu + Q^\nu Q_1^\mu) \right] \\
&+ \frac{1}{(\bar{k}^2 - \mu_{UV}^2)^2} \left[+ 4(1 - \varepsilon) g^{\mu\nu} (\mu_{UV}^2 + \bar{k} \cdot Q + \bar{k} \cdot Q_1) + (6 - 2\varepsilon) g^{\mu\nu} (Q^2 + Q_1^2) - 8g^{\mu\nu} Q \cdot Q_1 \right] \\
&+ \frac{1}{(\bar{k}^2 - \mu_{UV}^2)} \left[- 4(1 - \varepsilon) g^{\mu\nu} \right]
\end{aligned} \tag{D.8}$$

wherein

$$R_{gg,lc}^{UV,\ell_{gg}=2,\mu\nu}(p_1) = \frac{2}{3} (g^{\mu\nu} p_1^2 - p_1^\mu p_1^\nu) \tag{D.9}$$

Upon integration this yields

$$\begin{aligned}
i\Pi_{lc}^{(1)UV,\mu\nu}(p_1, \mu_{UV}/\mu) &= S_\varepsilon^{-1} \mu^{2\varepsilon} \int \frac{d^D \bar{k}}{(2\pi)^D} g_{gg,lc}^{UV,\ell_{gg}=2,\mu\nu}(\bar{k}, Q, p_1, \mu_{UV}) \\
&= \frac{i}{(4\pi)^2} \left[\left(\frac{10}{3}\right) (g^{\mu\nu} p_1^2 - p_1^\mu p_1^\nu) \left(\frac{1}{\varepsilon} - \log \frac{\mu_{UV}^2}{\mu^2}\right) \right] + \mathcal{O}(\varepsilon)
\end{aligned} \tag{D.10}$$

The result for the local counterterm to the subleading color part of the quark–gluon vertex correction reads

$$g_{3,2}^{qqg,\ell_{qqg}=0,UV,sc}(\bar{k}, \mu_{UV}) \equiv g_{qqg,sc}^{UV,\ell_{qqg}=0,\lambda}(\bar{k}, \mu_{UV}) = \left[\frac{4(1-\varepsilon)\bar{k}\bar{k}^\lambda + 2\mu_{UV}^2\gamma^\lambda}{(\bar{k}^2 - \mu_{UV}^2)^3} + \frac{-2(1-\varepsilon)\gamma^\lambda}{(\bar{k}^2 - \mu_{UV}^2)^2} \right] \tag{D.11}$$

wherein

$$R_{qqg,sc}^{UV,\ell_{qqg}=0,\lambda} = \gamma^\lambda \tag{D.12}$$

Upon integration this yields

$$\Gamma_{sc}^{(1)UV,\lambda}(\mu_{UV}/\mu) = S_\varepsilon^{-1} \mu^{2\varepsilon} \int \frac{d^D \bar{k}}{(2\pi)^D} g_{qqg,sc}^{UV,\ell_{qqg}=0,\lambda}(\bar{k}) = \frac{i}{(4\pi)^2} \left[(-1)(\gamma^\lambda) \left(\frac{1}{\varepsilon} - \log \frac{\mu_{UV}^2}{\mu^2}\right) \right] + \mathcal{O}(\varepsilon) \tag{D.13}$$

The result for the local counterterm to the leading color part of the quark–gluon vertex correction reads

$$g_{3,2}^{qqg,\ell_{qqg}=0,UV,lc}(\bar{k}, \mu_{UV}) \equiv g_{qqg,lc}^{UV,\ell_{qqg}=0,\lambda}(\bar{k}, \mu_{UV}) = \left[\frac{4(1-\varepsilon)\bar{k}\bar{k}^\lambda - 2\mu_{UV}^2\gamma^\lambda}{(\bar{k}^2 - \mu_{UV}^2)^3} + \frac{2\gamma^\lambda}{(\bar{k}^2 - \mu_{UV}^2)^2} \right] \tag{D.14}$$

wherein

$$R_{qqg,lc}^{UV,\ell_{qqg}=0,\lambda} = -\gamma^\lambda \tag{D.15}$$

Upon integration this yields

$$\Gamma_{lc}^{(1)UV,\lambda}(\mu_{UV}/\mu) = S_\varepsilon^{-1} \mu^{2\varepsilon} \int \frac{d^D \bar{k}}{(2\pi)^D} g_{qqg,lc}^{UV,\ell_{qqg}=0,\lambda}(\bar{k}, \mu_{UV}) = \frac{i}{(4\pi)^2} \left[(3) (\gamma^\lambda) \left(\frac{1}{\varepsilon} - \log \frac{\mu_{UV}^2}{\mu^2} \right) \right] + \mathcal{O}(\varepsilon) \quad (\text{D.16})$$

The result for the local counterterm to the n_f -part of the three-gluon vertex correction reads

$$\begin{aligned} g_{3,3}^{ggg,\ell_{ggg}=1,UV,nf}(\bar{k}, Q, p_1, p_2, \mu_{UV}) &\equiv g_{ggg,nf}^{UV,\ell_{ggg}=1,\mu\nu\lambda}(\bar{k}, Q, p_1, p_2, \mu_{UV}) = \\ &+ \frac{1}{(\bar{k}^2 - \mu_{UV}^2)^4} \left[-32 \bar{k}^\mu \bar{k}^\nu \bar{k}^\lambda (\bar{k} \cdot Q + \bar{k} \cdot Q_1 + \bar{k} \cdot Q_2) \right] \\ &+ \frac{1}{(\bar{k}^2 - \mu_{UV}^2)^3} \left[+16 \bar{k}^\mu \bar{k}^\nu \bar{k}^\lambda + 8U^{\mu\nu\lambda}(\bar{k}, Q, Q_1, Q_2) + 8T^{\mu\nu\lambda}(\bar{k}, Q, Q_1, Q_2) \right] \\ &+ \frac{1}{(\bar{k}^2 - \mu_{UV}^2)^2} \left[[-4g^{\mu\nu}(\bar{k}^\lambda + Q^\lambda + Q_1^\lambda + Q_2^\lambda)] + [\mu \leftrightarrow \nu \leftrightarrow \lambda] \right] \\ &+ \frac{1}{(\bar{k}^2 - \mu_{UV}^2)^2} \left[+8(g^{\mu\nu} Q_1^\lambda + g^{\mu\lambda} Q_1^\nu + g^{\nu\lambda} Q_1^\mu) \right] \end{aligned} \quad (\text{D.17})$$

wherein

$$R_{ggg,nf}^{UV,\ell_{ggg}=1,\mu\nu\lambda} = 0 \quad (\text{D.18})$$

and where

$$U^{\mu\nu\lambda}(\bar{k}, Q, Q_1, Q_2) \equiv g^{\mu\nu} \bar{k}^\lambda \bar{k} \cdot (Q + Q_2) + g^{\mu\lambda} \bar{k}^\nu \bar{k} \cdot (Q_1 + Q_2) + g^{\nu\lambda} \bar{k}^\mu \bar{k} \cdot (Q + Q_1) \quad (\text{D.19})$$

$$T^{\mu\nu\lambda}(\bar{k}, Q, Q_1, Q_2) \equiv \bar{k}^\mu \bar{k}^\nu (Q^\lambda + Q_2^\lambda) + \bar{k}^\mu \bar{k}^\lambda (Q_1^\nu + Q_2^\nu) + \bar{k}^\nu \bar{k}^\lambda (Q^\mu + Q_1^\mu) \quad (\text{D.20})$$

Upon integration this yields

$$\begin{aligned} V_{ggg,nf}^{(1)UV,\mu\nu\lambda}(p_1, p_2, p_3, \mu_{UV}/\mu) &= S_\varepsilon^{-1} \mu^{2\varepsilon} \int \frac{d^D \bar{k}}{(2\pi)^D} g_{ggg,nf}^{UV,\ell_{ggg}=1,\mu\nu\lambda}(\bar{k}, Q, p_1, p_2, \mu_{UV}) \\ &= \frac{i}{(4\pi)^2} \left[\left(\frac{4}{3} \right) (V_3^{\mu\nu\lambda}(p_1, p_2, p_3)) \left(\frac{1}{\varepsilon} - \log \frac{\mu_{UV}^2}{\mu^2} \right) \right] + \mathcal{O}(\varepsilon) \end{aligned} \quad (\text{D.21})$$

The result for the local counterterm to the leading color part of the three-gluon vertex correction

reads

$$\begin{aligned}
g_{3,3}^{ggg,\ell_{ggg}=1,UV,lc}(\bar{k}, Q, p_1, p_2, \mu_{UV}) &\equiv g_{ggg,lc}^{UV,\ell_{ggg}=1,\mu\nu\lambda}(\bar{k}, Q, p_1, p_2, \mu_{UV}) = \\
&+ \frac{1}{(\bar{k}^2 - \mu_{UV}^2)^4} \left[+ 32(1 - \varepsilon) \bar{k}^\mu \bar{k}^\nu \bar{k}^\lambda (\bar{k} \cdot Q + \bar{k} \cdot Q_1 + \bar{k} \cdot Q_2) \right] \\
&+ \frac{1}{(\bar{k}^2 - \mu_{UV}^2)^3} \left[- 16(1 - \varepsilon) \bar{k}^\mu \bar{k}^\nu \bar{k}^\lambda - 8(1 - \varepsilon) T^{\mu\nu\lambda}(\bar{k}, Q, Q_1, Q_2) \right] \\
&+ \frac{1}{(\bar{k}^2 - \mu_{UV}^2)^3} \left[+ 2\mu_{UV}^2 \left(- \frac{2}{3} V_3^{\mu\nu\lambda}(p_1, p_2, p_3) \right) \right] \\
&+ \frac{1}{(\bar{k}^2 - \mu_{UV}^2)^3} \left[- 8(1 - \varepsilon) U^{\mu\nu\lambda}(\bar{k}, Q, Q_1, Q_2) \right] \\
&+ \frac{1}{(\bar{k}^2 - \mu_{UV}^2)^2} \left[4(1 - \varepsilon) g^{\mu\nu} (\bar{k}^\lambda + Q^\lambda + Q_1^\lambda + Q_2^\lambda) + [\mu \leftrightarrow \nu \leftrightarrow \lambda] \right] \\
&+ \frac{1}{(\bar{k}^2 - \mu_{UV}^2)^2} \left[- 4(2 - \varepsilon) (g^{\mu\nu} Q_1^\lambda + g^{\mu\lambda} Q_1^\nu + g^{\nu\lambda} Q_2^\mu) \right] \\
&+ \frac{1}{(\bar{k}^2 - \mu_{UV}^2)^2} \left[+ 2\varepsilon H^{\mu\nu\lambda}(Q, Q_1, Q_2) \right] \tag{D.22}
\end{aligned}$$

wherein

$$R_{ggg,lc}^{UV,\ell_{ggg}=1,\mu\nu\lambda}(p_1, p_2, p_3) = -\frac{2}{3} V_3^{\mu\nu\lambda}(p_1, p_2, p_3) \tag{D.23}$$

and where

$$H^{\mu\nu\lambda}(Q, Q_1, Q_2) \equiv g^{\mu\nu} (Q^\lambda + Q_2^\lambda) + g^{\mu\lambda} (Q_1^\nu + Q_2^\nu) + g^{\nu\lambda} (Q^\mu + Q_1^\mu) \tag{D.24}$$

Upon integration this yields

$$\begin{aligned}
V_{ggg,lc}^{(1)UV\mu\nu\lambda}(p_1, p_2, p_3, \mu_{UV}/\mu) &= S_\varepsilon^{-1} \mu^{2\varepsilon} \int \frac{d^D \bar{k}}{(2\pi)^D} V_{ggg,lc}^{UV,\ell_{ggg}=1,\mu\nu\lambda}(\bar{k}, Q, p_1, p_2, \mu_{UV}) \\
&= \frac{i}{(4\pi)^2} \left[\left(-\frac{4}{3} \right) (V_3^{\mu\nu\lambda}(p_1, p_2, p_3)) \left(\frac{1}{\varepsilon} - \log \frac{\mu_{UV}^2}{\mu^2} \right) \right] + \mathcal{O}(\varepsilon) \tag{D.25}
\end{aligned}$$

The result for the local counterterm to the n_f -part of the four-gluon vertex correction reads

$$g_{4,4}^{gggg,\ell_{gggg}=0,UV,nf}(\bar{k}, \mu_{UV}) \equiv g_{gggg,nf}^{UV,\ell_{gggg}=0,\mu\nu\lambda\kappa}(\bar{k}, \mu_{UV}) = \left[\frac{-32\bar{k}^\mu\bar{k}^\nu\bar{k}^\lambda\bar{k}^\kappa}{(\bar{k}^2 - \mu_{UV}^2)^4} + \frac{8W(\bar{k})^{\mu\nu\lambda\kappa}}{(\bar{k}^2 - \mu_{UV}^2)^3} + \frac{4(V_4^{\mu\nu\lambda\kappa} - g^{\mu\lambda}g^{\nu\kappa})}{(\bar{k}^2 - \mu_{UV}^2)^2} \right] \quad (\text{D.26})$$

wherein

$$R_{gggg,nf}^{UV,\ell_{gggg}=0,\mu\nu\lambda\kappa} = 0 \quad (\text{D.27})$$

and where

$$W(\bar{k})^{\mu\nu\lambda\kappa} \equiv g^{\mu\nu}\bar{k}^\lambda\bar{k}^\kappa + g^{\mu\kappa}\bar{k}^\nu\bar{k}^\lambda + g^{\nu\lambda}\bar{k}^\mu\bar{k}^\kappa + g^{\lambda\kappa}\bar{k}^\mu\bar{k}^\nu \quad (\text{D.28})$$

Upon integration this yields

$$V_{gggg,nf}^{(1)UV,\mu\nu\lambda\kappa}(\mu_{UV}/\mu) = S_\varepsilon^{-1}\mu^{2\varepsilon} \int \frac{d^D\bar{k}}{(2\pi)^D} g_{gggg,nf}^{UV,\ell_{gggg}=0,\mu\nu\lambda\kappa}(\bar{k}, \mu_{UV}) = \frac{i}{(4\pi)^2} \left[\left(\frac{4}{3}\right) (V_4^{\mu\nu\lambda\kappa}) \left(\frac{1}{\varepsilon} - \log \frac{\mu_{UV}^2}{\mu^2}\right) \right] + \mathcal{O}(\varepsilon) \quad (\text{D.29})$$

The result for the local counterterm to the leading color part of the four–gluon vertex correction reads

$$g_{4,4}^{gggg,\ell_{gggg}=0,UV,lc}(\bar{k}, \mu_{UV}) \equiv g_{gggg,lc}^{UV,\ell_{gggg}=0,\mu\nu\lambda\kappa}(\bar{k}, \mu_{UV}) = \begin{aligned} & + \frac{1}{(\bar{k}^2 - \mu_{UV}^2)^4} \left[+ 32(1 - \varepsilon)\bar{k}^\mu\bar{k}^\nu\bar{k}^\lambda\bar{k}^\kappa \right] \\ & + \frac{1}{(\bar{k}^2 - \mu_{UV}^2)^3} \left[- 8(1 - \varepsilon)W(\bar{k})^{\mu\nu\lambda\kappa} - \frac{4}{3}\mu_{UV}^2 V_4^{\mu\nu\lambda\kappa} \right] \\ & + \frac{1}{(\bar{k}^2 - \mu_{UV}^2)^2} \left[+ 2(1 - \varepsilon)(g^{\mu\nu}g^{\lambda\kappa} + g^{\mu\kappa}g^{\nu\lambda}) \right] \end{aligned} \quad (\text{D.30})$$

wherein

$$R_{gggg,lc}^{UV,\ell_{gggg}=0,\mu\nu\lambda\kappa} = -\frac{2}{3}V_4^{\mu\nu\lambda\kappa} \quad (\text{D.31})$$

Upon integration this yields

$$\begin{aligned}
V_{gggg,lc}^{(1)UV,\mu\nu\lambda\kappa}(\mu_{UV}/\mu) &= S_\varepsilon^{-1} \mu^{2\varepsilon} \int \frac{d^D \bar{k}}{(2\pi)^D} g_{gggg,lc}^{UV,\ell_{gggg}=0,\mu\nu\lambda\kappa}(\bar{k}, \mu_{UV}) \\
&= \frac{i}{(4\pi)^2} \left[\left(\frac{2}{3}\right) (V_4^{\mu\nu\lambda\kappa}) \left(\frac{1}{\varepsilon} - \log \frac{\mu_{UV}^2}{\mu^2}\right) \right] + \mathcal{O}(\varepsilon)
\end{aligned} \tag{D.32}$$

In the above $[\mu \leftrightarrow \nu]$ or $[\mu \leftrightarrow \nu \leftrightarrow \lambda]$ denotes the remaining sum of terms of all possible permutations on the indices compared to the term in front. As before $\bar{k} \equiv k - Q$, $k_i \equiv k - (p_1 + p_2 + \dots + p_i)$, $Q_i \equiv Q - (p_1 + p_2 + \dots + p_i)$

The unintegrated local UV counterterms have been implemented in a set of C++ libraries, where we use them in the limit $\varepsilon = 0$ in the recursive construction of $G_{UV}^{(1)}$.

The integrated results can easily be cross-checked against the counterterms for the color-stripped propagators and vertices in chapter 3.1.

Appendix E

One–Loop Integrals to Integrate the Local UV Counterterms

In this appendix we collect those integral identities which are needed to analytically integrate the local UV counterterms in appendix D, but also those local UV counterterms to the propagators and three–valent vertices which one gets upon the further expansion to include also terms of the orders $\mathcal{O}(1/|k|^5)$ and $\mathcal{O}(1/|k|^6)$. For a more elaborate discussion about the subject of one–loop integration we refer the reader to the literature, where a selection can be found in [141, 150, 74, 75, 35, 36, 33, 34, 151].

For the algebraic reductions in D dimensions we use $g^{\mu\nu}g_{\mu\nu} = D$, $\gamma^\mu\gamma_\mu = D$, $\gamma^\mu\gamma^\nu\gamma_\mu = (2-D)\gamma^\nu$, $\gamma^\mu\gamma^\nu\gamma^\rho\gamma_\mu = 4g^{\nu\rho} - (4-D)\gamma^\nu\gamma^\rho$, $\gamma^\mu\gamma^\nu\gamma^\rho\gamma^\sigma\gamma_\mu = -2\gamma^\sigma\gamma^\rho\gamma^\nu + (4-D)\gamma^\nu\gamma^\rho\gamma^\sigma$. The Clifford algebra for the Dirac gamma matrices reads $\{\gamma^\mu, \gamma^\nu\} = \gamma^\mu\gamma^\nu + \gamma^\nu\gamma^\mu = 2g^{\mu\nu}$ and for the trace over Dirac gamma matrices we use the four–dimensional trace $Tr(\mathbf{1}) = 4$, $Tr(\text{odd \# of } \gamma \text{ matrices}) = 0$, $Tr(\gamma^\mu\gamma^\nu) = 4g^{\mu\nu}$, $Tr(\gamma^\mu\gamma^\nu\gamma^\rho\gamma^\sigma) = 4(g^{\mu\nu}g^{\rho\sigma} - g^{\mu\rho}g^{\nu\sigma} + g^{\mu\sigma}g^{\nu\rho})$.

We perform the analytical one–loop integrals in dimensional regularization, where $\int \frac{d^4k}{(2\pi)^4} \rightarrow S_\varepsilon^{-1}\mu^{2\varepsilon} \int \frac{d^Dk}{(2\pi)^D}$, with $D = 4 - 2\varepsilon$ for $|\varepsilon| \ll 1$. $S_\varepsilon = (4\pi)^\varepsilon e^{-\varepsilon\gamma_E}$ is hereby the typical volume factor in dimensional regularization, with γ_E the Euler–Mascheroni constant, and μ the typical mass scale in dimensional regularization. Multiplication by the factor S_ε^{-1} yields thereby directly the results in the $\overline{\text{MS}}$ –scheme. The combination of terms $+\log(4\pi) - \gamma_E$, which always appears in the expansion in the dimensional regularization parameter ε together with the pole term $\frac{1}{\varepsilon}$, is thereby dropped.

After replacing $k \rightarrow \bar{k} + Q$ in the integrands in appendix C and carrying out the series expansion and power counting in \bar{k} as described in chapter 3.2, we are left with tensor integrals of the type

$$\mathcal{I}_{n,a}^{UV}(\mu_{UV}^2)^{\alpha_1 \dots \alpha_{2a}} = S_\varepsilon^{-1} \mu^{2\varepsilon} \int \frac{d^D \bar{k}}{(2\pi)^D} \frac{\bar{k}^{\alpha_1} \dots \bar{k}^{\alpha_{2a}}}{(\bar{k}^2 - \mu_{UV}^2)^n} \equiv \frac{i}{(4\pi)^2} \frac{S_\varepsilon^{-1} (2\pi\mu)^{2\varepsilon}}{i\pi^2} I_{n,a}(\mu_{UV}^2)^{\alpha_1 \dots \alpha_{2a}} \quad (\text{E.1})$$

and further

$$I_{n,a}^{\alpha_1 \dots \alpha_{2a}} \equiv I_{n,a}(\mu_{UV}^2)^{\alpha_1 \dots \alpha_{2a}} = \int d^D \bar{k} \frac{\bar{k}^{\alpha_1} \dots \bar{k}^{\alpha_{2a}}}{(\bar{k}^2 - \mu_{UV}^2)^n} \quad (\text{E.2})$$

where the numerator of the integrand is of tensor rank $2a$ in \bar{k} . The symmetry of the denominator in these tensor integrals allows us to relate them to the corresponding scalar integrals $I_{n,a}$ via

$$I_{n,a}^{\alpha_1 \dots \alpha_{2a}} = I_{n,a} \frac{1}{D(D+2)(D+4)\dots(D+2a-2)} R_{2a}^{\alpha_1 \dots \alpha_{2a}} \quad (\text{E.3})$$

where

$$R_{2a}^{\alpha_1 \dots \alpha_{2a}} = \sum_{S(\alpha_1 \dots \alpha_{2a})} g^{\alpha_1 \alpha_2} \dots g^{\alpha_{2a-1} \alpha_{2a}} \quad (\text{E.4})$$

and the sum runs over all possible totally symmetric combinations of Lorentz indices on the given products of the Minkowski metric $g^{\mu\nu}$, without those that leave the Minkowski metric invariant $g^{\mu\nu} = g^{\nu\mu}$. For our purposes the following three are sufficient

$$I_{n,3}^{\alpha\beta\mu\nu\rho\sigma} = I_{n,3} \frac{1}{D(D+2)(D+4)} R_6^{\alpha\beta\mu\nu\rho\sigma} \quad (\text{E.5})$$

$$I_{n,2}^{\alpha\beta\mu\nu} = I_{n,2} \frac{1}{D(D+2)} R_4^{\alpha\beta\mu\nu} \quad (\text{E.6})$$

$$I_{n,1}^{\alpha\beta} = I_{n,1} \frac{1}{D} R_2^{\alpha\beta} \quad (\text{E.7})$$

with

$$\begin{aligned}
R_6^{\alpha\beta\mu\nu\rho\sigma} &= g^{\alpha\beta} g^{\mu\nu} g^{\rho\sigma} + g^{\alpha\beta} g^{\mu\rho} g^{\sigma\nu} + g^{\alpha\beta} g^{\mu\sigma} g^{\nu\rho} \\
&+ g^{\alpha\mu} g^{\nu\rho} g^{\sigma\beta} + g^{\alpha\mu} g^{\beta\rho} g^{\nu\sigma} + g^{\alpha\mu} g^{\nu\beta} g^{\rho\sigma} \\
&+ g^{\alpha\nu} g^{\beta\mu} g^{\rho\sigma} + g^{\alpha\nu} g^{\mu\sigma} g^{\rho\beta} + g^{\alpha\nu} g^{\rho\mu} g^{\sigma\beta} \\
&+ g^{\alpha\rho} g^{\mu\nu} g^{\sigma\beta} + g^{\alpha\rho} g^{\nu\beta} g^{\sigma\mu} + g^{\alpha\rho} g^{\beta\mu} g^{\sigma\nu} \\
&+ g^{\alpha\sigma} g^{\beta\mu} g^{\nu\rho} + g^{\alpha\sigma} g^{\beta\nu} g^{\rho\mu} + g^{\alpha\sigma} g^{\beta\rho} g^{\mu\nu}
\end{aligned} \tag{E.8}$$

$$R_4^{\alpha\beta\mu\nu} = g^{\alpha\beta} g^{\mu\nu} + g^{\alpha\mu} g^{\beta\nu} + g^{\alpha\nu} g^{\beta\mu} \tag{E.9}$$

$$R_2^{\alpha\beta} = g^{\alpha\beta} \tag{E.10}$$

The scalar integrals are thereby analytically known and given by

$$\begin{aligned}
I_{n,a} &\equiv I_{n,a}(\mu_{UV}^2) = \int d^D \bar{k} \frac{(\bar{k}^2)^a}{(\bar{k}^2 - \mu_{UV}^2)^n} \\
&= i(-1)^{n+a} \frac{\pi^{D/2}}{\Gamma(D/2)} (\mu_{UV}^2)^{(D/2+a-n)} \frac{\Gamma(D/2+a)\Gamma(n-D/2-a)}{\Gamma(n)}
\end{aligned} \tag{E.11}$$

where the numerator is of degree a in \bar{k}^2 , or $2a$ in $|\bar{k}|$. To obtain the above solution for these scalar integrals we have to introduce an infinitesimal regulator which shifts the pole in the time-component \bar{k}_0 of the Minkowski four-vector \bar{k} into complex space. This is usually done by virtue of Feynman's $+i\delta$ -prescription, with $\delta > 0$ and $|\delta| \ll 1$. The integral then acquires the form

$$I_{n,a} \equiv I_{n,a}(\mu_{UV}^2) = \int d^D \bar{k} \frac{(\bar{k}^2)^a}{(\bar{k}^2 - \mu_{UV}^2 + i\delta)^n} \tag{E.12}$$

which develops now a pole around $\bar{k}_0 = \pm\sqrt{\vec{k}^2 + \mu_{UV}^2} - i\delta = \pm\sqrt{\vec{k}^2 + \mu_{UV}^2} \mp i\delta'$. This shifts the poles into complex space by $+i\delta'$ for the negative branch $-\sqrt{\vec{k}^2 + \mu_{UV}^2}$ and by $-i\delta'$ for the positive branch $+\sqrt{\vec{k}^2 + \mu_{UV}^2}$, as shown in figure E.1. We can thus close the integration contour in the complex \bar{k}_0 -plane without enclosing a pole and Cauchy's integral theorem tells us then that $\oint d\bar{k}_0 (\bar{k}^2)^a (\bar{k}^2 - \mu_{UV}^2 + i\delta)^{-n} = 0$. It can be shown that the contributions of the arcs actually vanish at infinity, thus we have

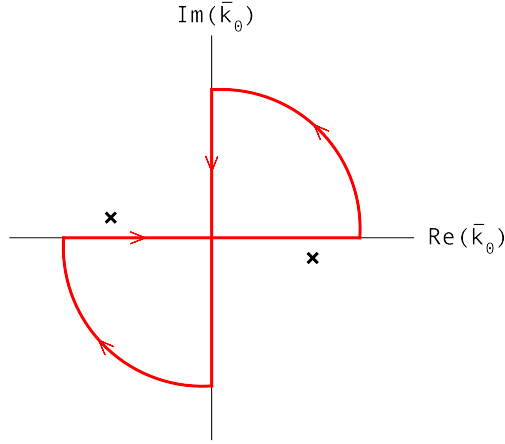


Figure E.1: Complex \bar{k}_0 -plane. Upon shifting the poles we can close the integration contour (red) without enclosing a pole (black crosses).

$$\int_{-\infty}^{+\infty} d\bar{k}_0 \dots = \int_{-i\infty}^{+i\infty} d\bar{k}_0 \dots \quad (\text{E.13})$$

and if we convert from Minkowskian to Euclidean coordinates via $\bar{k}_0 = i\bar{k}_{E,0}$ and $\vec{k} = \vec{k}_E$, which yields $\bar{k}^2 = -\bar{k}_E^2$, we have further

$$\int_{-\infty}^{+\infty} d\bar{k}_0 \dots = i \int_{-\infty}^{+\infty} d\bar{k}_{E,0} \dots \quad (\text{E.14})$$

and thus

$$I_{n,a} \equiv I_{n,a}(\mu_{UV}^2) = i \int d^D \bar{k}_E (-1)^{n+a} \frac{(\bar{k}_E^2)^a}{(\bar{k}_E^2 + \mu_{UV}^2 - i\delta)^n} \quad (\text{E.15})$$

This D -dimensional integral in Euclidean space can be solved with the use of D -dimensional polar coordinates, where the D -dimensional solid angle is given by $\Omega_D = \frac{2\pi^{D/2}}{\Gamma(D/2)}$ with $\Gamma(\dots)$ Euler's Gamma function, to read

$$\begin{aligned}
I_{n,a} &\equiv I_{n,a}(\mu_{UV}^2) = i(-1)^{n+a} \frac{1}{2} \Omega_D \int_0^{+\infty} d^D x \frac{x^{D/2+a-1}}{(x + \mu_{UV}^2 - i\delta)^n} \\
&= i(-1)^{n+a} \frac{1}{2} \Omega_D (\mu_{UV}^2 - i\delta)^{D/2+a-n} \int_0^{+\infty} d^D y \frac{y^{D/2+a-1}}{(1 + \mu_{UV}^2 - i\delta)^n} \\
&= i(-1)^{n+a} \frac{1}{2} \Omega_D (\mu_{UV}^2 - i\delta)^{D/2+a-n} B(D/2 + a, n - D/2 - a)
\end{aligned} \tag{E.16}$$

with $x = \mu_{UV}^2 y = \bar{k}_E^2$ and $B(x, y) = \frac{\Gamma(x)\Gamma(y)}{\Gamma(x+y)}$ Euler's Beta function. This leads finally to equation E.11. The scalar integrals $I_{n,a}(A)$ with $a > 0$ can also be written in terms of the corresponding scalar integrals with $a = 0$ via

$$I_{n,a}(A) = (-1)^a A^a I_{n,0}(A) \frac{(D/2)(D/2 + 1)(D/2 + 2)\dots(D/2 + (a - 1))}{((n - D/2) - 1)((n - D/2) - 2)\dots((n - D/2) - a)} \tag{E.17}$$

We can further express the scalar integrals $I_{n,a}(A)$ with $a > 0$ in terms of linear combinations of the corresponding scalar integrals of lower denominator degree $n' < n$ and $a = 0$, where the following identities are sufficient for our purposes

$$I_{n,3}(A) = I_{n-3,0}(A) + 3AI_{n-2,0}(A) + 3A^2I_{n-1,0}(A) + A^3I_{n,0}(A) \tag{E.18}$$

$$I_{n,2}(A) = I_{n-2,0}(A) + 2AI_{n-1,0}(A) + A^2I_{n,0}(A) \tag{E.19}$$

$$I_{n,1}(A) = I_{n-1,0}(A) + AI_{n,0}(A) \tag{E.20}$$

Odd powers of \bar{k} in the numerator lead to an antisymmetric integrand, which integrates to zero between $\bar{k} \rightarrow -\infty$ and $\bar{k} \rightarrow \infty$. Integrals with half-integer values in a thus vanish. For the expansion of the propagator and three-valent vertex correction to higher orders in \bar{k} , as discussed in chapter 3.2, the scalar integrals $I_{6,3}$, $I_{5,2}$, $I_{4,2}$, $I_{4,1}$, $I_{4,0}$, $I_{3,1}$, $I_{3,0}$, $I_{2,1}$, $I_{2,0}$ and $I_{1,0}$ are sufficient. These can be expressed in terms of $I_{2,0}$ and $I_{1,0}$ via

$$I_{6,3} = \frac{\varepsilon(\varepsilon - 2)(\varepsilon - 3)(\varepsilon - 4)}{(120\mu_{UV}^2)} I_{2,0} \tag{E.21}$$

$$I_{5,2} = -\frac{\varepsilon(\varepsilon-2)(\varepsilon-3)}{(24\mu_{UV}^2)} I_{2,0} \quad (\text{E.22})$$

$$I_{4,2} = \frac{(4-2\varepsilon)(4-2\varepsilon+2)}{24} I_{2,0} \quad (\text{E.23})$$

$$I_{4,1} = \frac{\varepsilon(\varepsilon-2)}{(6\mu_{UV}^2)} I_{2,0} \quad (\text{E.24})$$

$$I_{4,0} = \frac{\varepsilon(1+\varepsilon)}{(6\mu_{UV}^4)} I_{2,0} \quad (\text{E.25})$$

$$I_{3,1} = \frac{(4-2\varepsilon)}{4} I_{2,0} \quad (\text{E.26})$$

$$I_{3,0} = -\frac{\varepsilon}{(2\mu_{UV}^2)} I_{2,0} \quad (\text{E.27})$$

$$I_{2,1} = I_{1,0} + \mu_{UV}^2 I_{2,0} \quad (\text{E.28})$$

We finally need the expansions of $I_{2,0}$ and $I_{1,0}$ around $|\varepsilon| \ll 1$ up to finite order in ε , which read

$$S_\varepsilon^{-1} \frac{(2\pi\mu)^{2\varepsilon}}{i\pi^2} I_{2,0} = S_\varepsilon^{-1} \left(\frac{\mu_{UV}^2}{4\pi\mu^2} \right)^{-\varepsilon} \Gamma(\varepsilon) = \frac{1}{\varepsilon} - \log \frac{\mu_{UV}^2}{\mu^2} + \mathcal{O}(\varepsilon) \quad (\text{E.29})$$

$$S_\varepsilon^{-1} \frac{(2\pi\mu)^{2\varepsilon}}{i\pi^2} I_{1,0} = -\mu_{UV}^2 S_\varepsilon^{-1} \left(\frac{\mu_{UV}^2}{4\pi\mu^2} \right)^{-\varepsilon} \Gamma(\varepsilon-1) = \mu_{UV}^2 \left(\frac{1}{\varepsilon} - \log \frac{\mu_{UV}^2}{\mu^2} + 1 \right) + \mathcal{O}(\varepsilon) \quad (\text{E.30})$$

where the following expansions around $|\varepsilon| \ll 1$ are helpful

$$\Gamma(\varepsilon-1) = -\frac{1}{\varepsilon} + \gamma_E - 1 - \frac{1}{6} \left(1 - \gamma_E + 3\gamma_E^2 + \frac{\pi^2}{6} \right) \varepsilon + \mathcal{O}(\varepsilon^2) \quad (\text{E.31})$$

$$\Gamma(\varepsilon) = \frac{1}{\varepsilon} - \gamma_E + \frac{1}{6} \left(3\gamma_E^2 + \frac{\pi^2}{6} \right) \varepsilon + \mathcal{O}(\varepsilon^2) \quad (\text{E.32})$$

$$\Gamma(1+\varepsilon) = \varepsilon \Gamma(\varepsilon) = 1 - \varepsilon \gamma_E + \mathcal{O}(\varepsilon^2) \quad (\text{E.33})$$

$$\frac{1}{\Gamma(\varepsilon)} = \varepsilon + \gamma_E \varepsilon^2 + \mathcal{O}(\varepsilon^3) \quad (\text{E.34})$$

$$\frac{1}{\Gamma(\varepsilon - 1)} = \frac{(\varepsilon - 1)}{\Gamma(\varepsilon)} = (\varepsilon - 1)(\varepsilon + \gamma_E \varepsilon^2 + \mathcal{O}(\varepsilon^3)) \quad (\text{E.35})$$

$$\Gamma(1 - \varepsilon)\Gamma(1 + \varepsilon) = 1 + \frac{\pi^2 \varepsilon^2}{6} + \mathcal{O}(\varepsilon^4) \quad (\text{E.36})$$

$$\frac{e^{\varepsilon \gamma_E}}{\Gamma(1 - \varepsilon)} = 1 - \frac{\pi^2 \varepsilon^2}{12} + \mathcal{O}(\varepsilon^3) \quad (\text{E.37})$$

$$\left(\frac{a}{b}\right)^{\pm \varepsilon} = 1 \pm \log\left(\frac{a}{b}\right)\varepsilon + \frac{1}{2} \log^2\left(\frac{a}{b}\right)\varepsilon^2 + \mathcal{O}(\varepsilon^3) \quad (\text{E.38})$$

Appendix F

One–Loop Recurrence Relations in Leading Color Approximation

In this appendix we give all the recursive relations that are needed to construct the bare primitive gluon one–loop amplitudes, the bare primitive quark and antiquark one–loop amplitudes and the bare primitive one–loop amplitude to the process $e^+e^- \rightarrow n$ jets, in the leading color approximation.

F.1 Ordered One–Loop Gluon Currents

The recursive relation for the unintegrated ordered one–loop gluon off–shell current is depicted in figure F.1, where only the parts for the leading color approximation are accounted for, i.e. gluonic and ghost–gluon interactions but no closed fermion–loops. This is the recursive relation to construct the set of color–stripped diagrams for the leading color part $A_{n;1}^{[1]}(1, 2, \dots, n)$ in equation 2.42 for the n –gluon amplitude in equation 2.41 in chapter 2.5. In formula it reads

F.1 Ordered One-Loop Gluon Currents

$$\begin{aligned}
J_\alpha^{(1)}(m, \dots, n) &= \frac{-ig_{\alpha\mu}}{P(m, \dots, n)^2} \times \\
&\times \left[\sum_{i=m}^{n-1} V_{ggg}^{(0)\mu\nu\rho}(-P(m, \dots, n), P(m, \dots, i), P(i+1, \dots, n)) J_\nu^{(1)}(m, \dots, i) J_\rho^{(0)}(i+1, \dots, n) \right. \\
&+ \sum_{i=m}^{n-1} V_{ggg}^{(0)\mu\nu\rho}(-P(m, \dots, n), P(m, \dots, i), P(i+1, \dots, n)) J_\nu^{(0)}(m, \dots, i) J_\rho^{(1)}(i+1, \dots, n) \\
&+ \sum_{l=1}^4 V_{ggg}^{[l]\mu\rho}(-P(m, \dots, n), k_{m-1}, -k_n) K_\rho^{[l]}(m, \dots, n; k_{m-1}) \\
&+ \sum_{i=m}^{n-2} \sum_{j=i+1}^{n-1} V_{gggg}^{(0)\mu\nu\rho\sigma} J_\nu^{(1)}(m, \dots, i) J_\rho^{(0)}(i+1, \dots, j) J_\sigma^{(0)}(j+1, \dots, n) \\
&+ \sum_{i=m}^{n-2} \sum_{j=i+1}^{n-1} V_{gggg}^{(0)\mu\nu\rho\sigma} J_\nu^{(0)}(m, \dots, i) J_\rho^{(1)}(i+1, \dots, j) J_\sigma^{(0)}(j+1, \dots, n) \\
&+ \sum_{i=m}^{n-2} \sum_{j=i+1}^{n-1} V_{gggg}^{(0)\mu\nu\rho\sigma} J_\nu^{(0)}(m, \dots, i) J_\rho^{(0)}(i+1, \dots, j) J_\sigma^{(1)}(j+1, \dots, n) \\
&+ \sum_{i=m}^{n-1} \sum_{l=1}^4 V_{gggg}^{1[l]\mu\rho\sigma} K_\rho^{[l]}(m, \dots, i; k_{m-1}) J_\sigma^{(0)}(i+1, \dots, n) \\
&+ \sum_{i=m}^{n-1} \sum_{l=1}^4 V_{gggg}^{2[l]\mu\nu\sigma} J_\nu^{(0)}(m, \dots, i) K_\sigma^{[l]}(i+1, \dots, n; k_i) \\
&\left. + (-1)(-1)V_{ghg}^{(0)\mu}(k_{m-1})L^{(-)}(m, \dots, n; k_{m-1}) + (-1)(+1)V_{ghg}^{(0)\mu}(-k_n)L^{(+)}(m, \dots, n; k_{m-1}) \right] \tag{F.1}
\end{aligned}$$

where $V_{ggg}^{[l]\mu\rho}$ has been given in chapter 4.2, and

$$V_{gggg}^{1[l]\mu\rho\sigma} = V_{gggg}^{(0)\mu\nu\rho\sigma} a_\nu^{[l]} \tag{F.2}$$

and

$$V_{gggg}^{2[l]\mu\nu\sigma} = V_{gggg}^{(0)\mu\nu\rho\sigma} a_\rho^{[l]} \tag{F.3}$$

The two-leg off-shell current $K_\mu^{[l]}$, as described in chapter 4.2, receives an additional term in its recursive construction, via the four-gluon interaction. This is shown in figure F.2 and reads in formula

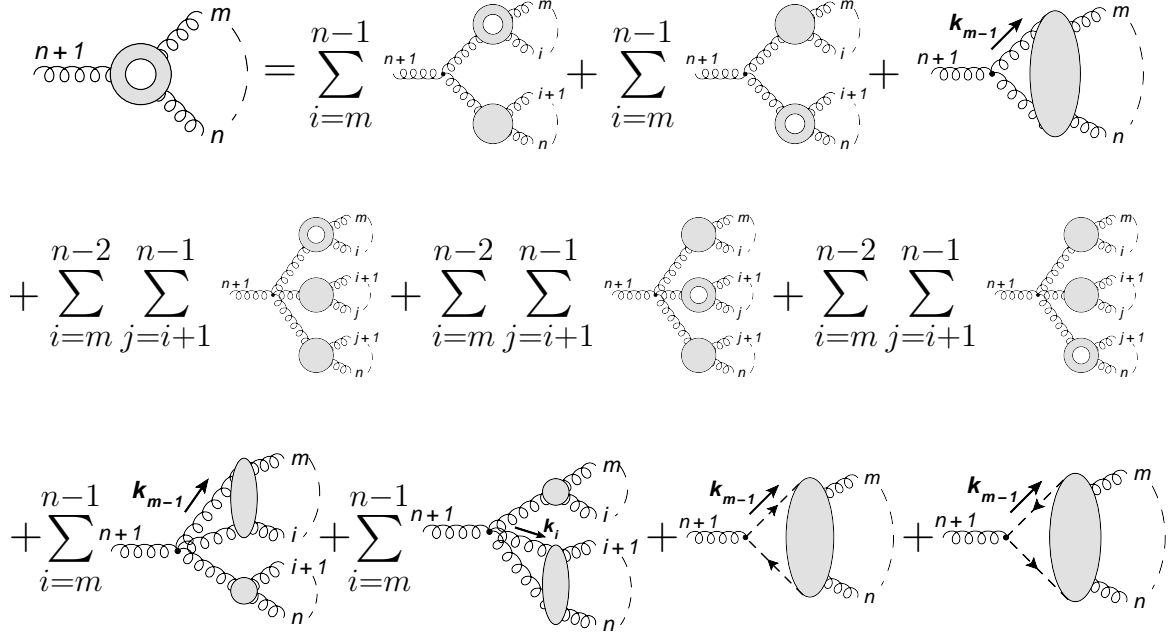


Figure F.1: Recursion relation for the one-loop gluon off-shell current in the leading color approximation. Wiggly lines denote gluons, dashed lines denote ghosts.

$$\begin{aligned}
 K_{\rho}^{[l]}(m, \dots, n; q) &= \frac{-ig_{\rho\lambda}}{(q - P(m, \dots, n))^2} \times \\
 &\times \left[\sum_{i=m-1}^{n-1} V_{ggg}^{(0)\lambda\sigma\tau}(q - P(m, \dots, n), -q + P(m, \dots, i), P(i+1, \dots, n)) \times \right. \\
 &\quad \times K_{\sigma}^{[l]}(m, \dots, i; q) J_{\tau}^{(0)}(i+1, \dots, n) \\
 &\quad \left. + \sum_{i=m-1}^{n-2} \sum_{j=i+1}^{n-1} V_{gggg}^{(0)\lambda\sigma\kappa\tau} K_{\sigma}^{[l]}(m, \dots, i; q) J_{\kappa}^{(0)}(i+1, \dots, j) J_{\tau}^{(0)}(j+1, \dots, n) \right] \quad (\text{F.4})
 \end{aligned}$$

The termination conditions and the retrieval of the integrand to the bare primitive amplitude are the same as given in chapter 4.2

$$G_{bare,lc}^{(1)}(1, \dots, n+1) = \varepsilon^{\mu}(p_{n+1}, q) i P(1, \dots, n)^2 J_{\mu}^{(1)}(1, \dots, n) \Big|_{P(1, \dots, n) = -p_{n+1}} \quad (\text{F.5})$$

The last two terms in equation F.1 represent the contributions of closed ghost loops, which have to be inserted because we use the gluon propagator in the Feynman gauge. A minus sign in both terms has to be included due to fermion statistics. Since we are dealing with ordered amplitudes

F.1 Ordered One-Loop Gluon Currents

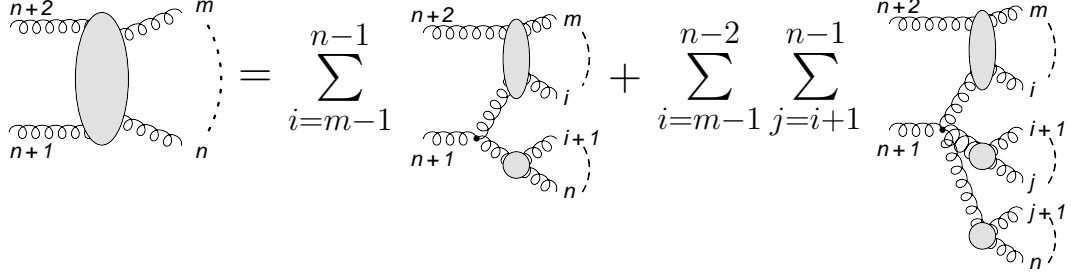


Figure F.2: Recursion relation for the two-leg gluon off-shell current. Wiggly lines denote gluons.

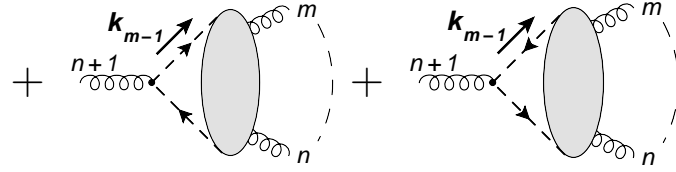


Figure F.3: Ghost loop contributions to the gluonic one-loop recursion. Wiggly lines denote gluons, dashed lines denote ghosts. In ordered diagrams we have to consider both fermionic directions.

here, we have to consider both fermionic directions of the ghost propagators in the loop, as shown in figure F.1. In the next-to-last term in equation F.1 we need an additional minus sign, since the off-shell gluon is a left-radiator, as described in appendix A. The additional two terms are shown in figure F.3. They can be recursively computed by cutting the ghost propagators in the loop, where we choose to cut the upper propagator. The recursive relations are depicted in figure F.4 and are given in formula by

$$\begin{aligned}
 L^{(-)}(m, \dots, n; q) &= \\
 &\frac{+i}{(q - P(m, \dots, n))^2} \left[\sum_{i=m-1}^{n-1} (-1) V_{ghg}^{(0)\mu}(k_n) J_\mu^{(0)}(i+1, \dots, n) L^{(-)}(m, \dots, i; q) \right] \\
 L^{(+)}(m, \dots, n; q) &= \\
 &\frac{+i}{(q - P(m, \dots, n))^2} \left[\sum_{i=m-1}^{n-1} (+1) V_{ghg}^{(0)\mu}(-k_i) J_\mu^{(0)}(i+1, \dots, n) L^{(+)}(m, \dots, i; q) \right] \quad (\text{F.6})
 \end{aligned}$$

where the right-radiating ghost-gluon vertex in $L^{(+)}$ is given by $V_{ghg}^{(0)\mu}(k) = -ik^\mu$ and we include this vertex as left-radiator with an extra minus sign $(-1)V_{ghg}^{(0)\mu}(k)$ in $L^{(-)}$. The recursions terminate with $L^{(\mp)}(m, m-1; q) = \frac{\pm i}{q^2}$ and the tree-level one-currents $J_\mu^{(0)}(l)$.

Figure F.4: Recursion relation for the two-leg ghost off-shell currents $L^{(-)}(m, \dots, n; q)$ (top) and $L^{(+)}(m, \dots, n; q)$ (bottom). Wiggly lines denote gluons, dashed lines denote ghosts.

This ends the discussion of the one-loop gluon recursions. We turn to the one-loop quark and antiquark currents in the next section.

F.2 Ordered One-Loop Quark and Antiquark Currents

The recursion for the unintegrated ordered one-loop off-shell quark current with one quark-antiquark pair in leading color approximation is depicted in figure F.5. This is the recursive relation to construct the set of color-stripped diagrams for the leading color part $A_n^{L,[1]}(1_{\bar{q}}, 2_q, 3, \dots, n)$ in equation 2.50 for the amplitude with one quark-antiquark pair and multiple gluons in equation 2.47 in chapter 2.5.2.

To compute the direct one-loop contribution one could cut the upper gluon line and state the recursion for the two-leg tree-level current, where the two off-shell legs are given by a gluon and a quark line. In the leading color approximation we are able to recursively construct the direct one-loop contribution by the means of only using the two-leg off-shell gluon current, as shown in figure F.6. The recursion formula then reads

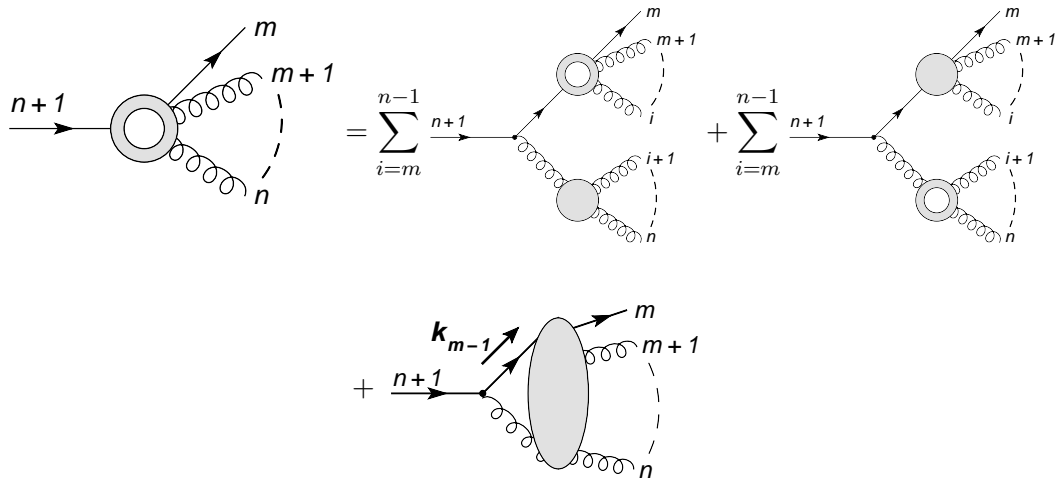


Figure F.5: Recursion relation for the ordered one-loop off-shell quark current in leading color approximation. Wiggly lines denote gluons, straight lines with fermion arrows denote fermions.

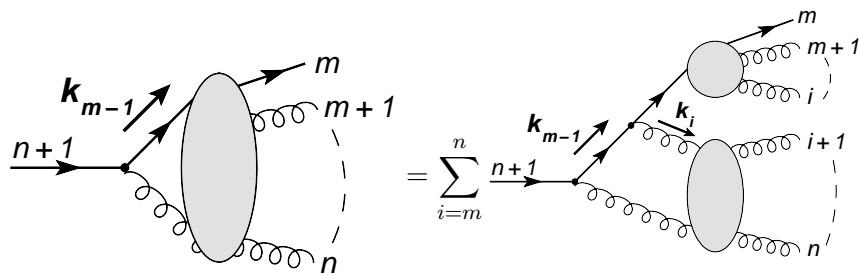


Figure F.6: The direct one-loop contribution in the one-loop off-shell quark current can in the leading color approximation be described with the two-leg tree-level off-shell gluon current. Wiggly lines denote gluons, straight lines with fermion arrows denote fermions.

$$\begin{aligned}
 \bar{U}^{(1)}(m_q, m+1, \dots, n) = & \left[\sum_{i=m}^{n-1} \bar{U}^{(1)}(m_q, m+1, \dots, i) \Gamma^{(0)\mu} J_\mu^{(0)}(i+1, \dots, n) \right. \\
 & + \sum_{i=m}^{n-1} \bar{U}^{(0)}(m_q, m+1, \dots, i) \Gamma^{(0)\mu} J_\mu^{(1)}(i+1, \dots, n) \\
 & \left. + \sum_{i=m}^n \bar{U}^{(0)}(m_q, m+1, \dots, i) \Gamma^{(0)\mu} \frac{ik_{m-1}^\mu}{k_{m-1}^2} \Gamma^{(0)\nu} K_{\mu\nu}(i+1, \dots, n; k_i) \right] \times \\
 & \times \frac{i[\not{p}_{m_q} + \not{P}(m+1, \dots, n)]}{[p_{m_q} + P(m+1, \dots, n)]^2} \quad (\text{F.7})
 \end{aligned}$$

Similar considerations lead to the recursion for the unintegrated ordered one-loop off-shell antiquark current with one quark-antiquark pair in leading color approximation, depicted in figure F.7 and figure F.8. This is the recursive relation to construct the set of color-stripped diagrams for the leading color part $A_n^{L,[1]}(1_{\bar{q}}, 2_q, 3, \dots, n)$ in equation 2.50 for the amplitude with one quark-antiquark pair and multiple gluons in equation 2.47 in chapter 2.5.2. In formula it reads

$$\begin{aligned}
 V^{(1)}(m, \dots, n-1, n_{\bar{q}}) = & \frac{i[-(\not{P}(m, \dots, n-1) + \not{p}_{n_{\bar{q}}})]}{[P(m, \dots, n-1) + p_{n_{\bar{q}}}]^2} \times \\
 & \times \left[\sum_{i=m}^{n-1} \Gamma^{(0)\mu} J_\mu^{(0)}(m, \dots, i) V^{(1)}(i+1, \dots, n-1, n_{\bar{q}}) \right. \\
 & + \sum_{i=m}^{n-1} \Gamma^{(0)\mu} J_\mu^{(1)}(m, \dots, i) V^{(0)}(i+1, \dots, n-1, n_{\bar{q}}) \\
 & \left. + \sum_{i=m-1}^{n-1} \Gamma^{(0)\mu} \frac{ik_n^\mu}{k_n^2} \Gamma^{(0)\nu} K_{\mu\nu}(m, \dots, i; k_{m-1}) V^{(0)}(i+1, \dots, n-1, n_{\bar{q}}) \right] \quad (\text{F.8})
 \end{aligned}$$

The one-loop quark and antiquark off-shell currents terminate with $\bar{U}^{(1)}(m_q)$ and $V^{(1)}(n_{\bar{q}})$, which describe self-energies on external quark lines and are therefore dropped. Just as in the tree-level case, $\bar{U}^{(1)}$ and $V^{(1)}$ are matrices in Dirac space, which means that their position with respect to the quark-gluon vertex and the quark and antiquark propagators matter. The integrand to the corresponding one-loop primitive amplitude is recovered from the quark or antiquark currents by

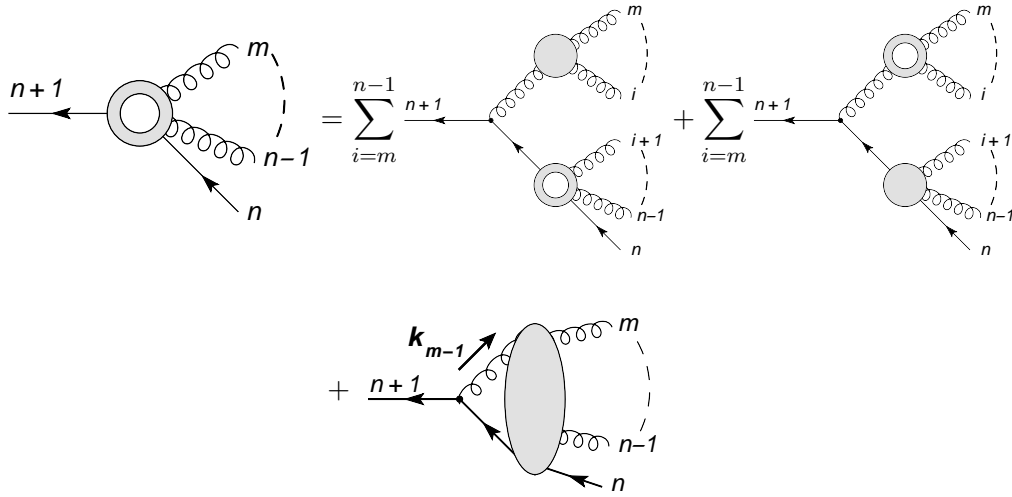


Figure F.7: Recursion relation for the ordered one-loop off-shell antiquark current in leading color approximation. Wiggly lines denote gluons, straight lines with fermion arrows denote fermions.

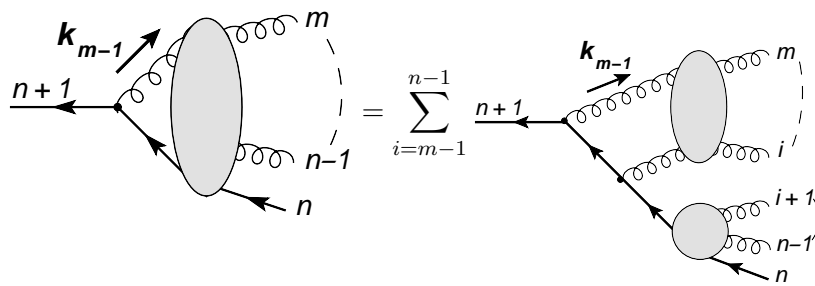


Figure F.8: The direct one-loop contribution in the one-loop off-shell antiquark current can in the leading color approximation be described with the two-leg tree-level off-shell gluon current. Wiggly lines denote gluons, straight lines with fermion arrows denote fermions.

$$\begin{aligned}
 G_{bare,lc}^{(1)}(1_q, 2, \dots, n-1, n_{\bar{q}}) &= \bar{U}^{(1)}(1_q, 2, \dots, n-1)(-i)[\not{p}_{1_q} + \not{P}(2, \dots, n-1)]v(p_{n_{\bar{q}}})|_{p_{1_q}+P(2,\dots,n-1)=-p_{n_{\bar{q}}}} \\
 &= \bar{u}(p_{1_q})(-i)[-(\not{P}(2, \dots, n-1) + \not{p}_{n_{\bar{q}}})]V^{(1)}(2, \dots, n-1, n_{\bar{q}})|_{P(2,\dots,n-1)+p_{n_{\bar{q}}}=-p_{1_q}} \quad (\text{F.9})
 \end{aligned}$$

Just as in the case of the one–loop gluon currents, attention has to be paid when self–energies appear on the off–shell legs of $\bar{U}^{(1)}(1_q, 2, \dots, n-1)$ or $V^{(1)}(2, \dots, n-1, n_{\bar{q}})$, since these off–shell legs are put on–shell in the end.

F.3 One–Loop Recursion for $e^+e^- \rightarrow (n-2)$ jets

The process $e^+e^- \rightarrow (n-2)$ jets in the leading color approximation is shown in figure F.9. The integrand to the corresponding primitive amplitude reads

$$\begin{aligned}
 G_{e^+e^- \rightarrow (n-2)\text{jets},lc}^{(1)bare} &= G^{(1)}(1_q, 2_g, \dots, (n-3)_g, (n-2)_{\bar{q}}, (n-1)_l, n_{\bar{l}}) \\
 &= \mathcal{Q}_{start}^{(1)\mu}(1_q, 2, \dots, n-3, (n-2)_{\bar{q}})J_{\mu}^{(0)EW}((n-1)_l, n_{\bar{l}}) \quad (\text{F.10})
 \end{aligned}$$

with $J_{\mu}^{(0)EW}((n-1)_l, n_{\bar{l}}) = \bar{v}(-p_{n-1})V_{ll\gamma/Z}^{(0)\alpha}u(-p_n)P_{\alpha\mu}^{\gamma/Z}$ and where the recursion start for the corresponding unintegrated one–loop current $\mathcal{Q}_{start}^{(1)\mu}(1_q, 2, \dots, n-3, (n-2)_{\bar{q}})$ is given by

$$\begin{aligned}
 \mathcal{Q}_{start}^{(1)\mu}(1_q, 2, \dots, n-3, (n-2)_{\bar{q}}) &= \\
 &\sum_{i=1}^{n-3} \bar{U}^{(1)}(1_q, 2, \dots, i)V_{qq\gamma/Z}^{(0)\mu}V(i+1, \dots, n-3, (n-2)_{\bar{q}}) \\
 &+ \sum_{i=1}^{n-3} \bar{U}(1_q, 2, \dots, i)V_{qq\gamma/Z}^{(0)\mu}V^{(1)}(i+1, \dots, n-3, (n-2)_{\bar{q}}) \\
 &+ \sum_{i=1}^{n-3} \sum_{j=i}^{n-3} \bar{U}(1_q, 2, \dots, i)\Gamma^{(0)\alpha} \frac{i\cancel{k}_0}{k_0^2} V_{qq\gamma/Z}^{(0)\mu} \frac{i\cancel{k}_{n-2}}{k_{n-2}^2} \Gamma^{(0)\beta} \times \\
 &\quad \times K_{\alpha\beta}(i+1, \dots, j; k_i)V(j+1, \dots, n-3, (n-2)_{\bar{q}}) \quad (\text{F.11})
 \end{aligned}$$

with $V_{ll\gamma/Z}^{(0)\mu}$ and $V_{qq\gamma/Z}^{(0)\mu}$ the appropriate γ/Z –fermion vertices and $P_{\mu\nu}^{\gamma/Z}$ the appropriate γ/Z propagator, as they can be found in every standard textbook. We drop the propagator in the start routine $\mathcal{Q}_{start}^{(1)\mu}(1_q, 2, \dots, n-3, (n-2)_{\bar{q}})$ since it is included already in $J_{\mu}^{(0)EW}((n-1)_l, n_{\bar{l}})$, as explained at the end of chapter 4.1. The electron and positron are taken to be as incoming

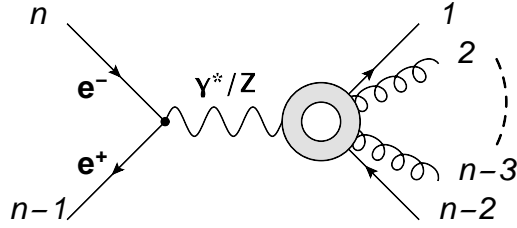


Figure F.9: One-loop amplitude to $e^+e^- \rightarrow (n-2)$ jets in leading color approximation. We choose the leptons as incoming.

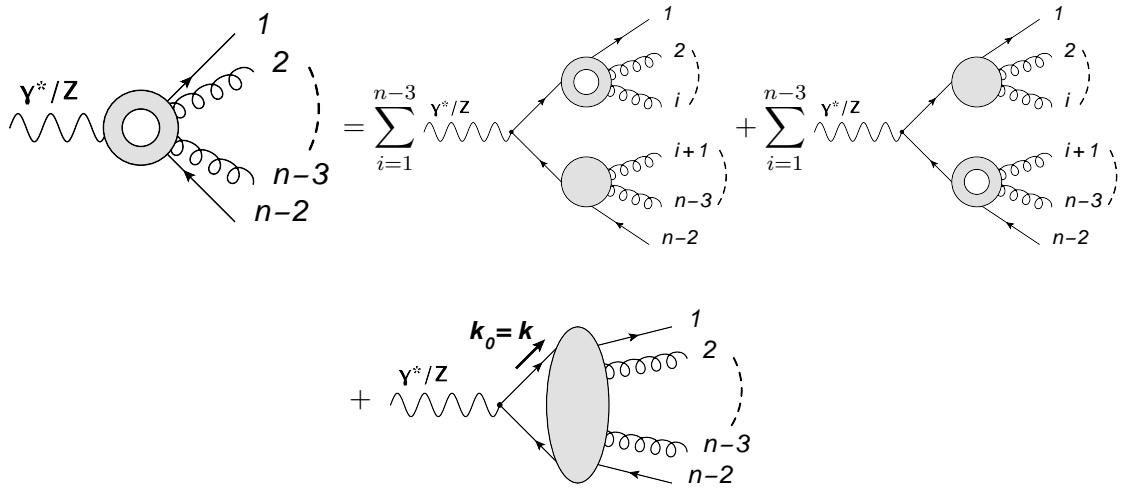


Figure F.10: Recursion start $\mathcal{Q}_{start}^{(1)\mu}(1_q, 2, \dots, n-3, (n-2)_{\bar{q}})$ to the unintegrated one-loop current in $e^+e^- \rightarrow (n-2)$ jets in leading color approximation. Wiggly lines denote gluons, straight lines with fermion arrows denote fermions.

particles, where we have an incoming electron with momentum $p_{e^-}^{in} = -p_n$ and an incoming positron with momentum $p_{e^+}^{in} = -p_{n-1}$. The recursions are depicted in figure F.10 and figure F.11. We note that in figure F.10 we could have cut one of the quark lines in the loop in the direct one-loop contribution. In the leading color approximation, however, it is sufficient to use the two-leg gluon off-shell currents as shown in figure F.11.

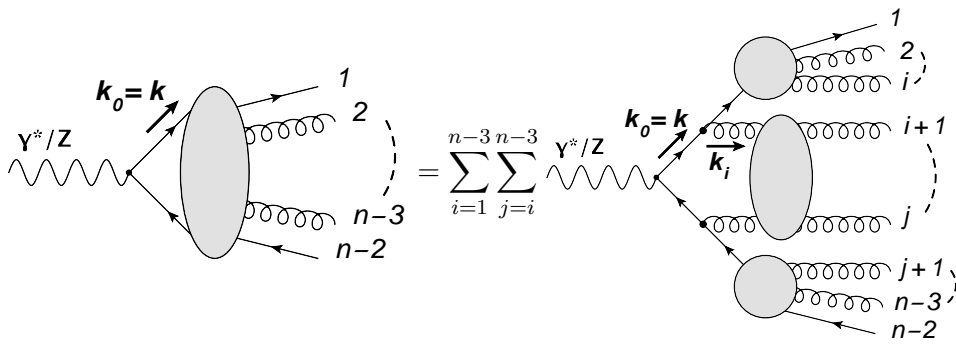


Figure F.11: The direct one-loop contribution in $\mathcal{Q}_{start}^{(1)\mu}(1_q, 2, \dots, n-3, (n-2)_{\bar{q}})$ can in the leading color approximation be described with the two-leg tree-level off-shell gluon current. Wiggly lines denote gluons, straight lines with fermion arrows denote fermions.

Appendix G

UV Recurrence Relations in Leading Color Approximation

In this appendix we give all the recursive relations that are needed to compute the total local UV subtraction terms to the bare primitive gluon one-loop amplitudes, the bare primitive quark and antiquark one-loop amplitudes and the bare primitive one-loop amplitude to the process $e^+e^- \rightarrow n$ jets, in the leading color approximation from the local UV counterterms. The local UV counterterms have been discussed in chapter 3.2 and are given in appendix D.

G.1 Ordered One-Loop Gluon Currents

The contributions from closed ghost-loops have been included in the derivation of the local UV counterterms. Whenever we place a local UV counterterm regarding a gluon propagator or a three- or four-gluon vertex, in our recursive construction, this will automatically also incorporate the necessary degrees of freedom from the respective ghost contributions. The UV recursion to the one-loop gluon currents in the leading color approximation are depicted in figure G.1. In formula it reads

$$\begin{aligned}
 J_{lc,\alpha}^{(1)UV}(m, \dots, n) &= \frac{-ig_{\alpha\mu}}{P(m, \dots, n)^2} \times \\
 &\times \left[\sum_{i=m}^{n-1} V_{ggg}^{(0)\mu\nu\rho}(-P(m, \dots, n), P(m, \dots, i), P(i+1, \dots, n)) J_{lc,\nu}^{(1)UV}(m, \dots, i) J_{\rho}^{(0)}(i+1, \dots, n) \right. \\
 &+ \sum_{i=m}^{n-1} V_{ggg}^{(0)\mu\nu\rho}(-P(m, \dots, n), P(m, \dots, i), P(i+1, \dots, n)) J_{\nu}^{(0)}(m, \dots, i) J_{lc,\rho}^{(1)UV}(i+1, \dots, n) \\
 &+ g_{gg,lc}^{UV,\ell_{gg}=2,\mu\beta}(\bar{k}, Q_{m-1}, P(m, \dots, n), \mu_{UV}) \frac{-ig_{\beta\gamma}}{P(m, \dots, n)^2} \times \\
 &\quad \times \sum_{i=m}^{n-1} V_{ggg}^{(0)\gamma\nu\rho}(-P(m, \dots, n), P(m, \dots, i), P(i+1, \dots, n)) J_{\nu}^{(0)}(m, \dots, i) J_{\rho}^{(0)}(i+1, \dots, n) \\
 &+ \sum_{i=m}^{n-1} g_{ggg,lc}^{UV,\ell_{ggg}=1,\mu\nu\rho}(\bar{k}, Q_{m-1}, P(m, \dots, i), P(i+1, \dots, n), \mu_{UV}) J_{\nu}^{(0)}(m, \dots, i) J_{\rho}^{(0)}(i+1, \dots, n) \\
 &+ \sum_{i=m}^{n-2} \sum_{j=i+1}^{n-1} V_{gggg}^{(0)\mu\nu\rho\sigma} J_{lc,\nu}^{(1)UV}(m, \dots, i) J_{\rho}^{(0)}(i+1, \dots, j) J_{\sigma}^{(0)}(j+1, \dots, n) \\
 &+ \sum_{i=m}^{n-2} \sum_{j=i+1}^{n-1} V_{gggg}^{(0)\mu\nu\rho\sigma} J_{\nu}^{(0)}(m, \dots, i) J_{lc,\rho}^{(1)UV}(i+1, \dots, j) J_{\sigma}^{(0)}(j+1, \dots, n) \\
 &+ \sum_{i=m}^{n-2} \sum_{j=i+1}^{n-1} V_{gggg}^{(0)\mu\nu\rho\sigma} J_{\nu}^{(0)}(m, \dots, i) J_{\rho}^{(0)}(i+1, \dots, j) J_{lc,\sigma}^{(1)UV}(j+1, \dots, n) \\
 &+ g_{gg,lc}^{UV,\ell_{gg}=2,\mu\beta}(\bar{k}, Q_{m-1}, P(m, \dots, n), \mu_{UV}) \frac{-ig_{\beta\gamma}}{P(m, \dots, n)^2} \times \\
 &\quad \times \sum_{i=m}^{n-2} \sum_{j=i+1}^{n-1} V_{gggg}^{(0)\gamma\nu\rho\sigma} J_{\nu}^{(0)}(m, \dots, i) J_{\rho}^{(0)}(i+1, \dots, j) J_{\sigma}^{(0)}(j+1, \dots, n) \\
 &\left. + \sum_{i=m}^{n-2} \sum_{j=i+1}^{n-1} g_{gggg,lc}^{UV,\ell_{gggg}=0,\mu\nu\lambda\kappa}(\bar{k}, \mu_{UV}) J_{\nu}^{(0)}(m, \dots, i) J_{\rho}^{(0)}(i+1, \dots, j) J_{\sigma}^{(0)}(j+1, \dots, n) \right] \quad (G.1)
 \end{aligned}$$

with $Q_i = Q - P(1, \dots, i)$ and the relation between k , \bar{k} and Q is in the above given by $k_i = \bar{k} + Q_i$. The local UV counterterms $g_{gg,lc}^{UV,\ell_{gg}=2,\mu\beta}(\dots)$, $g_{ggg,lc}^{UV,\ell_{ggg}=1,\mu\nu\rho}$ and $g_{gggg,lc}^{UV,\ell_{gggg}=0,\mu\nu\lambda\kappa}(\dots)$ that appear in the above are the leading color contributions of the local UV counterterms to the color-stripped gluon propagator, three-gluon vertex and four-gluon vertex respectively, as given in appendix D. The recursion terminates with the unintegrated UV one-current $J_{lc,\mu}^{(1)UV}(l)$, which corresponds to a counterterm for a self-energy correction on an external leg and is thus set to zero, or with the usual tree-level one-current $J_{\mu}(l) \equiv \varepsilon_{\mu}(p_l, q)$.

$$\begin{aligned}
 & \text{Diagram with } n+1 \text{ and } m \text{ and a cross} = \sum_{i=m}^{n-1} \left[\text{Diagram 1} + \text{Diagram 2} + \text{Diagram 3} + \text{Diagram 4} \right] \\
 & + \sum_{i=m}^{n-2} \sum_{j=i+1}^{n-1} \text{Diagram 5} + \sum_{i=m}^{n-2} \sum_{j=i+1}^{n-1} \text{Diagram 6} + \sum_{i=m}^{n-2} \sum_{j=i+1}^{n-1} \text{Diagram 7} \\
 & + \sum_{i=m}^{n-2} \sum_{j=i+1}^{n-1} \text{Diagram 8} + \sum_{i=m}^{n-2} \sum_{j=i+1}^{n-1} \text{Diagram 9}
 \end{aligned}$$

Figure G.1: UV recursion relation to the one-loop gluon off-shell current. Wiggly lines denote gluons. Crosses denote local UV counterterms. In leading color approximation we need to use the leading color parts of the local UV counterterms.

G.2 Ordered One–Loop Quark and Antiquark Currents

The total unintegrated UV subtraction term to the associated bare primitive one–loop amplitude is then retrieved similarly as before by

$$G_{UV,lc}^{(1)}(1, \dots, n+1) = \varepsilon^\mu(p_{n+1}, q) i P(1, \dots, n)^2 J_{lc,\mu}^{(1)UV}(1, \dots, n) \Big|_{P(1, \dots, n) = -p_{n+1}} \quad (\text{G.2})$$

Since we put the off–shell leg on–shell here again, care has to be taken when a the local UV counterterms to a self–energy correction appears on the off–shell leg. These terms also have to be set to zero.

G.2 Ordered One–Loop Quark and Antiquark Currents

The UV recursion to the quark current for one quark–antiquark pair is depicted in fig.G.2. In formula it reads

$$\begin{aligned} \overline{U}_{lc}^{(1)UV}(m_q, m+1, \dots, n) &= \frac{i}{[p_{m_q} + P(m+1, \dots, n)]^2} \times \\ &\times \left[\sum_{i=m}^{n-1} \overline{U}_{lc}^{(1)UV}(m_q, m+1, \dots, i) \Gamma^{(0)\mu} J_\mu^{(0)}(i+1, \dots, n) \right. \\ &+ \sum_{i=m}^{n-1} \overline{U}^{(0)}(m_q, m+1, \dots, i) \Gamma^{(0)\mu} J_{lc,\mu}^{(1)UV}(i+1, \dots, n) \\ &+ \sum_{i=m}^{n-1} \overline{U}^{(0)}(m_q, m+1, \dots, i) \Gamma^{(0)\mu} J_\mu^{(0)}(i+1, \dots, n) \frac{i [\not{p}_{m_q} + \not{P}(m+1, \dots, n)]}{[p_{m_q} + P(m+1, \dots, n)]^2} \times \\ &\quad \times g_{qq}^{UV, \ell_{qq}=1}(\bar{k}, Q_{m-1}, P(m, \dots, n), \mu_{UV}) \\ &\left. + \sum_{i=m}^{n-1} \overline{U}^{(0)}(m_q, m+1, \dots, i) g_{qqg,lc}^{UV, \ell_{qqg}=0, \lambda}(\bar{k}, \mu_{UV}) J_\mu^{(0)}(i+1, \dots, n) \right] [\not{p}_{m_q} + \not{P}(m+1, \dots, n)] \end{aligned} \quad (\text{G.3})$$

The local UV counterterms $g_{qq}^{UV, \ell_{qq}=1}(\dots)$ and $g_{qqg,lc}^{UV, \ell_{qqg}=0, \lambda}(\dots)$ that appear in the above are the leading color contributions of the local UV counterterms to the quark propagator and to the quark–gluon vertex respectively, as given in appendix D. The recursion terminates with the UV one–current $\overline{U}_{lc}^{(1)UV}(m_q)$, which corresponds to a counterterm for a self–energy correction on an external leg and is thus set to zero, or with the usual tree–level one–currents $J_\mu^{(0)}(l)$ or $\overline{U}^{(0)}(m_q)$.

The unintegrated total local UV subtraction term to the corresponding one–loop primitive am–

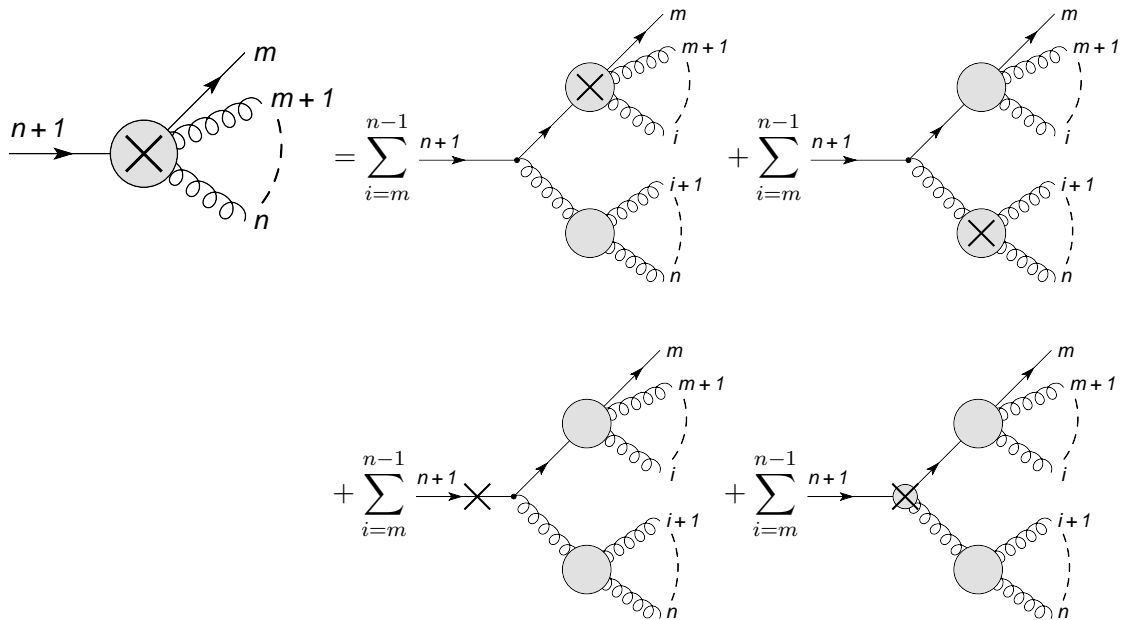


Figure G.2: UV recursion relation to the one-loop quark off-shell current. Wiggly lines denote gluons, straight lines with fermion arrows denote fermions. Crosses denote local UV counterterms. In leading color approximation we need to use the leading color parts of the local UV counterterms.

plitude is recovered from the quark currents by

$$\begin{aligned}
 G_{UV,lc}^{(1)}(1_q, 2, \dots, n-1, n_{\bar{q}}) \\
 = \overline{U}_{lc}^{(1)UV}(1_q, 2, \dots, n-1)(-i)[\not{p}_{1_q} + \not{P}(2, \dots, n-1)]v(p_{n_{\bar{q}}})|_{p_{1_q}+P(2,\dots,n-1)=-p_{n_{\bar{q}}}} \quad (\text{G.4})
 \end{aligned}$$

Since we put the off-shell leg on-shell here again, care has to be taken when a the local UV counterterms to a self-energy correction appears on the off-shell leg. These terms also have to be set to zero.

The UV recursion to the antiquark current for one quark-antiquark pair is depicted in fig.G.3. In formula it reads

$$\begin{aligned}
 V_{lc}^{(1)UV}(m, \dots, n-1, n_{\bar{q}}) &= \frac{i[-(\not{P}(m, \dots, n-1) + \not{p}_{n_{\bar{q}}})]}{[P(m, \dots, n-1) + p_{n_{\bar{q}}}]^2} \times \\
 &\times \left[\sum_{i=m}^{n-1} \Gamma^{(0)\mu} J_{\mu}^{(0)}(m, \dots, i) V_{lc}^{(1)UV}(i+1, \dots, n-1, n_{\bar{q}}) \right. \\
 &+ \sum_{i=m}^{n-1} \Gamma^{(0)\mu} J_{lc,\mu}^{(1)UV}(m, \dots, i) V^{(0)}(i+1, \dots, n-1, n_{\bar{q}}) \\
 &+ \sum_{i=m}^{n-1} \int \frac{d^4 k}{(2\pi)^4} g_{qq}^{UV, \ell_{qq}=1}(\bar{k}, Q_n, P(m, \dots, n), \mu_{UV}) \frac{i[-(\not{P}(m, \dots, n-1) + \not{p}_{n_{\bar{q}}})]}{[P(m, \dots, n-1) + p_{n_{\bar{q}}}]^2} \times \\
 &\quad \times \Gamma^{(0)\mu} J_{\mu}^{(0)}(m, \dots, i) V^{(0)}(i+1, \dots, n-1, n_{\bar{q}}) \\
 &\left. + \sum_{i=m}^{n-1} \int \frac{d^4 k}{(2\pi)^4} g_{qqg,lc}^{UV, \ell_{qq}=0, \lambda}(\bar{k}, \mu_{UV}) J_{\mu}^{(0)}(m, \dots, i) V^{(0)}(i+1, \dots, n-1, n_{\bar{q}}) \right] \quad (\text{G.5})
 \end{aligned}$$

In appendix C we defined in $i\Sigma^{(1)}$ the loop momentum k to sit on the quark line in the loop. For the recursion this means that we have to shift the arbitrary four-vector Q , as described in chapter 4.3, in the definition of $g_{qq}^{UV, \ell_{qq}=1}(\dots)$ to be Q_n instead of Q_{m-1} . The recursion terminates with the UV one-current $V_{lc}^{(1)UV}(n_q)$, which corresponds to a counterterm for a self-energy correction on an external leg and is thus set to zero, or with the usual tree-level one-currents $J_{\mu}^{(0)}(l)$ or $V^{(0)}(m_q)$.

The unintegrated total local UV subtraction term to the corresponding one-loop primitive amplitude is recovered from the antiquark currents by

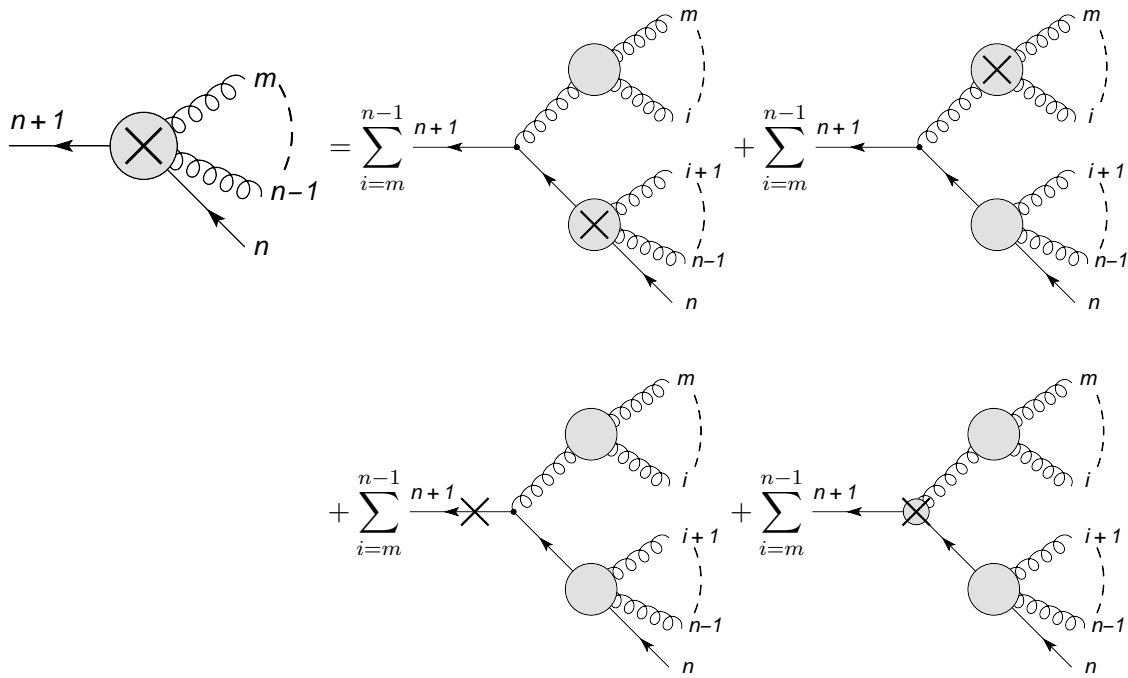


Figure G.3: UV recursion relation to the one-loop antiquark off-shell current. Wiggly lines denote gluons, straight lines with fermion arrows denote fermions. Crosses denote local UV counterterms. In leading color approximation we need to use the leading color parts of the local UV counterterms.

$$\begin{aligned}
G_{UV,lc}^{(1)}(1_q, 2, \dots, n-1, n_{\bar{q}}) \\
= \bar{u}(p_{1_q})(-i) \left[-(\not{P}(2, \dots, n-1) + \not{p}_{n_{\bar{q}}}) \right] V_{lc}^{(1)UV}(2, \dots, n-1, n_{\bar{q}}) |_{P(2, \dots, n-1) + p_{n_{\bar{q}}} = -p_{1_q}} \quad (\text{G.6})
\end{aligned}$$

Since we put the off-shell leg on-shell here again, care has to be taken when a the local UV counterterms to a self-energy correction appears on the off-shell leg. These terms also have to be set to zero.

G.3 UV Recursion for $e^+e^- \rightarrow (n-2)$ jets

The kinematics of the incoming e^+e^- -pair have been described above, where the electron and positron are taken to be as incoming particles with an incoming electron momentum $p_{e^-}^{in} = -p_n$ and an incoming positron momentum $p_{e^+}^{in} = -p_{n-1}$. The UV subtraction term to this process is depicted in figure G.4, the corresponding recursion start in figure G.5. The integrand to the corresponding primitive amplitude reads

$$\begin{aligned}
G_{e^+e^- \rightarrow (n-2)\text{jets},lc}^{(1)UV} &= G^{(1)UV}(1_q, 2_g, \dots, (n-3)_g, (n-2)_{\bar{q}}, (n-1)_l, n_{\bar{l}}) \\
&= \mathcal{Q}_{UV,start}^{(1)\mu}(1_q, 2, \dots, n-3, (n-2)_{\bar{q}}) J_{\mu}^{(0)EW}((n-1)_l, n_{\bar{l}}) \quad (\text{G.7})
\end{aligned}$$

with $J_{\mu}^{(0)EW}((n-1)_l, n_{\bar{l}}) = \bar{v}(-p_{n-1}) V_{ll\gamma/Z}^{(0)\alpha} u(-p_n) P_{\alpha\mu}^{\gamma/Z}$ and where the recursion start for the corresponding unintegrated UV current $\mathcal{Q}_{UV,start}^{(1)\mu}(1_q, 2, \dots, n-3, (n-2)_{\bar{q}})$ is given by

$$\begin{aligned}
\mathcal{Q}_{UV,start}^{(1)\mu}(1_q, 2, \dots, n-3, (n-2)_{\bar{q}}) &= \\
&\sum_{i=1}^{n-3} \bar{U}_{lc}^{(1)UV}(1_q, 2, \dots, i) V_{qq\gamma/Z}^{(0)\mu} V^{(0)}(i+1, \dots, n-3, (n-2)_{\bar{q}}) \\
&+ \sum_{i=1}^{n-3} \bar{U}^{(0)}(1_q, 2, \dots, i) V_{qq\gamma/Z}^{(0)\mu} V_{lc}^{(1)UV}(i+1, \dots, n-3, (n-2)_{\bar{q}}) \\
&+ \sum_{i=1}^{n-3} \bar{U}^{(0)}(1_q, 2, \dots, i) g_{qqg,sc}^{UV,\ell_{qqg}=0,\mu}(\bar{k}, \mu_{UV}) V^{(0)}(i+1, \dots, n-3, (n-2)_{\bar{q}}) \quad (\text{G.8})
\end{aligned}$$

with $V_{ll\gamma/Z}^{(0)\mu}$ and $V_{qq\gamma/Z}^{(0)\mu}$ the appropriate γ/Z -fermion vertices and $P_{\mu\nu}^{\gamma/Z}$ the appropriate γ/Z propagator. We drop the propagator in the start routine $\mathcal{Q}_{UV,start}^{(1)\mu}(1_q, 2, \dots, n-3, (n-2)_{\bar{q}})$ since it is included already in $J_{\mu}^{(0)EW}((n-1)_l, n_{\bar{l}})$.

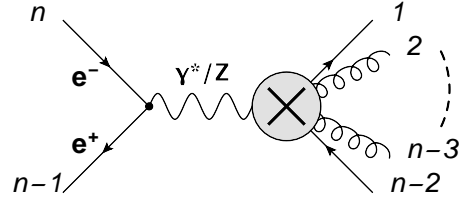


Figure G.4: UV subtraction term to $e^+e^- \rightarrow (n-2)$ jets in leading color approximation. We choose the leptons as incoming.

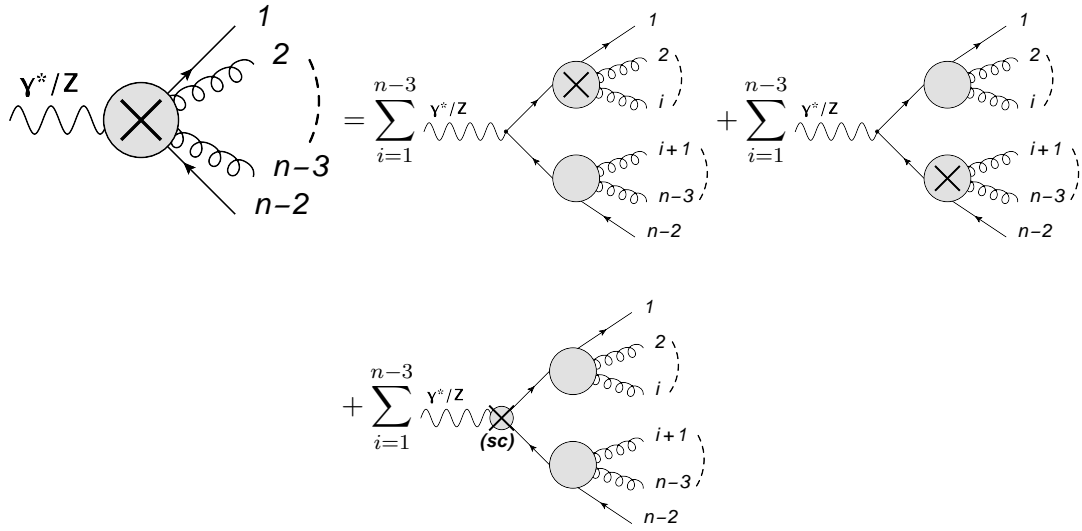


Figure G.5: Recursion start $\mathcal{Q}_{UV,start}^{(1)\mu}(1_q, 2, \dots, n-3, (n-2)_{\bar{q}})$ to the unintegrated UV counterterm in $e^+e^- \rightarrow (n-2)$ jets in leading color approximation. Wiggly lines denote gluons, straight lines with fermion arrows denote fermions.

In the third term in equation G.8 above we use $g_{qqg,sc}^{UV,\ell_{qqg}=0,\mu}(\bar{k}, \mu_{UV})$ instead of $g_{qqg,lc}^{UV,\ell_{qqg}=0,\mu}(\bar{k}, \mu_{UV})$. The subleading color term (*sc*) is the one that has to be used here in the start routine, since the leading color term (*lc*) does not contain a tree-level quark-boson vertex on the side of the external boson.

Appendix H

Monte Carlo Integration and Phase–Space Points for Small Two–Particle Invariants

In this appendix we want to give a brief overview on Monte Carlo integration and on the generation of phase–space points with small two–particle invariants, as used for the UV scaling plot at the end of chapter 4.4. Most of the contents below can be found in [19] and we introduce them here only in order to have a certain complete picture at hand.

H.1 Monte Carlo Integration

The Monte Carlo estimate for an integral of a function $f(u_1, \dots, u_d)$, depending on the variables u_1, \dots, u_d , over the unit hypercube $[0, 1]^d$

$$I = \int dx f(x) \equiv \int d^d u f(u_1, \dots, u_d) \quad (\text{H.1})$$

is given by

$$E = \frac{1}{N} \sum_{n=1}^N f(x_n) \quad (\text{H.2})$$

Due to the law of large numbers the Monte Carlo estimate converges to the true value of the integral

$$\lim_{N \rightarrow \infty} \frac{1}{N} \sum_{n=1}^N f(x_n) = I \quad (\text{H.3})$$

With the variance $\sigma^2(f)$ of the function $f(x)$ given by $\sigma^2(f) = \int dx (f(x) - I)^2$ we can show that

$$\int dx_1 \dots \int dx_N \left(\frac{1}{N} \sum_{n=1}^N f(x_n) - I \right)^2 = \frac{\sigma^2(f)}{N} \quad (\text{H.4})$$

which tells us that the error in the Monte Carlo estimate is on average $\sigma(f)/\sqrt{N}$ and shows essentially that the error in a Monte Carlo scales like $1/\sqrt{N}$, independent of the integration dimension d . In practice we can only have a finite number of Monte Carlo evaluations N , where one uses the Monte Carlo estimate

$$S^2 = \frac{1}{N-1} \sum_{n=1}^N (f(x_n) - E)^2 = \frac{1}{N} \sum_{n=1}^N (f(x_n))^2 - E^2 \quad (\text{H.5})$$

Although we have the advantage that the Monte Carlo error is independent of the integration dimension d , we have the disadvantage that the integral converges relatively slow to the true value. In order to enhance the behavior compared to the crude Monte Carlo there are several techniques, of which two important ones are stratified sampling and importance sampling.

In stratified sampling the integration space is divided into several subspaces, where in each a Monte Carlo integration is performed. Therefore one splits the integration region $M = [0, 1]^d$ into k subregions M_j , where $j = 1, \dots, k$ and performs in each subregion a Monte Carlo integration with N_j points. One then obtains the estimate

$$E = \sum_{j=1}^k \frac{\text{vol}(M_j)}{N_j} \sum_{n=1}^{N_j} f(x_{jn}) \quad (\text{H.6})$$

and instead of the variance $\sigma(f)/\sqrt{N}$ one has then the expression

$$\sum_{j=1}^k \frac{\text{vol}(M_j)}{N_j} \left(\int_{M_j} dx f(x)^2 - \frac{1}{\text{vol}(M_j)} \left(\int_{M_j} dx f(x) \right)^2 \right) \quad (\text{H.7})$$

If the subspaces and the corresponding numbers of points are chosen carefully, this can lead to a significant reduction in the variance, compared to the crude Monte Carlo.

Importance sampling corresponds to a change of integration variables according to

$$\int dx f(x) = \int \frac{f(x)}{p(x)} p(x) dx \equiv \int \frac{f(x)}{p(x)} dP(x) \quad (\text{H.8})$$

with $p(x) = \frac{\partial^d}{\partial x_1 \dots \partial x_d} P(x)$. If $p(x)$ is chosen as positive-valued and normalized to $\int dx p(x) = 1$ then $p(x)$ may be interpreted as probability density function. If one further has a random number generator for the distribution $P(x)$ then the integral may be estimated from a therefrom generated sample x_1, \dots, x_N of random numbers by

$$E = \frac{1}{N} \sum_{n=1}^N \frac{f(x_n)}{p(x_n)} \quad (\text{H.9})$$

The statistical error of the Monte Carlo integration is then given by $\sigma(f/p)/\sqrt{N}$ and an estimator for the variance $\sigma^2(f/p)$ by

$$S = \frac{1}{N} \sum_{n=1}^N \left(\frac{f(x_n)}{p(x_n)} \right)^2 - E^2 \quad (\text{H.10})$$

The relevant quantity is now $f(x)/p(x)$ and one tries to choose $p(x)$ as close in shape as possible to $f(x)$, where in practice one chooses $p(x)$ such that it approximates $|f(x)|$ reasonably well in shape and such that one can generate random points according to $P(x)$. It is, however, dangerous to choose functions $p(x)$ that become zero or approach zero too quickly.

In many cases it is quite difficult to estimate the behavior of the functions to be integrated. In particle physics for example the integrands to the phase-space integrals for a large number of particles possess a quite complicated peak structure, which is usually not known a priori. One prefers adaptive techniques in these cases, where e.g. the VEGAS algorithm [152] combines the basic ideas of stratified sampling and importance sampling in an iterative algorithm which learns about the function as it proceeds. VEGAS concentrates most on those regions where the integrand has the largest contribution. The strategy is thereby to subdivide the integration space into a rectangular grid and to perform integrations in each subspace on the grid. The results of this first iterative step are then used to adjust the grid for the next iteration, according

to the information about the dominant contributions gained from the first step. VEGAS tries therefore to approximate the optimal density function

$$p_{opt}(x) = \frac{|f(x)|}{\int dx |f(x)|} \quad (\text{H.11})$$

by a step function. Due to storage requirements one has to use separable density function in d dimensions $p(u_1, \dots, u_d) = p_1(u_1) \cdot \dots \cdot p_d(u_d)$. Further details about the various variance reduction techniques and about VEGAS can be found in [19], from where the above excerpt is taken.

H.2 Generating Phase–Space Points for Small Two–Particle Invariants

In this section we want to give a prescription of how to produce specific phase–space points with a small two–particle invariant, for the usage in the UV scaling plot which has been shown at then end of chapter 4.4. There are more efficient ways in order to generate such phase–space configurations, and we stress that the following is only used in the generation of the aforementioned plot, where essentially the ideas in [153] have been used.

In order to generate a phase–space point where two particles give rise to a small two–particle invariant we consider first a phase–space point for $(n - 1)$ massless particles, with $p_1^2 = \dots = p_{n-1}^2 = 0$ and a center–of–mass energy $p_1^0 + \dots + p_{n-1}^0 = Q$. The p_i are the external four–momenta of the massless particles and p_i^0 denotes their time–components respectively.

Now we take on the following equation

$$f(\xi) = Q - \sum_{i=1}^{n-1} \sqrt{m_i^2 + \xi^2 (p_i^0)^2} = 0 \quad (\text{H.12})$$

for $m_1 = \lambda_{coll}$ and $m_i = 0$ if $i > 1$, which leads to

$$f(\xi) = Q - \sqrt{\lambda_{coll}^2 + \xi^2 (p_1^0)^2} - \sum_{i=2}^{n-1} \sqrt{\xi^2 (p_i^0)^2} = 0 \quad (\text{H.13})$$

and solve (numerically) for ξ . It actually suffices to find one ξ which satisfies the equation. We consider then the following transformation

$$\tilde{p}_i^0 = \sqrt{m_i^2 + \xi^2(p_i^0)^2} \quad \text{and} \quad \tilde{\vec{p}}_i = \xi \vec{p}_i \quad (\text{H.14})$$

for $m_1 = \lambda_{coll}$ and $m_i = 0$ if $i > 1$, which leads to

$$\tilde{p}_1^0 = \sqrt{\lambda_{coll}^2 + \xi^2(p_1^0)^2} \quad \text{and} \quad \tilde{\vec{p}}_1 = \xi \vec{p}_1 \quad \text{for} \quad i = 1 \quad (\text{H.15})$$

$$\tilde{p}_i^0 = \sqrt{\xi^2(p_i^0)^2} \quad \text{and} \quad \tilde{\vec{p}}_i = \xi \vec{p}_i \quad \text{for} \quad i = 2, \dots, n-1 \quad (\text{H.16})$$

We have thus obtained a phase-space point for $(n-1)$ particles, where one particle is massive and $(n-2)$ particles are massless, with $\tilde{p}_1^2 = \lambda_{coll}^2$ and $\tilde{p}_2^2 = \dots = \tilde{p}_{n-1}^2 = 0$ respectively, and the center-of-mass energy is still given by $\tilde{p}_1^0 + \dots + \tilde{p}_{n-1}^0 = Q$.

We go on and determine further the parameters of a Lorentz transformation Λ , which transforms a four-vector with center-of-mass energy λ_{coll} from its rest-frame to $(\tilde{p}_1^0, \tilde{\vec{p}}_1)$, via $(\tilde{p}_1^0, \tilde{\vec{p}}_1) = \Lambda(\lambda_{coll}, \vec{0})$.

In a subsequent step we define two massless four-vectors with back-to-back spatial components via $\hat{p}_0 = (\frac{\lambda_{coll}}{2}, \vec{a})$ and $\hat{p}_1 = (\frac{\lambda_{coll}}{2}, -\vec{a})$ respectively. Upon $\hat{p}_0^2 = \hat{p}_1^2 = 0$ we see that the absolute value of \vec{a} is then determined by $\vec{a}^2 = \frac{\lambda_{coll}^2}{4}$ and we can for example choose \vec{a} such that $\vec{a} \perp \tilde{\vec{p}}_1$ and $|\vec{a}| = \frac{\lambda_{coll}}{2}$.

We now boost the vectors \hat{p}_0 and \hat{p}_1 , according to the Lorentz transformation Λ whose parameters we just have determined, to gain two new vectors

$$\hat{p}'_0 = \Lambda(\hat{p}_0) \quad \text{and} \quad \hat{p}'_1 = \Lambda(\hat{p}_1) \quad (\text{H.17})$$

Upon collecting the set of four-vectors $\{\hat{p}'_0, \hat{p}'_1, \tilde{p}_2, \dots, \tilde{p}_{n-1}\}$ we have thus created an n -particle phase-space point with n massless particles, where two of the four-vectors, namely \hat{p}'_0 and \hat{p}'_1 , have a common invariant mass λ_{coll} which can be varied to our will. If we choose to gradually decrease the value of λ_{coll} to a small value λ_{coll}^{small} , we subsequently generate an n -particle phase-space point for n massless particles at a certain center-of-mass energy Q , where the two four-vectors \hat{p}'_0 and \hat{p}'_1 give rise to a small two-particle invariant λ_{coll}^{small} .

Further details of how to generate an initial $(n-1)$ -particle phase-space in the first place and how to parametrize the Lorentz transformation Λ can be found in [121, 19]. Therein given is

H.2 Generating Phase-Space Points for Small Two-Particle Invariants

for example an algorithm which generates phase-space configurations according to the collinear and soft regions of the matrix elements and is ideally suited for the generation of final-state phase-space configurations for the process $e^+e^- \rightarrow jets$ and subsequent Monte Carlo integration with VEGAS.

Bibliography

- [1] Georges Aad et al. “Observation of a new particle in the search for the Standard Model Higgs boson with the ATLAS detector at the LHC”. In: *Phys.Lett.* B716 (2012), pp. 1–29. DOI: 10.1016/j.physletb.2012.08.020. eprint: 1207.7214.
- [2] Serguei Chatrchyan et al. “Observation of a new boson at a mass of 125 GeV with the CMS experiment at the LHC”. In: *Phys.Lett.* B716 (2012), pp. 30–61. DOI: 10.1016/j.physletb.2012.08.021. eprint: 1207.7235.
- [3] Rikkert Frederix, Stefano Frixione, Kirill Melnikov, and Giulia Zanderighi. “NLO QCD corrections to five-jet production at LEP and the extraction of $\alpha_s(M_Z)$ ”. In: *JHEP* 1011 (2010), p. 050. DOI: 10.1007/JHEP11(2010)050. eprint: 1008.5313.
- [4] Torbjorn Sjostrand, Stephen Mrenna, and Peter Z. Skands. “A Brief Introduction to PYTHIA 8.1”. In: *Comput.Phys.Commun.* 178 (2008), pp. 852–867. DOI: 10.1016/j.cpc.2008.01.036. eprint: 0710.3820.
- [5] M. Bahr, S. Gieseke, M.A. Gigg, D. Grellscheid, K. Hamilton, et al. “Herwig++ Physics and Manual”. In: *Eur.Phys.J.* C58 (2008), pp. 639–707. DOI: 10.1140/epjc/s10052-008-0798-9. eprint: 0803.0883.
- [6] T. Gleisberg, Stefan. Hoeche, F. Krauss, M. Schonherr, S. Schumann, et al. “Event generation with SHERPA 1.1”. In: *JHEP* 0902 (2009), p. 007. DOI: 10.1088/1126-6708/2009/02/007. eprint: 0811.4622.
- [7] C. Buttar, S. Dittmaier, V. Drollinger, S. Frixione, A. Nikitenko, et al. “Les houches physics at TeV colliders 2005, standard model and Higgs working group: Summary report”. In: (2006). eprint: hep-ph/0604120.
- [8] Stefan Weinzierl. “Automated calculations for multi-leg processes”. In: *PoS ACAT* (2007), p. 005. eprint: 0707.3342.
- [9] V.N. Gribov and L.N. Lipatov. “Deep inelastic e p scattering in perturbation theory”. In: *Sov.J.Nucl.Phys.* 15 (1972), pp. 438–450.

-
- [10] Guido Altarelli and G. Parisi. “Asymptotic Freedom in Parton Language”. In: *Nucl.Phys.* B126 (1977), p. 298. DOI: 10.1016/0550-3213(77)90384-4.
- [11] Yuri L. Dokshitzer. “Calculation of the Structure Functions for Deep Inelastic Scattering and $e^+ e^-$ Annihilation by Perturbation Theory in Quantum Chromodynamics.” In: *Sov.Phys.JETP* 46 (1977), pp. 641–653.
- [12] Andy Buckley, Jonathan Butterworth, Stefan Gieseke, David Grellscheid, Stefan Hoche, et al. “General-purpose event generators for LHC physics”. In: *Phys.Rept.* 504 (2011), pp. 145–233. DOI: 10.1016/j.physrep.2011.03.005. eprint: 1101.2599.
- [13] Stefan Weinzierl. “Jet algorithms in electron-positron annihilation: Perturbative higher order predictions”. In: *Eur.Phys.J.* C71 (2011), p. 1565. DOI: 10.1140/epjc/s10052-011-1717-z, 10.1140/epjc/s10052-011-1565-x. eprint: 1011.6247.
- [14] J. Beringer et al. “Review of Particle Physics (RPP)”. In: *Phys.Rev.* D86 (2012), p. 010001. DOI: 10.1103/PhysRevD.86.010001.
- [15] S. Dittmaier, P. Uwer, and S. Weinzierl. “NLO QCD corrections to t anti- t + jet production at hadron colliders”. In: *Phys.Rev.Lett.* 98 (2007), p. 262002. DOI: 10.1103/PhysRevLett.98.262002. eprint: hep-ph/0703120.
- [16] Byckling E. and Kajantie K. *Particle Kinematics*. John Wiley & Sons, 1973.
- [17] T. Kinoshita. “Mass singularities of Feynman amplitudes”. In: *J.Math.Phys.* 3 (1962), pp. 650–677.
- [18] T.D. Lee and M. Nauenberg. “Degenerate Systems and Mass Singularities”. In: *Phys.Rev.* 133 (1964), B1549–B1562. DOI: 10.1103/PhysRev.133.B1549.
- [19] Stefan Weinzierl. “Introduction to Monte Carlo methods”. In: (2000). eprint: hep-ph/0006269.
- [20] Zoltan Kunszt and Davison E. Soper. “Calculation of jet cross-sections in hadron collisions at order α_s^3 ”. In: *Phys.Rev.* D46 (1992), pp. 192–221. DOI: 10.1103/PhysRevD.46.192.
- [21] Z. Kunszt, P. Nason, G. Marchesini, and B.R. Webber. “QCD AT LEP”. In: (1989).
- [22] R. Keith Ellis, D.A. Ross, and A.E. Terrano. “The Perturbative Calculation of Jet Structure in $e^+ e^-$ Annihilation”. In: *Nucl.Phys.* B178 (1981), p. 421. DOI: 10.1016/0550-3213(81)90165-6.

-
- [23] Stephen D. Ellis, Zoltan Kunszt, and Davison E. Soper. “The One Jet Inclusive Cross-Section at Order α_s^3 . 1. Gluons Only”. In: *Phys.Rev.* D40 (1989), p. 2188. DOI: 10.1103/PhysRevD.40.2188.
- [24] Stephen D. Ellis, Zoltan Kunszt, and Davison E. Soper. “Two jet production in hadron collisions at order α_s^3 in QCD”. In: *Phys.Rev.Lett.* 69 (1992), pp. 1496–1499. DOI: 10.1103/PhysRevLett.69.1496.
- [25] Michelangelo L. Mangano, Paolo Nason, and Giovanni Ridolfi. “Heavy quark correlations in hadron collisions at next-to-leading order”. In: *Nucl.Phys.* B373 (1992), pp. 295–345. DOI: 10.1016/0550-3213(92)90435-E.
- [26] S. Catani and M. H. Seymour. “The Dipole Formalism for the Calculation of QCD Jet Cross Sections at Next-to-Leading Order”. In: *Phys. Lett.* B378 (1996), pp. 287–301. DOI: 10.1016/0370-2693(96)00425-X. eprint: hep-ph/9602277.
- [27] S. Catani and M. H. Seymour. “A general algorithm for calculating jet cross sections in NLO QCD”. In: *Nucl. Phys.* B485 (1997), pp. 291–419. DOI: 10.1016/S0550-3213(96)00589-5. eprint: hep-ph/9605323.
- [28] Stefano Catani, Stefan Dittmaier, Michael H. Seymour, and Zoltan Trocsanyi. “The Dipole formalism for next-to-leading order QCD calculations with massive partons”. In: *Nucl.Phys.* B627 (2002), pp. 189–265. DOI: 10.1016/S0550-3213(02)00098-6. eprint: hep-ph/0201036.
- [29] Stefan Dittmaier. “A General approach to photon radiation off fermions”. In: *Nucl.Phys.* B565 (2000), pp. 69–122. DOI: 10.1016/S0550-3213(99)00563-5. eprint: hep-ph/9904440.
- [30] Lukas Phaf and Stefan Weinzierl. “Dipole formalism with heavy fermions”. In: *JHEP* 0104 (2001), p. 006. eprint: hep-ph/0102207.
- [31] Stefan Weinzierl. “Automated computation of spin- and colour-correlated Born matrix elements”. In: *Eur. Phys. J.* C45 (2006), pp. 745–757. DOI: 10.1140/epjc/s2005-02467-6. eprint: hep-ph/0510157.
- [32] Daniel Goetz, Christopher Schwan, and Stefan Weinzierl. “Random Polarizations of the Dipoles”. In: (2012). eprint: 1205.4109.
- [33] Gerard 't Hooft and M.J.G. Veltman. “Scalar One Loop Integrals”. In: *Nucl.Phys.* B153 (1979), pp. 365–401. DOI: 10.1016/0550-3213(79)90605-9.

-
- [34] G. Passarino and M.J.G. Veltman. “One Loop Corrections for $e^+ e^-$ Annihilation Into $\mu^+ \mu^-$ in the Weinberg Model”. In: *Nucl.Phys.* B160 (1979), p. 151. DOI: 10.1016/0550-3213(79)90234-7.
- [35] Ansgar Denner and S. Dittmaier. “Reduction schemes for one-loop tensor integrals”. In: *Nucl.Phys.* B734 (2006), pp. 62–115. DOI: 10.1016/j.nuclphysb.2005.11.007. eprint: hep-ph/0509141.
- [36] Ansgar Denner and S. Dittmaier. “Reduction of one loop tensor five point integrals”. In: *Nucl.Phys.* B658 (2003), pp. 175–202. DOI: 10.1016/S0550-3213(03)00184-6. eprint: hep-ph/0212259.
- [37] Stefan Dittmaier. “Separation of soft and collinear singularities from one loop N point integrals”. In: *Nucl.Phys.* B675 (2003), pp. 447–466. DOI: 10.1016/j.nuclphysb.2003.10.003. eprint: hep-ph/0308246.
- [38] A. Denner and S. Dittmaier. “Scalar one-loop 4-point integrals”. In: *Nucl.Phys.* B844 (2011), pp. 199–242. DOI: 10.1016/j.nuclphysb.2010.11.002. eprint: 1005.2076.
- [39] W.T. Giele and E.W. Nigel Glover. “A Computational formalism for one loop integrals”. In: *JHEP* 0404 (2004), p. 029. DOI: 10.1088/1126-6708/2004/04/029. eprint: hep-ph/0402152.
- [40] Andre van Hameren, Jens Vollinga, and Stefan Weinzierl. “Automated computation of one-loop integrals in massless theories”. In: *Eur.Phys.J.* C41 (2005), pp. 361–375. DOI: 10.1140/epjc/s2005-02229-6. eprint: hep-ph/0502165.
- [41] R. Keith Ellis, W.T. Giele, and G. Zanderighi. “Semi-numerical evaluation of one-loop corrections”. In: *Phys.Rev.* D73 (2006), p. 014027. DOI: 10.1103/PhysRevD.73.014027. eprint: hep-ph/0508308.
- [42] J. Fleischer and T. Riemann. “A Complete algebraic reduction of one-loop tensor Feynman integrals”. In: *Phys.Rev.* D83 (2011), p. 073004. DOI: 10.1103/PhysRevD.83.073004. eprint: 1009.4436.
- [43] T. Diakonidis, J. Fleischer, T. Riemann, and J.B. Tausk. “A Recursive reduction of tensor Feynman integrals”. In: *Phys.Lett.* B683 (2010), pp. 69–74. DOI: 10.1016/j.physletb.2009.11.049. eprint: 0907.2115.
- [44] J. Fleischer, T. Riemann, and V. Yundin. “PJFry: A C++ package for tensor reduction of one-loop Feynman intergals”. In: (2011).
- [45] Roberto Pittau. “Formulae for a numerical computation of one-loop tensor integrals”. In: (2004). eprint: hep-ph/0406105.

-
- [46] T. Binoth, G. Heinrich, and N. Kauer. “A Numerical evaluation of the scalar hexagon integral in the physical region”. In: *Nucl.Phys.* B654 (2003), pp. 277–300. DOI: 10.1016/S0550-3213(03)00052-X. eprint: hep-ph/0210023.
- [47] T. Binoth, J. Ph. Guillet, G. Heinrich, E. Pilon, and C. Schubert. “An Algebraic/numerical formalism for one-loop multi-leg amplitudes”. In: *JHEP* 0510 (2005), p. 015. DOI: 10.1088/1126-6708/2005/10/015. eprint: hep-ph/0504267.
- [48] Janusz Gluza, Krzysztof Kajda, Tord Riemann, and Valery Yundin. “Numerical Evaluation of Tensor Feynman Integrals in Euclidean Kinematics”. In: *Eur.Phys.J.* C71 (2011), p. 1516. DOI: 10.1140/epjc/s10052-010-1516-y. eprint: 1010.1667.
- [49] F. del Aguila and R. Pittau. “Recursive numerical calculus of one-loop tensor integrals”. In: *JHEP* 0407 (2004), p. 017. DOI: 10.1088/1126-6708/2004/07/017. eprint: hep-ph/0404120.
- [50] A. van Hameren. “Recursive calculation of multi-gluon one-loop amplitudes”. In: *Acta Phys.Polon.* B40 (2009), pp. 3119–3125.
- [51] A. van Hameren. “Multi-gluon one-loop amplitudes using tensor integrals”. In: *JHEP* 0907 (2009), p. 088. DOI: 10.1088/1126-6708/2009/07/088. eprint: 0905.1005.
- [52] Zvi Bern, Lance J. Dixon, David C. Dunbar, and David A. Kosower. “Fusing gauge theory tree amplitudes into loop amplitudes”. In: *Nucl.Phys.* B435 (1995), pp. 59–101. DOI: 10.1016/0550-3213(94)00488-Z. eprint: hep-ph/9409265.
- [53] C.F. Berger, Z. Bern, L.J. Dixon, F. Febres Cordero, D. Forde, et al. “An Automated Implementation of On-Shell Methods for One-Loop Amplitudes”. In: *Phys.Rev.* D78 (2008), p. 036003. DOI: 10.1103/PhysRevD.78.036003. eprint: 0803.4180.
- [54] Darren Forde. “Direct extraction of one-loop integral coefficients”. In: *Phys.Rev.* D75 (2007), p. 125019. DOI: 10.1103/PhysRevD.75.125019. eprint: 0704.1835.
- [55] Giovanni Ossola, Costas G. Papadopoulos, and Roberto Pittau. “Reducing full one-loop amplitudes to scalar integrals at the integrand level”. In: *Nucl.Phys.* B763 (2007), pp. 147–169. DOI: 10.1016/j.nuclphysb.2006.11.012. eprint: hep-ph/0609007.
- [56] Giovanni Ossola, Costas G. Papadopoulos, and Roberto Pittau. “CutTools: A Program implementing the OPP reduction method to compute one-loop amplitudes”. In: *JHEP* 0803 (2008), p. 042. DOI: 10.1088/1126-6708/2008/03/042. eprint: 0711.3596.
- [57] Giovanni Ossola, Costas G. Papadopoulos, and Roberto Pittau. “On the Rational Terms of the one-loop amplitudes”. In: *JHEP* 0805 (2008), p. 004. DOI: 10.1088/1126-6708/2008/05/004. eprint: 0802.1876.

-
- [58] P. Mastrolia, G. Ossola, C.G. Papadopoulos, and R. Pittau. “Optimizing the Reduction of One-Loop Amplitudes”. In: *JHEP* 0806 (2008), p. 030. DOI: 10.1088/1126-6708/2008/06/030. eprint: 0803.3964.
- [59] P. Draggiotis, M.V. Garzelli, C.G. Papadopoulos, and R. Pittau. “Feynman Rules for the Rational Part of the QCD 1-loop amplitudes”. In: *JHEP* 0904 (2009), p. 072. DOI: 10.1088/1126-6708/2009/04/072. eprint: 0903.0356.
- [60] M.V. Garzelli, I. Malamos, and R. Pittau. “Feynman rules for the rational part of the Electroweak 1-loop amplitudes”. In: *JHEP* 1001 (2010), p. 040. DOI: 10.1007/JHEP10(2010)097, 10.1007/JHEP01(2010)040. eprint: 0910.3130.
- [61] A. van Hameren, C.G. Papadopoulos, and R. Pittau. “Automated one-loop calculations: A Proof of concept”. In: *JHEP* 0909 (2009), p. 106. DOI: 10.1088/1126-6708/2009/09/106. eprint: 0903.4665.
- [62] William B. Kilgore. “One-loop Integral Coefficients from Generalized Unitarity”. In: (2007). eprint: 0711.5015.
- [63] Charalampos Anastasiou, Ruth Britto, Bo Feng, Zoltan Kunszt, and Pierpaolo Mastrolia. “Unitarity cuts and Reduction to master integrals in d dimensions for one-loop amplitudes”. In: *JHEP* 0703 (2007), p. 111. DOI: 10.1088/1126-6708/2007/03/111. eprint: hep-ph/0612277.
- [64] Charalampos Anastasiou, Ruth Britto, Bo Feng, Zoltan Kunszt, and Pierpaolo Mastrolia. “D-dimensional unitarity cut method”. In: *Phys.Lett.* B645 (2007), pp. 213–216. DOI: 10.1016/j.physletb.2006.12.022. eprint: hep-ph/0609191.
- [65] Ruth Britto and Bo Feng. “Integral coefficients for one-loop amplitudes”. In: *JHEP* 0802 (2008), p. 095. DOI: 10.1088/1126-6708/2008/02/095. eprint: 0711.4284.
- [66] Ruth Britto and Bo Feng. “Unitarity cuts with massive propagators and algebraic expressions for coefficients”. In: *Phys.Rev.* D75 (2007), p. 105006. DOI: 10.1103/PhysRevD.75.105006. eprint: hep-ph/0612089.
- [67] R. Keith Ellis, W.T. Giele, and Z. Kunszt. “A Numerical Unitarity Formalism for Evaluating One-Loop Amplitudes”. In: *JHEP* 0803 (2008), p. 003. DOI: 10.1088/1126-6708/2008/03/003. eprint: 0708.2398.
- [68] Walter T. Giele, Zoltan Kunszt, and Kirill Melnikov. “Full one-loop amplitudes from tree amplitudes”. In: *JHEP* 0804 (2008), p. 049. DOI: 10.1088/1126-6708/2008/04/049. eprint: 0801.2237.

-
- [69] R. Keith Ellis, W.T. Giele, Zoltan Kunszt, Kirill Melnikov, and Giulia Zanderighi. “One-loop amplitudes for W^+ 3 jet production in hadron collisions”. In: *JHEP* 0901 (2009), p. 012. DOI: 10.1088/1126-6708/2009/01/012. eprint: 0810.2762.
- [70] W.T. Giele and G. Zanderighi. “On the Numerical Evaluation of One-Loop Amplitudes: The Gluonic Case”. In: *JHEP* 0806 (2008), p. 038. DOI: 10.1088/1126-6708/2008/06/038. eprint: 0805.2152.
- [71] R. Keith Ellis, Walter T. Giele, Zoltan Kunszt, and Kirill Melnikov. “Masses, fermions and generalized D -dimensional unitarity”. In: *Nucl.Phys.* B822 (2009), pp. 270–282. DOI: 10.1016/j.nuclphysb.2009.07.023. eprint: 0806.3467.
- [72] Simon Badger, Benedikt Biedermann, and Peter Uwer. “Numerical Evaluation of One-Loop QCD Amplitudes”. In: *J.Phys.Conf.Ser.* 368 (2012), p. 012055. DOI: 10.1088/1742-6596/368/1/012055. eprint: 1112.0412.
- [73] Simon Badger, Benedikt Biedermann, Peter Uwer, and Valery Yundin. “Numerical evaluation of virtual corrections to multi-jet production in massless QCD”. In: (2012). eprint: 1209.0100.
- [74] Stefan Weinzierl. “The Art of computing loop integrals”. In: (2006), pp. 345–395. eprint: hep-ph/0604068.
- [75] Matthias Steinhauser. “Uebungen zu Strahlungskorrekturen, Herbstschule fuer Hochenergiephysik in Maria Laach”. In: (2003).
- [76] Zvi Bern, Lance J. Dixon, and David A. Kosower. “Progress in one loop QCD computations”. In: *Ann.Rev.Nucl.Part.Sci.* 46 (1996), pp. 109–148. DOI: 10.1146/annurev.nucl.46.1.109. eprint: hep-ph/9602280.
- [77] R. Keith Ellis, Zoltan Kunszt, Kirill Melnikov, and Giulia Zanderighi. “One-loop calculations in quantum field theory: from Feynman diagrams to unitarity cuts”. In: *Phys.Rept.* 518 (2012), pp. 141–250. DOI: 10.1016/j.physrep.2012.01.008. eprint: 1105.4319.
- [78] Davison E. Soper. “QCD calculations by numerical integration”. In: *Phys.Rev.Lett.* 81 (1998), pp. 2638–2641. DOI: 10.1103/PhysRevLett.81.2638. eprint: hep-ph/9804454.
- [79] Davison E. Soper. “Techniques for QCD calculations by numerical integration”. In: *Phys.Rev.* D62 (2000), p. 014009. DOI: 10.1103/PhysRevD.62.014009. eprint: hep-ph/9910292.
- [80] Davison E. Soper. “Choosing integration points for QCD calculations by numerical integration”. In: *Phys. Rev.* D64 (2001), p. 034018. DOI: 10.1103/PhysRevD.64.034018. eprint: hep-ph/0103262.

-
- [81] 1 Kramer Michael and Davison E. Soper. “Next-to-leading order numerical calculations in Coulomb gauge”. In: *Phys.Rev.* D66 (2002), p. 054017. DOI: 10.1103/PhysRevD.66.054017. eprint: hep-ph/0204113.
- [82] Zoltan Nagy and Davison E. Soper. “Numerical integration of one-loop Feynman diagrams for N- photon amplitudes”. In: *Phys. Rev.* D74 (2006), p. 093006. DOI: 10.1103/PhysRevD.74.093006. eprint: hep-ph/0610028.
- [83] Wei Gong, Zoltan Nagy, and Davison E. Soper. “Direct numerical integration of one-loop Feynman diagrams for N-photon amplitudes”. In: *Phys. Rev.* D79 (2009), p. 033005. DOI: 10.1103/PhysRevD.79.033005. eprint: 0812.3686.
- [84] Giampiero Passarino. “An Approach toward the numerical evaluation of multiloop Feynman diagrams”. In: *Nucl.Phys.* B619 (2001), pp. 257–312. DOI: 10.1016/S0550-3213(01)00528-4. eprint: hep-ph/0108252.
- [85] Andrea Ferroglia, Massimo Passera, Giampiero Passarino, and Sandro Uccirati. “All purpose numerical evaluation of one loop multileg Feynman diagrams”. In: *Nucl.Phys.* B650 (2003), pp. 162–228. DOI: 10.1016/S0550-3213(02)01070-2. eprint: hep-ph/0209219.
- [86] Charalampos Anastasiou, Stefan Beerli, and Alejandro Daleo. “Evaluating multi-loop Feynman diagrams with infrared and threshold singularities numerically”. In: *JHEP* 0705 (2007), p. 071. DOI: 10.1088/1126-6708/2007/05/071. eprint: hep-ph/0703282.
- [87] Sebastian Becker, Christian Reuschle, and Stefan Weinzierl. “Numerical NLO QCD calculations”. In: *JHEP* 12 (2010), p. 013. DOI: 10.1007/JHEP12(2010)013. eprint: 1010.4187.
- [88] Sebastian Becker and Stefan Weinzierl. “Direct contour deformation with arbitrary masses in the loop”. In: (2012). eprint: 1208.4088.
- [89] Sebastian Becker and Stefan Weinzierl. “Direct numerical integration for multi-loop integrals”. In: (2012). eprint: 1211.0509.
- [90] Sebastian Becker, Daniel Goetz, Christian Reuschle, Christopher Schwan, and Stefan Weinzierl. “NLO results for five, six and seven jets in electron-positron annihilation”. In: *Phys.Rev.Lett.* 108 (2012). 5 pages, p. 032005. DOI: 10.1103/PhysRevLett.108.032005. eprint: 1111.1733.
- [91] Sebastian Becker, Christian Reuschle, and Stefan Weinzierl. “Efficiency Improvements for the Numerical Computation of NLO Corrections”. In: *JHEP* 1207 (2012), p. 090. DOI: 10.1007/JHEP07(2012)090. eprint: 1205.2096.

-
- [92] Zoltan Nagy and Davison E. Soper. “General subtraction method for numerical calculation of one-loop QCD matrix elements”. In: *JHEP* 09 (2003), p. 055. eprint: [hep-ph/0308127](#).
- [93] Mohammad Assadsolimani, Sebastian Becker, and Stefan Weinzierl. “A Simple formula for the infrared singular part of the integrand of one-loop QCD amplitudes”. In: *Phys.Rev.D* 81 (2010), p. 094002. DOI: [10.1103/PhysRevD.81.094002](#). eprint: [0912.1680](#).
- [94] M. Assadsolimani, S. Becker, Ch. Reuschle, and S. Weinzierl. “Infrared singularities in one-loop amplitudes”. In: *Nucl.Phys.Proc.Suppl.* 205-206 (2010), pp. 224–229. DOI: [10.1016/j.nuclphysbps.2010.08.047](#). eprint: [1006.4609](#).
- [95] S. Becker, D. Goetz, C. Reuschle, C. Schwan, and S. Weinzierl. “Multiparton NLO Corrections by Numerical Methods”. In: (2011). eprint: [1112.3521](#).
- [96] S. Becker, D. Goetz, C. Reuschle, C. Schwan, and S. Weinzierl. “Numerical evaluation of NLO multiparton processes”. In: (2012). eprint: [1209.2846](#).
- [97] F. Maltoni, K. Paul, T. Stelzer, and S. Willenbrock. “Color-flow decomposition of QCD amplitudes”. In: *Phys. Rev. D* 67 (2003), p. 014026. DOI: [10.1103/PhysRevD.67.014026](#). eprint: [hep-ph/0209271](#).
- [98] Frits A. Berends and W.T. Giele. “Recursive Calculations for Processes with n Gluons”. In: *Nucl.Phys.* B306 (1988), p. 759. DOI: [10.1016/0550-3213\(88\)90442-7](#).
- [99] Frits A. Berends and W.T. Giele. “Multiple Soft Gluon Radiation in Parton Processes”. In: *Nucl.Phys.* B313 (1989), p. 595. DOI: [10.1016/0550-3213\(89\)90398-2](#).
- [100] Ronald Kleiss and Hans Kuijf. “MULTI - GLUON CROSS-SECTIONS AND FIVE JET PRODUCTION AT HADRON COLLIDERS”. In: *Nucl.Phys.* B312 (1989), p. 616. DOI: [10.1016/0550-3213\(89\)90574-9](#).
- [101] Frits A. Berends, W.T. Giele, and H. Kuijf. “EXACT AND APPROXIMATE EXPRESSIONS FOR MULTI - GLUON SCATTERING”. In: *Nucl.Phys.* B333 (1990), p. 120. DOI: [10.1016/0550-3213\(90\)90225-3](#).
- [102] Stephen J. Parke and T.R. Taylor. “An Amplitude for n Gluon Scattering”. In: *Phys.Rev.Lett.* 56 (1986), p. 2459. DOI: [10.1103/PhysRevLett.56.2459](#).
- [103] Michelangelo L. Mangano, Stephen J. Parke, and Zhan Xu. “Dual Amplitudes and Multi - Gluon Processes”. In: (1987).
- [104] Michelangelo L. Mangano and Stephen J. Parke. “Soft and Collinear Behavior of Dual Amplitudes”. In: (1987).

-
- [105] Michelangelo L. Mangano, Stephen J. Parke, and Zhan Xu. “Duality and Multi - Gluon Scattering”. In: *Nucl.Phys.* B298 (1988), p. 653. DOI: 10.1016/0550-3213(88)90001-6.
- [106] Michelangelo L. Mangano. “The Color Structure of Gluon Emission”. In: *Nucl.Phys.* B309 (1988), p. 461. DOI: 10.1016/0550-3213(88)90453-1.
- [107] Stephen J. Parke and Michelangelo L. Mangano. “The Structure of Gluon Radiation in QCD”. In: (1989).
- [108] Gerard 't Hooft. “A Planar Diagram Theory for Strong Interactions”. In: *Nucl.Phys.* B72 (1974), p. 461. DOI: 10.1016/0550-3213(74)90154-0.
- [109] Hong-Mo Chan and Jack E. Paton. “Generalized Veneziano Model with Isospin”. In: *Nucl.Phys.* B10 (1969), p. 516.
- [110] Z. Koba and Nielsen H.B. “Reaction Amplitude for n-Mesons. A Generalization of the Veneziano-Bardakci-Ruegg-Virasoro Model”. In: *Nucl.Phys.* B10 (1969), p. 633.
- [111] Michelangelo L. Mangano and Stephen J. Parke. “Quark - Gluon Amplitudes in the Dual Expansion”. In: *Nucl.Phys.* B299 (1988), p. 673. DOI: 10.1016/0550-3213(88)90368-9.
- [112] David A. Kosower. “COLOR FACTORIZATION FOR FERMIONIC AMPLITUDES”. In: *Nucl.Phys.* B315 (1989), p. 391. DOI: 10.1016/0550-3213(89)90361-1.
- [113] Michelangelo L. Mangano and Stephen J. Parke. “Multi-Parton Amplitudes in Gauge Theories”. In: *Phys. Rept.* 200 (1991), pp. 301-367. DOI: 10.1016/0370-1573(91)90091-Y. eprint: [hep-th/0509223](#).
- [114] Zvi Bern and David A. Kosower. “Color decomposition of one loop amplitudes in gauge theories”. In: *Nucl. Phys.* B362 (1991), pp. 389-448. DOI: 10.1016/0550-3213(91)90567-H.
- [115] Zvi Bern and David A. Kosower. “The Computation of loop amplitudes in gauge theories”. In: *Nucl.Phys.* B379 (1992), pp. 451-561. DOI: 10.1016/0550-3213(92)90134-W.
- [116] Zvi Bern, Lance J. Dixon, David C. Dunbar, and David A. Kosower. “One-loop n-point gauge theory amplitudes, unitarity and collinear limits”. In: *Nucl.Phys.* B425 (1994), pp. 217-260. DOI: 10.1016/0550-3213(94)90179-1. eprint: [hep-ph/9403226](#).
- [117] Zvi Bern, Lance J. Dixon, and David A. Kosower. “One loop corrections to two quark three gluon amplitudes”. In: *Nucl. Phys.* B437 (1995), pp. 259-304. DOI: 10.1016/0550-3213(94)00542-M. eprint: [hep-ph/9409393](#).

-
- [118] Vittorio Del Duca, William B. Kilgore, and Fabio Maltoni. “Multiphoton amplitudes for next-to-leading order QCD”. In: *Nucl.Phys.* B566 (2000), pp. 252–274. DOI: 10.1016/S0550-3213(99)00663-X. eprint: hep-ph/9910253.
- [119] Vittorio Del Duca, Lance J. Dixon, and Fabio Maltoni. “New color decompositions for gauge amplitudes at tree and loop level”. In: *Nucl. Phys.* B571 (2000), pp. 51–70. DOI: 10.1016/S0550-3213(99)00809-3. eprint: hep-ph/9910563.
- [120] Harald Ita and Kemal Ozeren. “Colour Decompositions of Multi-quark One-loop QCD Amplitudes”. In: *JHEP* 1202 (2012), p. 118. DOI: 10.1007/JHEP02(2012)118. eprint: 1111.4193.
- [121] S. Weinzierl. “QCD corrections to $e^+ e^- \rightarrow j$ 4jets”. In: (1998).
- [122] Stefan Weinzierl and David A. Kosower. “QCD corrections to four jet production and three jet structure in $e^+ e^-$ annihilation”. In: *Phys.Rev.* D60 (1999), p. 054028. DOI: 10.1103/PhysRevD.60.054028. eprint: hep-ph/9901277.
- [123] Simon Badger, Benedikt Biedermann, Peter Uwer, and Valery Yundin. “NLO QCD corrections to multi-jet production at the LHC with a centre-of-mass energy of $\sqrt{s}=8$ TeV”. In: (2012). eprint: 1209.0098.
- [124] P. De Causmaecker, R. Gastmans, W. Troost, and Tai Tsun Wu. “Helicity Amplitudes for Massless QED”. In: *Phys.Lett.* B105 (1981), p. 215. DOI: 10.1016/0370-2693(81)91025-X.
- [125] R. Kleiss and W. James Stirling. “Spinor Techniques for Calculating p anti- $p \rightarrow j$ $W^{+-} / Z^0 +$ Jets”. In: *Nucl.Phys.* B262 (1985), pp. 235–262. DOI: 10.1016/0550-3213(85)90285-8.
- [126] Stefan Dittmaier. “Weyl-van der Waerden formalism for helicity amplitudes of massive particles”. In: *Phys.Rev.* D59 (1998), p. 016007. DOI: 10.1103/PhysRevD.59.016007. eprint: hep-ph/9805445.
- [127] Ruth Britto, Freddy Cachazo, and Bo Feng. “New recursion relations for tree amplitudes of gluons”. In: *Nucl.Phys.* B715 (2005), pp. 499–522. DOI: 10.1016/j.nuclphysb.2005.02.030. eprint: hep-th/0412308.
- [128] Marcus T. Grisaru and H.N. Pendleton. “Some Properties of Scattering Amplitudes in Supersymmetric Theories”. In: *Nucl.Phys.* B124 (1977), p. 81. DOI: 10.1016/0550-3213(77)90277-2.
- [129] Stephen J. Parke and T.R. Taylor. “Perturbative QCD Utilizing Extended Supersymmetry”. In: *Phys.Lett.* B157 (1985), p. 81. DOI: 10.1016/0370-2693(85)91216-X.

-
- [130] Jurgen Reuter. “Supersymmetry of scattering amplitudes and Green functions in perturbation theory”. In: (2002). eprint: [hep-th/0212154](#).
- [131] Christian Schwinn and Stefan Weinzierl. “SUSY ward identities for multi-gluon helicity amplitudes with massive quarks”. In: *JHEP* 0603 (2006), p. 030. DOI: [10.1088/1126-6708/2006/03/030](#). eprint: [hep-th/0602012](#).
- [132] Tanju Gleisberg and Stefan Hoeche. “Comix, a new matrix element generator”. In: *JHEP* 0812 (2008), p. 039. DOI: [10.1088/1126-6708/2008/12/039](#). eprint: [0808.3674](#).
- [133] Daniel Goetz. “Efficient Automated Computation of Tree-Level Amplitudes in QCD and QED”. MA thesis. Johannes-Gutenberg Universitaet in Mainz, Germany, 2011.
- [134] C. Schwan. “Numerical computation of matrix elements at leading order for QCD with photons”. MA thesis. Johannes-Gutenberg Universitaet in Mainz, Germany, 2011.
- [135] D. Zeppenfeld. “DIAGONALIZATION OF COLOR FACTORS”. In: *Int.J.Mod.Phys. A3* (1988), pp. 2175–2179. DOI: [10.1142/S0217751X88000916](#).
- [136] John M. Campbell and E.W. Nigel Glover. “Double unresolved approximations to multiparton scattering amplitudes”. In: *Nucl.Phys. B527* (1998), pp. 264–288. DOI: [10.1016/S0550-3213\(98\)00295-8](#). eprint: [hep-ph/9710255](#).
- [137] Thomas Becher and Matthias Neubert. “Infrared singularities of scattering amplitudes in perturbative QCD”. In: *Phys.Rev.Lett.* 102 (2009), p. 162001. DOI: [10.1103/PhysRevLett.102.162001](#). eprint: [0901.0722](#).
- [138] Einan Gardi and Lorenzo Magnea. “Factorization constraints for soft anomalous dimensions in QCD scattering amplitudes”. In: *JHEP* 0903 (2009), p. 079. DOI: [10.1088/1126-6708/2009/03/079](#). eprint: [0901.1091](#).
- [139] W.T. Giele and E.W. Nigel Glover. “Higher order corrections to jet cross-sections in $e^+ e^-$ annihilation”. In: *Phys.Rev. D46* (1992), pp. 1980–2010. DOI: [10.1103/PhysRevD.46.1980](#).
- [140] Zoltan Kunszt, Adrian Signer, and Zoltan Trocsanyi. “Singular terms of helicity amplitudes at one loop in QCD and the soft limit of the cross-sections of multiparton processes”. In: *Nucl.Phys. B420* (1994), pp. 550–564. DOI: [10.1016/0550-3213\(94\)90077-9](#). eprint: [hep-ph/9401294](#).
- [141] Peskin M. and Schroeder D. *An Introduction to Quantum Field Theory*. Westview Press, 1995.
- [142] Ryder L. *Quantum Field Theory*. Cambridge University Press, 1985.

- [143] Claude Duhr, Stefan Hoeche, and Fabio Maltoni. “Color-dressed recursive relations for multi-parton amplitudes”. In: *JHEP* 0608 (2006), p. 062. DOI: 10.1088/1126-6708/2006/08/062. eprint: hep-ph/0607057.
- [144] Walter Giele, Zoltan Kunszt, and Jan Winter. “Efficient Color-Dressed Calculation of Virtual Corrections”. In: *Nucl.Phys.* B840 (2010), pp. 214–270. DOI: 10.1016/j.nuclphysb.2010.07.007. eprint: 0911.1962.
- [145] Christian Schwinn and Stefan Weinzierl. “On-shell recursion relations for all Born QCD amplitudes”. In: *JHEP* 0704 (2007), p. 072. DOI: 10.1088/1126-6708/2007/04/072. eprint: hep-ph/0703021.
- [146] Michael Dinsdale, Marko Ternick, and Stefan Weinzierl. “A Comparison of efficient methods for the computation of Born gluon amplitudes”. In: *JHEP* 0603 (2006), p. 056. DOI: 10.1088/1126-6708/2006/03/056. eprint: hep-ph/0602204.
- [147] Fabio Cascioli, Philipp Maierhofer, and Stefano Pozzorini. “Scattering Amplitudes with Open Loops”. In: *Phys.Rev.Lett.* 108 (2012), p. 111601. DOI: 10.1103/PhysRevLett.108.111601. eprint: 1111.5206.
- [148] W. James Stirling. “Hard QCD working group: Theory summary”. In: *J.Phys.* G17 (1991), pp. 1567–1574. DOI: 10.1088/0954-3899/17/10/014.
- [149] J.A.M. Vermaseren. “New features of FORM”. In: (2000). eprint: math-ph/0010025.
- [150] Stefan Weinzierl. “Introduction to Feynman Integrals”. In: (2010). eprint: 1005.1855.
- [151] Christian Reuschle. “Gravitational Corrections to QED Form Factors”. MA thesis. Albert-Ludwigs-Universitaet in Freiburg, Germany, 2009.
- [152] G. Peter Lepage. “A New Algorithm for Adaptive Multidimensional Integration”. In: *J.Comput.Phys.* 27 (1978), p. 192. DOI: 10.1016/0021-9991(78)90004-9.
- [153] R. Kleiss, W. James Stirling, and S.D. Ellis. “A NEW MONTE CARLO TREATMENT OF MULTIPARTICLE PHASE SPACE AT HIGH-ENERGIES”. In: *Comput.Phys.Commun.* 40 (1986), p. 359. DOI: 10.1016/0010-4655(86)90119-0.

Acknowledgements

I would like to owe my gratitude first and foremost to my supervisor, who has provided for me the opportunity to work on a very interesting and highly applicable topic. It was a great pleasure to gain from his deep insights during the course of the last three years. My thanks belongs also to my second assessor.

I would like give thanks to my office mates, who provided an inspiring atmosphere and were always prepared to discuss extensively about any upcoming topic.

Many thanks belongs to the THEP secretariat for always being patient enough to endure any bureaucratic adventure.

My deepest gratitude, however, belongs to my parents for always backing me up and to my girlfriend, with whom I am deeply in love and who has been along my side during the last years to provide me with confidence and encouragement.

Erklärung der Originalität / Statement of Originality

Hiermit erkläre ich, dass ich diese Dissertation selbstständig verfasst und keine anderen als die angegebenen Quellen und Hilfsmittel benutzt habe. Die Stellen in meiner Arbeit, welche dem Wortlaut oder Sinn nach anderen Werken entnommen sind, habe ich in jedem Fall unter Angabe der Quelle als Entlehnung kenntlich gemacht. Dasselbe gilt sinngemäß für Tabellen und Abbildungen. Diese Arbeit hat in dieser oder einer ähnlichen Form noch nicht im Rahmen einer anderen Prüfung vorgelegen.

The author hereby declares, that this doctoral thesis has been composed independently on his own and no other than the referenced literary sources and appliances have been used. Those statements, formulas, lists and figures, which have been borrowed in formulation or meaning from other works, have been referenced accordingly. This thesis has not yet been presented, in neither this nor any other similar form, within the context of any other examination.

Place, Date

Signature

Curriculum Vitae

Family Name: Reuschle
First Name(s): Christian Andreas
Date of birth: 03/26/1980
Place of birth: Heilbronn, Germany

Academic Information

- Since 10/2012* Karlsruhe Institute of Technology, Germany. Employment as postdoctoral researcher in the "Institute for Theoretical Physics" (ITP).
- 12/2009 to 09/2012* University of Mainz, Germany. Enrolled as PhD student in the Physics Department. Research and teaching assistant in the group for "Theoretical High Energy Physics" (WA THEP).
- Oral PhD exam: February 05, 2013.
 - PhD thesis submission: November 15, 2012. Title of the thesis: "Numerical precision calculations for LHC physics".
- 05/2007 to 09/2009* University of Freiburg, Germany. Enrolled as "Diplom" student in the Physics Dept. Advanced studies.
- Awarded "Diplom-Physiker" by the University of Freiburg (09/2009). Title of the thesis: "Gravitational Corrections to QED Form Factors".
 - "Diplom" student in the group for "Elementary Particle Phenomenology" (05/2008).
 - "Hauptpraktikant" in the group for "Elementary Particle Phenomenology" (11/2007).
 - Oral "Diplom" exams in Astrophysics (01/2007 during a visit in Germany), Quantum Field Theory and General Relativity (09/2007) and Experimental as well as Theoretical Physics in general (10/2007).
- 09/2005 to 04/2007* University of Massachusetts, Amherst MA, USA. Graduate Student with an Exchange Program between Massachusetts, USA and the "Land Baden-Württemberg", Germany.
- Awarded "Master of Science" in Physics by UMASS (05/2008), Title of the thesis: „A Neural Network Based Background Suppression Technique applied to VHE Gamma Ray Data coming from the Crab Pulsar“.
 - Research assistant and enrollment in the Master's program in the group for "Elementary Particle and Gravitational Physics Experiment" at UMASS (02/2006).
- 08/2002 to 08/2005* University of Freiburg, Germany. Enrolled as "Diplom" student in the Physics Dept. Basic studies. "Vordiplom" in Mathematics, Physics and Microsystems Technology (2003/04).

Further Professional Information

- 07/2003 to 03/2005* Research Assistant at the "Fraunhofer Institute for High-Speed Dynamics" ("Enst-Mach-Institut") in Freiburg, Germany.
- 07/2001 to 04/2002* Civilian Service in a community for the physically challenged, "Lindhain Wohngruppe" in Bietigheim-Bissingen, Germany.
- 09/1996 to 07/1999* Vocational Training as Electronic Technician at „Valeo Auto-Electrics“ in Bietigheim-Bissingen, Germany and Vocational School, "Carl-Schaefer Schule" in Ludwigsburg, Germany.
- Electronic Technician Diploma (07/1999).
 - Vocational School Diploma (06/1999).

Further Skills

Languages	German (native), English (fluent, spoken/written, 6 years in school, 1.5 years in the US, TOEFL)
Programming	C++, GSL, CINT, ROOT, Fortran, PAW++, MLPfit, FORM, Mathematica, FeynRules, GNUPLOT

Publications and Publicly Available Theses

Becker, Reuschle, Weinzierl, "Efficiency Improvements for the Numerical Computation of NLO Corrections", JHEP 1207 (2012) 090. arXiv:1205.2096 [hep-ph].
Becker, Goetz, Reuschle, Schwan, Weinzierl, "Numerical evaluation of NLO multiparton processes", PoS (2012), arXiv:1209.2846 [hep-ph].
Becker, Goetz, Reuschle, Schwan, Weinzierl, "Multiparton NLO corrections by numerical methods", PoS (2011), arXiv:1112.3521 [hep-ph].
Becker, Goetz, Reuschle, Schwan, Weinzierl, "NLO results for five, six and seven jets in electron-positron annihilation". Phys.Rev.Lett. 108 (2012) 032005. arXiv:1111.1733 [hep-ph].
Becker, Reuschle, Weinzierl, "Numerical NLO QCD calculations", JHEP 12 (2010) 013, arXiv:1010.4187 [hep-ph].
Assadsolimani, Becker, Reuschle, Weinzierl, "Infrared singularities in one-loop amplitudes", Nucl.Phys.Proc.Suppl. 205-206 (2010) 224, arXiv:1006.4609 [hep-ph].
C. Reuschle, "Gravitational Corrections to QED Form Factors", Master's ("Diplom") thesis (2009), University of Freiburg. http://www.thep.physik.uni-mainz.de/~reuschle/Homepage/Presentations/Files/Theses/DA/DA_CR_Main.pdf
C. Reuschle, "A Neural Network based Background Suppression Technique applied to VHE Gamma Ray Data coming from the Crab Pulsar", Master's thesis (2008), University of Massachusetts. http://scholarworks.umass.edu/theses/145/

Conferences, Workshops and Schools

April 19, 2012	Presentation at the "Loops And Legs 2012" conference in Wernigerode, Germany. Title "Numerical Evaluation of NLO Multiparton Processes"
August 25, 2011	Presentation at the "QCD @ LHC 2011" conference in St. Andrews, Scotland. Title "Numerical evaluation of loop corrections"
March 31, 2011	Presentation at the "DPG Frühjahrstagung 2011" in Karlsruhe, Germany. Title "Numerical NLO QCD calculations - Subtraction method for the virtual contributions"
September 16, 2010	Presentation at the "SRFN-Workshop 2010" at the Ebernburg in Bad-Münster am Stein, Germany. Title "Numerical QCD Calculations for LHC physics"
September 11 - 16, 2011	University of Mainz GK and EMG Summer School on "Symmetries, Fundamental Interactions and Cosmology 2011", Chiemsee Island "Frauenchiemsee" in Bavaria, Germany.
March 14 - 17, 2011	Helmholtz Alliance - Physics at the Terascale, "Monte Carlo School 2011", DESY Hamburg, Germany.
September 27 - 29, 2010	Second Annual Retreat of the Graduate School "Symmetry Breaking in Fundamental Interactions" in Bingen am Rhein, Germany
August 1 - 7, 2010	PSI Summerschool "Gearing up for LHC Physics" in Zuz, Switzerland.

Teaching Experience and Seminar Organization

Fall '11/Spring '12, Mainz	Friday Seminar "Selected Topics in Collider Physics", THEP and ETAP	Convener
Fall '11	University of Mainz GK and EMG Summer School on "Symmetries, Fundamental Interactions and Cosmology 2011". Short lecture on "Introduction to theory and higher order corrections of (g-2)".	Topical Talk
Spring '11, Mainz	Theoretical Physics 3 (Introductory QM)	Personal Assistant
Fall '10, Mainz	Theoretical Physics IV (Advanced QM)	Personal Assistant
Spring '10, Mainz	Theoretical Physics 1 (Mechanics/Electrodynamics)	Personal Assistant
Spring '09, Freiburg	Practical Laboratory Course for Physics Minors	Teaching Assistant
Fall '08, Freiburg	Practical Laboratory Course for Physics Majors (Beginners)	Teaching Assistant
Fall '08, Freiburg	Mathematical Introduction for Beginners	Teaching Assistant
Spring '08, Freiburg	Theoretical Physics 2 (Classical Mechanics)	Teaching Assistant
Fall '07, Freiburg	Practical Laboratory Course for Physics Majors (Beginners)	Teaching Assistant